NASA/TP—1998-207687

Comparison of Five System Identification Algorithms for Rotorcraft Higher Harmonic Control

Stephen A. Jacklin
Ames Research Center, Moffett Field, California

National Aeronautics and
Space Administration

Ames Research Center
Moffett Field, California 94035-1000

May 1998

Available from:

NASA Center for AeroSpace Information
7121 Standard Drive
Hanover, MD 21076-1320

National Technical Information Service
5285 Port Royal Road
Springfield, VA 22161

CONTENTS

SYMBOLS

ABS or | |	absolute value
CA	cycles-averaged
E[]	expected value
G_1	gain for transfer-matrix variation
G_2	gain for constant noise input
G_3	gain for random noise input
g	measure of acceleration, 9.81 m/sec^2
HHC	higher harmonic control
I	identity matrix
i	indicates row of tensor or row dimension of a matrix
J_{ID}	quadratic identification index
J_P	quadratic performance index
J_Z	measured vibration index
J_{Z0}	uncontrolled vibration index
J_θ	total HHC pitch index
j	indicates column of tensor or column dimension of a matrix
$\mathbf{K_S}$	LMS and generalized LMS stability gain matrix (i x i)
$\mathbf{K_{Si}}$	diagonal element of K_S, scalar
k	discrete computation step index
LMS	least-mean-squares
LSE	least-square-error
M	initial process-noise covariance matrix (j x j)

M_i	M for ith row of T_i (j x j)
N	number of rotor blades
N_T	number of elements in **T** matrix
n	number of measurements; multi-step batch size
P	process-noise covariance matrix computed after measurement (j x j)
$\mathbf{P}_i$	P for ith row of $\mathbf{T}_i$ (j x j)
Q	Kalman filter probing noise matrix (j x j)
R	measurement-noise covariance matrix, (n x n)
r	measurement-noise covariance, scalar
r_i	measurement-noise covariance for ith row of T, scalar
T	local or global transfer matrix (i x j)
$\mathbf{T}_{Global}$	global transfer matrix (i x j+1)
$\mathbf{T}_{ID}$	identified transfer matrix (i x j)
$\mathbf{T}_i$	ith row of transfer matrix (1 x j)
$\mathbf{T}_{Local}$	local transfer matrix (i x j)
$\mathbf{T}_{NS}$	invariant-noise matrix (i x j)
$\mathbf{T}_{NUS}$	random-noise matrix (i x j)
$\mathbf{T}_{True}$	true transfer matrix (i x j)
$\mathbf{T}_0$	base transfer matrix (i x j)
W	WLSE diagonal-weighting matrix (n x n)
$\mathbf{W}_{GLMS}$	GLMS diagonal-weighting matrix (n x n)
$\mathbf{W}_Z$	diagonal vibration-weighting matrix (i x i)
$W_{\Delta\theta}$	diagonal control-rate weighting matrix (j x j)

W_θ	diagonal total control weighting matrix (j x j)
WLSE	weighted least-square error
w	Kalman filter transfer-matrix process noise, scalar
w(k)	measurement error weight for kth measurement
$\mathbf{Z}$	vibration measurement matrix (i x n)
$\mathbf{Z}_i$	ith row of Z matrix (1 x n)
Z_1	gain for z_0 variation
Z_2	z_0 phase lag constant
z	vibration vector (i x 1)
z_{DV}	abrupt changes to z_0 (i x k)
z_i	ith element of vibration vector scalar
z_N	vibration measurement noise (i x 1)
z_0	uncontrolled vibration (i x 1)
α, γ	weighting factors for WLSE
ϕ	estimate transition matrix
Γ	Kalman filter influence matrix (i x j)
ε	error vector, scalar or (1 x n)
ε_i	adaptation error vector (1+ n)
Δz	change in vibration vector (i x 1)
$\Delta\theta$	change in HHC pitch vector (j x 1)
Θ	HHC block control matrix (j x n)
θ	HHC pitch vector (j x 1)

θ^*	repartitioned control vector
λ	matrix eigenvalue
Ψ	Kalman filter transition matrix (j x j)
ω_T	rate of transfer-matrix variation
ω_Z	rate of z_0 vibration variation

Superscripts

T	transpose
-1	inverse
*	estimate

Note: Throughout the text, letters that designate matrices are printed in boldface.

COMPARISON OF FIVE SYSTEM IDENTIFICATION ALGORITHMS FOR ROTORCRAFT HIGHER HARMONIC CONTROL

Stephen A. Jacklin

Ames Research Center

SUMMARY

This report presents an analysis and performance comparison of five system-identification algorithms. The methods are presented in the context of identifying a frequency-domain transfer matrix for the higher harmonic control (HHC) of helicopter vibration. The five system-identification algorithms include three previously proposed methods: (1) the weighted-least-squares-error approach (in moving-block format), (2) the Kalman filter method, and (3) the least-mean-squares (LMS) filter method. In addition there are two new ones: (4) a generalized Kalman filter method and (5) a generalized LMS filter method. The generalized Kalman filter method and the generalized LMS filter method were derived as extensions of the classic methods to permit identification by using more than one measurement per identification cycle. Simulation results are presented for conditions ranging from the ideal case of a stationary transfer matrix and no measurement noise to the more complex cases involving both measurement noise and transfer-matrix variation. Both open-loop identification and closed-loop identification were simulated. Closed-loop mode identification was more challenging than open-loop identification because of the decreasing signal-to-noise ratio as the vibration became reduced. The closed-loop simulation considered both local-model identification, with measured vibration feedback and global-model identification with feedback of the identified uncontrolled vibration. The algorithms were evaluated in terms of their accuracy, stability, convergence properties, computation speeds, and relative ease of implementation. With the exception of the weighted-least-squares-error technique, all of the identification methods were found to be suitable for on-line system identification, and all were found to produce about the same amount of identification error in closed-loop operation. However, the algorithms clearly differed with respect to their formulation, ease of implementation, and computational speed. The single-step LMS filter was not only computationally the fastest identification method, but was also the easiest to implement because it required the specification of only one tuning parameter. Although the generalized LMS filter implemented with a batch size of 4 was slower than the single-step version, it also produced somewhat superior identification accuracy. The generalized Kalman filter, though not as fast nor as easy to tune as the LMS methods, produced the lowest system identification error using a batch size of 4 with the local model. Neither the elimination of a recursive equation in the generalized Kalman filter formulation nor the reduction of tuning parameters by the LMS and generalized LMS formulations was seen to impair identification accuracy when compared to the classic Kalman filter.

1. INTRODUCTION

In forward flight, asymmetrical airflow through the helicopter rotor causes large vibratory forces and moments to be generated on the rotor blades. The blade loads may be additionally affected by the presence of rotor blade stall, shock waves (compressibility effects), or by the blades striking the trailed vortices of other blades at one or more places around the rotor azimuth (fig. 1). For an N-bladed rotor, these harmonic air loads produce large oscillatory blade-root shear forces and bending moments which are experienced as N-per-revolution (N/rev) vibration in the fuselage reference frame. This vibration degrades the ride quality of the helicopter and shortens the life of critical rotor hardware.

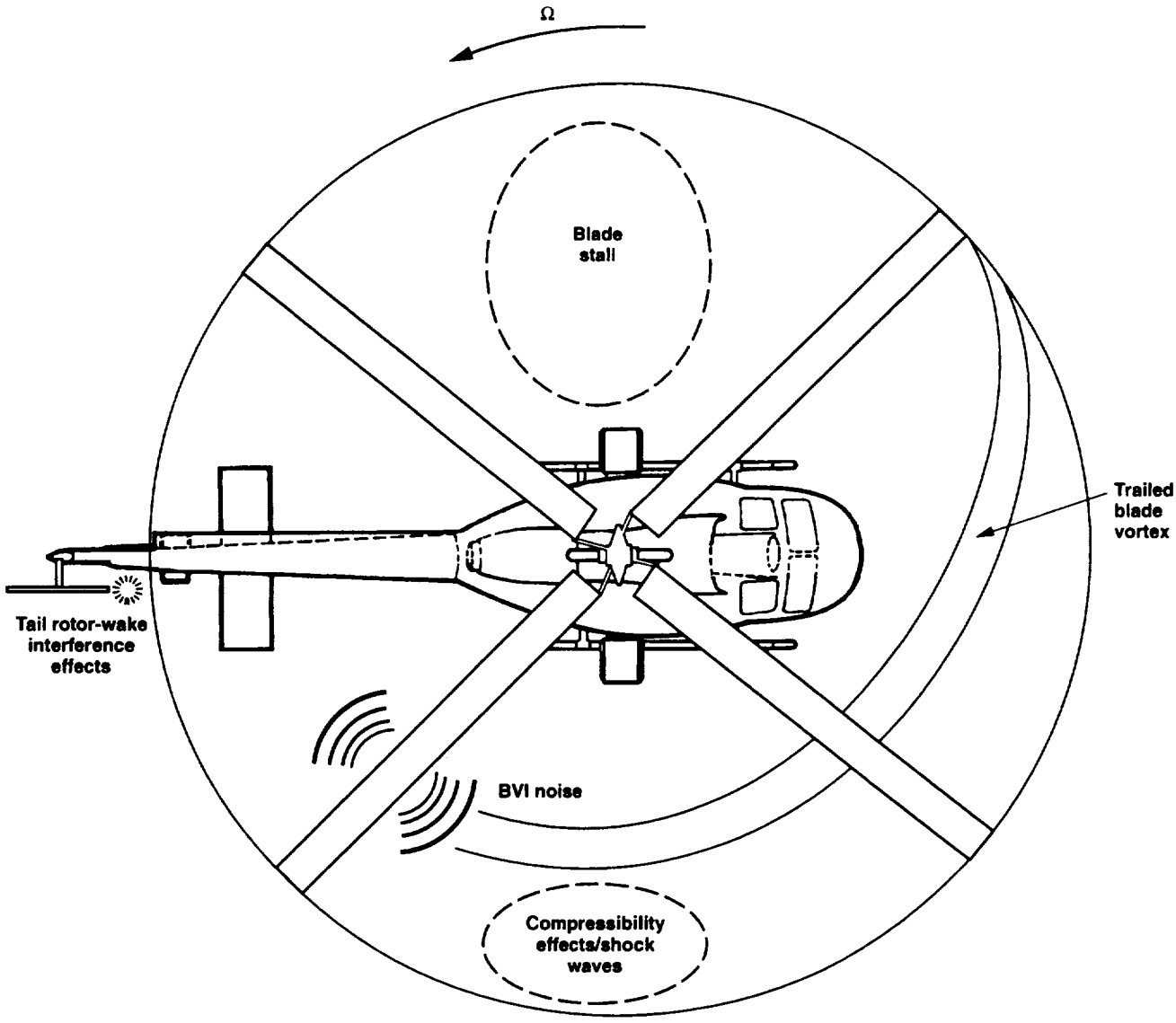

Figure 1. Origin of rotorcraft N/rev air loads and vibration.

Since passive vibration control methods (such as pendulum absorber and modal placement methods) have not been totally successful (ref. 1), active control methods have been proposed to help alleviate the helicopter vibration problem. The most widely studied method is the higher harmonic control (HHC) technique whereby the rotor blades are oscillated at the N/rev frequency to cancel the vibration at its source. In this approach, accelerometers can be used to measure the fuselage vibration while suitable swashplate actuators can be used to induce the N/rev blade-pitch commands. Figure 2 illustrates the basic HHC vibration control-loop. To implement this control scheme, however, it is necessary to know the manner in which the N/rev blade-pitch inputs influence the N/rev components of vibration.

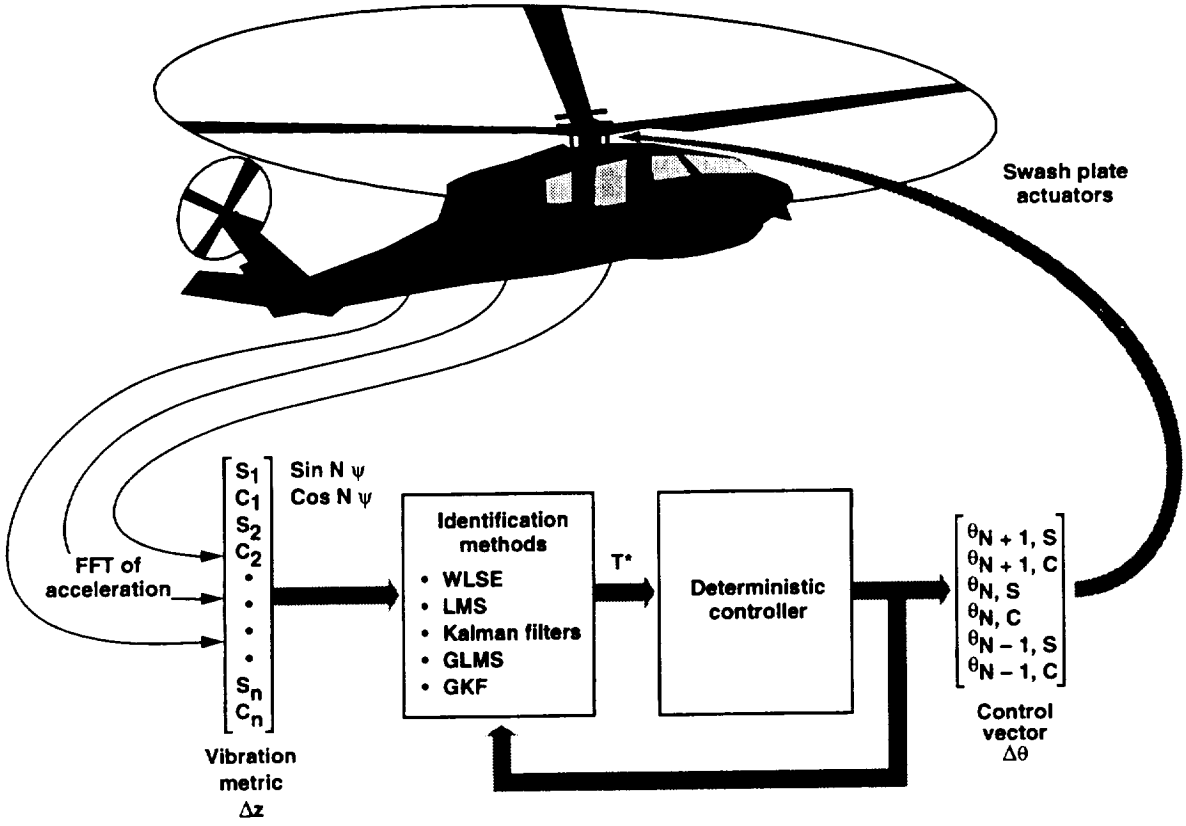

Figure 2. Helicopter vibration control loop.

Early work in achieving this understanding focused primarily on seeking a simple set of HHC input amplitudes and phases that would allow reduction of the vibration throughout the flight regime of the helicopter. Stewart (ref. 2) proposed the application of 2/rev control inputs to delay the onset of retreating-blade stall. The method was extended to include 3/rev input by Arcidiacono (ref. 3) in 1961, and then flight tested on a UH-1A, two-bladed, teetering rotor. This test showed that the 2/rev input had a marked effect on rotor vibration (ref. 4). Nearly a decade later, Sissingh and Donham (ref. 5) and McCloud and Kretz (ref. 6) applied HHC to four-bladed rotors. Sissingh and Donham showed that HHC could suppress the blade flap-bending oscillatory loads, while McCloud and Kretz, using a jet-flap rotor, showed that substantial fuselage vibration reduction could be achieved by using HHC. Moreover, McCloud also calculated a set of influence

coefficients which attempted to relate the effects of harmonic control input on the harmonics of measured vibration. This originated the idea of the transfer-matrix model.

In 1975, McCloud further advanced the idea of a transfer matrix relating the harmonics of control input to the harmonics of measured vibration for a four-bladed, articulated, controllable-twist rotor (ref. 7). This transfer matrix was used to determine the HHC input magnitudes and phases required to minimize the sum of the squares of the vibratory loads. When tested full-scale in two wind tunnel tests, it was shown that HHC could substantially reduce the rotor-blade bending loads (McCloud and Weisbrich (ref. 8)), as well as the N/rev vibration at fuselage (test stand) stations instrumented with accelerometers (Brown and McCloud (ref. 9)). This work clearly established the validity of using a linear transfer matrix to relate the harmonics of HHC input to the harmonics of measured vibration output. However, at the same time, this work also showed that the transfer matrix was not invariant with airspeed, but rather was strongly dependent on the flight conditions. This finding was subsequently confirmed by Shaw and Albion (ref. 10) using a model-scale, four-bladed, hingeless rotor.

Shaw and Albion also demonstrated the feasibility of designing a closed-loop, HHC vibration control system based on using a transfer matrix in a deterministic control law (discussed in sec. 5.3). To be effective at several flight speeds, however, a way had to be found to adapt or re-identify the transfer-matrix elements with each flight condition. For this purpose, Shaw decided to use a Kalman filter which proved to be successful in low-speed flight. In a later work however, testing HHC on a three-bladed, small-scale CH47D rotor, Shaw achieved the same vibration reduction performance (up to 90% reduction) using transfer matrices identified off-line. In this approach, separate transfer matrices were identified at each flight condition off-line, and then subsequently used in the controller (ref. 11). This approach was preferred over the Kalman filter, which sometimes had difficulties. Indeed, several other researchers of HHC also reported similar problems when using the classic Kalman filter system identification method (refs. 12–18).

The classic Kalman filter approach, which many believe to be the best on-line method of system identification, performs the system identification using only the most recent measurement to update the estimate of the identified parameters (or transfer matrix). This makes the Kalman filter computationally efficient. The difficulty in using the classic Kalman filter, however, is that the statistical information needed to implement the filter is often poorly known. For example, exact knowledge of the vibration measurement-noise spectrum and error covariance is required. If not tuned correctly, the Kalman filter may not be able to distinguish errors in the measurements from true changes in the parameters, leading to either unresponsive identification performance or a display of stability and convergence problems. These problems motivate the search for alternative system-identification algorithms which can produce near optimal Kalman filter identification accuracy, yet are more easily implemented and less prone to the destabilizing effects of measurement noise and un-modeled dynamic behavior.

With this goal in mind, this report seeks to compare the identification performance of four other system identification methods with that of the classic Kalman filter. These algorithms are the weighted-least-squares method in moving-block format, the generalized Kalman filter method, the least-mean-square (LMS) filter method, and generalized LMS filter methods. These algorithms differ from the classic Kalman filter method in that they place less reliance on user-supplied tuning

information than the classic Kalman filter method or in that they are computationally more efficient. In fact, the LMS filter method is a single-step identification technique which resembles the Kalman filter method in some ways, but is considerably less complex in its implementation.

The order of the report is as follows. After a brief description of the helicopter system-identification problem for HHC, a detailed description and derivation of each of the five system-identification methods is presented. Then the computer program used to simulate the identification methods is briefly described, and the computational efficiencies of the identification methods are compared. After that, the open-loop and closed-loop identification performance results are presented. The closed-loop simulation considered both local-model identification with measured vibration feedback and global-model identification with feedback of the identified uncontrolled vibration. Last, some comparisons between the methods are made and the conclusions are presented.

Note that throughout the text, letters designating matrices are printed in boldface.

2. SYSTEM IDENTIFICATION MODELS

Adopting the transfer-matrix modeling approach, the relationship between the HHC control input harmonics and the harmonics of vibration output can be linearly expressed as

$$z_k = \mathbf{T}\theta_k + z_o \tag{1}$$

In this representation, z_k is an (i x 1) vector representing the sine and cosine harmonics of vibration at step k, θ_k is a (j x 1) vector representing the sine and cosine harmonics of N/rev blade-pitch control at step k, and $\mathbf{T}$ is the (i x j) transfer matrix relating the harmonics of vibration to the harmonics of control. The vibration vector, z, could represent the N/rev sine and cosine accelerations measured by i/2 fuselage accelerometers. Since most helicopter swashplates are controlled using three actuators in the fixed-system, the dimension of j is usually 6. Equation (1) is referred to as the global model of helicopter harmonic vibration. Note that the baseline vibration present with no HHC control ($\theta = 0$) is therefore z_o.

An alternative representation is to model the relationship linearly in a local region about the current conditions. If equation (1) is applied to two successive simulation steps, namely k and k-1, two equations are formed,

$$z_k = \mathbf{T}\,\theta_k + z_o$$

$$z_{k-1} = \mathbf{T}\,\theta_{k-1} + z_o$$

which, if subtracted from each other yield the local-model representation as

$$\Delta z = \mathbf{T}\,\Delta\theta \tag{2}$$

where the changes in vibration, Δz, and the changes in control, $\Delta\theta$, are computed for simulation step k as

$$\Delta z = z_k - z_{k-1}$$

$$\Delta\theta = \theta_k - \theta_{k-1} \tag{3}$$

Using either model, the identification problem is to determine the coefficients of the transfer matrix, given knowledge of the control inputs and measured vibration outputs. Since the transfer matrix will typically vary with the helicopter operating conditions (e.g., thrust, airspeed), the methods used for transfer-matrix identification should be "on-line" methods which can track or estimate the transfer matrix based on the information contained in the most recent control inputs and vibration outputs.

Given knowledge of the transfer matrix, it is possible to compute a minimum-variance control law of the type described in section 5.3 below. When using the local modeling, the identified transfer matrix and measured vibration are used in the control law to calculate the optimal change in control needed to cancel the measured vibration. Using equation (2), the optimal change in control is computed as

$$\Delta\theta_{OPT} = -\mathbf{T}^{-1}z \tag{4}$$

since the change in vibration desired is the opposite of the amount of remaining measured vibration z. Note that in this nomenclature, $\mathbf{T}^{-1}$ is regarded as a pseudo-inverse, since $\mathbf{T}$ is not required to be a square matrix. If the global modeling is used, the identification routine is also used to identify the uncontrolled vibration, z_0. Using equation (1) to cancel the vibration (i.e., make z = 0),

$$\theta_{OPT} = -\mathbf{T}^{-1}z_o \tag{5}$$

Therefore, it can be seen that if the transfer matrices defined by equations (1) or (2) exist, computing the optimal vibration controls is a relatively simple matter after the transfer matrices have been identified.

3. ANALYSIS OF IDENTIFICATION ALGORITHMS

This section presents an analysis of the five identification algorithms. Through analysis, the important limitations of the methods can be more fully understood. Of central importance is a review of the underlying assumptions concerning the stochastic environment in which each method is designed to operate.

The following analyses for each of the five identification methods are presented in terms of the local-model notation. The derivations, however, are exactly the same for the global model because equations (1) and (2) can be transformed into the same equation form. This is easily seen by rewriting these equations in matrix form and using partitioned matrices and vectors for the global model. If that is done, then the global model ($z = T\theta + z_0$) can be written as

$$\begin{bmatrix} z_1 \\ \vdots \\ \vdots \\ z_i \end{bmatrix} = \left[\begin{array}{ccc|c} T_{11} & \cdots & \cdots & T_{1j} \,|\, z_{o1} \\ \vdots & \ddots & & \vdots \;| \\ \vdots & & \ddots & \vdots \;| \\ T_{i1} & \cdots & \cdots & T_{ij} \,|\, z_{oi} \end{array}\right] \begin{bmatrix} \theta_1 \\ \vdots \\ \theta_j \\ \hline 1 \end{bmatrix} \tag{6}$$

and the local model can be written as

$$\begin{bmatrix} \Delta z_1 \\ \vdots \\ \vdots \\ \Delta z_i \end{bmatrix} = \begin{bmatrix} T_{11} & \cdots & \cdots & T_{1j} \\ \vdots & \ddots & & \vdots \\ \vdots & & \ddots & \vdots \\ T_{i1} & \cdots & \cdots & T_{ij} \end{bmatrix} \begin{bmatrix} \Delta\theta_1 \\ \vdots \\ \vdots \\ \Delta\theta_j \end{bmatrix} \tag{7}$$

Equations (6) and (7) are of the same form and are equivalent mathematical expressions of equations (1) and (2), respectively, assuming that the system is truly linear. The only difference is that the global model (eq. (6)) requires that a "1" be appended onto the control vector so that the last column of the identified transfer matrix represents the uncontrolled vibration. In actual application, however, nonlinearities in the plant dynamics cause these models to differ. They are only truly equivalent for the case of a time-invariant linear system.

3.1 Weighted-Least-Squares-Error Method

The technique of ordinary least squares has been around as long as the concept of identification. It was independently formulated by Legendre and Gauss in the early 1800s to identify constant parameters in the presence of measurement noise. Today, nearly all methods of parameter identification, whether off-line or on-line, stem from this important technique. This method assumes that a batch, or set of command inputs and response outputs, is available at the start of the calculation. The method makes no assumptions other than that the measurement errors have a normal distribution about the mean (i.e., broadband measurement noise). The batch size must be no less than the number of parameters (per row) to be identified, and may be made larger to reduce the effects of measurement noise on the identification process. The method is non-recursive and is therefore always convergent, provided that the plant excitation commands used in the identification are always linearly independent.

In order to adapt the weighted-least-squares-error (WLSE) method to the helicopter on-line system identification problem, the calculations must be limited to a history of the number of the most recent control commands and vibration measurements (n). Then the excitation commands and

corresponding response measurements can be grouped into block matrices. Using the local-model representation, these block matrices are

$$\Theta = \begin{bmatrix} \vdots & \vdots & \vdots & \vdots \\ \Delta\theta(1), \Delta\theta(2), ,.., , \Delta\theta(n-1), \Delta\theta(n) \\ \vdots & \vdots & \vdots & \vdots \end{bmatrix} \tag{8}$$

$$\mathbf{Z} = \begin{bmatrix} \vdots & \vdots & \vdots & \vdots \\ \Delta z(1), \Delta z(2), ,.., , \Delta z(n-1), \Delta z(n) \\ \vdots & \vdots & \vdots & \vdots \end{bmatrix} \tag{9}$$

In this context, the $\Delta\theta()$ terms represent the changes to the (j x 1) input control commands, the $\Delta z()$ terms represent the corresponding changes to the (i x 1) vibration outputs, and n is the number of measurements in the batch. The identification problem is to identify **T** given knowledge of **Z** and Θ.

The approach used by the WLSE method (and basically by all other identification methods) is to find an estimate of **T** which minimizes the errors produced between the measured output and the output predicted using the estimate of **T** and the input. This error can be expressed for each row of the transfer matrix as

$$\varepsilon_i = \mathbf{Z}_i - \mathbf{T}_i\Theta \tag{10}$$

$$(1 \text{ x } n) = (1 \text{ x } n) - (1 \text{ x } j)(j \text{ x } n)$$

where ε_i is the error and $\mathbf{T}_i$ is any row of the transfer matrix. (Note well: z(1) is a column vector denoting the first measurement over all output channels or, equivalently, the first column of **Z**. However, $\mathbf{Z}_1$ is a (1 x n) row vector denoting the n measurements from channel 1 or, equivalently, row 1 of the **Z** matrix.) As the name implies, the approach used by the WLSE method is to minimize the weighted sum of the squares of the errors for the inputs and outputs used in the calculation batch. (The error is raised to an even power so that positive and negative errors are treated uniformly.) By taking the weighted dot product of the error vector, a scalar identification index, J_{ID}, can be formed as

$$\begin{aligned} \mathbf{J}_{ID} &= \varepsilon_i \mathbf{W} \varepsilon_i^T \\ \mathbf{J}_{ID} &= (\mathbf{Z}_i - \mathbf{T}_i\Theta)\mathbf{W}(\mathbf{Z}_i - \mathbf{T}_i\Theta)^T \\ \mathbf{J}_{ID} &= \mathbf{Z}_i\mathbf{W}\mathbf{Z}_i^T - \mathbf{Z}_i\mathbf{W}\Theta^T\mathbf{T}_i^T - \mathbf{T}_i\Theta\mathbf{W}\mathbf{Z}_i^T + \mathbf{T}_i\Theta\mathbf{W}\Theta^T\mathbf{T}_i^T \end{aligned} \tag{11}$$

where **W** is an (n x n) diagonal weighting matrix. As will be seen in comparison to the other system identification methods, this type of quadratic error equation is common to all the other methods of system identification presented in this report.

To find the value of $\mathbf{T}_i$ which minimizes the quadratic performance index of equation (11), the partial derivative with respect to $\mathbf{T}_i$ is computed,

$$\frac{\partial \mathbf{J}_{ID}}{\partial \mathbf{T}_i} = -2\Theta\mathbf{W}\mathbf{Z}_i^T + 2\Theta\mathbf{W}\Theta^T\mathbf{T}_i^T \tag{12}$$

Setting this partial derivative equal to zero (to find the minimum), the WLSE estimate of $\mathbf{T}_i$ is

$$\mathbf{T}_i = \mathbf{Z}_i\mathbf{W}\Theta^T(\Theta\mathbf{W}\Theta^T)^{-1} \tag{13}$$

$$(1 \times j) = (1 \times n)(n \times n)(n \times j)\ [\ (j \times n)(n \times n)(n \times j)\ ]\text{-}1$$

This linear equation is the weighted-least-squares estimate of the transfer-matrix row. Note that if the performance index had been quartic, ε^4, the derivative would have been cubic. The difficulty of handling a cubic identification law (with three minimas possible) is why the least squares-approach is so convenient for analysis.

It follows from equation (13) that the WLSE estimate for the entire transfer matrix can be formed as

$$\mathbf{T} = \mathbf{Z}\mathbf{W}\Theta^T(\Theta\mathbf{W}\Theta^T)^{-1} \tag{14}$$

$$(i \times j) = (i \times n)(n \times n)(n \times j)\ [\ (j \times n)(n \times n)(n \times j)\ ]^{-1}$$

where the weighting matrix **W** is the same for all measurement channels. (Note that a different weighting matrix for each input channel could be accommodated by applying equation (13) for each row of the transfer matrix.) For ordinary least squares, **W** is an identity matrix. Then identification errors at all steps are counted equally in the optimization process. As n becomes larger, the effect of equal weighting at each time-step is to average out white or wideband measurement noise.

However, it often arises that variations in the system parameters over time create a situation in which the more recent measurements will better reflect the true system state. For example, the helicopter air speed may suddenly change. In that case, the identification performance may be improved by placing greater weight on the more recent measurements. It has been shown (refs. 19, 20) that the optimal weighting matrix is the inverse of the measurement-noise covariance matrix. For measurement noise with a normal distribution, this choice of weighting produces the well-known maximum likelihood or best linear unbiased estimate. In general, however, the values of the measurement-noise covariance matrix (see eq. (18) for the scalar definition) are unknown because the system transfer matrix is unavailable for use in the computational process.

A more convenient method of weight selection is presented in reference 19, where the weights for the diagonal elements of **W**, w(k), are generated as

$$w(k) = \alpha\gamma^{(n-k)} \qquad 0 < \gamma < 1 \tag{15}$$

where n is the number of measurements in the batch and k denotes a specific measurement in the batch for which k = n is the most recent measurement. If $\gamma = 1$ and $\alpha = 1$, the weighting matrix is the identity matrix. As γ is reduced, less weight is placed on the least recent measurements. One consideration governing how far γ should be reduced is that smaller values will tend to amplify the effects of measurement noise on the most recent measurements by making the batch size effectively smaller.

It should be noted that equation (14) has certain limitations. First, the calculation batch size n must be larger than the row dimension of **T** (or larger than the number of elements in the control vector). Second, the weighted control-covariance matrix, $[\Theta\, \mathbf{W}\, \Theta^T]$ must not have a lower rank than the number of elements in the control vector θ. If that happens, the control covariance matrix becomes singular, and the inversion cannot be performed. This situation arises when the control vectors within the covariance matrix are redundant or linearly dependent. Of course, this problem is easily avoided in open-loop identification by selecting excitation commands randomly. However, for closed-loop control, when the commands are selected to minimize the (vibration) response vector, avoidance of this problem is not easy. If the controller should calculate nearly the same control input from one cycle to the next (as should happen about the steady-state optimal input), the control covariance matrix will tend toward singularity, and the identification accuracy will degrade as the singularity worsens.

A good way to avoid the singularity problem is a subject of debate. The most obvious possibility would be to ignore the singularity problem altogether and allow the identification process to produce an improper transfer matrix. The control based on the resulting erroneous estimate would then serve to automatically generate a perturbation excitation signal. However, steady-state controller performance would likely be erratic. Another solution would be to prevent the control commands from ever becoming linearly dependent by constantly introducing a random perturbation component to the control signal. This would also degrade steady-state control performance, but might make the controller behavior less erratic. A third solution might be to shut off the identification process during periods when the changes in control are sufficiently small. The merits of each approach were evaluated through simulation.

3.2 Classic Kalman Filter Method

Though identification by the WLSE method is relatively easy to implement and to understand, its calculation batch size limits its ability to identify rapidly changing variables. This provides the motivation to find faster identification algorithms that have fewer computations and that use fewer measurements. The Kalman filter method is perhaps the most widely known and accepted method of a class of computationally efficient algorithms designed to update parameter estimates on the basis of a single measurement. The Kalman filter has been widely used in a number of aerospace

applications. In fact, many investigators of higher harmonic control concepts have proposed using the Kalman filter to identify frequency-domain transfer matrices (for example, see refs. 10, 12-14, 16-18, 21). The Kalman filter is derived by converting the least squares algorithm into a recursive method by accumulating the rank of the first inversion. This solution is referred to as the recursive-least-squares-estimation method. However, the recursive-least-squares algorithm was not simulated separately in this study because, as will be shown, it is a special case of the more general Kalman filter theory.

The computational speed of the Kalman filter results from not computing the values of certain quantities that define the stochastic identification environment. These values are presumed to be known. As will be shown below, they include knowledge of starting estimates for the transfer matrix, the transfer-matrix covariance, the measurement-noise covariance, and the process-noise covariance. The degree to which this information is actually known is critical in designing the filter for optimal performance and stability. Usually, however, this information is not readily available, and the user must use trial and error to find the correct values.

Since the complete derivation of the Kalman filter is well explained by many excellent texts (refs. 19-22), only the essentials of the derivation process will be outlined here. Derivation of the Kalman filter begins by assuming that the measurement and process noises have zero (or known constant) mean values:

$$E(\Delta z_i - \mathbf{T}_i \Delta\theta) = 0 \tag{16}$$

$$E(\mathbf{T}_i - \mathbf{T}_i^*) = 0 \tag{17}$$

respectively, where $\mathbf{T}_i^*$ represents an estimate of the ith transfer-matrix row and $E\{...\}$ denotes "expected value." The associated covariance matrices (also assumed to be known) are represented by diagonal, positive definite matrices, r_i and $\mathbf{M}_i$, as

$$E\left[(\Delta z_i - \mathbf{T}_i \Delta\theta)^T (\Delta z_i - \mathbf{T}_i \Delta\theta)\right] = r_i \tag{18}$$

$$E\left[(\mathbf{T}_i - \mathbf{T}_i^*)^T (\mathbf{T}_i - \mathbf{T}_i^*)\right] = \mathbf{M}_i \tag{19}$$

where r_i is a scalar which is the measurement-noise variance and $\mathbf{M}_i$ is the process-noise covariance matrix. Equations (16) and (17) state that the distributions of measurement and process noises have a zero mean value. Equations (18) and (19) state that the variance and covariance of the measurement (18) and process (19) noises are known, assuming a Gaussian distribution of measurement and process noises. Although obtaining an estimate of the transfer-matrix row $\mathbf{T}_i^*$ is not difficult (from least squares), evaluation of r_i and $\mathbf{M}_i$ requires operation of the filter to produce $\mathbf{T}_i$. This is troublesome, since r_i and $\mathbf{M}_i$ must be specified to start the filter.

The solution to this dilemma is to guess the correct initial values for r_i and $\mathbf{M}_i$. This is called "tuning the filter." Sometimes, r_i and $\mathbf{M}_i$ can be selected on the basis of some rationale (refs. 14

and 22 give some), but in most cases guessing is required. This is an awesome task for the proposed helicopter identification problem, because for a typical (6 × 6) transfer-matrix, 6 values for r_i and 146 values for $\mathbf{M}_i$ (6 * [6 × 6]) would require specification. (Note that the $\mathbf{M}_i$ covariance matrix is symmetric.)

A sensible alternative commonly employed is to make more assumptions regarding the nature of r_i and $\mathbf{M}_i$ in order to simplify the tuning problem. One assumption often made is that the $\mathbf{M}_i$ matrices are diagonal matrices, whose diagonal elements are all equal. A further assumption is that the r_i and the $\mathbf{M}_i$ are the same for each row of the transfer-matrix. These assumptions may or may not be justifiable. However, with these assumptions, the tuning parameter selection problem can be reduced to a two-parameter selection problem. In the above example with the (6 × 6) transfer matrix, for example, the 6 + 146 tuning parameters reduce to only two. $\mathbf{M}_i$ is still a matrix, but with diagonal form and all the diagonal elements are equal. Its specification is then like choosing a scalar quantity.

It is very important to note that although these assumptions are convenient, they corrupt the most basic premises of the Kalman filter theory. The filter is only optimal if the input values for the measurement- and process-noise covariances (r_i and $\mathbf{M}_i$) are correct. To see this, consider the Kalman filter as one minimizing the weighted sum of the process and measurement noises. Like the least-squares method, this can be expressed as the minimization of a quadratic identification performance index, J_{ID},

$$J_{ID} = (\Delta z_i - \mathbf{T}_i \Delta\theta) r_i^{-1} (\Delta z_i - \mathbf{T}_i \Delta\theta)^T + (\mathbf{T}_i - \mathbf{T}_i^*) \mathbf{M}_i^{-1} (\mathbf{T}_i - \mathbf{T}_i^*)^T \tag{20}$$

where r_i^{-1} and $\mathbf{M}_i^{-1}$ are the optimal weighting parameters. The minimum value of J_{ID} occurs when the partial derivative of J_{ID} with respect to $\mathbf{T}_i$ is zero, or

$$0 = (\mathbf{T}_i \Delta\theta r_i^{-1} \Delta\theta^T) - (\Delta z_i r_i^{-1} \Delta\theta^T) - \mathbf{T}_i^* \mathbf{M}_i^{-1} + \mathbf{T}_i \mathbf{M}_i^{-1} \tag{21}$$

It is then possible to arrange the terms in equation (21) to produce an update equation for $\mathbf{T}_i$ as follows:

$$\mathbf{T}_i (\mathbf{M}_i^{-1} + \Delta\theta r_i^{-1} \Delta\theta^T) = \mathbf{T}_i^* \mathbf{M}_i^{-1} + \Delta z_i r_i^{-1} \Delta\theta^T$$

or,

$$\mathbf{T}_i (\mathbf{M}_i^{-1} + \Delta\theta r_i^{-1} \Delta\theta^T) = \mathbf{T}_i^* (\mathbf{M}_i^{-1} + \Delta\theta r_i^{-1} \Delta\theta^T) + (\Delta z_i - \mathbf{T}_i^* \Delta\theta) r_i^{-1} \Delta\theta^T \tag{22}$$

which can be rewritten as

$$\mathbf{T}_i = \mathbf{T}_i^* + (\Delta z_i - \mathbf{T}_i^* \Delta\theta) r_i^{-1} \Delta\theta^T \mathbf{P}_i \tag{23}$$

where, by definition, $\mathbf{P}_i$ is

$$\mathbf{P}_i = (\mathbf{M}_i^{-1} + \Delta\theta r_i^{-1} \Delta\theta^T)^{-1} \tag{24}$$

Equations (23) and (24) define a formula for the calculation of $\mathbf{T}_i$, given $\mathbf{M}_i$ and r_i. Unfortunately, equation (24) requires inversion of a (j × j) matrix, which is computationally troublesome. This can be avoided, however, by using the matrix inversion lemma,

$$(A + BCD)^{-1} = A^{-1} - A^{-1}B(C^{-1} + DA^{-1}B)^{-1}DA^{-1} \tag{25}$$

Assigning

$$A = \mathbf{M}_i^{-1}$$
$$B = \Delta\theta$$
$$C = r_i^{-1}$$
$$D = \Delta\theta^T$$

equation (24) may be expressed as

$$\mathbf{P}_i = \mathbf{M}_i - \mathbf{M}_i \Delta\theta (r_i + \Delta\theta^T \mathbf{M}_i \Delta\theta)^{-1} \Delta\theta^T \mathbf{M}_i \tag{26}$$

which now only requires inversion of a scalar. Equations (23) and (26) are update equations for the transfer-matrix row identification and may be computed after each new measurement. Equation (23) shows that the new estimate of the transfer-matrix row is equal to the old estimate plus a correction term. The correction term is proportional to the error between the change in measured vibration state Δz_i and the predicted change in vibration state ($\mathbf{T}_i^* \Delta\theta$), which would be zero, except for measurement error in Δz_i and identification errors in $\mathbf{T}_i$. Since the Kalman filter is designed for recursive calculation, $\mathbf{T}_i^*$ is usually understood to mean $\mathbf{T}_i$ at the previous time-step (it is estimated for the first calculation). Starting values for the (j × j) $\mathbf{P}_i$ matrix can be computed from equation (26) given $\mathbf{M}_i$ and r_i. Note that if $\mathbf{P}_i$ is too large at the start or if it becomes too large, the filter will tend to overcorrect, and the identification performance will be unstable. However, if $\mathbf{P}_i$ is too small, the identification method will not be able to track rapidly changing $\mathbf{T}_i$ values.

Specification of the Kalman filter method is completed by appending equations that specify the manner in which the parameter estimates ($\mathbf{T}_i$) and the covariance matrix ($\mathbf{M}_i$) change between measurements. Usually, the $\mathbf{T}_i$ variation is assumed to be a Gauss-Markov process whereby the value of the parameter estimate at the next step is a function only of the estimate at the current step and some process noise, or

$$\mathbf{T}_i(k+1) = \mathbf{T}_i(k)\Phi + \omega_i(k) \tag{27}$$

where Φ is the estimate transition matrix and ω_i is a random variable vector with an expected value of zero. Then, subtracting the expected transfer-matrix value from both sides of equation (27) we have,

$$\mathbf{T}_i(k+1) - \mathbf{T}_i^*(k+1) = [\mathbf{T}_i(k) - \mathbf{T}_i^*(k)]\Phi + \omega_i(k) \tag{28}$$

where $\mathbf{T}_i^*$ is the expected value of $\mathbf{T}_i$. From equation (19) it can be seen that an update equation for the process-noise covariance matrix can be formed by manipulating each side of equation (28) as follows:

$$E\left\{[\mathbf{T}_i(k+1) - \mathbf{T}_i^*(k+1)]^T[\mathbf{T}_i(k+1) - \mathbf{T}_i^*(k+1)]\right\} =$$

$$E\left\{\left[\Phi^T(\mathbf{T}_i(k) - \mathbf{T}_i^*(k))^T + \omega_i^T(k)\right]\left[(\mathbf{T}_i(k) - \mathbf{T}_i^*(k))\Phi + \omega_i(k)\right]\right\} \tag{29}$$

From which it is obtained directly that

$$\mathbf{M}_i(k+1) = \Phi\mathbf{M}_i(k)\Phi^T + \mathbf{Q}_i \tag{30}$$

where

$$E[\omega_i(k)^T\omega_i(k)] = \mathbf{Q}_i \tag{31}$$

Equation (30) derives directly from equation (29), keeping in mind that the $\mathbf{T}_i$ and ω_i are uncorrelated so that the expected value of the cross-product terms vanish. In order to use equation (30), it is necessary to pick values for Φ and $\mathbf{Q}_i$, similar to that done for r_i and $\mathbf{M}_i$ above. Again, this information is assumed to be known to the user, which is rarely the case in general, and certainly not for the helicopter vibration control problem. Very commonly, Φ is chosen as the identity matrix and $\mathbf{Q}_i$ is left variable for algorithm tuning. Exactly analogous to the assumptions made to simplify the selection of $\mathbf{M}_i$, the $(j \times j)$ $\mathbf{Q}_i$ matrix is usually reduced to the selection of a diagonal matrix whose elements are all the same.

Equations (27) and (30) are to be computed between measurements. In the days of limited on-line computational resources, it might have been useful to compute the variation in $\mathbf{T}_i$ and $\mathbf{P}_i$ between measurements. However, with today's computational power, the time between measurements is so short that the application of these equations takes on a different purpose. This is that $\mathbf{Q}_i$ adds a perturbation to $\mathbf{M}_i$ to prevent it from ever becoming zero; if that were to happen, no further identification could take place. Similarly, ω_i is a perturbation to $\mathbf{T}_i$ which serves to add probing, or a disturbance, to the identification process, desirable to keep the filter from becoming nonadaptive.

The Kalman filter equations can be placed into matrix form by assuming that the r_i values and the $\mathbf{Q}_i$ and $\mathbf{M}_i$ matrices are the same for all rows of $\mathbf{T}$, and that they are denoted as r, $\mathbf{Q}$, and $\mathbf{M}$, respectively. Arranged in the order of their computational sequence after measurement, the Kalman filter equations are then as follows:

$$\mathbf{P} = \mathbf{M}^* - \mathbf{M}^* \Delta\theta(r + \Delta\theta^T \mathbf{M}^* \Delta\theta)^{-1} \Delta\theta^T \mathbf{M}^* \tag{32}$$

$$\mathbf{T} = \mathbf{T}^* + (\mathbf{Z} - \mathbf{T}^* \Delta\theta) r^{-1} \Delta\theta^T \mathbf{P} \tag{33}$$

$$\mathbf{M}^* = \Phi \mathbf{P} \Phi^T + \mathbf{Q} \tag{34}$$

$$\mathbf{T}^* = \mathbf{T}\Phi + \omega \tag{35}$$

These equations represent an optimal filter, given perfect knowledge of r, $\mathbf{M}$, $\mathbf{Q}$, Φ, and ω. In most applications proposed for higher harmonic control, equation (34) is rewritten as

$$\mathbf{M}^* = \mathbf{P} + \mathbf{Q} \tag{36}$$

$$(j \times j) = (j \times j) + (j \times j)$$

assuming $\Phi = I$ and equation (35) is neglected. Equation (32) shows that a small value $\mathbf{M}^*$, once obtained in the steady-state, will cause $\mathbf{P}$ to approach zero. This will make the Kalman filter update in equation (33) zero, and no further improvement of the estimated transfer matrix will take place. The $\mathbf{Q}$ matrix, therefore, serves to keep the $\mathbf{P}$ matrix from ever becoming zero. This is the key strength of the Kalman filter over the recursive least-squares estimation technique. Although that technique is not explicitly developed in this report, the recursive least-squares solution is a special case of Kalman filter theory. As shown in reference 19, the recursive least-squares estimate is obtained by iteratively computing equations (33) and (34) only. Then $\mathbf{M}^*$ is redefined as $\mathbf{P}(k+1)$, and equations (32), (35), and (36) are omitted.

Equation (33) displays the basic dynamics of the Kalman filter method. The new estimate of the transfer-matrix $\mathbf{T}$, formed after measurement, is equal to the old estimate plus a correction term. The correction term is proportional to the error between the change in the measured vibration state, Δz, and the change in the vibration state predicted using the estimated value of the vibration, $\mathbf{T}^*\Delta\theta$. As shown by Kalman filter analysis (ref. 19), identification of the unknown transfer matrix then occurs in the limit of a sufficient number of measurements, assuming that $\mathbf{T}$ and ΔZ are stationary in the mean for as many measurements as are needed to define the expectation values for r, $\mathbf{M}$, and $\mathbf{Q}$.

The Kalman filter is tuned by making good guesses for the r, $\mathbf{M}$, and $\mathbf{Q}$ tuning parameters. If r and $\mathbf{M}$ are chosen so that $\mathbf{P}$ becomes too large, the Kalman filter will become unstable and diverge the identification process. If chosen such that $\mathbf{P}$ becomes too small, the identification process will

become sluggish. It is also probable that more than one combination of r and **M** may produce the same identification performance. Similarly, if **Q** is chosen too small, the filter might not be able to adjust to new conditions, and if chosen too large, may degrade steady-state performance. Moreover, the highly coupled nature of equations (33) through (36) implies that the filter performance will not be linear with regard to the selection of the tuning parameters.

3.3 Classic Least-Mean-Squares Filter Method

The least-mean-squares (LMS) filter method is a single-step identification technique which resembles the Kalman filter, yet is considerably less complex in its implementation. The simplicity of this algorithm derives from the manner in which it is formulated. The LMS filter was developed by Widrow and Hoff (ref. 23) and Widrow (ref. 24), for multiple-input, single-output systems; it was later applied to the multiple-input, multiple-output rotorcraft identification problem in reference 25.

An obvious problem with the Kalman filter method is that the information needed to assign initial values for r, **M**, and **Q** is usually unavailable. Although good estimates can sometimes be experimentally determined for some applications, in many instances a lack of information requires that the initial values be assigned by guessing. When the filter does not perform correctly (as it usually will not at first), there is no good rationale for deciding how the tuning parameters should be adjusted; that takes some trial and error.

In the LMS approach to system identification, this tuning difficulty is circumvented by modeling the identification process in a more direct manner. Both the Kalman and LMS filters require a starting estimate for the transfer matrix, **T**. However, whereas the Kalman filter forms an update equation for **T** assuming knowledge of r, **M**, and **Q**, the LMS approach begins by assuming that corrections to the estimate should be made proportional to the square of the identification error. This identification process is referred to by Widrow (ref. 24) as the steepest descent approach and is motivated by equation (33) of the Kalman filter. A useful mental image of the steepest descent approach for a one-dimensional system is shown in figure 3. In that figure, the estimate of the parameter x is plotted on the horizontal axis and the square of the corresponding identification error ε is plotted on the vertical axis to form a bucket-shaped curve about the value of x having the minimum identification error. It can be seen that given the slope of the identification error about any arbitrary starting value of x, the amount of correction to be made to the estimate is proportional to the slope of the identification error and in the opposite direction, or

$$x(k+1) = x(k) - \mathbf{K}\left[\frac{\partial \varepsilon^2}{\partial x}\right] \tag{37}$$

This states that the correction to the estimate of x is proportional and opposite to the gradient of the squared identification error, ε^2, with respect to x. The identification problem is now to find a good value for **K** and the gradient. If **K** is too large, the identification process may become divergent, and if too small, it may produce very slow convergence.

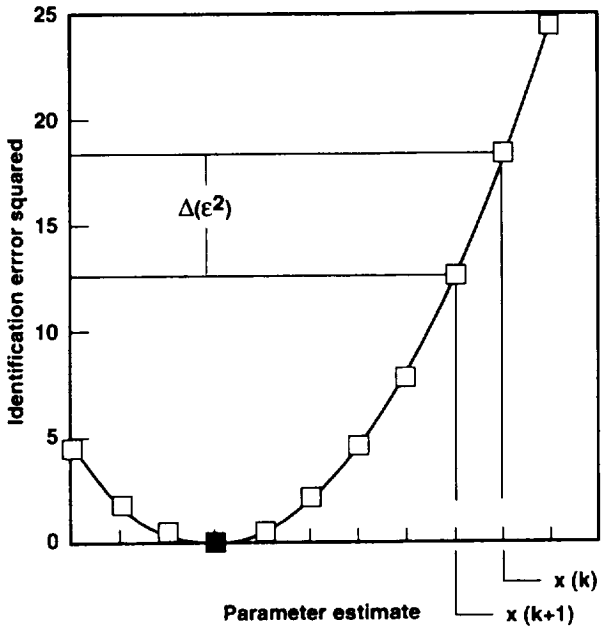

Figure 3. One-dimensional view of LMS gradient.

Equation (37) may be rewritten in terms of the helicopter transfer-matrix identification problem by forming an identification error for each row of the transfer matrix as

$$\varepsilon_i = \left[\Delta z_i(k) - \mathbf{T}_i(k)\Delta\theta(k)\right] \tag{38}$$

where, as before, $\mathbf{T}_i$ is a row of the transfer matrix relating the change in the control inputs $\Delta\theta$ to the change in the ith vibration component output. (Henceforth the digital step indicator k will be assumed and not explicitly written.) The square of the identification error is therefore,

$$\varepsilon_i^2 = \varepsilon_i \varepsilon_i^T \tag{39}$$

$$\varepsilon_i^2 = (\Delta z_i - \mathbf{T}_i\Delta\theta)(\Delta z_i - \mathbf{T}_i\Delta\theta)^T \tag{40}$$

$$\varepsilon_i^2 = \Delta z_i \Delta z_i^T - \Delta z_i \Delta\theta^T \mathbf{T}_i^T - \mathbf{T}_i\Delta\theta\Delta z_i^T + \mathbf{T}_i\Delta\theta\Delta\theta^T\mathbf{T}_i^T \tag{41}$$

Since Δ_{zi} is a scalar, differentiation of equation (41) with respect to the transfer-matrix row produces an expression for the error gradient

$$\frac{\partial\varepsilon^2}{\partial\mathbf{T}_i} = -2(\Delta z_i - \mathbf{T}_i\Delta\theta)\Delta\theta^T \tag{42}$$

Substituting equation (42) into equation (37) and substituting $\mathbf{T}_i$ for x produces

$$\mathbf{T}_i(k+1) = \mathbf{T}_i(k) + 2k_i\left[\Delta z_i(k) - \mathbf{T}_i(k)\Delta\theta(k)\right]\Delta\theta(k)^T \tag{43}$$

$$(1 \times j) = (1 \times j) + (1)(1)\,[\,(1) - (1 \times j)(j \times 1)\,]\,(1 \times j)$$

which is a remarkably computationally efficient algorithm for recursive identification of $\mathbf{T}_i$. This can also be written in matrix form:

$$\mathbf{T}(k+1) = \mathbf{T}(k) + 2\mathbf{K}\left[\Delta z(k) - \mathbf{T}(k)\Delta\theta(k)\right]\Delta\theta^T(k) \tag{44}$$

$$(i \times j) = (i \times j) + (1)(i \times i)\,[\,(i \times 1) - (i \times j)(j \times 1)\,]\,(1 \times j)$$

in which $\mathbf{K}$ is a diagonal matrix of the corresponding k coefficients. Equation (44) is the LMS filter for system identification. It is like equation (33) of the Kalman filter, with the $[r]^{-1}\Delta\theta^T\mathbf{P}$ gains term replaced with $2\mathbf{K}\Delta\theta^T$. Unlike the usual Kalman filter simplifications that $\mathbf{M}$ and $\mathbf{Q}$ are diagonal matrices, $\mathbf{K}$ is diagonal from its derivation. Compared to the full Kalman filter equations, the LMS method is very elegant and computationally efficient. At the same time, however, it should also be noted that the simplicity of the LMS algorithm (compared to the Kalman filter) is achieved at the expense of not using any knowledge about the theoretical quality of the estimate. In fact, no apriori knowledge was required in the formulation. This makes the LMS filter more computationally robust than the Kalman filter, but does not take advantage of any good information describing the stochastic nature of the system, if available.

To analyze the convergence properties of the LMS filter, the expected value of equation (44) is taken as

$$E\left[\mathbf{T}(k+1)\right] = E\mathbf{T}(k) + 2\mathbf{K}E\left[\Delta z(k)\Delta\theta(k)^T\right] - 2\mathbf{K}E\mathbf{T}(k)\Delta\theta(k)\Delta\theta(k)^T \tag{45}$$

Then, by defining

$$E\left[\Delta z(k)\Delta\theta(k)^T\right] = \Phi_{\Delta z\Delta\theta} \tag{46}$$

$$E\left[\Delta z(k)\Delta\theta(k)^T\right] = \Phi_{\Delta\theta\Delta\theta} \tag{47}$$

equation (45) may be rewritten

$$E\left[\mathbf{T}(k+1)\right] = E\mathbf{T}(k) + 2\mathbf{K}\Phi_{\Delta z,\Delta\theta} - 2\mathbf{K}E\mathbf{T}(k)\Phi_{\Delta\theta,\Delta\theta} \tag{48}$$

$$E[\mathbf{T}(k+1)] = E\mathbf{T}(k)(I - 2\mathbf{K}\Phi_{\Delta\theta,\Delta\theta}) + 2\mathbf{K}\Phi_{\Delta z,\Delta\theta} \tag{49}$$

From equation (49) it can be seen that as long as the absolute values of the eigenvalues of $[I\text{-}2\mathbf{K}\Phi_{\Delta\theta,\Delta\theta}]$ are less than 1, the algorithm is stable. Thus, the theoretical stability range for the k_i gain elements is

$$0 < k_i < 1/\lambda_{max}$$

where λ_{max} is the largest eigenvalue of the control information matrix $\Phi_{\Delta\theta,\Delta\theta}$. Values of k_i near $1/\lambda_{max}$ will cause rapid adaptation, but will also be more prone to tracking random noise disturbances. Good values for the k_i are ones that result in convergence at a sufficiently rapid rate, yet do not track noise signals too closely.

Although the above analysis provides some insight into the selection of elements for **K**, it should be noted that $\Phi_{\Delta\theta,\Delta\theta}$ is unknown for the general case of closed-loop identification. In order to determine it, the control commands at all future time-steps would need to be known, which is, of course, only possible for open-loop control. Therefore, in closed-loop, the selection of terms for **K** is a matter of guessing. Nevertheless, this is a vast simplification over the Kalman filter method. Whereas the Kalman filter method required selection of r, **M**, and **Q**, only **K** is required to implement the LMS filter. This means the parameters in **K** can be adjusted without regard to the effect on other tuning parameters, making the tuning task much less difficult.

Further tuning ease could be gained by assuming that the diagonal elements of **K** (the k_i's) are all the same. This choice would make tuning very simple. However, the filter would become non-optimal since k_i would be limited by the largest eigenvalue of $\Phi_{\Delta\theta,\Delta\theta}$.

3.4 Generalized Kalman Filter Method

In this section, an extension of the classic Kalman filter is presented which is referred to as the generalized or multi-step Kalman filter method. This algorithm uses more than the most recent measurement (and control) so that less reliance is placed on user-supplied tuning information, which may be only poorly known.

In the derivation of the generalized Kalman filter method, it is assumed that the last n control command and measurement vectors are available in computer memory. As was done for the weighted-least-squares method, these controls and measurements are grouped into the Φ and **Z** block matrices defined by equations (8) and (9). Then for each row of the parameter matrix to be identified, $\mathbf{T}_i$ and each row in the measurement matrix, $\mathbf{Z}_i$, the process and measurement noises are defined in a manner directly analogous to that of the classic Kalman filter, as

$$E(\mathbf{Z}_i - \mathbf{T}_i\Theta) = 0 \tag{50}$$

$$E\left[(\mathbf{Z}_i - \mathbf{T}_i\Theta)^T(\mathbf{Z}_i - \mathbf{T}_i\Theta)\right] = \mathbf{R}_i \tag{51}$$

$$E(\mathbf{T}_i - \mathbf{T}_i^*) = 0 \tag{52}$$

$$E[(\mathbf{T}_i - \mathbf{T}_i^*)^T(\mathbf{T}_i - \mathbf{T}_i^*)] = \mathbf{M}_i \tag{53}$$

As for the classic version, these equations state that the means of the measurement and process noises are zero and that the covariance matrices are known. However, $\mathbf{R}_i$ is an $(n \times n)$ matrix to take into account n measurements in $\mathbf{Z}_i$ and n controls in Θ. The generalized Kalman filter estimate of $\mathbf{T}_i$ is defined as the one that minimizes the quadratic identification performance index J_{ID},

$$J_{ID} = (\mathbf{Z}_i - \mathbf{T}_i\Theta)\mathbf{R}_i^{-1}(\mathbf{Z}_i - \mathbf{T}_i\Theta)^T + (\mathbf{T}_i - \mathbf{T}_i^*\mathbf{M}_i^{-1}(\mathbf{T}_i - \mathbf{T}_i^*)^T \tag{54}$$

where $\mathbf{R}_i^{-1}$ and $\mathbf{M}_i^{-1}$ are the optimal weighting parameters. For a minimum of this performance index to exist, the partial derivative of J_{ID} with respect to the row estimate $\mathbf{T}_i$ must be zero. Applying this condition to equation (54) gives

$$0 = \mathbf{T}_i\Theta\mathbf{R}_i^{-1}\Theta^T - \mathbf{Z}_i\mathbf{R}_i^{-1}\Theta^T - \mathbf{T}_i^*\mathbf{M}_i^{-1} + \mathbf{T}_i\mathbf{M}_i^{-1} \tag{55}$$

From which it follows that

$$\begin{aligned}\mathbf{T}_i(\mathbf{M}_i^{-1} + \Theta\mathbf{R}_i^{-1}\Theta^T) &= \mathbf{T}_i^*\mathbf{M}_i^{-1} + \mathbf{Z}_i\mathbf{R}_i^{-1}\Theta^T \\ \mathbf{T}_i(\mathbf{M}_i^{-1} + \Theta\mathbf{R}_i^{-1}\Theta^T) &= \mathbf{T}_i^*(\mathbf{M}_i^{-1} + \Theta\mathbf{R}_i^{-1}\Theta^T) \\ &\quad +(\mathbf{Z}_i - \mathbf{T}_i^*\Theta)\mathbf{R}_i^{-1}\Theta^T\end{aligned} \tag{56}$$

$$\mathbf{T}_i = \mathbf{T}_i^* + (\mathbf{Z}_i - \mathbf{T}_i^*\Theta)\mathbf{R}_i^{-1}\Theta^T\mathbf{P}_i \tag{57}$$

$$(1 \times j) = (1 \times j) + [\,(1 \times n) - (1 \times j)(j \times n)]\,[n \times n]\,(n \times j)(j \times j)$$

where $\mathbf{P}_i$ is defined as

$$\mathbf{P}_i = (\mathbf{M}_i^{-1} + \Theta\mathbf{R}_i^{-1}\Theta^T)^{-1} \tag{58}$$

$$(j \times j) = [(j \times j) + (j \times n)(n \times n)(n \times j)\,]^{-1}$$

Equations (57) and (58) define the generalized Kalman filter equations to be computed for each row of the transfer matrix. To place these in a convenient matrix formulation requires the assumption that the $\mathbf{R}_i$ and $\mathbf{M}_i$ matrices are the same for all rows of the transfer matrix. These are the same assumptions made for tuning the classic Kalman filter. Though they may not be valid,

they are necessary to make the tuning problem tractable. In matrix form, the equations for the generalized Kalman filter are

$$\mathbf{T} = \mathbf{T}^* + (\mathbf{Z} - \mathbf{T}^* \Theta)\mathbf{R}^{-1}\Theta^T\mathbf{P} \tag{59}$$

$$(i \times j) = (i \times j) + [\,(i \times n) - (i \times j)(j \times n)\,]\,(n \times n)\,(n \times j)(j \times j)$$

$$\mathbf{P} = (\mathbf{M}^{-1} + \Theta\mathbf{R}^{-1}\Theta^T)^{-1} \tag{60}$$

$$(j \times j) = [(j \times j) + (j \times n)\,(n \times n)\,(n \times j)\,]^{-1}$$

where $\mathbf{R}$ and $\mathbf{M}$ are specified to be diagonal matrices having their respective diagonal terms equal (i.e., $\mathbf{R} = rI_n$; $\mathbf{M} = mI_j$; where r and m are scalars). These equations bear strong resemblance to the ordinary Kalman filter, but are fewer in number and do not recursively propagate the covariance matrix. Unlike the ordinary Kalman filter method, the matrix inversion lemma is not used in the derivation of the generalized version, because $\mathbf{R}$ is no longer a scalar.

Comparing equation (59) with equation (44), it is seen that the generalized Kalman filter is computationally similar to the LMS algorithm. Whereas the LMS algorithm uses a gain based on $\Delta\theta^T$ and $\mathbf{K}$, the generalized Kalman filter bases the gain on $\mathbf{R}$, $\mathbf{M}$, and Θ^T. From equations (59) and (60), it is also seen that if $\mathbf{R}$ is chosen large, $\mathbf{R}^{-1}$ will be small to make the identification update rate slow. If $\mathbf{R}$ is chosen very large ($\mathbf{R}^{-1}$ very small), then an appropriately sized $\mathbf{M}^{-1}$ matrix is required to prevent singularity in the calculation of $\mathbf{P}$ (eq. (60)). It can also be noted that if $\mathbf{M}^{-1}$ were very small, then the update gains would be essentially proportional only to Θ.

The multi-step approach of the generalized Kalman filter makes it less computationally efficient. However, by possessing a "memory" of the n preceding measurements, the filter can theoretically obtain improved accuracy and better noise rejection properties, even though using less user-supplied tuning information.

3.5 Generalized Least-Mean-Squares Filter Method

Analogous to the generalization done for the Kalman filter, the generalized least-mean-squares (LMS) filter method extends the classic LMS method to allow the identification to be based on more than the most recent measurement and control input. The goal of the multi-step expansion is to obtain a filter having improved accuracy and better noise rejection properties.

The generalization of the classic LMS filter is done by grouping the most recent sequence of control and measurement vectors into the Θ and $\mathbf{Z}$ block matrices as defined by equations (8) and (9). As for the classic LMS method, the generalized version assumes that the update equation for transfer-matrix identification can be written in the steepest descent form of equation (37). The generalization of the LMS filter is done by expressing the error gradient in multi-step format as

$$\varepsilon_i = (\mathbf{Z}_i - \mathbf{T}_i\Theta) \tag{61}$$

$$(1 \times n) = (1 \times n) - (1 \times j)(j \times n)$$

Then, the weighted-mean-square error is expressed as

$$\varepsilon_i^2 = \varepsilon_i \mathbf{W} \varepsilon_i^T \tag{62}$$

$$\varepsilon_i^2 = (\mathbf{Z}_i - \mathbf{T}_i\Theta)\mathbf{W}(\mathbf{Z}_i - \mathbf{T}_i\Theta)^T \tag{63}$$

$$\varepsilon_i^2 = \mathbf{Z}_i\mathbf{W}\mathbf{Z}_i^T - \mathbf{Z}_i\mathbf{W}\Theta^T\mathbf{T}_i^T - \mathbf{T}_i\Theta\mathbf{W}\mathbf{Z}_i^T + \mathbf{T}_i\Theta\mathbf{W}\Theta^T\mathbf{T}_i^T \tag{64}$$

where **W** is a diagonal weighting matrix which can be used to place greater weight on the most recent measurements. The gradient of the square error with respect to $\mathbf{T}_i$ is then found from equation (64) as

$$\frac{\partial \varepsilon^2}{\partial \mathbf{T}_i} = -2(\mathbf{Z}_i - \mathbf{T}_i\Theta)\mathbf{W}\Theta^T \tag{65}$$

Substituting this expression into equation (37) and substituting $\mathbf{T}_i$ for **x** produces

$$\mathbf{T}_i(k+1) = \mathbf{T}_i(k) + 2k_i\left[Z_i(k) - \mathbf{T}_i(k)\Theta(k)\right]\Theta(k)^T \tag{66}$$

$$(1 \times j) = (1 \times j) + (1)(1)\,[\,(1 \times n) - (1 \times j)(j \times n)\,]\,(n \times n)\,(n \times j)$$

or in matrix form

$$\mathbf{T}(k+1) = \mathbf{T}(k) + 2\mathbf{K}\left[Z(k) - \mathbf{T}(k)\Theta(k)\right]\Theta(k)^T \tag{67}$$

$$(i \times j) = (i \times j) + (1)(i \times i)\,[\,(i \times n) - (i \times j)(j \times n)\,]\,(n \times n)\,(n \times j)$$

Since the structure of the identification equations in equation (67) is the same as that of the classic LMS filter, for a multi-step batch size of 1, the classic and generalized LMS filters are the same. Therefore, the considerations governing the selection of **K** for stability and convergence are the same as those presented for the classic LMS algorithm.

4. COMPUTATIONAL EFFICIENCY

The computational burden of each method was analyzed by calculating the number of additions, subtractions, multiplications, and inverse operations required by each method to identify a transfer matrix of dimension (6 x 6). This information is presented in table 1, along with the time required to implement each operation.

TABLE 1. Comparison of operations required to identify a (6 x 6) transfer matrix.

Type of operation	Computation time* msec n = 1 (6, 18)	WLSE	Kalman filter	LMS filter	Generalized Kalman filter	Generalized LMS filter
Scalar add	1		1			
Scalar inverse	2		1			
(6 x 1)(1 x 1)	6		2			
(6 x 6) ± (6 x 6)	33		3	1	2	1
(6 x 1) - (6 x 1)	7		1	1		
(6 x n) - (6 x n)	7 (33, 91)				1	1
(1 x 6)(6 x 1)	5		1			
(6 x 1)(1 x 6)	10		2	1		
(6 x 6)(6 x 1)	4		2	1		
(6 x 6)(6 x 6)	20	1	2	1	1	1
(6 x 6)(6 x n)	4 (20, 60)				1	1
(6 x n)(n x 6)	10 (20, 42)	2			2	1
(n x n)(n x 6)	6 (20, 112)	1				
(6 x n)(n x n)	6 (20, 118)				2	1
Inverse (6 x 6)	170	1			1	

*Approximate computation times are based on IBM 386 architecture with a WE DSP32C processing board run at 50 MHz.

The time needed for each operation, of course, is dependent on the type of computer and programming language used to implement the on-line identification. The types of machines available range from personal computer lap-top configurations to dedicated array processor systems having several microprocessors and several data paths to facilitate high-speed, pipe-lined operations (see ref. 26 for further details). To be conservative, the author has decided to calculate the computation time based on a personal computer hosting a WE DSP32C processing board running at 50 MHz.

Figure 4 presents a graphical comparison of the computation times for each of the identification methods. Here it is seen that the generalized LMS (GLMS) algorithm using a batch size of 6 was still faster than the classic Kalman filter. The generalized Kalman filter (GKF) and weighted-least-squares-error (WLSE) methods were the slowest. Their computation times,

however, are still sufficiently fast compared to the average helicopter rotor-revolution period of 150 to 200 msec. Therefore, the desire to update the transfer-matrix parameters as often as once every rotor revolution certainly does not eliminate any of the algorithms on the basis of computational speed.

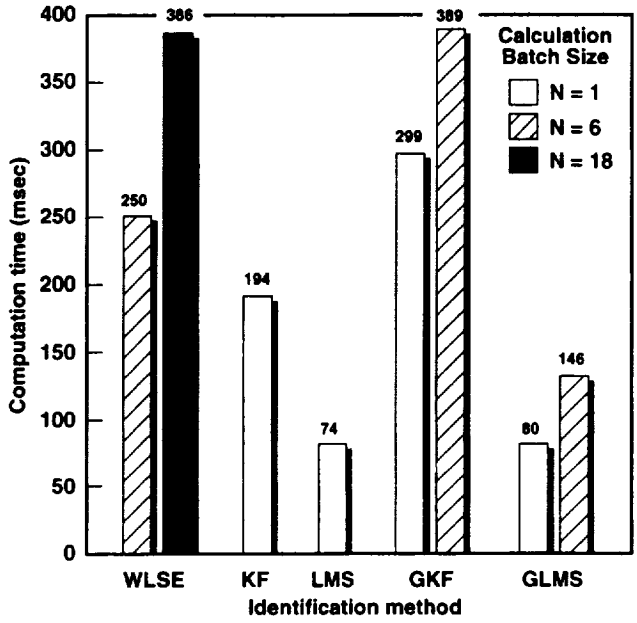

Figure 4. Comparison of identification algorithm computation times based on IBM 386 architecture with a WE DSP32C processing board running at 50 MHz.

5. SIMULATION PROGRAM

Identification performance was evaluated by modeling the rotorcraft as a quasi-steady, linear system, in which the harmonics of vibration were related to the harmonics of blade-pitch control by a linear transfer matrix. Though this type of modeling could not predict helicopter vibration in units of g's, the purpose of simulating the system-identification algorithms was fully achieved.

A comprehensive helicopter dynamics analysis code for modeling the complexities of the helicopter aerodynamic environment and airframe/rotor dynamics was not used to evaluate the performance of the system-identification methods. The reason was that it was doubtful that a sufficiently accurate wake model could be found to represent the high-frequency air loads and resulting fuselage vibrations. In fact, the development of such a code would have been a more formidable research problem than the original task of simulating the identification algorithms. Therefore, for the limited purposes of this study, it was simply more efficient to generate the helicopter transfer matrix artificially, using some ordinary matrix algebra. This simplification allowed the performance of the identification algorithms to be evaluated quickly. The limitation of this simplified approach, however, was that with the approach it was not possible to study the influence of the helicopter dynamics on the identification performance.

The simulation program consisted of three basic parts: (1) generation of the transfer-matrix model and uncontrolled vibration (response metric), (2) computation of the control command, and (3) simulation of the system-identification code (fig. 5). Coupling the identification and controller formed an adaptive regulator for vibration control. The function of the controller was to either excite the system dynamics for open-loop identification or to minimize the rotorcraft vibration to permit study of closed-loop system identification. The transfer-matrix model was used to generate the N/rev vibration coefficients as the sum of the uncontrolled vibration, the measurement noise, and the vibration induced from the application of the HHC commands. Using the HHC inputs and the plant-generated vibration outputs, the identification code was able to simulate the system-identification methods. Many types of system-identification problems—for example, singularity of the control covariance matrix, low signal-to-noise ratio, high measurement noise, high process noise (unmodeled dynamics), and error in the tuning parameters—could be modeled using this simulation.

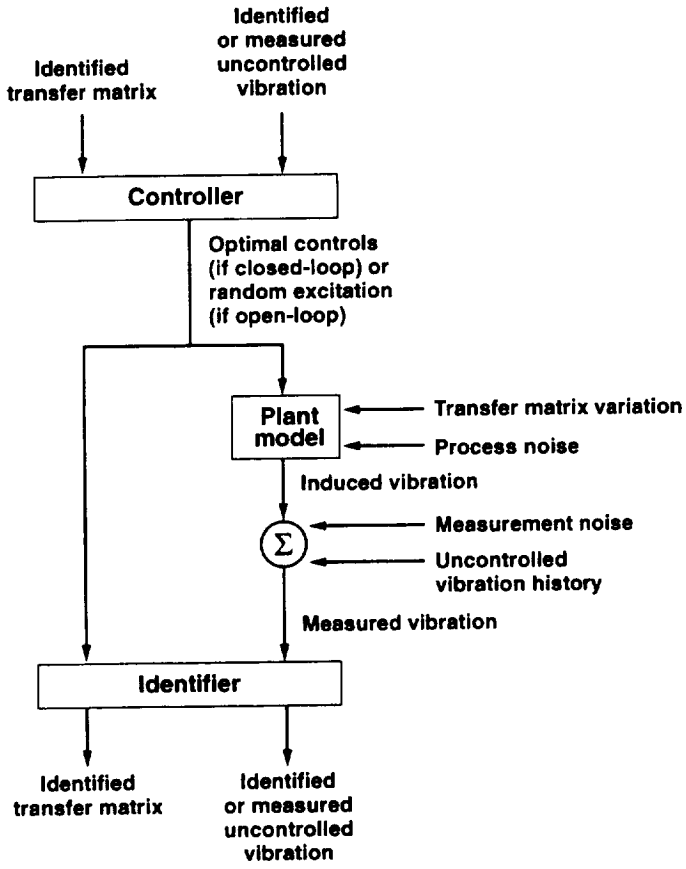

Figure 5. Outline of simulation program.

5.1 Transfer-Matrix Modeling

A transfer matrix was used to translate changes in the input HHC control vector θ to changes in the response measurement z. The transfer matrix had six columns, corresponding to six control inputs, and from 1 to 12 rows, depending on the number of outputs being simulated. For example,

this size transfer matrix would be needed between a (6 x 1) input control vector (composed of the sine and cosine coefficients of collective, lateral, and longitudinal 4/rev swashplate excitation) and the response vector composed of 2 -12 sine and cosine coefficients of measured vibration. The simulation program could change all the elements of the transfer matrix **T** in order to study the ability of system-identification methods to track changes in the transfer matrix. The propagation of the transfer matrix with simulation step (k) was programmed as

$$\mathbf{T}(k) = \mathbf{T_0}(k) + G_1\left[-1^{(i+j)}\right]\sin(\Omega_T k) + \mathbf{T_N}(k) \tag{68}$$

$$\text{with } T_0(k) = T_A \text{ for k 100th step} \tag{69}$$

With this representation, the transfer-matrix elements could be held constant, varied continuously, varied randomly, or changed in a step-wise manner.

The initial value of the transfer matrix, $\mathbf{T}_0$, was composed of randomly selected numbers between 0 and 1. Such a matrix would generally be representative of a well-scaled actual helicopter transfer matrix. By choosing the transfer-matrix values as random numbers between -1.0 and 1.0, a process-noise matrix ($\mathbf{T}_N$) of 10% could therefore be defined as a matrix of random numbers between 0.1 and -0.1.

After simulation step 100, the $\mathbf{T}_0$ matrix was allowed to remain constant or to change in a prescribed manner. Most identification performance was evaluated for the condition of a single-step change in the matrix at simulation step 100. Physically, this type of change might be encountered when taking the helicopter rapidly from one constant flight speed to another. This type of single-step change in the transfer matrix represented the easiest identification task to analyze. The identification process would either succeed in re-identifying the new transfer matrix, display convergence or stability problems, or simply be nonadaptive. For some simulation runs, the transfer matrix was varied continuously after step 100. These variations are described in section 7.1.

5.2 Vibration Generation

As mentioned in section 2, the harmonics of the measurement vector to be reduced consisted of the sine and cosine coefficient harmonics of the vibration. This vector, denoted as z, was computed for simulation step k as

$$z(k+1) = [\mathbf{T}(k)]\theta(k+1) + z_0(k+1) + z_N(k+1) \tag{70}$$

where $\mathbf{T}(k)$ represented the transfer matrix at step k, θ was the control vector, z_0 was the uncontrolled vibration, and z_N represented the measurement noise. The z_0 and z_N quantities could be zero, held constant, made random, or given some other prescribed variation. In most of the simulated conditions, z_0 was held constant to indicate a steady flight condition. Identification was always first studied for the ideal case of no measurement noise (z_N = null vector). For the simulation cases showing good identification performance under ideal conditions, the simulations

were repeated with various amounts of measurement noise. By changing z_N, the signal-to-noise ratio (i.e., z/z_N) could be adjusted.

5.3 Controller Simulation

The controller generated the (6 x 1) θ-vector, representing the harmonics of the blade-pitch control motion. For the case of open-loop identification, the controller generated random controls to excite the plant dynamics. For the case of identification during closed-loop vibration control, the controls were computed using a one-step deterministic control law of the type described in reference 14. This controller sought to minimize the value of a quadratic performance index, J_C,

$$J_C = z^T(k)\mathbf{W}_z z(k) + \theta^T(k)\mathbf{W}_\theta \theta(k) + \Delta\theta^T(k)\mathbf{W}_{\Delta\theta}\Delta\theta(k) \tag{71}$$

where $\mathbf{W}_z$, $\mathbf{W}_\theta$, and $\mathbf{W}_{\Delta\theta}$ were defined as diagonal, positive definite matrices specifying the relative weighting given toward minimizing the vibration, blade-pitch control amplitude, and blade-pitch control rate, respectively. By substituting the identities

$$z(k) = \mathbf{T}[\theta(k) - \theta(k-1)] + z(k-1) \tag{72}$$

$$\Delta\theta(k) = \theta(k) - \theta(k-1) \tag{73}$$

in equation (71), and then setting the partial derivative of J_C with respect to θ equal to zero, the deterministic control laws were produced. For the case of global transfer-matrix model representation, the deterministic control law was given by

$$\theta(k) = D\left[\mathbf{W}_{\Delta\theta}\theta(k-1) - \mathbf{T}^T\mathbf{W}_z z_0\right] \tag{74}$$

and for the local model by

$$\theta(k) = D(\mathbf{T}^T\mathbf{W}_z\mathbf{T} + \mathbf{W}_{\Delta\theta})\theta(k-1) - D(\mathbf{T}^T\mathbf{W}_z)z(k-1) \tag{75}$$

where for both cases

$$D = (\mathbf{T}^T\mathbf{W}_z\mathbf{T} + \mathbf{W}_{\Delta\theta} + \mathbf{W}_\theta)^{-1} \tag{76}$$

Note that when using the global model, the identified uncontrolled vibration was used, whereas when using the local model, the measured vibration was used.

For closed-loop identification, the controller was usually tuned to balance the trade-off between minimizing vibration, control rate, and absolute control by specifying the weighting matrix diagonal values to be $\mathbf{W}_z = 1.0$, $\mathbf{W}_{\Delta\theta} = 0.05$, and $\mathbf{W}_\theta = 0.0$. These weightings were found by trial

and error to produce good controller performance. With these settings, the controller would generally converge rapidly to the proper vibration control setting without manifesting unstable behavior. On the basis of results not presented herein, it was found that varying the weighting on $\mathbf{W}_{\Delta\theta}$ and $\mathbf{W}_{\theta}$ from 0 to 0.20 did not change the basic vibration control or identification convergence pattern significantly. Values of $\mathbf{W}_{\Delta\theta}$ and $\mathbf{W}_{\theta}$ from 0.20 to 0.50 were found to provide too much damping on the control action and to cause poor controller performance, though they did not generally affect identification performance.

5.4 Identification Algorithms

The system-identification equations presented in section 3 were used to form the identifier modules which derived an estimate of the transfer matrix $\mathbf{T}_{ID}$ at each step of the simulation. Identification performance was then measured by the error between the true plant transfer matrix and the identified transfer matrix. Since the system transfer matrix could range in dimension from (1×6) to (12×6), it was necessary to create an identification performance comparison index. The index chosen was the sum of the absolute value of the identification errors for all elements of the matrix divided by the number of elements N_T in the matrix,

$$J_{ID} = \frac{\sum_{i=1}^{I=12} \sum_{j=1}^{6} |\mathbf{T}_{ID}(i,j) - \mathbf{T}(i,j)|}{N_T} \tag{77}$$

This index made possible a graphical presentation of the identification error as a function of the simulation step. However, it masked the variation of the individual matrix elements and also obscured some details of the identification process. A subtle point of this index is that it is necessary to recognize that a $J_{ID} = 0.25$ implies a 50% identification error in the transfer-matrix elements. The reason for this is that with the elements of $\mathbf{T}$ chosen as random numbers between -1 and +1, random errors in $\mathbf{T}$ ranging between -0.5 and 0.5 would have an absolute value range of 0.0 to 0.5, with the average error being 0.25.

6. OPEN-LOOP IDENTIFICATION OF THE LOCAL MODEL

Open-loop identification of the local transfer-matrix model was studied by having the controller generate random input commands to excite the system dynamics. This represented the ideal case for system identification, because the level of excitation did not diminish as the simulation progressed. Identification performance with and without measurement noise was compared for all of the identification methods. For all cases presented below, the initial estimate of the transfer matrix was specified without any starting error.

After simulation step 100, the system transfer matrix was changed to a new matrix in order to determine how fast each identification method could re-identify the new transfer matrix. The transfer matrix used after step 100 was generated as the sum of the first transfer matrix plus a matrix of random numbers between -0.5 and +0.5. Since the original transfer matrix was composed

of numbers between -1.0 and +1.0, this was a change of about 50% from the original transfer matrix. The transfer matrices before and after the change at simulation step 100 are presented in table 2.

TABLE 2. Comparison (6 x 6) transfer matrix before and after simulation step 100.

Before step 100							After step 100					
−1.00	0.67	−0.64	0.02	0.12	0.00	→	−0.75	1.17	−0.40	−0.35	−0.18	−0.20
−1.00	0.26	0.70	0.14	0.70	−0.57		−0.82	0.13	0.33	0.48	0.41	−0.34
−0.78	−0.26	−0.29	0.22	0.61	0.39		−1.01	−0.53	−0.66	−0.15	0.59	0.86
0.53	−0.60	−0.33	0.09	0.98	0.83		0.38	−0.46	−0.07	0.37	0.68	0.43
−0.64	−0.93	−0.88	−0.39	−0.33	0.70		−0.91	−0.60	−0.51	−0.42	−0.56	1.02
0.81	0.97	0.37	−0.94	0.23	0.75		0.67	1.34	0.16	−0.49	−0.19	0.70

Identification performance was then judged by the amount of identification error remaining after simulation step 100. Without identification, the identification error remaining after step 100 would be constant (fig. 6). (The shading in fig. 6 under the identification error is only for visual effect and has no special significance.) Identification plots resembling that of figure 6 would therefore be indicative of little or no identification improvement. With good identification, the identification error would be brought back to zero.

Note. The simulation results presented in figures 6–99 appear at the end of the report.

6.1 Open-Loop Weighted-Least-Squares-Error Simulation

Least-squares identification was studied using a (6 x 6) transfer matrix. A minimum batch size of n = 6 was therefore required for the least-squares identification. Figure 7 shows that for a batch size of 6, no measurement noise, and **W** set equal to a (6 x 6) identity matrix, the identification of the new transfer matrix occurred within six steps after the change in **T** at simulation step 100. However, with 10% measurement noise, the identification process became very erratic (fig. 8(a)). Some of the identification-error peaks went substantially beyond the plot border. Figure 8(b) shows that by increasing the batch size to 8, the peaks of high identification error were attenuated. As the batch size was made larger still, the identification error was further reduced. Figure 8 shows the identification error using batch sizes of 10 (fig. 8(c)), 12 (fig. 8(d)), and 24 (fig. 8(e)). The steady-state identification error was clearly lowest for batch size 24 (fig. 8(e)), the batch size that also required the longest computation time. Since each measurement had some measurement error, the only way to lower the identification error to zero would have been to use an infinitely large batch size. Figures 9(a) and 9(b) show that the effect of higher measurement noise was to raise the steady-state identification error.

The effect of using exponential weighting was to increase the rate of convergence. Figure 10 shows the identification error (for batch size 24) with γ set equal to 1.0 (i.e., no relative weighting, fig. 10(a)); to 0.9 (fig. 10(b)); to 0.8 (fig. 10(c)); and to 0.7 (fig. 10(d)). Although there was an improvement in the identification convergence speed after the disturbance at simulation step 100,

the steady-state identification error was higher. It was concluded that a batch size of about 12 with no exponential weighting was comparable to using a batch size of 24 with γ equal to 0.7. Considering that the computational burden increased by more than the square of the batch size (see eq. (15)), the choice of using a batch size of 12 with no exponential weighting is computationally preferable.

Figures 11(a) and 11(b) show that increasing the dimension of the transfer matrix from (6 x 6) to (12 x 6) had little effect on the identification performance. This was expected, since theoretically only the column dimension of **T** relative to the batch size is important. In practice, for good identification performance, the batch size must be about 1.5 to 2 times the column dimension of the transfer matrix. The number of rows in the transfer matrix did not influence the overall identification performance.

6.2 Open-Loop Kalman Filter Simulation

The ordinary Kalman filter was simulated for the same test condition as the weighted-least-squares-error (WLSE) method. As discussed in section 3, the Kalman filter required that starting estimates for the transfer matrix, $\mathbf{T}_0$, and for the r, **M**, and **Q** tuning parameters be selected. In actual application, a good starting estimate of $\mathbf{T}_0$ could be found using the least squares method. For the present investigation, the transfer-matrix estimate was initialized to the true transfer matrix for simplicity. (This assumption was later removed, as explained in sec. 6.6 below.) Ignoring (for the moment) the possibility of **P** going to zero, **Q** was set equal to zero to simplify the tuning task. In this way, tuning was reduced to the selection of two parameters, r and **M**.

In the first simulation runs, a parametric variation of r and **M** was studied for the case of no measurement noise. Figures 12-15 show results for various values of r and with the diagonal elements of **M** having values of 0.1, 1.0, 10.0, and 100.0. The results for r = 0.1 are shown in figure 12; for r = 1.0 in figure 13; for r = 10.0 in figure 14; and for r = 100.0 in figure 15. The results of these 16 cases displayed fairly similar behavior. In most cases, the identification error was reduced, though sometimes somewhat slowly. This indicated that precise specification of r and **M** was not very important. Table 3 presents the identification error at step 180 for each of the identification trials shown in figures 12–15. From this table, it was observed that runs made with the same **M**/r ratio had the same identification error. Table 4 shows that increasing the **M**/r ratio improved the identification performance until a ratio of about 1 or 10 was reached.

TABLE 3. Classic Kalman filter open-loop identification error at step 180 for no measurement noise.

	M			
r	**0.1**	**1.0**	**10.0**	**100.0**
0.1	0.1625	0.1614	0.1613	0.1613
1.0	0.1719	0.1625	0.1614	0.1613
10.0	0.2191	0.1719	0.1625	0.1614
100.0	0.2691	0.2191	0.1719	0.1625

TABLE 4. Classic Kalman filter open-loop identification error at step 180 as a function of the **M**/r ratio.

M/r	**Identification error at step 180**
0.001	0.2691
0.01	0.2191
0.1	0.1719
1	0.1625
10	0.1614
100	0.1613
1,000	0.1613
1,000,000	0.1611

The identification performance of the Kalman filter did not appear to be as good as that of the least-squares method. Further investigation determined that the identification was poorer because the **P** matrix was approaching zero as the simulation progressed. By raising the value of the **Q** matrix from zero, considerable identification improvement was obtained. (Recall that **Q** serves to keep **P** from ever going to zero.) Using $\mathbf{M} = 10.0 * \mathbf{I}_6$ and r = 1.0, even the smallest value of **Q** simulated (0.01) improved the identification convergence time (fig. 16). As **Q** was made larger, the identification error continued to be further reduced, until a value for the **Q** diagonal elements of about 10 was reached. For values of **Q** higher than 10, the identification performance was not further improved.

The identification performance of the open-loop Kalman filter with 10% measurement noise was evaluated using the filter tuning $\mathbf{M} = 10.0 * \mathbf{I}_6$, r = 1.0, and $\mathbf{Q} = 10.0 * \mathbf{I}_6$. Figure 17(a) shows that the addition of measurement noise had an effect similar to the that seen for weighted least squares, and that the convergence to the steady-state error after the disturbance at simulation step 100 was fairly fast. In fact, it was just as good as the least-squares approach. Figure 17(b) shows that setting $\mathbf{M} = 1.0 * \mathbf{I}_6$ and r = 0.1 with **Q** left at 10.0 did not change the identification performance, because the **M**/r ratio remained the same.

6.3 Open-Loop Least-Mean-Squares Filter Simulation

Since the least-mean-squares (LMS) algorithm had only one tuning parameter, $\mathbf{K}_S$, tuning the filter required no strategy like the kind used to tune the Kalman filter (e.g., keeping **Q** zero while adjusting the **M**/r ratio). Figure 18 shows the identification behavior with the $\mathbf{K}_S$ matrix diagonal elements varied from 0.001 to 0.5, for the case of no measurement noise. When $\mathbf{K}_S$ was very small, very little re-identification was observed after step 100 (fig. 18(a)). As $\mathbf{K}_S$ was made larger, the identification improved until $\mathbf{K}_S$ was made too large, and the identification process became unstable (fig. 18(e)). Figure 18(d) shows that the $\mathbf{K}_S$ diagonals equal to about 0.3 produced the best identification performance for the condition of no measurement noise.

The addition of 10% measurement noise raised the baseline level of identification error, but did not prevent convergence to the correct transfer matrix to within the bounds allowed by the measurement noise. As shown in figure 19, re-identification of the transfer matrix occurred within about 20 simulation steps.

6.4 Open-Loop Generalized Kalman Filter Simulation

The generalized Kalman filter required the specification of the $\mathbf{R} * \mathbf{I}_n$ and $\mathbf{M} * \mathbf{I}_6$ tuning matrices. Although specification of **Q** was not required, the calculation batch size n needed to be chosen. Of course, as the batch size was increased, so was the computation time.

In the simulations performed for the case of no measurement noise and a batch size n = 1, it was seen that the ratio of **M/R** was the primary factor governing identification performance. Figure 20 presents the identification error for several **M/R** ratios. For small values of **M/R**, virtually no identification took place after simulation step 100 (fig. 20(a)). As the **M/R** ratio was increased, the identification performance improved until the ratio approached a value of about 10 (fig. 20(d)). Because higher values did not continue to improve identification performance, an **M/R** ratio of 10 was judged to be good.

Using a value of 10 for the **M/R** ratio, the identification error was reduced much faster as the batch size was increased (fig. 21). Even a batch size of 2 made a noticeable improvement. A batch size of 8 increased the initial identification error slightly, but reduced the identification error convergence time greatly. With a batch size of 1, identification convergence did not occur within 200 simulation steps (fig. 21(a)); whereas for a batch size of 8, only 13 simulation steps were required (fig. 21(d)). A batch size of about 4 seemed to provide the best compromise between minimizing the identification error produced at simulation step 100 and maximizing the identification convergence rate after step 100.

It was anticipated that this multi-step method would also improve identification for the case of 10% measurement noise. Although this proved to be true, re-tuning of the **M/R** ratio was required. Figure 22 shows that the identification performance did not improve as the batch size was made larger if an **M/R** ratio of 10 was used. Figure 23 shows the identification performance using a batch size of 4 with **M/R** ratios of 100, 10, 1, 0.1, and 0.01. These plots show that by decreasing the **M/R** ratio, the performance of the generalized Kalman filter was much improved. An **M/R** ratio of about 0.1 appeared to provide the best identification performance for a batch size of 4 and 10% measurement noise (fig. 23(d)). Smaller **M/R** ratios continued to decrease the steady-state error, but lengthened the convergence time.

6.5 Open-Loop Generalized Least-Mean-Squares Filter Simulation

Since the generalized and classic least-mean-squares (LMS) filters were the same algorithm for a batch size of 1, simulation of the generalized LMS method was done primarily using batch sizes greater than 1. Figure 24 shows that for the case of no measurement noise, increasing the batch size to 2 improved the identification convergence time slightly. Although not shown in figure 24, increasing the batch size to 4 with $\mathbf{K}_S = 0.3$ made the identification very unstable and quickly aborted the simulation program. Figure 25 shows that by decreasing $\mathbf{K}_S$, good identification

performance could be regained with a batch size of 4. Figure 25(a) shows that the identification error became very large after simulation step 130 for $\mathbf{K}_S = 0.2$. (Fig. 25(a) does not show the exact magnitude of the error, but any error greater than 1 is not good.) Figure 25(b) shows that excellent identification performance was obtained by decreasing $\mathbf{K}_S$ to 0.15. This value of $\mathbf{K}_S$ also produced stable identification for batch sizes of 6 and 8 for the case of no measurement noise (fig. 26).

When 10% measurement noise was introduced into the simulation, however, $\mathbf{K}_S$ needed to be made smaller to maintain identification stability. Figure 27(a) shows that for a multi-step batch size of 6 and $\mathbf{K}_S = 0.15$, the identification error tended to be large at times, and the convergence was unstable, as noted by the large spikes in the identification error near the end of the record. Figure 27(b) shows that good identification performance could be regained by decreasing $\mathbf{K}_S$ to 0.05. Figure 28 shows that further reduction in $\mathbf{K}_S$ allowed identification stability to be maintained as the multi-step batch size was made larger.

Figure 28 also shows that the steady-state identification error was made smaller by increasing the batch size. However, since larger batch sizes also required smaller values of $\mathbf{K}_S$ for stability, the identification convergence time was also increased. For example, in figure 28(e) it is shown that the identification error at the end of the run was the smallest, but the decay in the identification error after step 100 was the slowest. Overall, a $\mathbf{K}_S$ of 0.1 with a batch size of 4 seemed to provide the best compromise between identification convergence speed and steady-state identification accuracy (fig. 28(c)). A batch size of 1 with $\mathbf{K}_S = 0.3$ also produced good identification performance (fig. 28(a)).

6.6 Effect of Transfer-Matrix Initial Conditions

In the simulations described above, the initial estimate of the transfer matrix was initialized to the true system transfer matrix so that the identification could start with zero identification error. Of course, this was unimportant for the least-squares method, since its formulation did not rely on a current estimate of the transfer matrix to form a new estimate. The other methods, however, used a starting transfer-matrix estimate in their recursive formulations.

Figure 29 compares the identification error of the four recursive methods for the case of 10% measurement noise and starting from an initial $\mathbf{T}$ matrix of all 1's. The tuning values used for r, $\mathbf{R}$, $\mathbf{M}$, $\mathbf{Q}$, and $\mathbf{K}_S$ were the best values found for each method above. Each of the methods was seen to converge without difficulty after about 50 simulation steps. It was also observed that the generalized methods using a batch size of 4 or 6 were able to perform the initial identification more accurately. Since the identification of the true transfer matrix from a starting matrix of all 1's was sufficiently general, any filter initialized with an estimate of $\mathbf{T}$ found by the least-squares method should perform even better. Other simulation data (not presented here) showed that different values of r, $\mathbf{R}$, $\mathbf{M}$, $\mathbf{Q}$, and $\mathbf{K}_S$ did not change the basic conclusion that the initial conditions on the transfer matrix were relatively unimportant for open-loop identification purposes.

7. CLOSED-LOOP IDENTIFICATION OF THE LOCAL MODEL

It is generally believed that closed-loop and open-loop system identification are fundamentally the same, but they are not. During open-loop identification, random excitation of the system insures that the system output will always be large enough to produce a good signal-to-noise ratio. In closed-loop identification, however, the control commands are chosen to perform some useful purpose like controlling helicopter vibration as in the present application. As the controller reduces the vibration, the point may be reached where the noise begins to dominate the residual measured vibration signal. At the same time, as the controller approaches a steady-state optimal control solution, the control commands from one step to the next will not be very different since they are nearly optimal. In this situation, the small changes in the command signal are real, but the changes in the measured vibration are mostly a result of measurement noise. The system-identification algorithm may therefore erroneously attempt to identify a matrix relating the small changes in control to the random changes in the measurement signal. This matrix is, of course, the null matrix.

The results discussed in this section are for identification of the local-system model in closed-loop operation. Just as for the case of open-loop identification, simulation of closed-loop identification was initially studied by abruptly changing the transfer-matrix elements at simulation step 100. The new matrix was again formed by adding a matrix of random numbers between -0.5 and +0.5 (50% random noise) to the transfer matrix. This simulation studied how effectively the identification algorithms could accommodate a mild, one-time change in the system transfer matrix during closed-loop operation. After tuning each of the methods for the one-time change, the five identification algorithms were examined to see how well they could track a continuously changing system transfer matrix.

During the simulation, the performance of the closed-loop regulator was also studied. Because the controller used the identified transfer matrix to compute the vibration controls, the level of vibration suppression achieved also served as an indirect indicator of system-identification performance. However, several times the controller masked or made up for identification errors. Occasionally, it was observed that identified matrices having the same overall level of identification error did not always control vibration with equal effectiveness. Whereas one matrix might be identified well enough for use in a control law, the other might produce unstable behavior. A relevant analogy is two people lost in the wilderness who need to travel 8 miles west to find their desired destination. The person saying "Let's go one mile west" gives better advice than a person saying "Let's go one mile north." Even though both will be in error by about 7 miles, successive approximation will enable the one who knows to go west to find the destination after a number of iterations. In the same way, the identified system transfer matrices also point the way to minimize the system vibration, though not always in one step. Transfer matrices that allow the controller to iteratively suppress the vibration are the ones having the right relative proportion between the matrix elements. These matrices ultimately work much better for vibration control.

The performance of the vibration controller was calculated by comparing the levels of controlled versus uncontrolled vibration. This was possible in simulation, since both the uncontrolled and controlled vibration levels were always known. However, because plotting all of

the vibration channels versus simulation step would have presented a complex picture, a vibration index was defined as

$$J_{Z0} = \frac{\sum_{i=1}^{1-12} |Z_0(i)|}{1-12} \tag{78}$$

and

$$J_Z = \frac{\sum_{i=1}^{1-12} |Z(i)|}{1-12} \tag{79}$$

where J_{Z0} represented the uncontrolled vibration index, and J_Z represented the controlled vibration index. These scalar quantities could be easily plotted and compared, just like the index used to plot the mean identification error. By plotting these values along with the system identification error, it could be seen how the identification error influenced closed-loop control performance.

Figure 30 presents the identification error and vibration indices for the case of control without identification. The level of vibration for no control was chosen to be 1 for all six channels (hence the sum squares average was 1 also) and is indicated by the dashed line. The vibration reduction/increase with control applied is indicated by the cross-hatched area under the solid line. The cross-hatched shading was used to avoid confusion with the identification-error solid shading. Before simulation step 100, the uncontrolled vibration level was reduced very smoothly because the transfer matrix was initialized without error. In fact, the vibration would have gone to zero in one step had not a relaxation constant of 10% been used to slow the control action. The relaxation was used to improve controller stability. (Alternatively, values for $\mathbf{W}_\theta$ and $\mathbf{W}_{\Delta\theta}$ could have been selected as well, but using a relaxation constant was computationally more efficient because it replaces several matrix multiplications with a single vector-scalar multiplication, namely $\theta^* = k\theta$. See how equations (74)–(76) simplify with $\mathbf{W}_\theta$ and $\mathbf{W}_{\Delta\theta}$ removed.) After step 100, the transfer-matrix elements were given a step-change identical to the one given for the open-loop identification runs. As can be seen, the uncontrolled vibration level became very large as the controller diverged. The divergence occurred because the transfer matrix used by the controller was not updated after the change at simulation step 100. For this reason, the controller calculated control values that made the uncontrolled vibration worse rather than better.

7.1 Closed-Loop Weighted-Least-Squares-Error Identification: Local Model

Simulation of the closed-loop weighted-least-squares-error (WLSE) identification was done using a 6 x 6 local transfer-matrix model. A batch size of 8 with no exponential weighting was used, since that configuration showed good open-loop identification performance. However, the identification performance was unstable, even for the case of no measurement noise (fig. 31). In fact, after step 170, the identified transfer matrix became the null matrix. Surprisingly, the vibration control was very good. This warrants special discussion.

It seems paradoxical that the vibration could be so effectively controlled during periods when the transfer matrix was so poorly identified. The reason was that the controller found the optimal vibration-control input before the transfer matrix became corrupted. Shortly after the new transfer matrix was correctly identified at about step 110, the controller found the correct steady-state control settings to reduce the vibration. However, as the control-vector elements became nearly optimal, the changes to it became very small for successive simulation steps and the control-covariance matrix, $\Theta\mathbf{W}\Theta^T$ (see eq. (14)) became singular. When this happened, the least-squares identification method diverged. Yet, because the controller produced its control updates proportional to $\mathbf{Z}_{(k-1)}$ (see eq. (75)), and because $\mathbf{Z}_{(k-1)}$ was near zero, the controller did not change the control settings even though $\mathbf{T}$ was greatly in error. For this reason, good vibration-control performance was maintained even when the identified transfer matrix became inaccurately defined. Most likely, if the vibration amplitudes and phases had been changed abruptly at about step 170, the controller would have also diverged.

The key to improving the identification performance of the least-squares method is to prevent the control-covariance matrix, $\Theta\mathbf{W}\Theta^T$, from becoming singular. Two methods of achieving this were evaluated: (1) to skip the identification and moving-block sequence update whenever the vibration fell below a predefined level and (2) to add an open-loop perturbation component to the control vector.

Figure 32 shows the resulting identification and control performance for the same case as that shown in figure 31, except that a software switch was added to allow the identification code and moving-block process to be skipped whenever the vibration level was below an index of 0.05 (or 5% of the baseline uncontrolled vibration level). This seemed to work very well at first. However, skipping the identification cycle whenever the vibration level was below 0.05 did not work for the case of 10% measurement noise (fig. 33). Since the vibration level was always above 0.05, the software switch was rendered ineffective as a means of stabilizing the identification process. (Note that because the identification error was greater than 1, it exceeded the plot boundaries.) As shown in figure 34, increasing the switching value to 0.20 did not eliminate the problem. In fact, for that case, the 10% error in $\mathbf{Z}_{(k-1)}$ was evidently enough to diverge the controller solution, and both identification and controller performances were degraded. Also of note in figure 34 were the points of constant identification error near the 0.50 mark for periods when the identification routine was bypassed. Examination of the transfer matrix near the 0.50 mark revealed a matrix of zeros. This was the expected value of the transfer matrix relating smaller changes in the deterministic control solution to random measurement noise.

More simulation runs were conducted to refine the switching points for other amounts of measurement noise. Figures 35(a) and 35(b) show for 1% and 3% measurement noise that skipping the identification for a vibration threshold of 0.15 made the identification and controller performance very acceptable. At 5% measurement noise, the identification and vibration control were still fairly good, but were beginning to degrade (fig. 35(c)). For 7.5% measurement noise, the identification performance was seriously degraded (fig. 35(d)). As was already shown in figure 34, for 10% measurement noise, both identification and controller performance were poor. Therefore, as a means of improving identification, the method of skipping the identification code for vibration levels below a certain set point was not very effective.

The second method (of adding a perturbation signal to improve identification performance) was also found to be unsuccessful in improving the overall identification performance. For the case of 10% measurement noise, adding ±10% perturbation signal to the control vector did not improve the identification performance, but did make the controller performance better (fig. 36(a)). Figure 36(b) shows that increasing the amount of random perturbation to ±50 % made both identification and controller performance much worse.

However, increasing the batch size from 8 to 24 considerably improved both identification and controller performance for the 10% measurement-noise case (fig. 37). Figure 37(a) shows that fairly good identification performance was obtained using a batch size of 24, a zero-vibration definition of 0.20, and random forcing perturbation of 10%. The controller performance was also good. Figure 37(b) shows that reducing the zero-vibration definition to 0.10 degraded the identification accuracy, but did improve the controller performance a little. Figure 37(c) shows that decreasing the random forcing to 0.05 further increased the identification error.

Lastly, the effect of removing the zero-vibration definition and using only random perturbation to improve the identification performance was studied using a batch size of 18. Figure 38 shows the identification and controller performance for random forcing of 30% (fig. 38(a)), 60% (fig. 38(b)), and 100% (fig. 38(c)) of the baseline control. It can be seen that as the amount of random forcing was increased, the steady-state identification error was reduced, but the steady-state controller performance was severely degraded. Moreover, in comparing these figures with figure 37(a), it can be seen that removing the zero-vibration definition made the identification and controller performance worse overall, regardless of the amount of random forcing.

Since the least-squares method produced the lowest identification errors using a batch size of 24, a zero-vibration definition of 0.20, and a random forcing perturbation of 10%, that configuration was tested for identification of a continuously varied transfer matrix. In this test, sinusoidal variation of the transfer matrix from one matrix to another began after simulation step 100 and was conducted according to the following schedule.

Simulation Steps	System Transfer Matrix
0-100	$\mathbf{T} = \mathbf{T}_0$
101-300	$\mathbf{T} = \mathbf{T}_0 + 0.25 *(\mathbf{T}_{RANDOM})*\sin(k\,\pi/500)$
301-500	$\mathbf{T} = \mathbf{T}_0 - 0.50 *(\mathbf{T}_{RANDOM})*\sin(k\,\pi/500)$
501-700	$\mathbf{T} = \mathbf{T}_0 + 0.75 *(\mathbf{T}_{RANDOM})*\sin(k\,\pi/500)$
701-900	$\mathbf{T} = \mathbf{T}_0 - 1.00 *(\mathbf{T}_{RANDOM})*\sin(k\,\pi/500)$
901-1000	$\mathbf{T} = \mathbf{T}_0$

In the above schedule, $\mathbf{T}_{RANDOM}$ was a matrix of random numbers between -1 and +1. Therefore, the magnitudes of the disturbances were 25%, 50%, 75%, and 100% from the baseline transfer matrix. Note also that the sign of the disturbance changed every 200 simulation steps to make the identification problem more challenging. Figure 39 shows the identification-error index produced by this variation for the case of no system identification. It should be noted that although the

absolute value of the identification error is seen to have discontinuities of only 0.25 (or 25% of the baseline matrix)—because the sign of the disturbance changed every 200 simulation steps—the actual magnitude of the change was much larger. For example, note from the schedule above that at simulation step 301, the transfer matrix was actually disturbed by 0.75 [0.25 - (-0.5)]. Had the identification metric been able to show both positive and negative errors, the plot in figure 39 would have shown the second and fourth 1/4 cosine waves as being negative.

Figure 40 shows the identification error and vibration produced by the least-squares method using a batch size of 24. Although the vibration control was not too bad, the identification error was higher than in the case of no identification. Exponential weighting was also simulated, but this did not improve the identification performance. The poor identification performance probably resulted from skipping the identification cycle during times of low vibration, thereby allowing the transfer matrix to change too much between identification updates.

7.2 Closed-Loop Kalman Filter Identification: Local Model

Since the classic Kalman filter appeared to work best in open-loop for the tuning selection of r = 1, **M** = 10, (or any **M**/r ratio of 10) and **Q** = 10, this tuning was initially selected for the closed-loop simulations. Figure 41(a) presents the baseline case of no noise and with the same 50% step-change in the transfer-matrix values at simulation step 100 as was done previously for the closed-loop, weighted-least-squares simulation. The vibration was suppressed in one iteration at the start of the simulation, since the initial estimate of the identified transfer matrix had no error. After simulation step 100, the controller initially made the vibration worse than the uncontrolled state, but then quickly regained control after a few simulation steps. During this period, the Kalman filter began to slowly correct the identified transfer matrix, as seen by the decrease in the identification error beginning after simulation step 100 (fig. 41(a)). However, before the identification process progressed very far, the deterministic controller achieved a nearly zero controlled vibration level. As the vibration neared zero, the identification process was effectively shut down. Equation (33) shows that as the change in control and the change in vibration both approach zero, the identification updates become very small. Figure 41(b) shows that the introduction of a 10% probing signal to the control vector allowed the identification process to continue to reduce the identification error after simulation step 100.

The introduction of 10% measurement noise caused the identification process to become divergent (fig. 42). The divergence occurred because the Kalman filter was identifying the local transfer matrix relating the changes in (mostly) measurement noise to the small changes in deterministic control. Nevertheless, the vibration controller produced surprisingly good control considering the high amount of identification error. Once again, having successfully arrived very close to the optimal control setting, the deterministic controller did not make large changes to the control vector because the measured vibration was small. Thus, the vibration remained well controlled, even though the transfer-matrix identification error was large.

The identification divergence problem caused by the introduction of measurement noise was remedied in two ways. First, it was found that adding a 10% probing signal to the control input stabilized the identification process and eliminated almost all growth in the identification error

(fig. 43). The probing signal stabilized the identification process by increasing the signal-to-noise ratio. The vibration control, however, was made slightly worse than without probing.

The second method of stabilizing the identification process in the presence of measurement noise was to make adjustments in the r, **M**, and **Q** tuning parameters. After another parametric variation similar to that performed for the open-loop tuning, it was found that increasing the r/**M** ratio made the closed-loop Kalman filter identification more stable. Without measurement noise, setting r = 100 and $\mathbf{M} = \mathbf{I}_6$ seemed to almost halt the identification process. As shown in figure 44, the identification error after simulation step 100 looked very much like the plot for no identification. However, whereas the vibration could not be controlled at all for the case of no identification (fig. 30), the vibration control shown in figure 44 was excellent. Therefore, even though convergence to the correct transfer matrix after step 100 was very slight, because the vibration control was so effective, it was concluded that the Kalman filter made important changes to the identified transfer matrix which allowed the controller to successfully iterate to the optimal control. The identification scheme, though not converged, appeared to alter the ratio of the transfer-matrix elements so that the deterministic controller could iteratively step toward the optimal control. Once this optimal control was found, however, the identification process halted.

For the case of 10% measurement noise, the (r = 100, $\mathbf{M} = \mathbf{I}_6$) tuning produced an identification error that did not grow with 10% measurement noise, but instead was very constant after the disturbance at step 100 (fig. 45). The vibration control was also more stable compared with that shown in figure 43.

Figure 46(a) shows that the addition of 10% control probing did not lessen the identification errors by a noticeable amount. Figure 46(b) shows that a very slight reduction in identification error was achieved by simulation step 200 by using 30% control probing, but that the steady-state vibration control was much worse. For 100% and 200% control probing, figures 46(c) and 46(d), show that the identification error could be driven lower. However, in those cases, all vibration control was forgone in order to produce large enough perturbations in the control vector to yield better system identification.

The 100% control probing case was then repeated using the previous (r = 1, $\mathbf{M} = 10 * \mathbf{I}_6$) tuning which had produced the best system identification in open-loop. The measurement noise level was 10% as before. The identification error was reduced much faster than with the (r = 100, $\mathbf{M} = \mathbf{I}_6$) tuning (fig. 47). Comparing figures 47 and 46(c) it was observed that before the transfer-matrix change at step 100, figure 47 showed higher identification error than did figure 46(c). Yet after the change at step 100, figure 47 showed less identification error. The reason was that the tuning used for figure 47 effectively gave the Kalman filter a higher identification gain. So, although it was more adaptive in the sense of being better able to re-identify the new transfer matrix, it was also more sensitive to the spurious effects of measurement noise.

The classic Kalman filter identification performance was also tested for the case of continuous transfer-matrix variation (see sec. 7.1). With r = 1 and $\mathbf{M} = 10 * \mathbf{I}_6$, the identification error was higher than the baseline (no identification) case, but the vibration control was good (fig. 48(a)). On the other hand, with r =100 and $\mathbf{M} = \mathbf{I}_6$, the identification error was lower than the baseline, but the vibration control was not as good (fig. 48(b)). The latter tuning seemed to provide better

identification, but also made the control more erratic. The former tuning produced a higher Kalman filter identification "gain" (or $r^{-1}\Delta\theta^T\mathbf{P}$ of eq. (33); with $\mathbf{P}$ computed from eq. (32)), which apparently drove the identification process unstable.

7.3 Closed-Loop Least-Mean-Squares Filter Identification: Local Model

The diagonal elements of $\mathbf{K}_S$ were set equal to 0.30 for the LMS filter, since that tuning worked well in open-loop identification. For the ideal case of no measurement noise, the identification process was convergent after the transfer matrix was changed at simulation step 100 (fig. 49). However, the identification process was effectively turned off when the uncontrolled vibration became small. Similar to the Kalman filter, equation (44) shows that the identification updates become very small as the changes in the control vector, $\Delta\theta$, become small. The identification error continued to be reduced only until the vibration approached zero. When that occurred (at about step 130), the changes in the control vector became small, and the identification process stopped. For this reason, the identification error remained nearly constant after the vibration was reduced to zero.

The addition of 10% measurement noise produced little change in the LMS identification performance (fig. 50). Figure 51 shows the effect of changing the $\mathbf{K}_S$ gains for the case of 10% measurement noise. Figure 51(a) shows that reducing the gain to 0.1 produced slightly better identification performance. The higher identification error shown in figure 51(b) resulted from using too high a value for the $\mathbf{K}_S$ gain elements ($\mathbf{K}_S = 0.5 * \mathbf{I}_6$).

Figure 52 shows that the addition of 10% probing to the control vector (with $\mathbf{K}_S = 0.1* \mathbf{I}_6$) made the identification process slightly more convergent after step 100. Figure 53 shows that the identification convergence could be further improved by increasing the amount of random forcing to 100%. Although clearly too much for practical vibration control, this proved that the problem of slow convergence was the result of having a poor signal-to-noise ratio in closed-loop operation.

Lastly, identification performance for the case of continuous variation of the transfer matrix was evaluated (see sec. 7.1). Just as before, the measurement noise level was 10%. Compared with the baseline case having no identification (fig. 39), the overall identification error was reduced (fig. 54). The vibration controller using the identified transfer matrix was fairly good.

7.4 Closed-Loop Generalized Kalman Filter Identification: Local Model

Closed-loop identification of the local model using the generalized Kalman filter was initially simulated with $\mathbf{R} = 1$ and $\mathbf{M} = 10$ ($\mathbf{R} = \mathbf{I}_N$ and $\mathbf{M} = 10\ \mathbf{I}_6$), because that tuning worked well in open-loop identification. Using a batch size of 1 for the case of no measurement noise and no probing, the identification process stopped when the uncontrolled vibration approached zero (fig. 55(a)). In fact, after about 10 simulation steps, the identification error was seen to be almost constant. However, the addition of a 10% probing signal allowed convergence to a much lower identification error by the end of the simulation run at step 200 (fig. 55(b)).

With 10% measurement noise, the identification process became highly divergent (fig. 56). Interestingly, the vibration control remained very good. Figure 57 shows that increasing the multi-

step batch size helped delay the identification error growth, but did not prevent the identification error from becoming large by iteration 200.

Figure 58 shows that the unbounded increase in the identification error was halted by introduction of a 10% probing signal. This did not degrade the vibration control to a large extent. For a batch size of 1, the overall level of identification error was about the same as that found using the classic Kalman filter (fig. 58(a)). This was encouraging, because it meant that decoupling the recursive equations and reducing the number of tuning parameters (compared to the classic version) did not worsen the identification accuracy of the generalized Kalman filter. Increasing the multi-step batch size, however, did not improve identification performance until a batch size of 48 was used (fig. 58(f)). With that batch size, however, the algorithm was very slow. Since multi-step batch sizes of 4 (fig. 58(b)), 8 (fig. 58(c)), 12 (fig. 58(d)), and 24 (fig. 58(e)) actually produced greater identification error, a batch size of only 1 was determined to be the best choice. Evidently, the inaccuracies introduced by inversion of the (n x n) $\mathbf{R}$ matrix in equation (55) had a slightly negative trade-off with the additional information contained in the greater number of measurements as the batch size became larger. For a batch size of 48, the identification performance was improved somewhat, but at the expense of a much increased computation time.

In an effort to reduce identification errors with the multi-step Kalman filter, a technique termed "cycle averaging" was utilized. In this method, the actual control and vibration vectors were not used in the identification process. Instead, the average values of these quantities were computed and used. In effect, this averaging process helped attenuate the effects of measurement noise. Figure 59 shows the effect of averaging over 1, 4, 8, and 12 cycles while using a multi-step batch size of 1. Compared to the baseline case shown in figure 59(a), cycle averaging over 4 cycles substantially lowered the identification error (fig. 59(b)). Contrary to expectations, averaging over 8 and 12 cycles (figs. 59(c) and 59(d)) was not as effective as it was with 4 cycles. Figures 60 and 61 show that similar results were obtained using batch sizes of 4 and 8, respectively. For these batch sizes, averaging over 8 cycles produced the best identification.

Overall, the best identification with $\mathbf{R} = 1$ and $\mathbf{M} = 10 * \mathbf{I}_6$ was obtained using a batch size of 4 and 8-cycle averaging (fig. 62). For this case, the addition of 10% probing to the control produced lower identification errors, but made the steady-state vibration control slightly worse.

The identification performance using the alternative Kalman filter tuning of $\mathbf{R} = 100$ and $\mathbf{M} = 1 * \mathbf{I}_6$ was then tested for the same case of 10% measurement noise and a batch size of 4. Figure 63(a) shows that the addition of 10% probing made the identification slightly convergent after step 100 for the case of no cycle averaging. Figure 63(b) shows that averaging over 8 cycles made the identification worse. Therefore, with $\mathbf{R} = 100$ and $\mathbf{M} = \mathbf{I}_6$, the best results were obtained using a batch size of 4 without cycle averaging.

The identification results for the case of continuously varying the transfer matrix (see sec. 7.1) are shown in figure 64. Figure 64(a) presents the results for the $\mathbf{R} = 1$ and $\mathbf{M} = 10 * \mathbf{I}_6$ tuning with averaging over 8 cycles; figure 64(b) shows the results having $\mathbf{R} = 100$ and $\mathbf{M} = 1$ with no averaging. Though the identification and vibration control results were similar, the $\mathbf{R} = 1$ and $\mathbf{M} = 10 * \mathbf{I}_6$ tuning yielded lower identification errors and produced slightly better vibration

control throughout most of the simulation run. With this tuning, the identification error was kept at a fairly constant level, even though the disturbances became greater as the simulation progressed.

7.5 Closed-Loop Generalized Least-Mean-Squares Filter Identification: Local Model

The generalized LMS filter simulation was started with $\mathbf{K}_S = 0.3 * \mathbf{I}_6$ since that value worked well in open-loop simulation. Figure 65(a) shows that for no measurement noise, the identification process was convergent until about simulation step 130, from which point it did not decrease further. Figure 65(b) shows that by adding 10% probing, the identification error was further reduced, but not greatly.

The generalized LMS filter identification process was not destabilized by the addition of 10% measurement noise. Figure 66(a) shows that without probing, the 10% measurement noise did not cause the identification errors to grow large; however, the addition of 10% probing did not greatly improve the identification performance either (fig. 66(b)).

The effect of multi-step batch sizes was also simulated for the 10% measurement noise case. For batch sizes of 4 or greater, it was found necessary to reduce $\mathbf{K}_S$ to $0.1 * \mathbf{I}_6$ in order to maintain identification stability. Figure 67 shows the identification error and vibration control using multi-step batch sizes of 4, 8, and 12. A multi-step batch size of 8 produced the lowest identification errors. A batch size of 12 displayed unstable identification and control. However, other simulation results (not presented herein) showed that identification stability could be regained by reducing $\mathbf{K}_S$ further. Unfortunately, that reduction also slowed the identification process greatly, and thereby made the identification performance poor overall.

With a multi-step batch size of 8, figure 68 shows that adding 10% probing to the control signal for the case of 10% measurement noise lowered the identification error somewhat, compared to that shown in figure 67(b).

Lastly, the effect of cycle averaging, previously used with the generalized Kalman filter, was simulated for the case of 10% measurement noise. Figure 69 presents the identification error obtained for a multi-step batch size of 8 with averaging over 4, 8, and 12 cycles. These results showed that averaging over 4 cycles (fig. 68(a)) improved the identification stability. Averaging over 8 and 12 cycles did not help to further lower the identification error.

Since the generalized LMS filter was seen to work the best when a batch size of 8 and 4-cycle averaging was used, that configuration was also evaluated for identification of a continuously varied transfer matrix (see sec. 7.1). Using $\mathbf{K}_S = 0.1 * \mathbf{I}_6$, the identification was found to be very erratic. However, by reducing $\mathbf{K}_S$ to $0.01 * \mathbf{I}_6$, identification convergence was regained. The identification error was somewhat controlled, but grew larger as the simulation progressed (fig. 70). The vibration controller performance was also poor.

8. CLOSED-LOOP IDENTIFICATION OF THE GLOBAL MODEL

Thus far, all the simulation results presented were those obtained when using a local transfer-matrix model relating small changes in the control (cyclic pitch) vector to small changes in the measurement (vibration) vector. Whereas the local model assumes linearity only about a local operating point, the global model assumes global linearization about the identified uncontrolled vibration. (Recall that the uncontrolled vibration, z_0, is defined as the vibration level with the control vector elements all set to zero.) While global linearization might present certain problems for a highly nonlinear system, a possible advantage of the global model is that by using the identified uncontrolled vibration, the controller might work better. That is, by using an identified feedback variable, rather than a measured one, the effects of measurement-noise disturbances might be better rejected.

In the global-model formulation, the last column of the identified transfer matrix represents the uncontrolled vibration. For the (6 x 6) transfer matrix considered here, equation (6) becomes

$$\begin{bmatrix} z_1 \\ z_2 \\ \vdots \\ z_n \end{bmatrix} = \begin{bmatrix} \mathbf{T}_{11} & \cdots & \mathbf{T}_{16} & z_{01} \\ \mathbf{T}_{21} & \cdots & \mathbf{T}_{26} & z_{02} \\ \vdots & \vdots & \vdots & \vdots \\ \mathbf{T}_{n1} & \cdots & \mathbf{T}_{n6} & z_{0n} \end{bmatrix} \begin{bmatrix} \theta_1 \\ \vdots \\ \theta_6 \\ 1 \end{bmatrix} \tag{80}$$

In this equation, the new (7 x 1) control vector consists of a (6 x 1) control vector and "1" appended as the seventh element to add in the z_0 terms. Placed in this form, the model can be identified by using exactly the same equations developed for the local model ($\Delta z = \mathbf{T}\Delta\theta$) by substituting z for Δz and θ for $\Delta\theta$.

Presented below are some results obtained in simulation of the global-model identification and vibration control using feedback of the identified uncontrolled vibration.

8.1 Closed-Loop Weighted-Least-Squares-Error Identification: Global Model

Identification of the global model using the weighted-least-squares-error (WLSE) method was first simulated with a batch size of 12. Random changes to the input vector were made to excite the plant matrix. Figure 71 shows that even for the case of no measurement noise, the identification process was very erratic and produced high amounts of identification error. The vibration control was also noted to be poor.

As it did with the local model, skipping the identification cycle for vibration lower than 0.05 (of the nominal value = 1.0) resulted in a stabilization of both the control and identification processes (fig. 72). However, introduction of 10% measurement noise upset the performance greatly. Acceptable identification and controller performances were regained by skipping the identification cycle for vibration lower than 20% of the nominal value. Figures 73(a) and 73(b) present the identification and control performance for the case of 10% measurement noise with

identification-cycle skipping for vibration lower than 20% of the uncontrolled level for batch sizes of 12 and 24, respectively. The identification error obtained using a batch size of 24 was clearly much lower than that for a batch size of 12. The controller performance was very good using either batch size.

The batch-size-24 configuration with 10% probing and zero-vibration defined at 0.20 was also simulated for identification of a continuously varying transfer matrix previously described in section 7.1. Figure 74 shows that the identification error grew large after simulation step 300. Although not shown in that plot, the actual error was of the order of about 4 and was fairly constant. Even with that amount of error in the identified transfer matrix, the vibration control was remarkably good. This reflects favorably on the deterministic control law, since it was able to step to the optimal control input, even though the identified matrix was not very close to the actual plant model.

8.2 Closed-Loop Kalman Filter Identification: Global Model

Simulation results for the global model showed that just as for identification using the local model, the ratio of r to the **M** diagonal elements was the factor that most influenced closed-loop identification. The identification error and vibration control for the case of no noise and $\mathbf{M} = 1 * \mathbf{I}_6$, are shown in figure 75 for r values of 1, 10, and 100. The ($r = 100$, $\mathbf{M} = \mathbf{I}_6$) tuning provided the lowest identification errors (fig. 75(c)). The tuning ratio of $r = 1$ and $\mathbf{M} = 10 * \mathbf{I}_6$ was also tried, since those values sometimes worked well with the local model. However, that tuning destabilized the global-model identification entirely.

The addition of 10% measurement noise did not greatly affect the identification performance. Figure 76 shows the results obtained for $\mathbf{M} = \mathbf{I}_6$, and for r values of 1 (fig. 76(a)), 10 (fig. 76(b)), and 100 (fig. 76(c)). Just as for the no-noise case, $\mathbf{M} = \mathbf{I}_6$ and $r = 100$ provided the lowest identification errors and the best vibration control. Figure 77 shows that the addition of a 10% probing signal did not improve the identification performance beyond that of figure 76(c).

Identification performance for the case of continuously varying the transfer matrix (see sec. 7.1) was evaluated with $r = 100$, $\mathbf{M} = \mathbf{I}_6$, $\mathbf{Q} = 10 * \mathbf{I}_6$, and with 10% measurement noise (fig. 78). The sinusoidal bump in the identification error seen after step 500 indicated that the identified transfer matrix was unchanging, thereby allowing the sinusoidal variation in the system transfer matrix to show up in the identification error metric. The Kalman filter could not adapt the matrix during this time because the vibration was so well controlled. As already mentioned for the local model, the Kalman filter identification stopped as the change in control approached zero.

8.3 Closed-Loop Least-Mean-Squares Filter Identification: Global Model

Global model identification using the classic least-mean-squares (LMS) filter was initially begun using $\mathbf{K}_S = 0.3 * \mathbf{I}_6$, since that worked in both open-loop simulation and closed-loop simulation using the local model. However, even for the case of no measurement, that gain destabilized both the identification and control processes. Figure 79(a) shows that even $\mathbf{K}_S = 0.05 * \mathbf{I}_6$ produced unstable identification results. The result was oscillatory behavior of the controller. Figure 79(b) shows that by reducing $\mathbf{K}_S$ to $0.02 * \mathbf{I}_6$, the oscillatory nature of the controller was

eliminated. Although the identification error still exceeded the boundaries of the plot after simulation step 100, the stability of the controller indicated that the identification process was working better than before. Figure 79(c) shows that by further reducing $\mathbf{K}_S$ to 0.01 * $\mathbf{I}_6$, the performance of both identification and controller was much improved. Reducing $\mathbf{K}_S$ below 0.01 * $\mathbf{I}_6$, however, did not improve identification or control, because the identification response time was greatly slowed.

With $\mathbf{K}_S$ = 0.01 * $\mathbf{I}_6$, the introduction of 10% measurement noise did not noticeably affect the identification or controller performance (fig. 80). Of course, the measurement noise did prevent the vibration from being completely eliminated.

Figure 81 shows that slightly lower identification error could be obtained by introducing a control probing signal of 0.1 magnitude; since it also degraded the vibration suppression only slightly, however, its value was deemed to be of marginal importance.

Lastly, the identification error produced for the case of continuously varying the transfer matrix was evaluated. With $\mathbf{K}_S$ = 0.01, the identification error became very large after simulation step 400 (fig. 82(a)). The vibration control was also poor after that point. By reducing $\mathbf{K}_S$ to 0.001 * $\mathbf{I}_6$, the vibration was better reduced (fig. 82(b)). Although the identification error was still high, the transfer matrix was better identified for the purpose of control.

8.4 Closed-Loop Generalized Kalman Filter Identification: Global Model

With $\mathbf{R}$ = 100 and $\mathbf{M} = \mathbf{I}_6$, the generalized Kalman filter was found to be insensitive to batch size, cycle-averaging size, and control probing. Figure 83(a) shows the identification error and controller performance using a batch size of 1 for the case of no measurement noise. This performance was not greatly affected by the introduction of 10% measurement noise (fig. 83(b)). Figures 84(a) and 84(b) show that increasing the multi-step batch size to 4 and 8, respectively, did not change the identification performance noticeably from that found using a batch size of only 1 (fig. 84(b)). Figures 85(a) and 85(b) show that for a batch size of 4, using 4- and 8-cycle averaging also had little effect on the identification performance. Lastly, the addition of 10% control probing did not serve to lower the identification error (fig. 86). The behavior of the controller using the identified transfer matrix and uncontrolled vibration feedback appeared to work very well in each case.

Identification of a continuously varied transfer matrix of the type described in section 7.1 was then simulated with $\mathbf{R}$ = 100 and $\mathbf{M} = \mathbf{I}_6$, batch size = 1, no probing, and no cycle averaging. The resulting identification error and vibration control history are presented in figure 87. This shows that the controller worked well except after the step changes in the transfer matrix. The vibration was ultimately well controlled after each step, implying that the identification process was working. However, convergence to zero identification error was not achieved.

8.5 Closed-Loop Generalized Least-Mean-Squares Filter Identification: Global Model

The generalized LMS filter was simulated with $\mathbf{K}_s$ = 0.01 * $\mathbf{I}_6$, since that value worked well for the classic LMS filter. For the case of 10% measurement noise, figure 88 shows the identifi-

cation error and vibration control for a multi-step batch size of 4 and 4-cycle averaging. The identification performance did not change appreciably without cycle averaging. Reductions in $\mathbf{K}_S$ also had little effect. Figure 89 shows that the identification performance with batch size 4, 10% probing, $\mathbf{K}_S = 0.001 * \mathbf{I}_6$, and no cycle averaging was almost identical to that seen in figure 88.

Figure 90 shows the identification error found for the continuously varied transfer-matrix identification test of section 7.1. As before, the measurement noise was 10%, the batch size was 4, and $\mathbf{K}_S$ was set to $0.001 * \mathbf{I}_6$. The resulting vibration control was fairly good, indicating that the identification algorithm was working fairly well near the end of the simulation, even though the identification index was somewhat high.

9. SUMMARY AND COMPARISON OF THE IDENTIFICATION METHODS

In the preceding sections, the open-loop and closed-loop simulation results were presented for each of the five system-identification techniques. In this section, the best results for each method are compared so that relevant conclusions may be drawn. For simplicity, the matrix dimension of the diagonal matrices is assumed since all simulations presented before were for the case of a (6 x 6) transfer matrix. Hence, for example, $\mathbf{M} = 0.1$ is used rather than the more correct but longer $\mathbf{M} = 0.1 * \mathbf{I}_6$ notation.

9.1 Comparison of Open-Loop Identification

Figure 91 compares the overall best open-loop results obtained for each of the five identification methods. The identification performances shown in these cases are roughly equivalent. All plots show about the same level of identification error versus simulation step.

The weighted-least-squares-error (WLSE) approach using a batch size of 24 clearly produced the lowest identification error (fig. 91(a)). Moreover, the identification error might have been reduced slightly further using a batch size of 48. The fact that a batch size of 48 would have required significantly more computation time than batch sizes of 12 or 24 is unimportant for the open-loop identification case. It should also be remembered that absolutely no tuning was required by this method.

The other identification methods, although providing similar identification accuracy (relative to each other), required different amounts of tuning. The classic LMS filter required the least tuning, having only a single tuning parameter, $\mathbf{K}_S$. The tuning was very easy because it was known, from theory, that small enough values of $\mathbf{K}_S$ would always produce stable and convergent identification. The LMS filter was also computationally the fastest method. Although the Kalman filter was almost as fast computationally, finding the correct **M**/r ratio was more difficult. The multi-step methods were computationally more intensive, but by using multiple measurements, the multi-step methods yielded somewhat lower steady-state identification errors. For the same reason however, they showed slightly higher identification errors after the transient step change to the transfer matrix at simulation step 100.

For these reasons, the weighted-least-squares approach was judged to have the best open-loop identification performance. Of the recursive identification methods, the classic LMS filter was preferred for its computational efficiency and ease of tuning.

9.2 Comparison of Closed-Loop Local-Model Identification

Figure 92 presents the best identification performance obtained by each of the five methods in attempting to identify the local transfer-matrix model before and after a change in the system transfer matrix after simulation step 100. For comparison purposes, the identification error for no identification is presented in figure 92(a). Figure 92(b) shows the weighted ($\alpha = 1$, $\gamma = 1$) least-squares-error method using a batch size of 24 and zero vibration defined as being 0.20 of the baseline vibration. Figure 92(c) presents the identification error obtained using the classic Kalman filter with r = 100, $\mathbf{M} = 1$, $\mathbf{Q} = 10$, and with probing set at 10%. Figure 92(d) shows the LMS filter identification with $\mathbf{K}_S = 0.1$ and probing of 10%. Figure 92(e) shows results for the generalized Kalman filter with $\mathbf{R} = 1$, $\mathbf{M} = 10$, a batch size 4, a cycle-averaging size of 8, and 10% probing. Figure 92(f) shows the results for the generalized LMS filter with $\mathbf{K}_S = 0.1$, a batch size of 4, and a cycle-averaging size of 4.

In comparing the figures, it is seen that none of the methods succeed in totally eliminating the identification error. The weighted-least-squares method showed the most identification error after the transfer-matrix step change at simulation step 100 and also had the highest steady-state error (fig. 92(b)). Figures 92(c) and 92(d) show that the classic Kalman and LMS filter algorithms reduced the identification error slowly as the simulation progressed, with the LMS filter being slightly better. The generalized Kalman filter did the best job of reducing the identification error (fig. 92(e)) because it continued to reduce the error as the simulation progressed. All the methods used probing to assist the identification process. Without probing, the generalized methods reduced the identification error, but very slowly.

The corresponding closed-loop vibration control records are shown in figure 93. As expected, it is seen that the weighted-least-squares method, which showed the largest transient identification error at simulation step 100, also displayed the worst vibration control (fig. 93(b)). Remarkably, as the simulation progressed, it attained virtually the same level of vibration control as the other methods. Correlating the vibration reduction to the identification-error reduction in figure 92, it is seen that the identification error was not eliminated by any of the recursive methods, because the optimal control vector was found before the transfer matrix was fully identified. That is, using only a partially identified matrix, the deterministic control law was able to step to the optimum in a few steps. Once found, the control did not change, and the identification process virtually stopped. The generalized LMS and Kalman multi-step methods produced better vibration control during the transient change introduced at simulation step 100.

Therefore, it appears that for closed-loop identification using the local model, that the best methods were the LMS filter and the generalized Kalman filter. The LMS filter was computationally efficient and used a single tuning parameter, whereas the generalized Kalman filter offered somewhat improved identification accuracy. However, the difference in identification performance appeared to be relatively unimportant in terms of vibration control.

Figure 94 compares the local model, closed-loop identification error obtained for the case of continuous variation of the transfer matrix (see sec. 7.1). The baseline identification error without on-line identification is shown in figure 94(a). The performance of the least-squares method is shown in figure 94(b); of the Kalman filter in figure 94(c); of the LMS filter in figure 94(d); of the generalized Kalman filter in figure 94(e); and of the generalized LMS filter in figure 94(f). Each of the methods was tuned as before, with the exception of the generalized LMS method, which was tuned having $\mathbf{K}_S = 0.1$, a batch size of 8, and a cycle-averaging size of 4. The least-squares method clearly produced the largest identification errors. The identification errors of the remaining recursive methods were similar, though again the generalized Kalman filter was the best (fig. 94(e)). The generalized LMS filter identification error was higher near simulation step 1000.

Figure 95 shows the corresponding closed-loop vibration control for the same identification cases shown in figure 94. The vibration control was found to be similar for each of the methods except for the weighted-least-squares method (fig. 95(b)). The vibration control using this identification method was better than that of any of the recursive methods. The reason for this gain, however, might not be the identification performance per se; rather, the gain might be a result of the artificial bypassing of the identification process for vibration levels below the set threshold vibration limit. All of the recursive methods produced good vibration control near the middle of the simulation, but they became more erratic as the changes in the plant-matrix model were made larger near the end of the simulation. The multi-step methods appeared to offer no advantage over their more computationally efficient, single-step counterparts.

9.3 Comparison of Closed-Loop Global-Model Identification

The best global-model identification results that were achieved with each of the five methods are shown in figure 96 for the case of 10% measurement noise and a 50% change in the system transfer matrix at simulation step 100. Figure 96(a) shows the identification error resulting after step 100 without identification. Figure 96(b) shows the weighted-least-squares identification error obtained using a batch size of 24 and with "zero-vibration" defined as 0.20 of the nominal value. Figure 96(c) shows the identification error obtained using the classic Kalman filter with $r = 100$, $\mathbf{M} = 1$, $\mathbf{Q} = 10$, and with 10% probing of the control vector. Figure 96(d) shows the classic LMS filter identification results with $\mathbf{K}_S = 0.01$ and 10% probing. Figure 96(e) shows the identification error of the generalized Kalman filter with $\mathbf{R} = 100$, $\mathbf{M} = 10$, a batch size of 4, a cycle-averaging size of 8, and with 10% probing. Finally figure 96(f) shows the identification error for the generalized LMS filter with $\mathbf{K}_S = 0.01$ and with a multi-step batch size of only 1 and no cycle averaging.

Comparing the plots shown in figure 96 with those shown in figure 92, it is seen that with the global model, each of the identification methods produced lower identification errors than using the local model. Each method appeared to produce the same identification accuracy. Moreover, figure 97 shows that the vibration control was equally similar for each of the methods. Therefore, the classic LMS algorithm was in some respects the best algorithm to use because it required the fewest tuning parameters and was computationally the fastest method.

Figure 98 compares the identification error obtained with each of the five methods for the case of the continuously varied global-model transfer matrix (see sec. 7.1). Figure 98(a) shows the baseline identification error without on-line identification. The identification error of the weighted-

least-squares method is shown in figure 98(b); of the classic Kalman filter in figure 98(c); of the classic LMS filter in figure 98(d); of the generalized Kalman filter in figure 98(e); and of the generalized LMS filter in figure 98(f). The filters were all tuned as described above, except that the classic and generalized LMS filter identification gains $\mathbf{K}_S$ were reduced to 0.001 to improve their identification performance.

The plots in figure 98 (compared with those in fig. 94) show that the weighted-least-squares and the classic LMS filter methods produced higher identification errors using the global model (figs. 98(b), 98(d)) than when using the local model. The identification performance of the classic and generalized Kalman filters (figs. 98(c), 98(e)) were virtually identical. Since the generalized Kalman filter was implemented using few tuning parameters, it was judged superior to the classic version.

Figure 99 shows results similar to those for the local model; that is, the best vibration control, by far, was obtained using the weighted-least-squares-error method (fig. 99(b)). The vibration suppression obtained using this identification method was nearly perfect, displaying only a few small glitches of vibration. All of the recursive versions displayed erratic vibration control. Although vibration control was sometimes very good, the recursive methods generally failed to control vibration after the discontinuities in the transfer matrix were introduced using the global model. For these methods, vibration control using the local model was clearly better, especially during the first half of the simulation run when the system transfer matrix was varied slowly.

The superior vibration control (fig. 99(b)) using the weighted-least-squares method in moving block format with a batch size of 24 was a surprise, considering the apparently high identification error shown in figure 98(b). Although the transfer matrix was computed to be more in error according to the absolute value of each element in the identified transfer matrix compared to its true value, it obviously worked well with the deterministic control law. Perhaps the memory of 24 measurements allowed the least-squares method to find a matrix that worked well with the deterministic control law. This identified matrix, even though in error relative to the true transfer matrix, may have had the row elements identified well in proportion to each other, thereby allowing the deterministic controller to step toward the optimum control input without being fully identified. Had the identification error metric been designed with the transfer-matrix element ratios in mind, the good vibration control results might have been expected.

9.4 Conclusions

Two general conclusions can be drawn from this system identification study. First, alternatives to the classic Kalman filter identification method exist that offer greater ease of implementation or faster computation or both. The accuracy of these methods, however, is not necessarily better than that of the classic Kalman filter method, given correct tuning information. Second, it is noteworthy that none of the identification methods simulated herein were found to be capable of identification convergence as the vibration level became reduced to the same level as the measurement noise including the classic Kalman filter method. This advocates the need for continued system identification research, since it is not an uncommon event that once good vibration control is achieved, the signal-to-noise ratio becomes high, thereby creating an environment that is very unamenable to system identification.

The principal specific findings of this investigation are noted below.

1. The only reliable method of transfer-matrix identification was open-loop excitation of the plant dynamics. In open-loop, all identification methods produced similar identification accuracy and stability. Measurement noise raised the amount of steady-state identification error, but did not prevent identification convergence toward the true estimate, because the open-loop excitation commands were always large enough to produce a sufficiently high signal-to-noise ratio for identification purposes. As was shown in figure 91, the multi-step Kalman and LMS filters may have yielded a slight improvement in identification accuracy. However, because these methods also required some tuning to work correctly, the method of weighted-least-squares (with identity matrix weighting) is recommended for open-loop identification. A batch size of 24–48 measurements for identification of the (6 x 6) transfer matrix is recommended to reduce the effects of measurement noise. Transfer matrices having more columns may require more measurements. As a general rule, the number of input-output pairs acquired should be about 3 times the column dimension of the transfer matrix. The lower computational speed of the least-squares method is irrelevant since the computations done for open-loop identification do not need to be done under a time constraint.

2. In closed-loop operation, in which the identified transfer matrix was used in a deterministic control law to reduce the measured vibration (or measurement vector), suppression of the vibration was clearly no indicator of correct transfer-matrix identification. Each of the identification methods was found to be capable of adjusting the identified transfer-matrix elements in such a way that the deterministic controller could find the optimum vibration control settings long before the transfer matrix was correctly identified.

3. Closed-loop identification was much more difficult than open-loop identification because the control commands were chosen to control the helicopter vibration, rather than to provide excitation. As the vibration became well reduced in closed-loop operation, the signal-to-noise ratio decreased, because the measurement noise became an increasingly larger portion of the measurement signal. As the optimum control solution was achieved, the changes to the identified transfer matrix became very small, because the recursive algorithms formulated the changes proportionally to both the change in control and to the difference between the measured and estimated vibration (i.e., $z - \mathbf{T}\theta$). As one or both of these approached zero as the vibration was controlled, the identification process was effectively shut down. In addition, since the changes to the control input were very small, they appeared less correlated to the changes in the measured vibration; a result of the random measurement noise. This made the updates to the identified matrix also take on a largely random nature. For these reasons, convergence to the correct transfer matrix was very slow once good vibration control was achieved. This resulted in the identification error taking on a constant value, even though convergence to the correct transfer matrix was far from completed.

4. The addition of perturbation or probing signals to the control vector increased the rate of closed-loop transfer-matrix identification and also prevented the identification algorithms from producing large constant error values in steady-state operation. However, the amount of steady-state vibration remaining was also increased, thereby degrading controller performance. For this reason, the technique of probing seems impractical for real vibration-control applications.

5. In closed-loop operation, the weighted-least-squares method always produced the highest identification errors, but the best vibration control. As the controller reached a steady-state solution for optimal control, the control-covariance matrix became singular, thereby producing poor identification in closed-loop. Adding a perturbation signal to the control vector did not greatly improve the situation. However, not performing the identification (and moving-block sequencing) for vibration below 0.20 of the baseline vibration level offered surprisingly good vibration control (see figs. 95, 99). Although not evaluated, it is possible that the recursive methods might have also produced better vibration control with the application of this logic. Therefore, using the weighted-least-squares-error method in moving-block format was determined to be very feasible. The selection of the correct threshold vibration level represents selection of a tuning parameter no more difficult to select than those used by the recursive identification methods.

6. The most computationally efficient and least complex recursive algorithm was the LMS filter method: its speed and simplicity highly recommend this identification algorithm as the method of choice since the more complicated recursive methods (i.e., Kalman filter, multi-step) offered only slightly improved identification accuracy.

7. The Kalman filter, although sometimes observed to produce very good identification results, was difficult to tune. The values chosen for r and **M**, as expected from theory, were found to govern the trade-off between responsive identification and superior noise rejection. It was also noted that over a wide range of r and **M** values, the ratio of r/**M** was generally the factor which most influenced the system identification convergence behavior. In addition, whereas a non-zero **Q** value was clearly required for good identification, almost any value of **Q** from 0.01 to 100 produced the same identification performance. However, tuning the filter was not a straightforward exercise. For example, the tuning values that were found to be optimal for open-loop identification (r = 1, **M** = 10, **Q** = 10), produced divergent identification in closed-loop operation. Although the instability was eliminated by re-tuning the filter (r = 100, **M** = 1, **Q** = 10), this task would likely prove to be difficult in real-world applications where strict simulation conditions cannot be so easily maintained.

8. By using multiple measurements, the multi-step methods yielded somewhat lower steady-state identification errors; yet, for the same reason, they gave slightly higher identification errors after the transient step change to the transfer matrix. The generalized Kalman filter differed from the classic Kalman filter not only because it allowed multiple measurements to be used in the identification process, but also because its formulation did not recursively propagate the process-noise covariance matrix. Although the generalized Kalman filter provided somewhat lower identification error relative to the generalized LMS filter and the other recursive methods, the difference was found to be unimportant in terms of closed-loop vibration-control performance. In view of this, the classic LMS filter might be preferred for its computational efficiency, whereas the weighted-least-squares method in moving-block format might be preferred for its superior vibration control.

9. As was found using the weighted-least-squares method in moving-block format, in closed-loop operation large identification errors in the transfer matrix did not necessarily preclude excellent vibration control. The reason was, apparently, that the identified matrix, even though in error compared to the true transfer matrix, may have had the row elements identified well in

proportion to each other, thereby allowing the deterministic controller to step toward the optimum control input without being fully identified.

10. Taken overall, both local and global models investigated by this study produced equivalent identification accuracy and closed-loop vibration control performance. Neither model was preferred over the other.

REFERENCES

1. Clay, D.; and Chadwick, J.: "Helicopter Vibration Analysis and Control." Proceedings of the 44th Annual National Forum of the American Helicopter Society, Washington, D. C., June 1988, pp. 243-250.

2. Stewart, W.: "Second Harmonic Control on the Helicopter Rotor." Aeronautical Research Council, Reports and Memoranda No. 2997, August 1952.

3. Arcidiacono, P. J.: "Theoretical Performance of Helicopters Having Second and Higher Harmonic Feathering Control." J. Am. Helicopter Soc., vol. 6, no. 2, April 1961, pp. 8-19.

4. Wernicke, R. K.; and Drees, J. M.: "Second Harmonic Control." 19th Annual National Forum of the American Helicopter Society, May 1963, pp. 1-7.

5. Sissingh, G. J.; and Donham, R. E.: "Hingeless Rotor Theory and Experiment on Vibration Reduction by Periodic Variation of Conventional Controls." NASA SP-352, 1974, pp. 261-277.

6. McCloud, J. L., III; and Kretz, M.: "Multicyclic Jet-Flap Control for Alleviation of Helicopter Blade Stresses and Fuselage Vibration." NASA SP-352, 1974, pp. 233-238.

7. McCloud, J. L. III: "An Analytical Study of a Multicyclic Controllable Twist Rotor." Proceedings of the 31st Annual National Forum of the American Helicopter Society, May 1975.

8. McCloud, J. L. III; and Weisbrich, A. L.: "Wind Tunnel Test Results of a Full-Scale Multicyclic Controllable-Twist Rotor." Proceedings of the 24th Annual National Forum of the American Helicopter Society, Washington, D. C., May 1978.

9. Brown, T. J.; and McCloud, J. L., III: "Multicyclic Control of a Helicopter Rotor Considering the Influence of Vibration, Loads, and Control Motion." AIAA Paper 80-673, May 1980.

10. Shaw, J.; and Albion, N.: "Active Control of the Helicopter Rotor for Vibration Reduction." Paper No. 80-68, Proceedings of the 36th Annual National Forum of the American Helicopter Society, Washington, D. C., 1980.

11. Shaw, J.; Albion, N.; Hanker, E. J.; and Teal, R. S.: "Higher Harmonic Control: Wind Tunnel Demonstration of Fully Effective Vibratory Hub Force Suppression." Proceedings of the 41st Annual National Forum of the American Helicopter Society, Fort Worth, TX, May 1985, pp. 1-15.

12. Molusis, J. A.; Hammond, C. E.; and Cline, J. H.: "A Unified Approach to the Optimal Design of Adaptive and Gain Scheduled Controllers to Achieve Minimum Helicopter Rotor Vibration." Proceedings of the 37th Annual National Forum of the American Helicopter Society, New Orleans, LA, May 1981, pp. 188-203.

13. Chopra, I.; and McCloud, J. L., III: "Considerations of Open-Loop, Closed-Loop, and Adaptive Multicyclic Control Systems." Proceedings of the American Helicopter Society National Specialist's Meeting on Helicopter Vibration Technology for the Jet Smooth Ride, Hartford, CT, 1981.

14. Johnson, W.: "Self-Tuning Regulators for Multicyclic Control of Helicopter Vibration." NASA TP-1996, 1982.

15. Molusis, J. A.: "Investigation of Unexplained Behavior and Nonlinearity Observed in Wind Tunnel Tests of Higher Harmonic Control." U.S. Army Research and Technology Laboratories, TR-83-D8, Fort Eutis, VA, August 1983.

16. Wood, E. R.; Powers, R. W.; Cline, J. H.; and Hammond, C. E.: "On Developing and Flight Testing a Higher Harmonic Control System." Proceedings of the 39th Annual National Forum of the American Helicopter Society, St. Louis, MO, May 1983, pp. 592-612.

17. Davis, M. W.: "Refinement and Evaluation of Helicopter Real-Time Self-Adaptive Active Vibration Controller Algorithms," NASA CR-3821, August 1984.

18. Haviland, J. K.; and Knospe, C.: "A Wide-Band, Time-Domain Adaptive Control for Helicopter Vibrations." Proceedings of the First Army Research Office Workshop on Rotorcraft, Boca Raton, FL, November 1986.

19. Franklin, G. F.; and Powell, J. D.: "Digital Control of Dynamic Systems." Addison-Wesley Publishing Co., Reading, MA, 1980.

20. Bryson, A. E., Jr.; and Ho, Y-C.: "Applied Optimal Control: Optimization, Estimation, and Control." Blaisdell Publishing Corp., New York, 1969.

21. Chen, R. T. N.; Eulrich, B. J.; and Lebacqz, J. V.: "Development of Advanced Techniques for the Identification of V/STOL Aircraft Stability and Control Parameters." Cornell Aeronautical Laboratories Technical Report (AD-730121), CAL No. BM-2820-F-1, August 1971.

22. Goodwin, G. C.; and Payne, R. L.: "Dynamic System Identification: Experiment Design and Data Analysis," Academic Press, New York, 1977.

23. Widrow, B.; and Hoff, M. E., Jr.: "Adaptive Switching Circuits." IRE WESCON Convention Record, 1960, pp. 96-104.

24. Widrow, B.: "Adaptive Filters, Aspects of Network and System Theory." Holt, Rinehart, and Winston, Inc., New York, 1970.

25. Jacklin, S. A.: "Adaptive Inverse Control for Rotorcraft Vibration Reduction," NASA TM-86829, 1985.

26. Jacklin, S. A.: "Arranging Computer Architectures to Create Higher Performance Controllers." Advances in Algorithms and Computational Techniques for Dynamic Control Systems, Academic Press, New York, 1988.

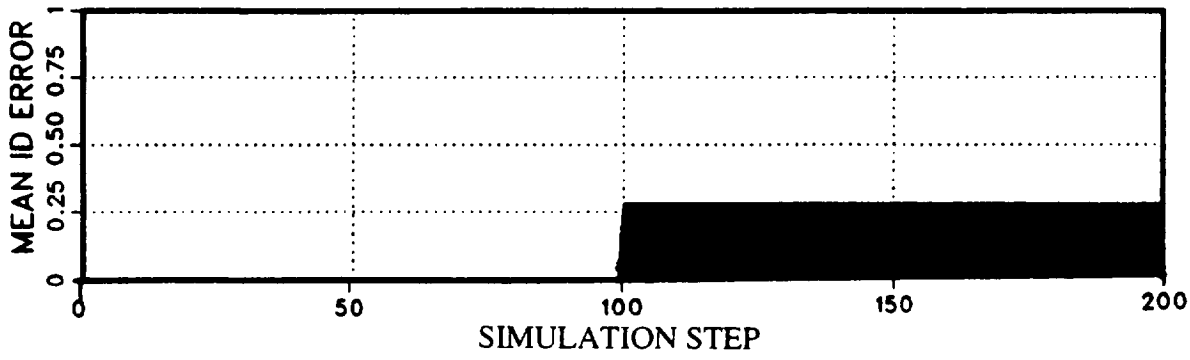

Figure 6. Plot of baseline identification error and open-loop excitation for the case of no identification.

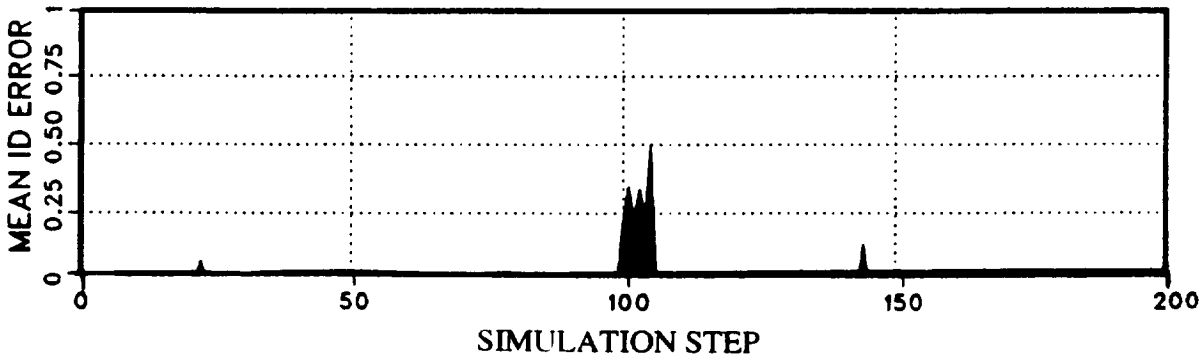

Figure 7. Open-loop weighted-least-squares identification error for no measurement noise using batch size n = 6 (Local Model).

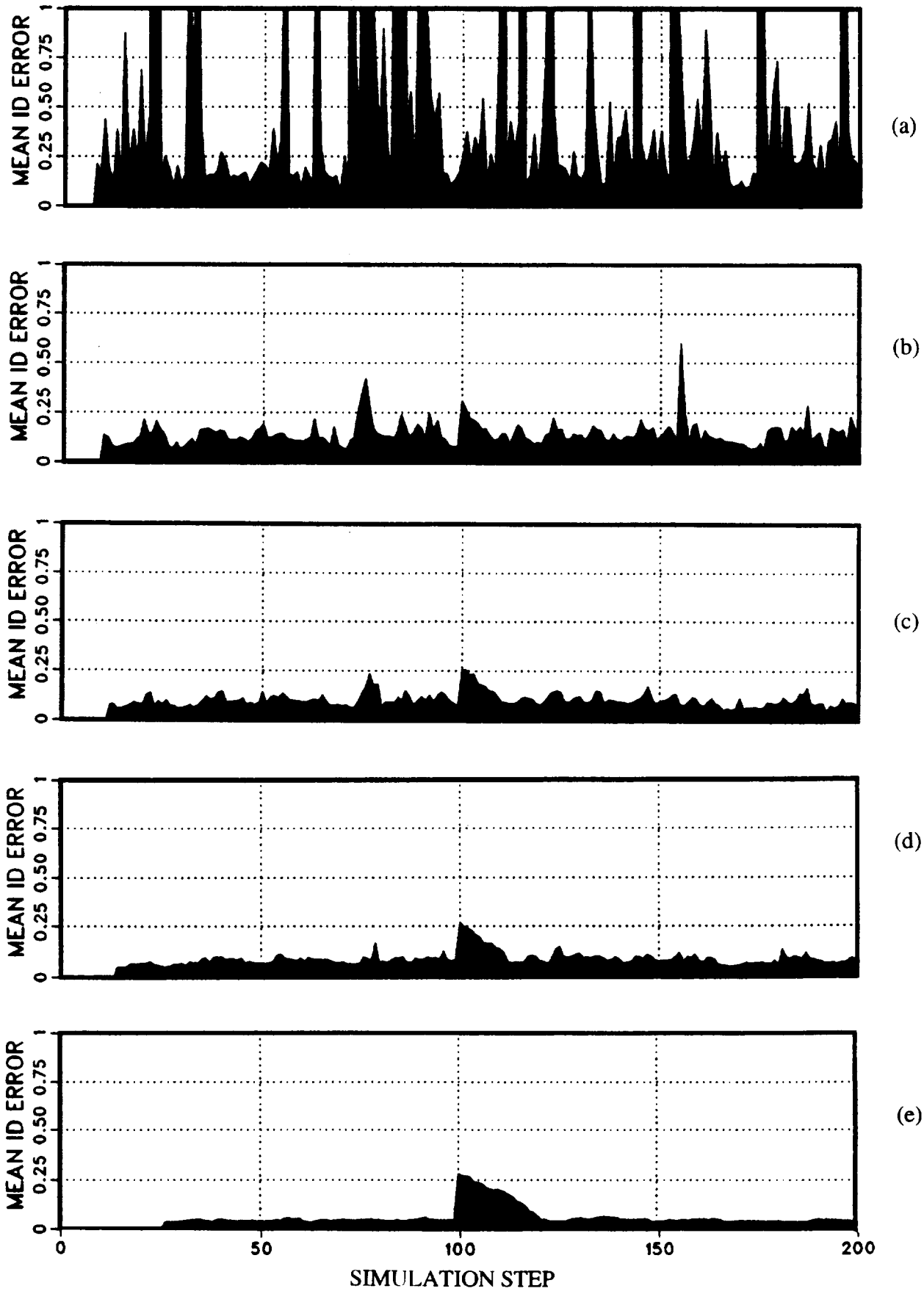

Figure 8. Open-loop weighted-least-squares identification error with 10% measurement noise showing effect of using different batch sizes n: (a) n = 6; (b) n = 8; (c) n = 10; (d) n = 12; (e) n = 24 (Local Model).

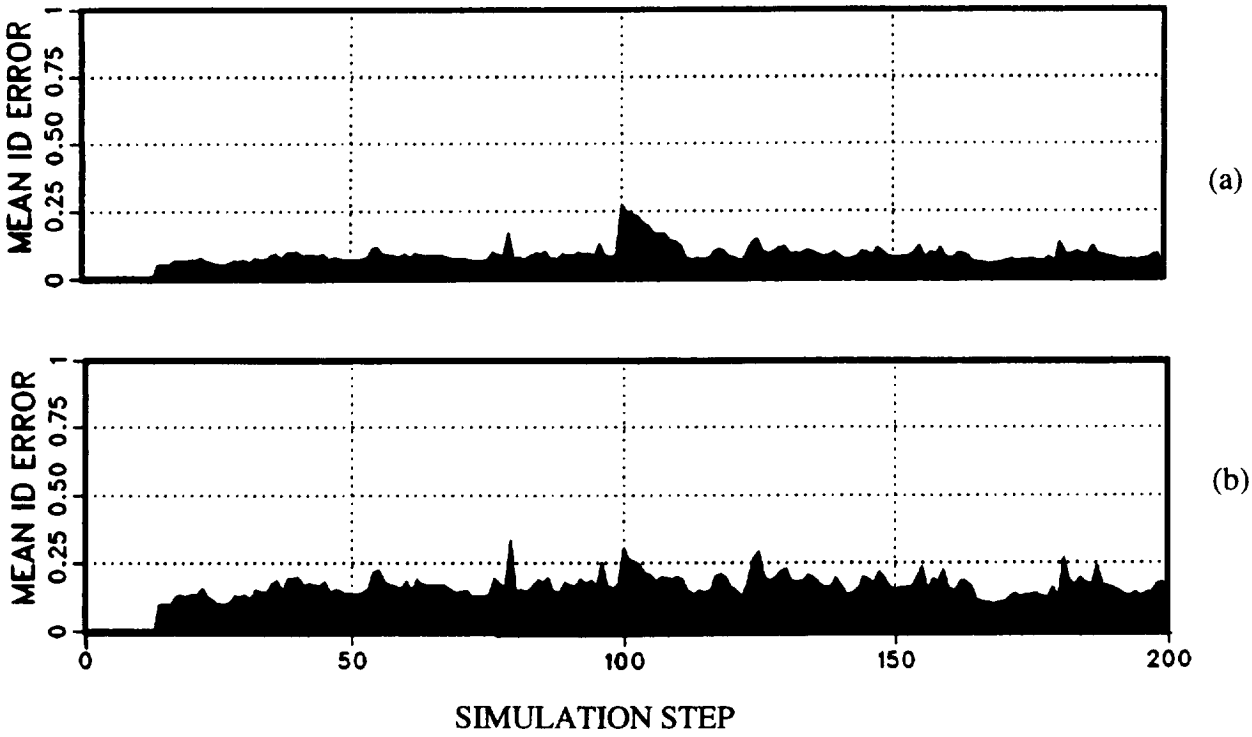

Figure 9. Open-loop weighted-least-squares identification error for batch size n = 12 showing effect of different amounts of measurement noise: (a) 10%, (b) 20% (Local Model).

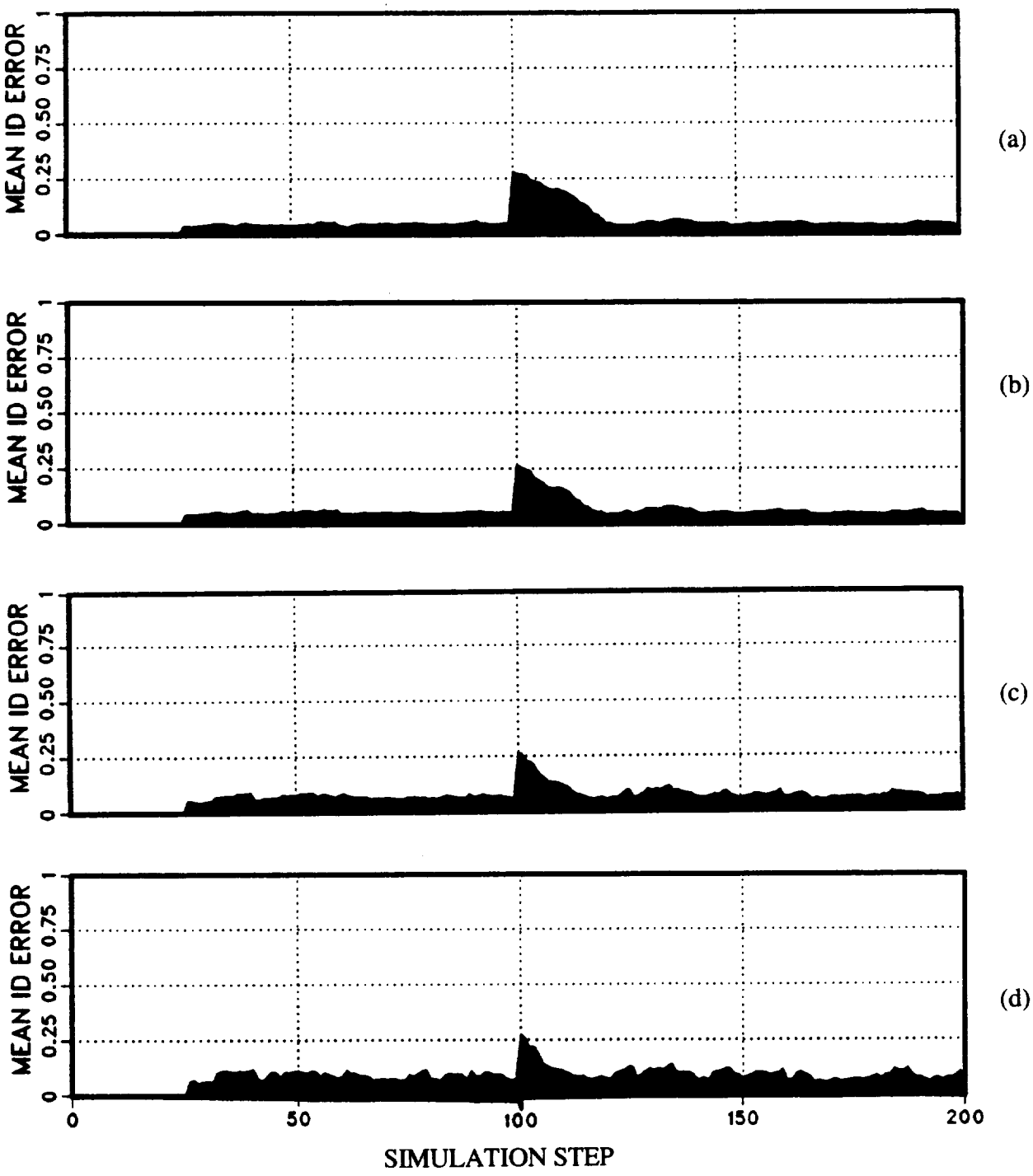

Figure 10. Open-loop weighted-least-squares identification error with 10% measurement noise and batch size n = 24 showing effect of using different exponential weighting γ: (a) $\gamma = 1$; (b) $\gamma = 0.9$; (c) $\gamma = 0.8$; (d) $\gamma = 0.7$ (Local Model).

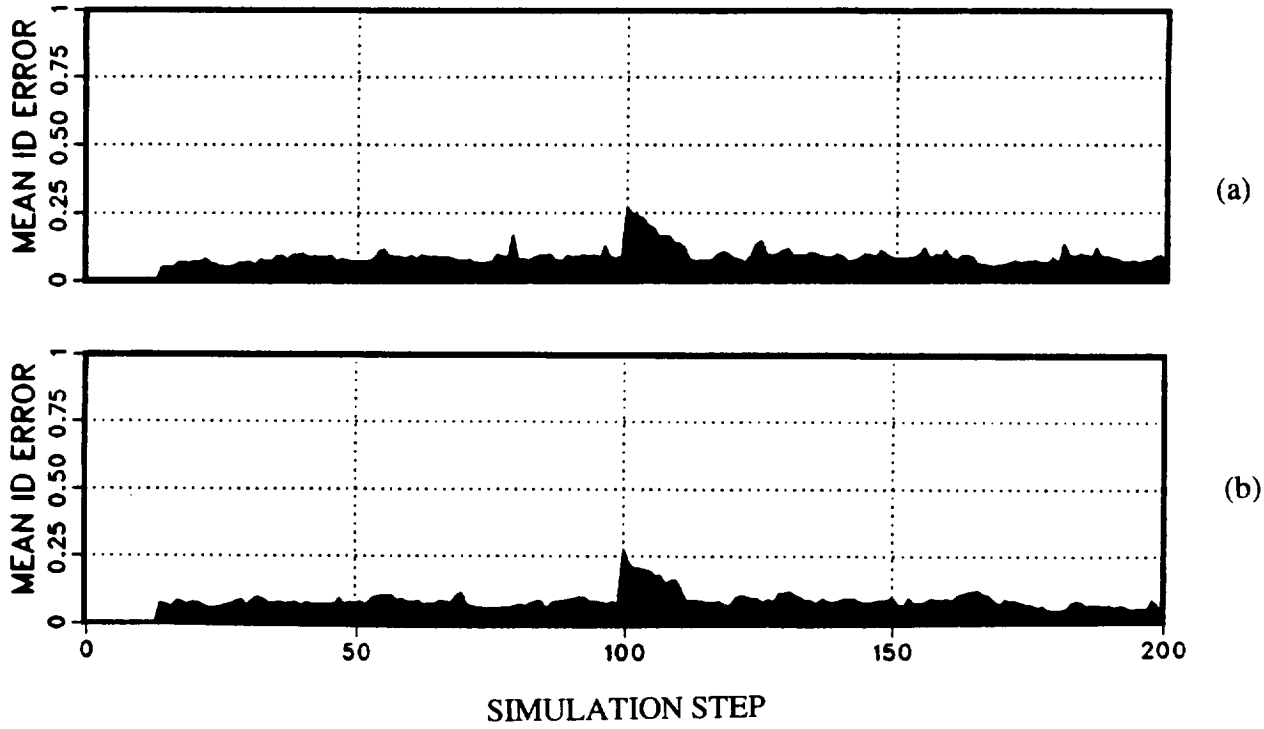

Figure 11. Open-loop weighted-least-squares identification error with 10% measurement noise and batch size n = 12 showing effect of transfer-matrix size: (a) 6 x 6, (b) 12 x 6 (Local Model).

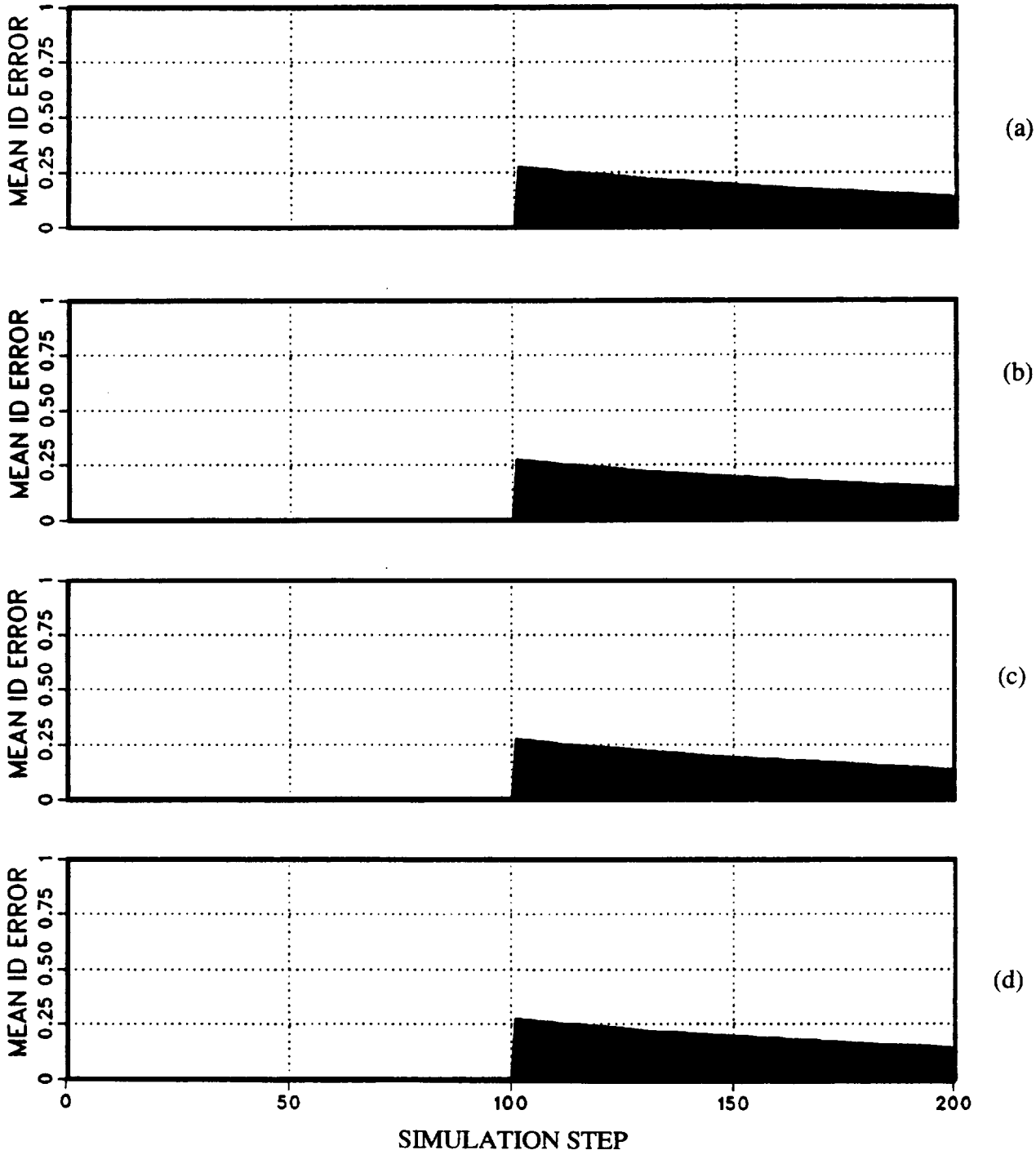

Figure 12. Open-loop Kalman filter identification error for no measurement noise, $\mathbf{Q} = 0.0 * \mathbf{I}_6$, r = 0.1: (a) $\mathbf{M} = 0.1 * \mathbf{I}_6$; (b) $\mathbf{M} = \mathbf{I}_6$; (c) $\mathbf{M} = 10 * \mathbf{I}_6$; (d) $\mathbf{M} = 100 * \mathbf{I}_6$ (Local Model).

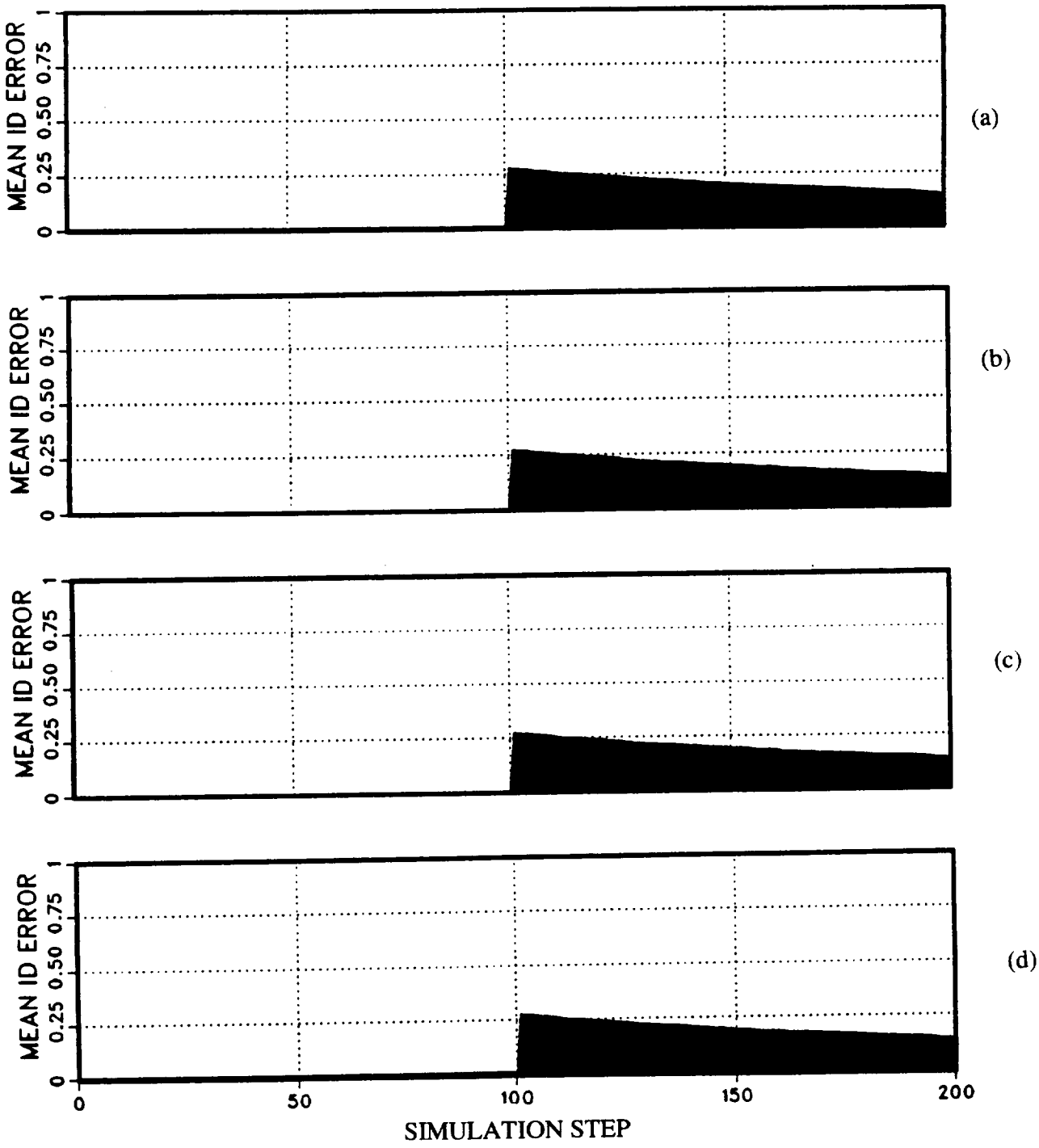

Figure 13. Open-loop Kalman filter identification error for no measurement noise, $\mathbf{Q} = 0.0 * \mathbf{I}_6$, r = 1: (a) $\mathbf{M} = 0.1 * \mathbf{I}_6$; (b) $\mathbf{M} = \mathbf{I}_6$; (c) $\mathbf{M} = 10 * \mathbf{I}_6$; (d) $\mathbf{M} = 100 * \mathbf{I}_6$ (Local Model).

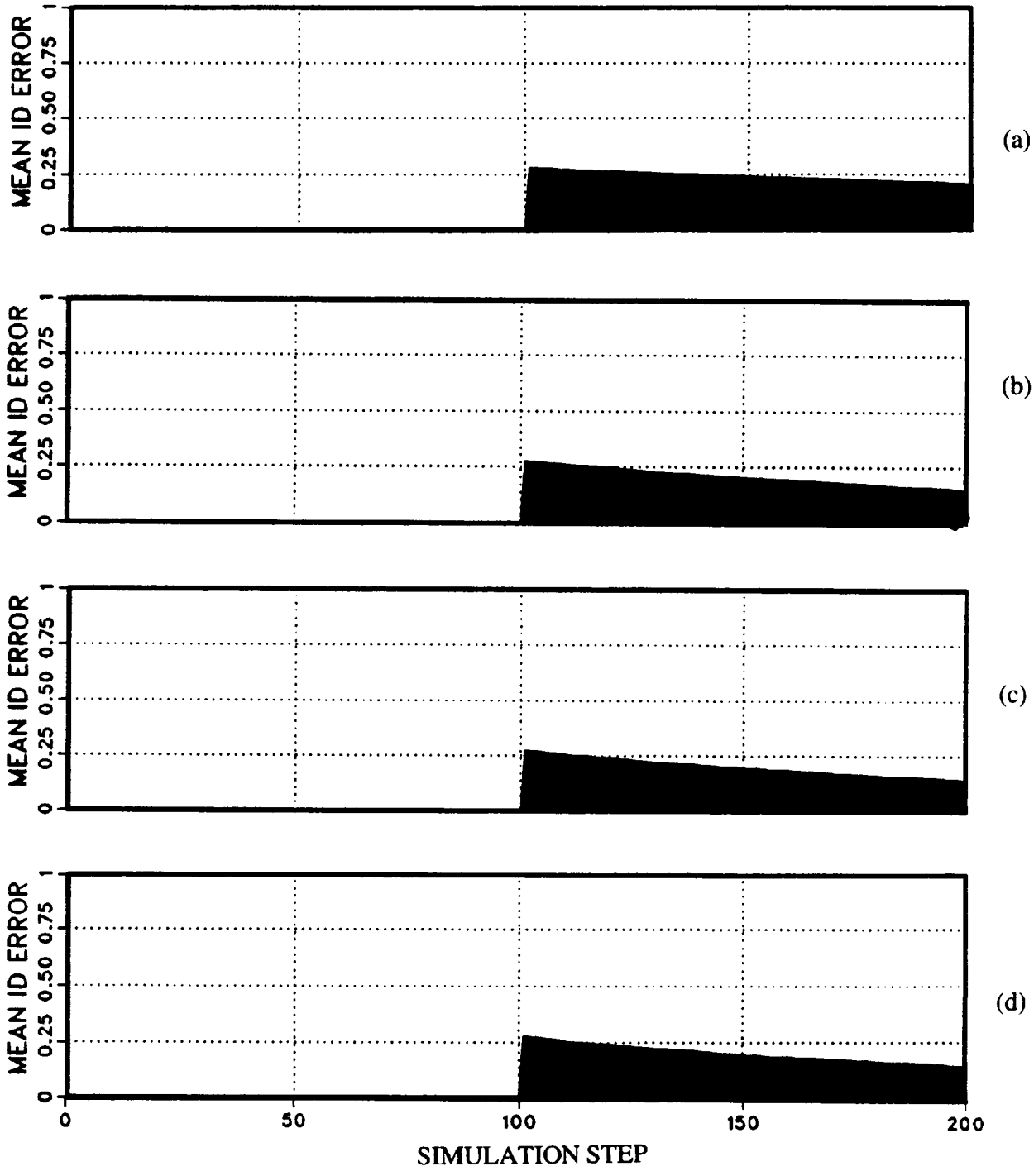

Figure 14. Open-loop Kalman filter identification error for no measurement noise, $\mathbf{Q} = 0.0 * \mathbf{I}_6$, r = 10: (a) $\mathbf{M} = 0.1 * \mathbf{I}_6$; (b) $\mathbf{M} = \mathbf{I}_6$; (c) $\mathbf{M} = 10 * \mathbf{I}_6$; (d) $\mathbf{M} = 100 * \mathbf{I}_6$ (Local Model).

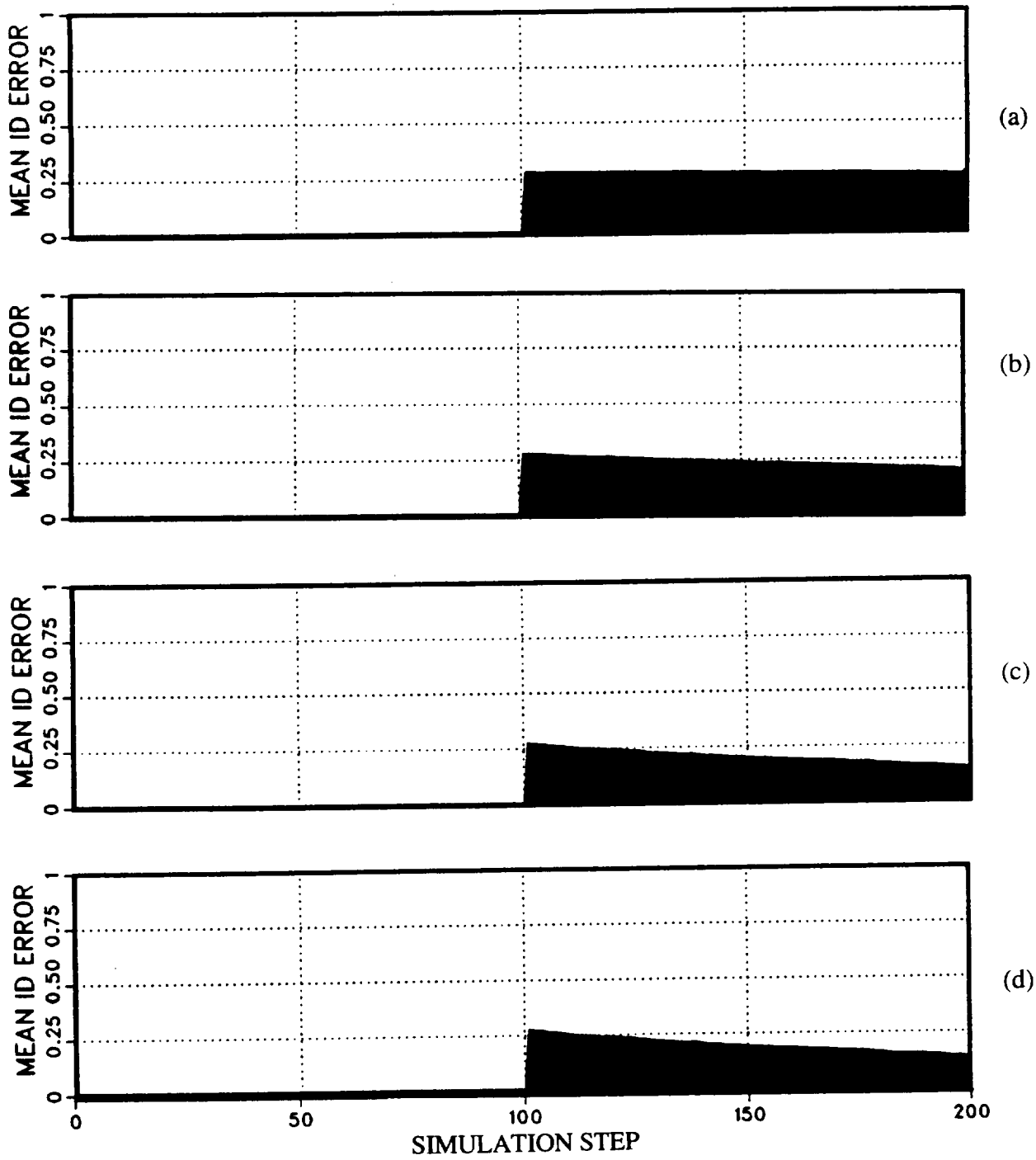

Figure 15. Open-loop Kalman filter identification error for no measurement noise, $\mathbf{Q} = 0.0 * \mathbf{I}_6$, $\mathbf{r} = 1$: (a) $\mathbf{M} = 0.1 * \mathbf{I}_6$; (b) $\mathbf{M} = \mathbf{I}_6$; (c) $\mathbf{M} = 10 * \mathbf{I}_6$; (d) $\mathbf{M} = 100 * \mathbf{I}_6$ (Local Model).

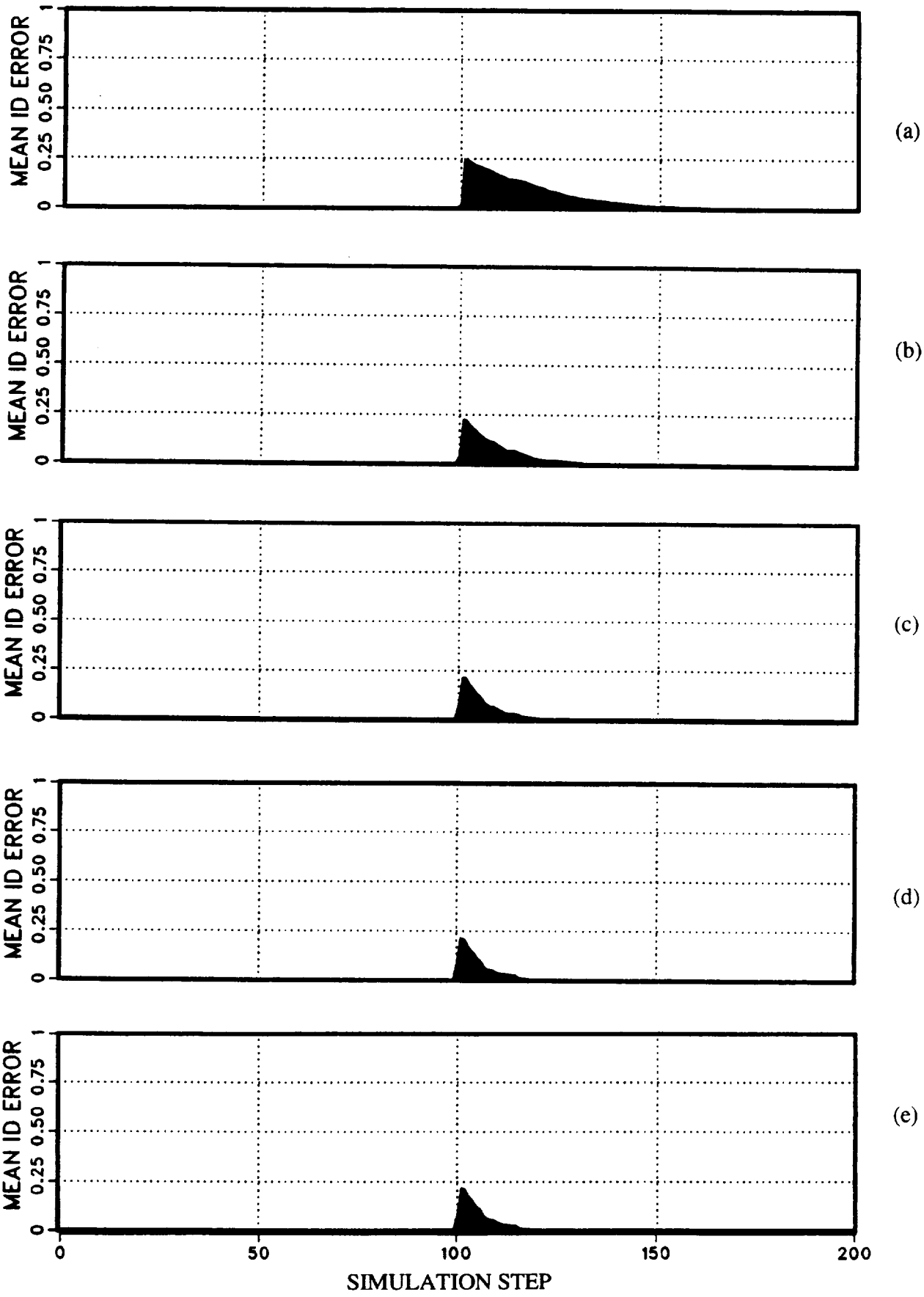

Figure 16. Open-loop Kalman filter identification error for no measurement noise, $\mathbf{r} = 1$, $\mathbf{M} = 10 * \mathbf{I}_6$: (a) $\mathbf{Q} = 0.01 * \mathbf{I}_6$; (b) $\mathbf{Q} = 0.1 * \mathbf{I}_6$; (c) $\mathbf{Q} = \mathbf{I}_6$; (d) $\mathbf{Q} = 10 * \mathbf{I}_6$; (e) $\mathbf{Q} = 100 * \mathbf{I}_6$ (Local Model).

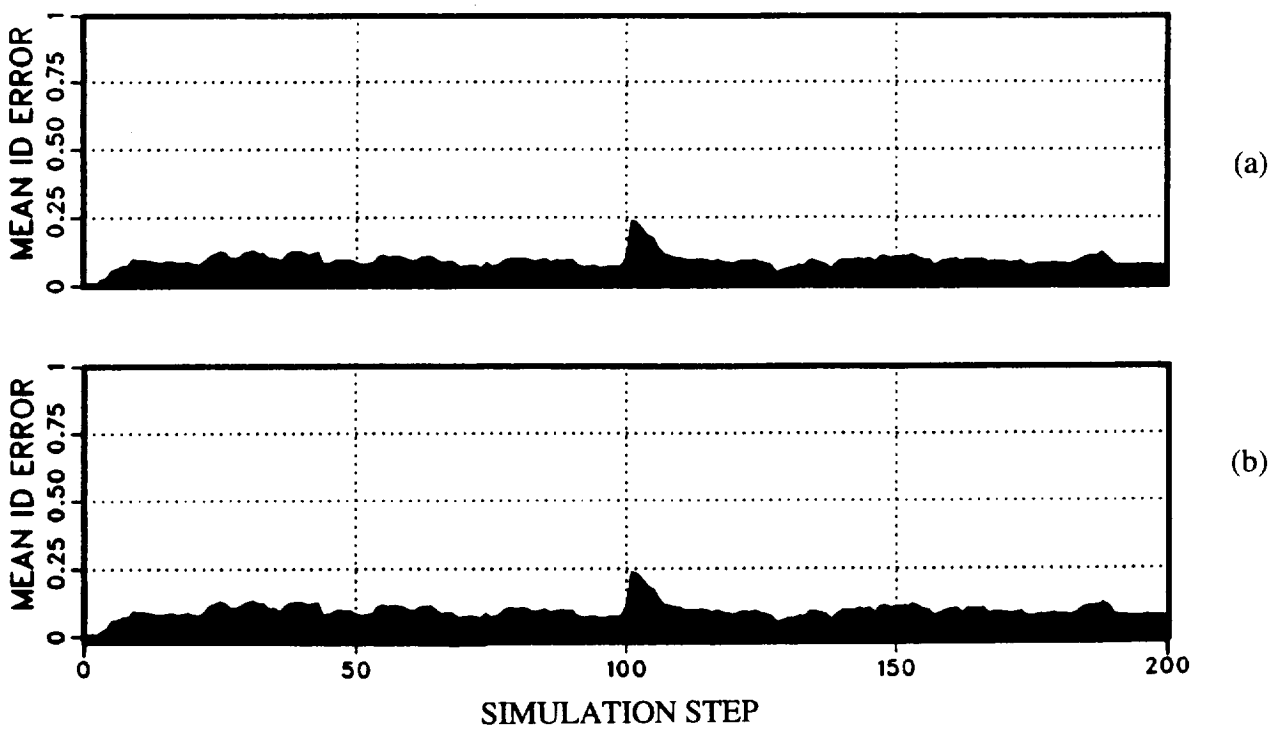

Figure 17. Open-loop Kalman filter identification error for 10% measurement noise, $\mathbf{Q} = 10 * \mathbf{I}_6$: (a) r = 1, $\mathbf{M} = 10 * \mathbf{I}_6$; (b) r = 0.1, $\mathbf{M} = \mathbf{I}_6$ (Local Model).

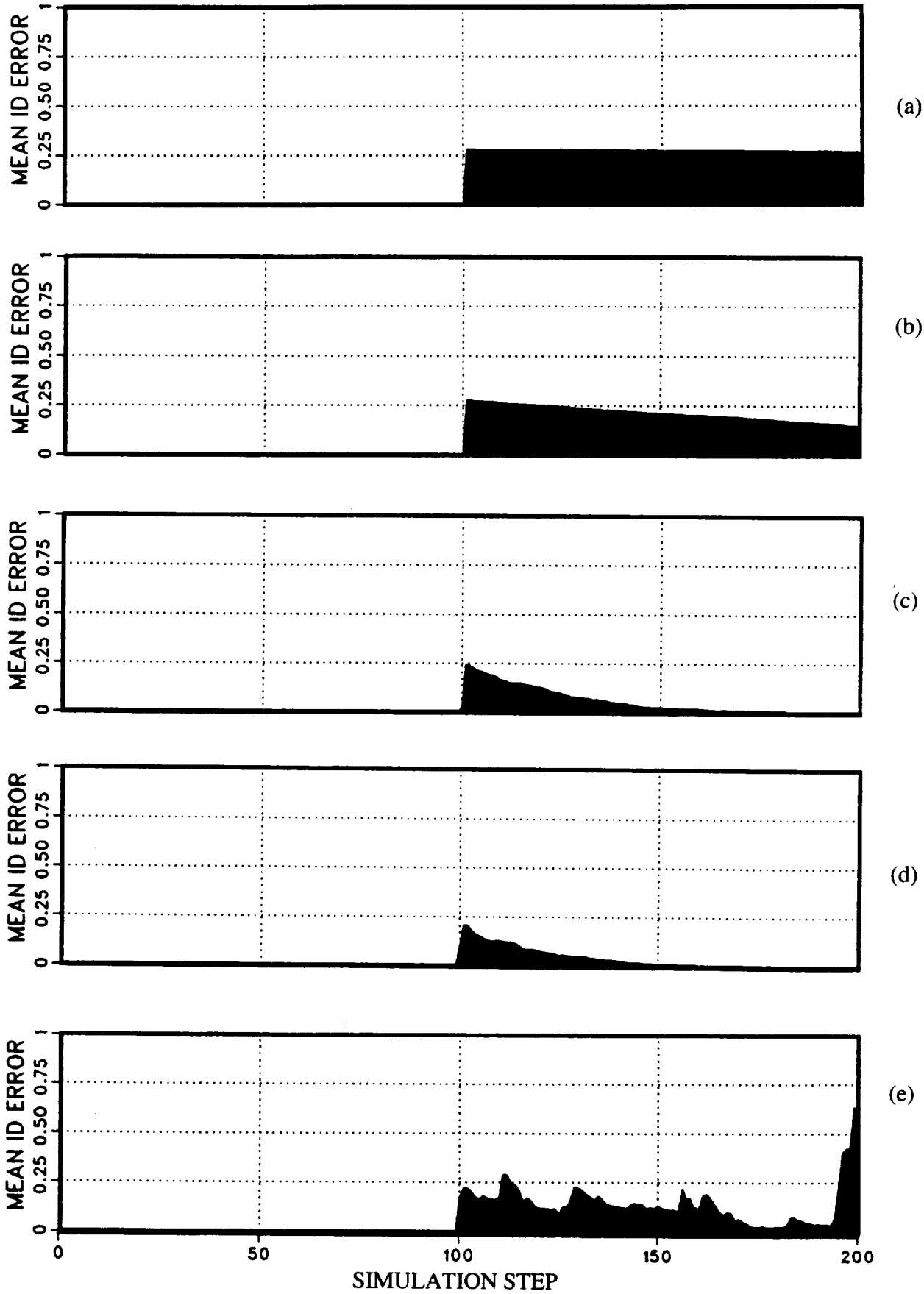

Figure 18. Open-loop LMS filter identification error for no measurement noise: (a) $\mathbf{K}_S = 0.001$; (b) $\mathbf{K}_S = 0.01$; (c) $\mathbf{K}_S = 0.1$; (d) $\mathbf{K}_S = 0.3$; (e) $\mathbf{K}_S = 0.5$ (Local Model).

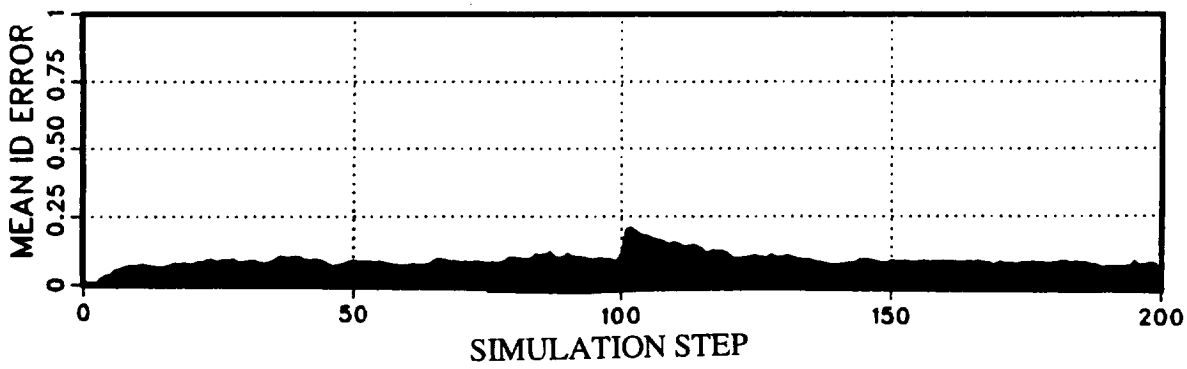

Figure 19. Open-loop LMS filter identification error for 10% measurement noise and $\mathbf{K}_S = 0.3$ (Local Model).

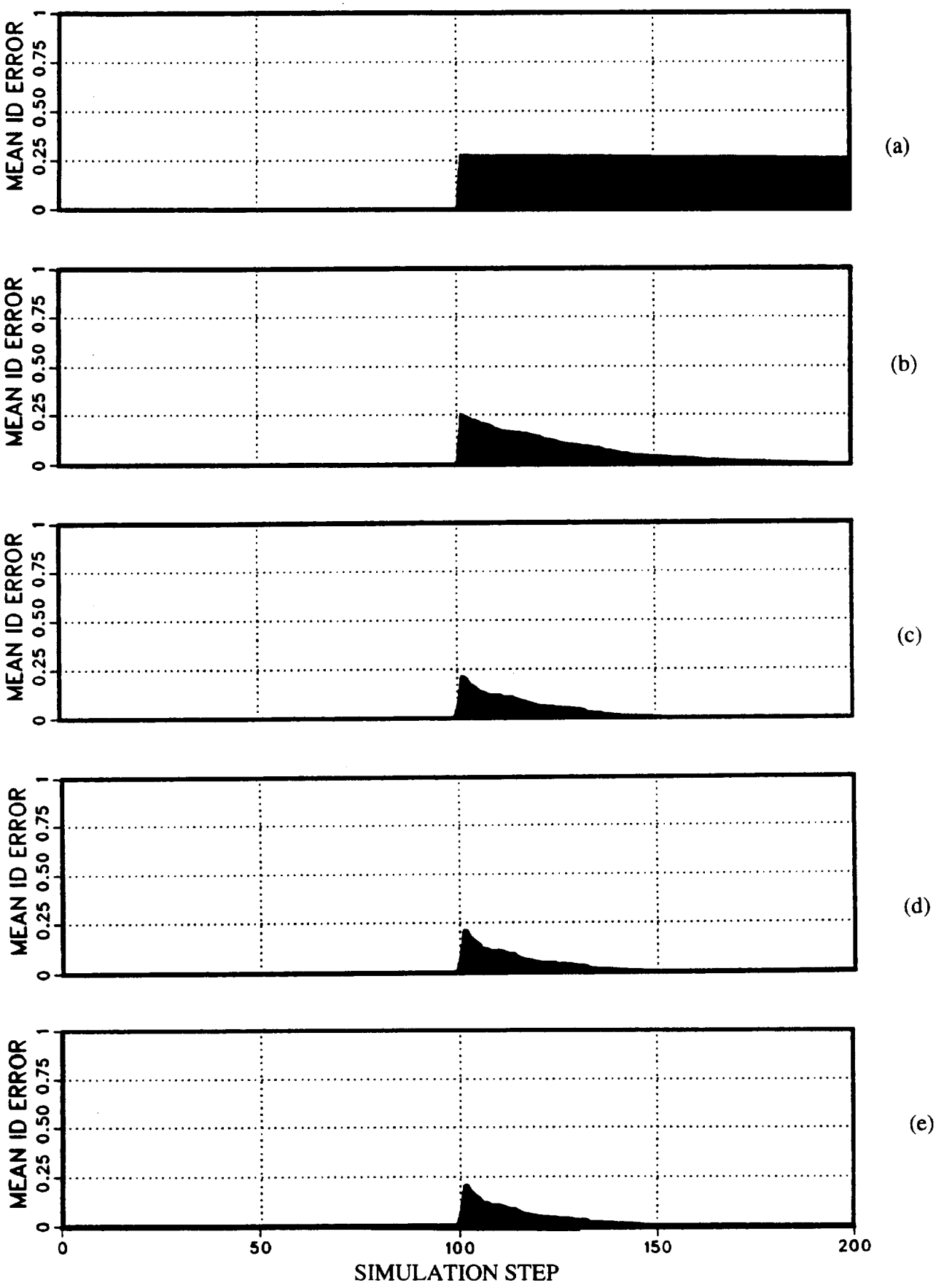

Figure 20. Open-loop generalized Kalman filter identification error for no measurement noise and multi-step batch size n = 1, showing effect of different **M/R** ratios: (a) $\mathbf{M} = 0.1 * \mathbf{I}_6$, $\mathbf{R} = 100$; (b) $\mathbf{M} = \mathbf{I}_6$, $\mathbf{R} = 10$; (c) $\mathbf{M} = \mathbf{I}_6$, $\mathbf{R} = 1$; (d) $\mathbf{M} = 10 * \mathbf{I}_6$, $\mathbf{R} = 1$; (e) $\mathbf{M} = 100 * \mathbf{I}_6$, $\mathbf{R} = 0.1$ (Local Model).

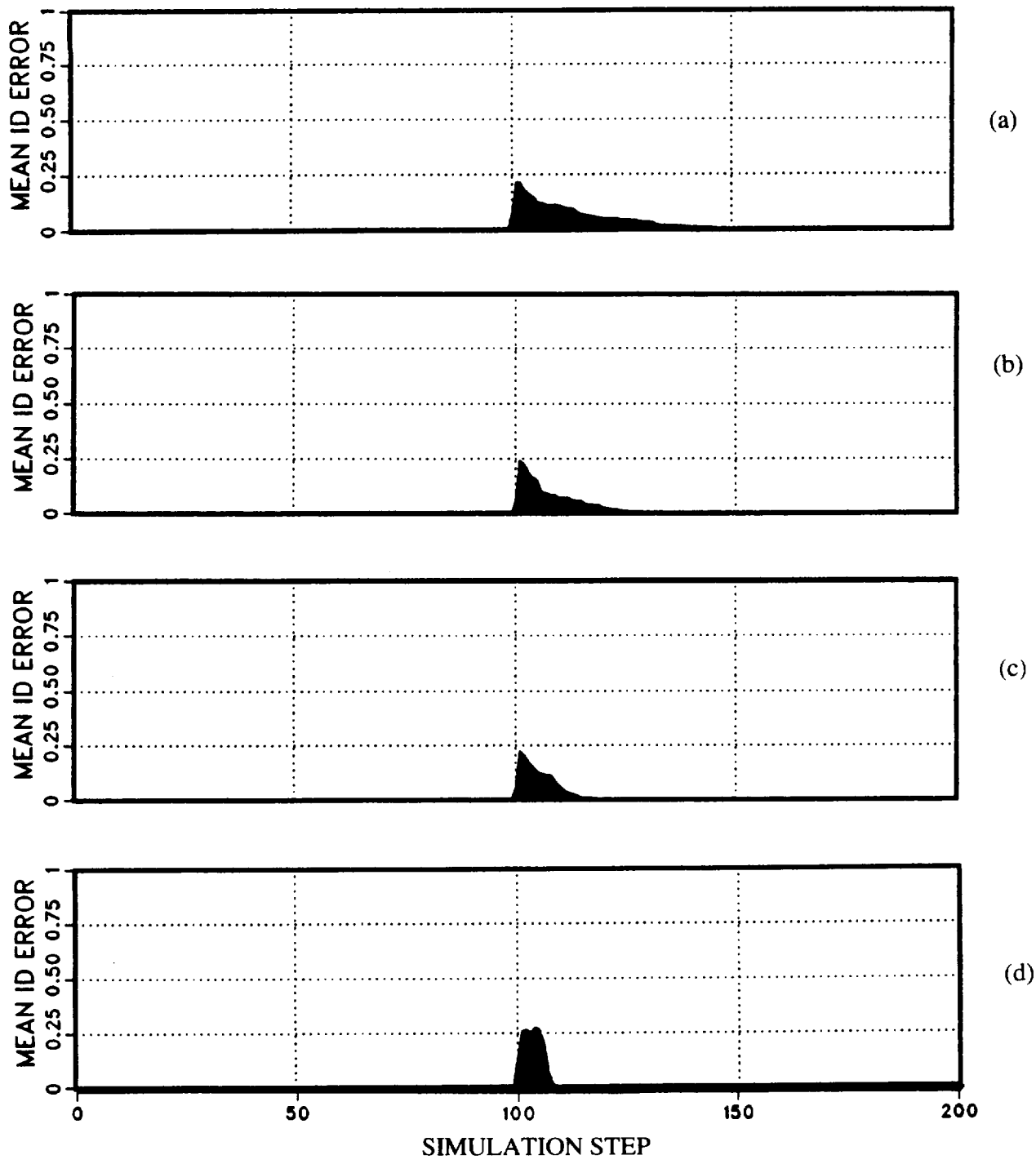

Figure 21. Open-loop generalized Kalman filter identification error for no measurement noise, $\mathbf{M} = 10 * \mathbf{I}_6$, and $\mathbf{R} = 1$, showing effect of different multi-step batch sizes: (a) n = 1; (b) n = 2; (c) n = 4; (d) n = 8 (Local Model).

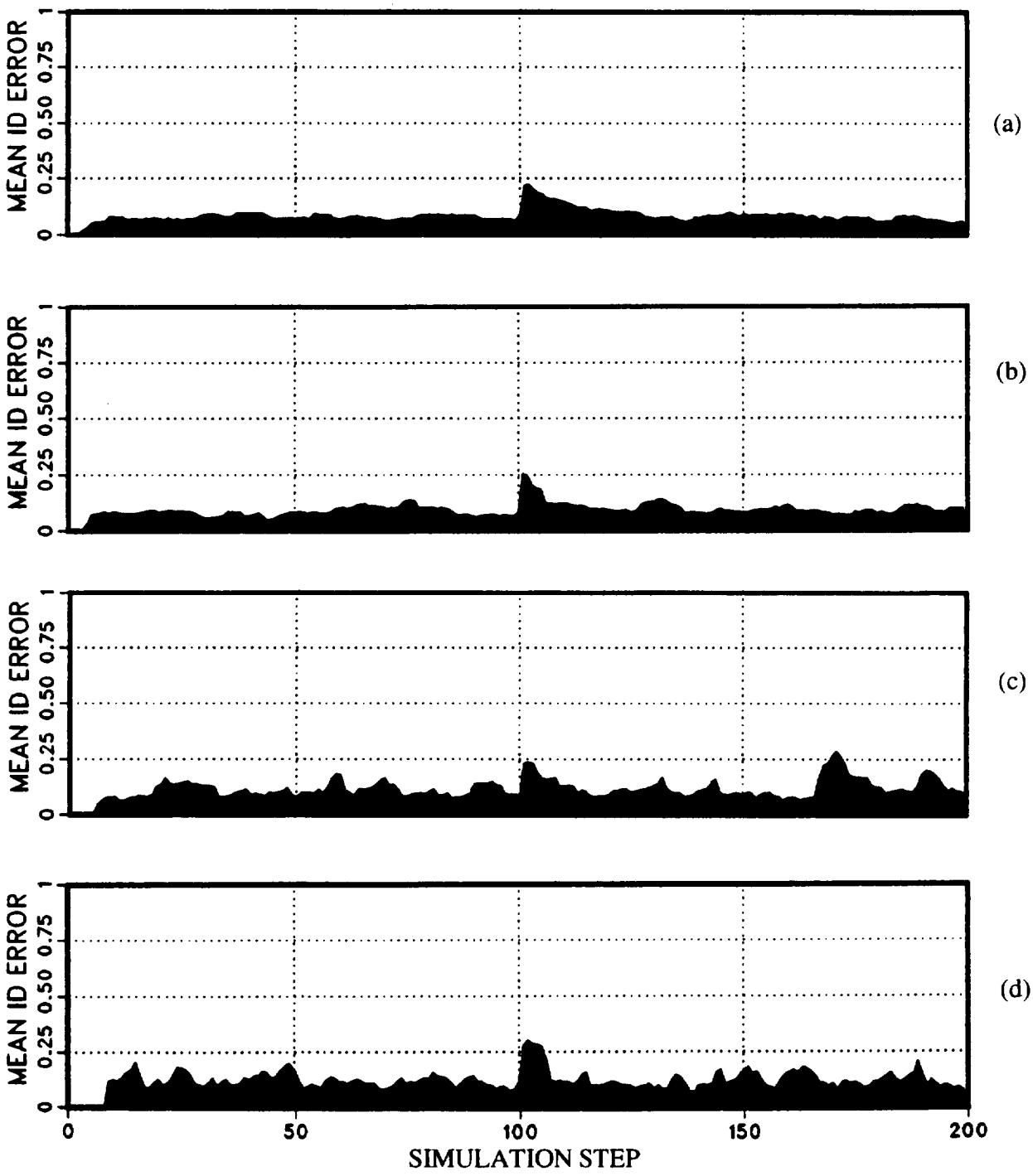

Figure 22. Open-loop generalized Kalman filter identification error for 10% measurement noise, $\mathbf{M} = 10 * \mathbf{I}_6$, and $\mathbf{R} = 1$, showing effect of different multi-step batch sizes: (a) n = 1, (b) n = 2, (c) n = 4, (d) n = 8 (Local Model).

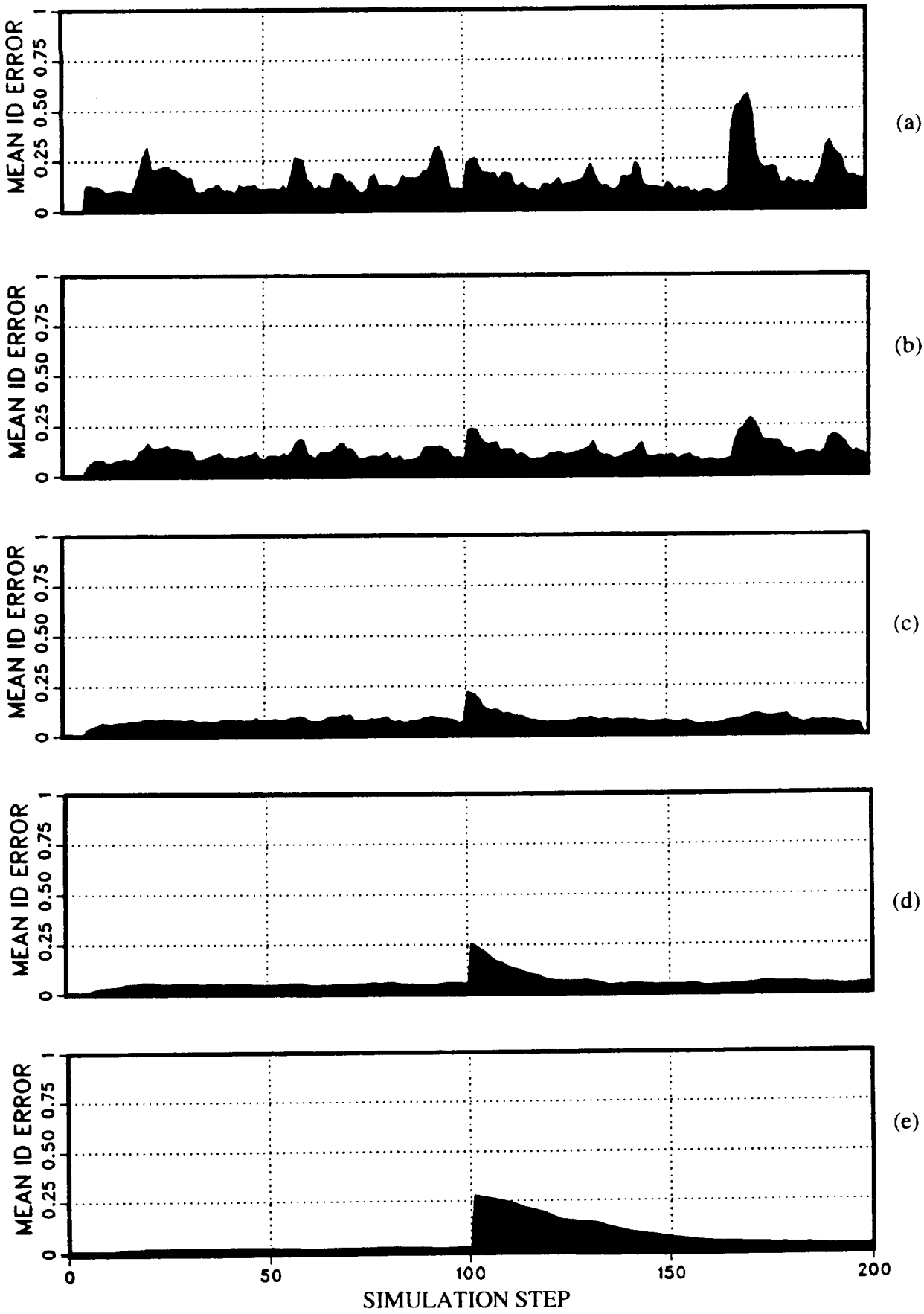

Figure 23. Open-loop generalized Kalman filter identification error for 10% measurement noise and multi-step batch size n = 4, showing effect of different **M/R** ratios: (a) $\mathbf{M} = 100 * \mathbf{I}_6$, $\mathbf{R} = 1$; (b) $\mathbf{M} = 10 * \mathbf{I}_6$, $\mathbf{R} = 1$; (c) $\mathbf{M} = \mathbf{I}_6$, $\mathbf{R} = 1$; (d) $\mathbf{M} = \mathbf{I}_6$, $\mathbf{R} = 10$; (e) $\mathbf{M} = \mathbf{I}_6$, $\mathbf{R} = 100$ (Local Model).

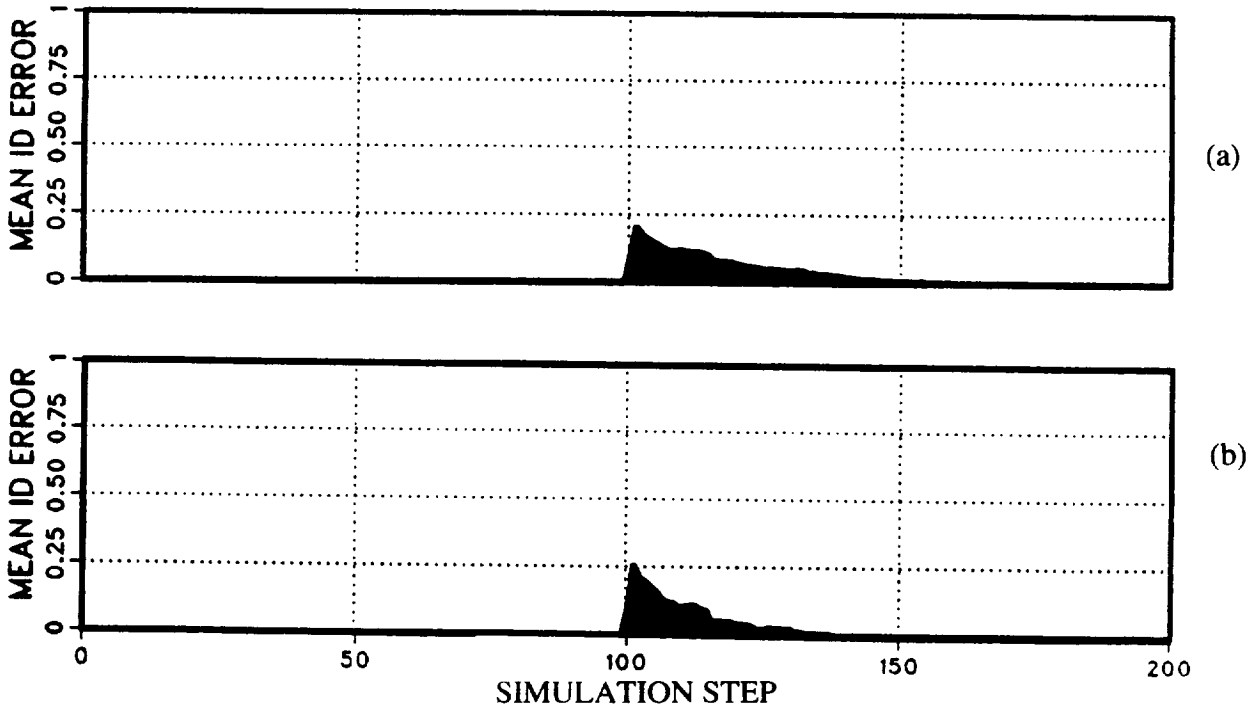

Figure 24. Open-loop generalized LMS filter identification error for no measurement noise and $\mathbf{K}_S = 0.3 * \mathbf{I}_6$, showing effect of different multi-step batch sizes n: (a) n = 1; (b) n = 2 (Local Model).

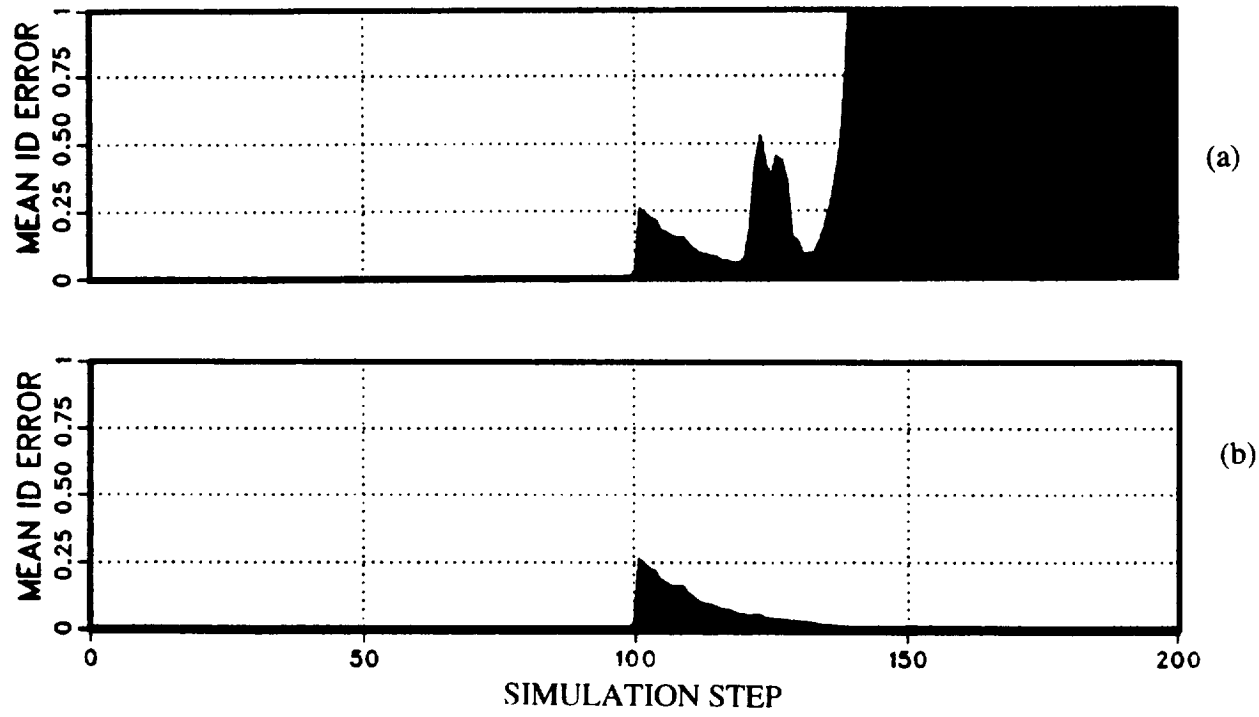

Figure 25. Open-loop generalized LMS filter identification error for no measurement noise and multi-step batch size n = 4: (a) $\mathbf{K}_S * \mathbf{I}_6 = 0.2$; (b) $\mathbf{K}_S * \mathbf{I}_6 = 0.15$ (Local Model).

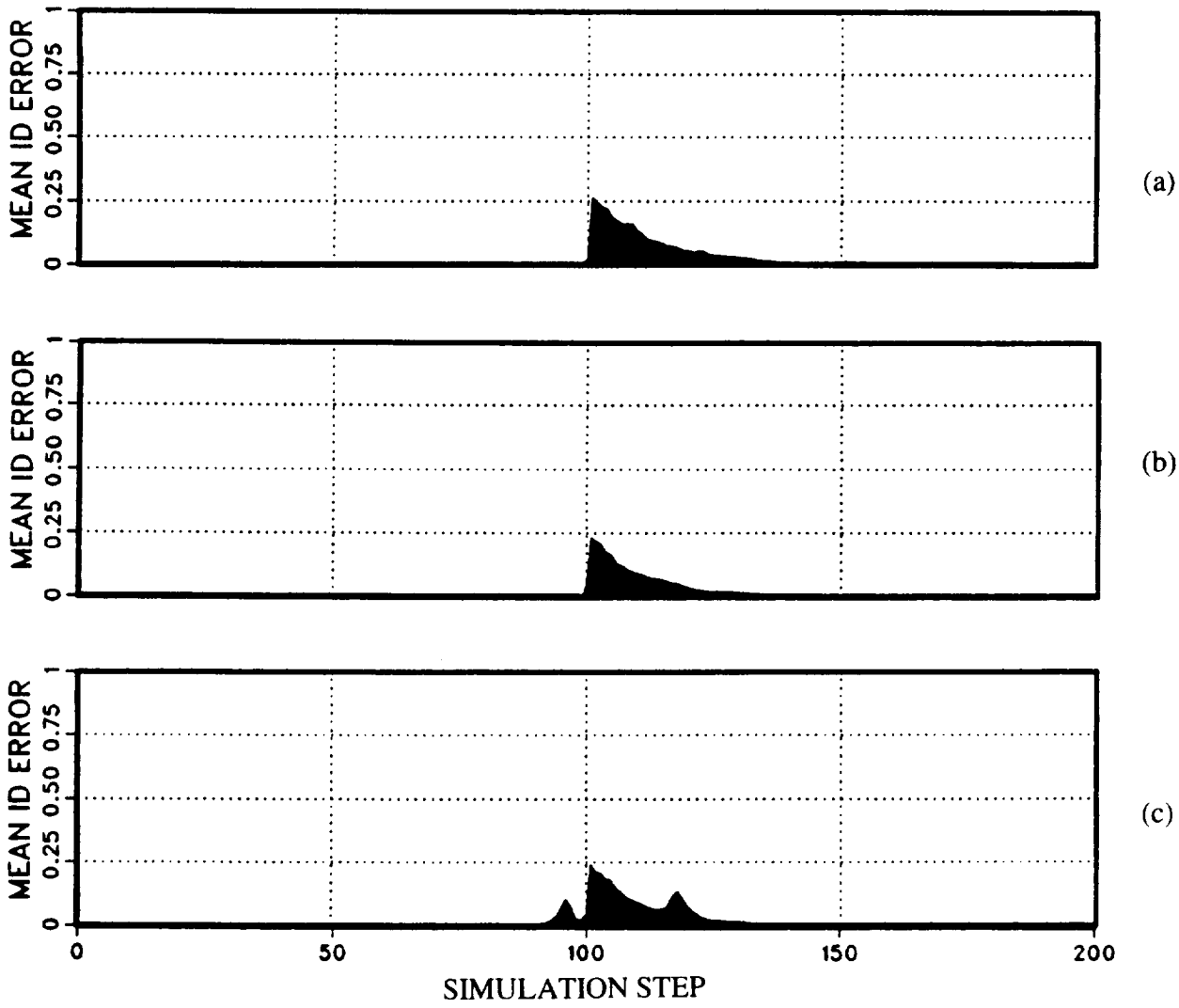

Figure 26. Open-loop generalized LMS filter identification error for no measurement noise and $\mathbf{K}_S = 0.15 * \mathbf{I}_6$, showing effect of different multi-step batch sizes n: (a) n = 4; (b) n = 6; (c) n = 8 (Local Model).

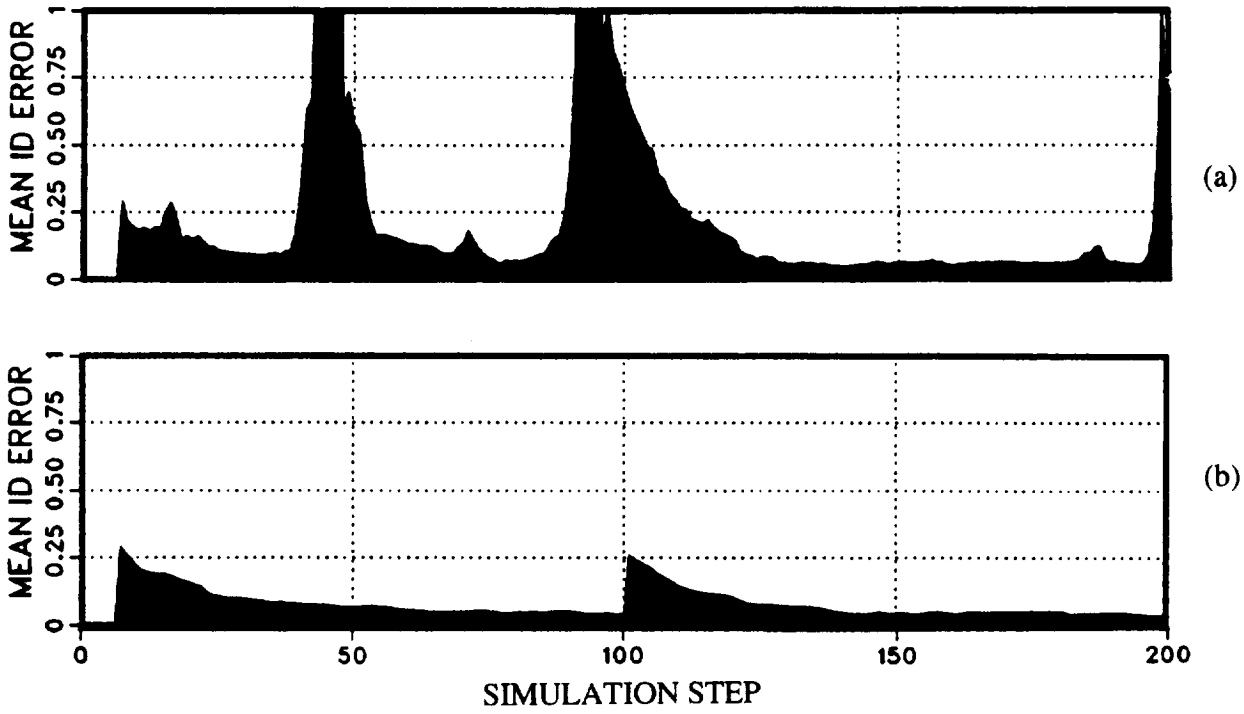

Figure 27. Open-loop generalized LMS filter identification error for 10% measurement noise and multi-step batch size n = 6: (a) $\mathbf{K}_S = 0.15 * \mathbf{I}_6$; (b) $\mathbf{K}_S = 0.05 * \mathbf{I}_6$ (Local Model).

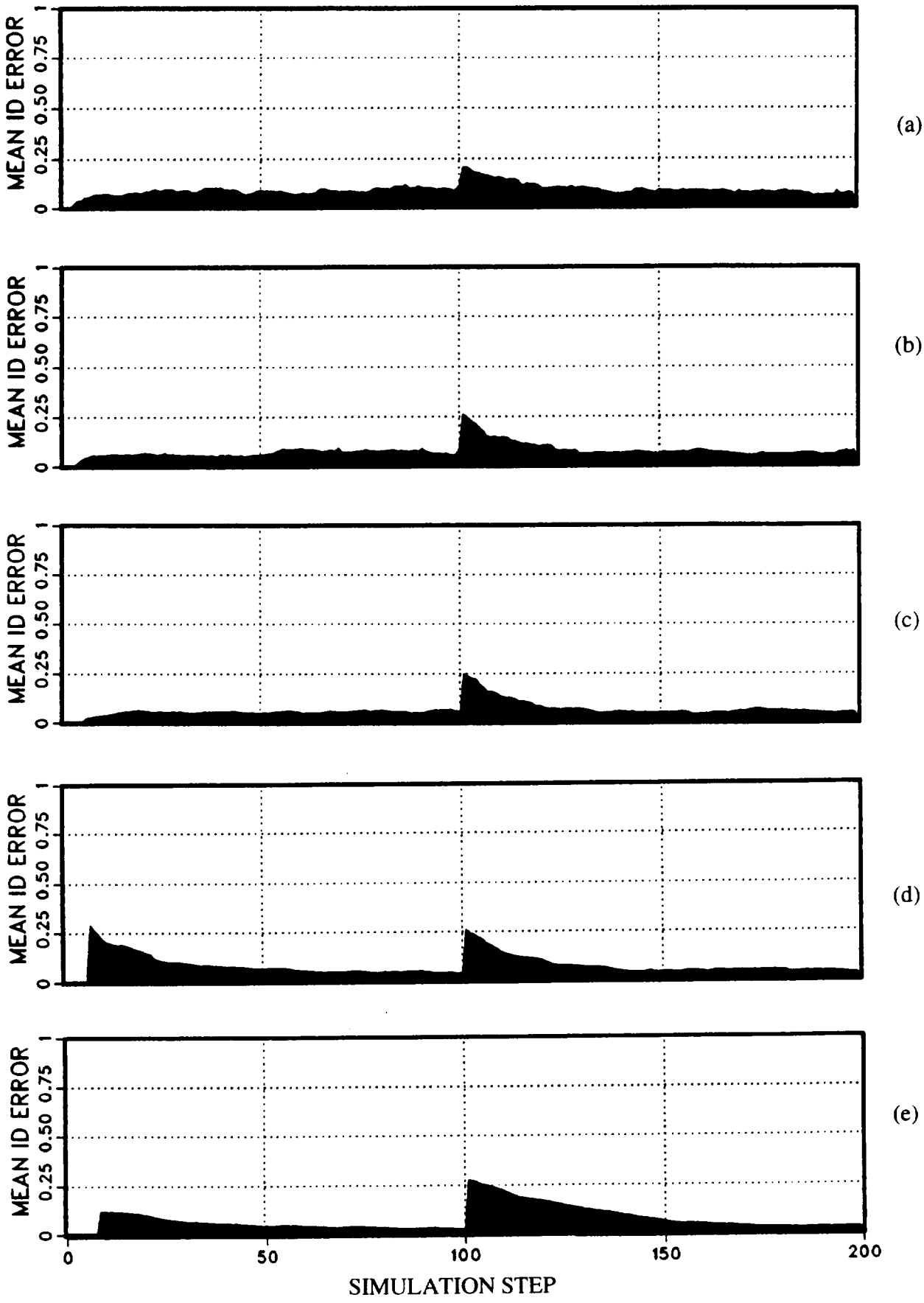

Figure 28. Open-loop generalized LMS filter identification error for 10% measurement noise showing that $\mathbf{K}_S$ must be reduced as multi-step batch size n is increased: (a) n = 1, $\mathbf{K}_S = 0.3 * \mathbf{I}_6$; (b) n = 2, $\mathbf{K}_S = 0.2 * \mathbf{I}_6$; (c) n = 4, $\mathbf{K}_S = 0.1 * \mathbf{I}_6$; (d) n = 6, $\mathbf{K}_S = 0.05 * \mathbf{I}_6$; (e) n = 8, $\mathbf{K}_S = 0.01 * \mathbf{I}_6$ (Local Model).

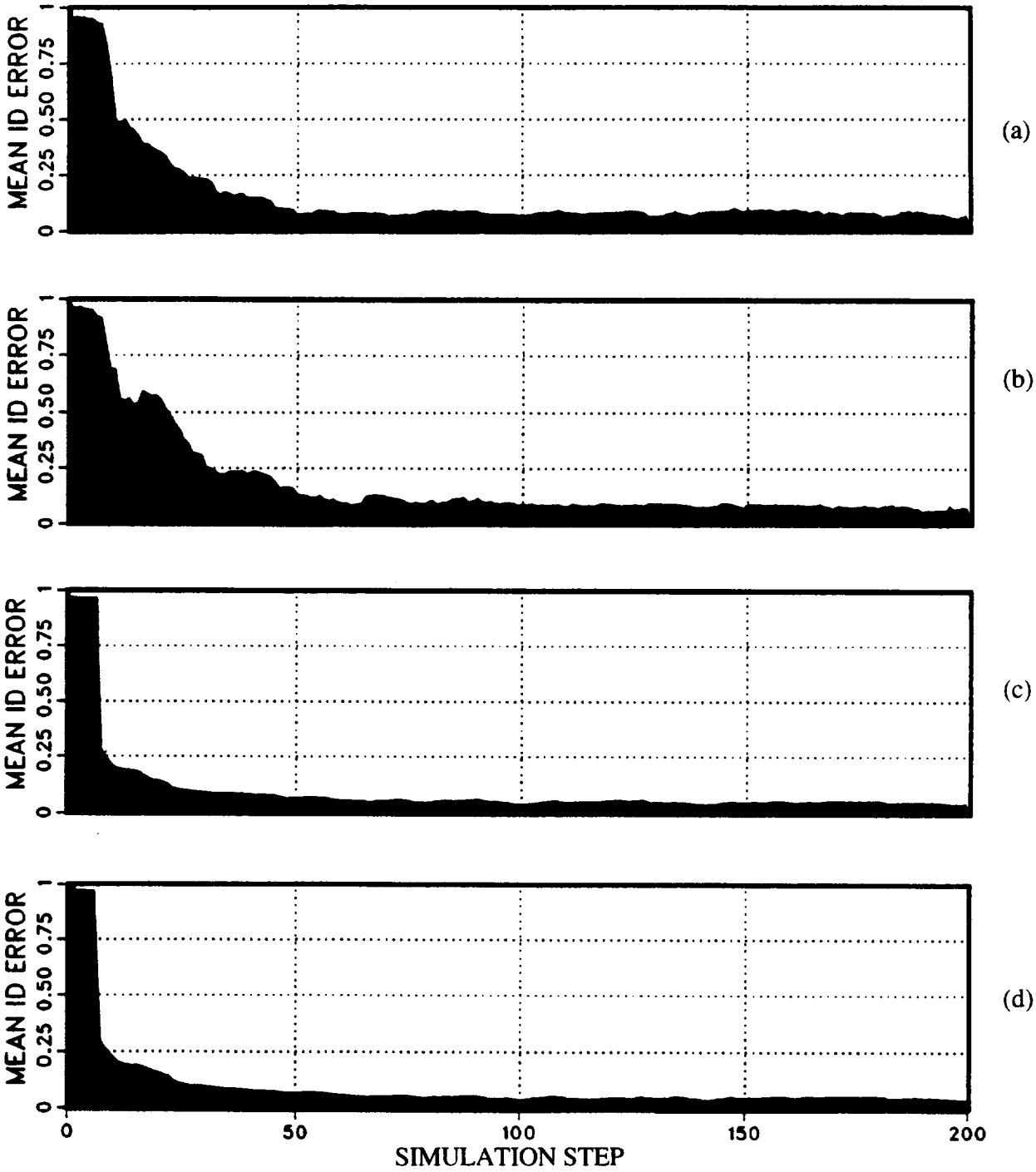

Figure 29. Comparison of open-loop identification error for 10% measurement noise and identity transfer-matrix initial conditions: (a) Kalman filter, $\mathbf{M} = 10 * \mathbf{I}_6$, $r = 1$, $\mathbf{Q} = 10 * \mathbf{I}_6$; (b) LMS filter, $\mathbf{K}_S = 0.3$; (c) generalized Kalman filter, multi-step batch size $n = 6$, $\mathbf{M} = \mathbf{I}_6$, $R = 10$; (d) generalized LMS filter, multi-step batch size $n = 6$, $\mathbf{K}_S = 0.05 * \mathbf{I}_6$ (Local Model).

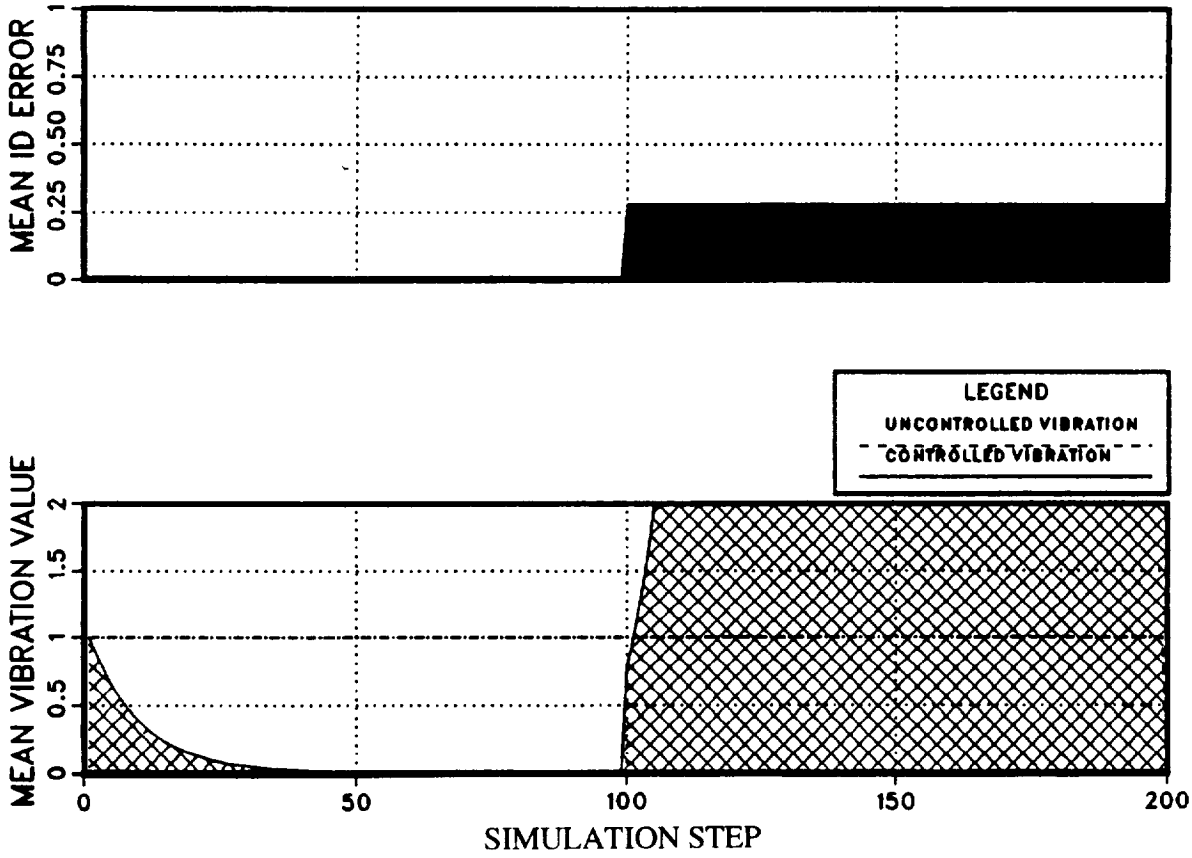

Figure 30. Plot of open-loop identification error, uncontrolled vibration, and controlled vibration levels for the case of no identification and no measurement noise (Local Model).

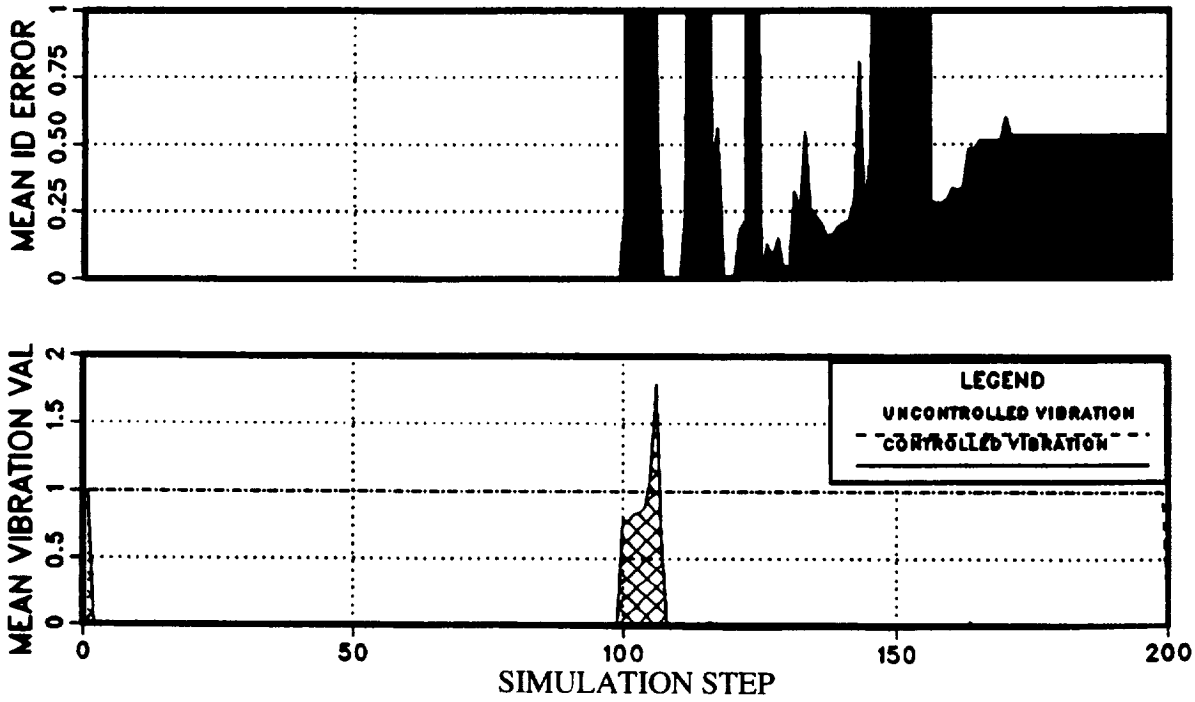

Figure 31. Closed-loop weighted-least-squares identification error and vibration for no measurement noise using batch size n = 8 (Local Model).

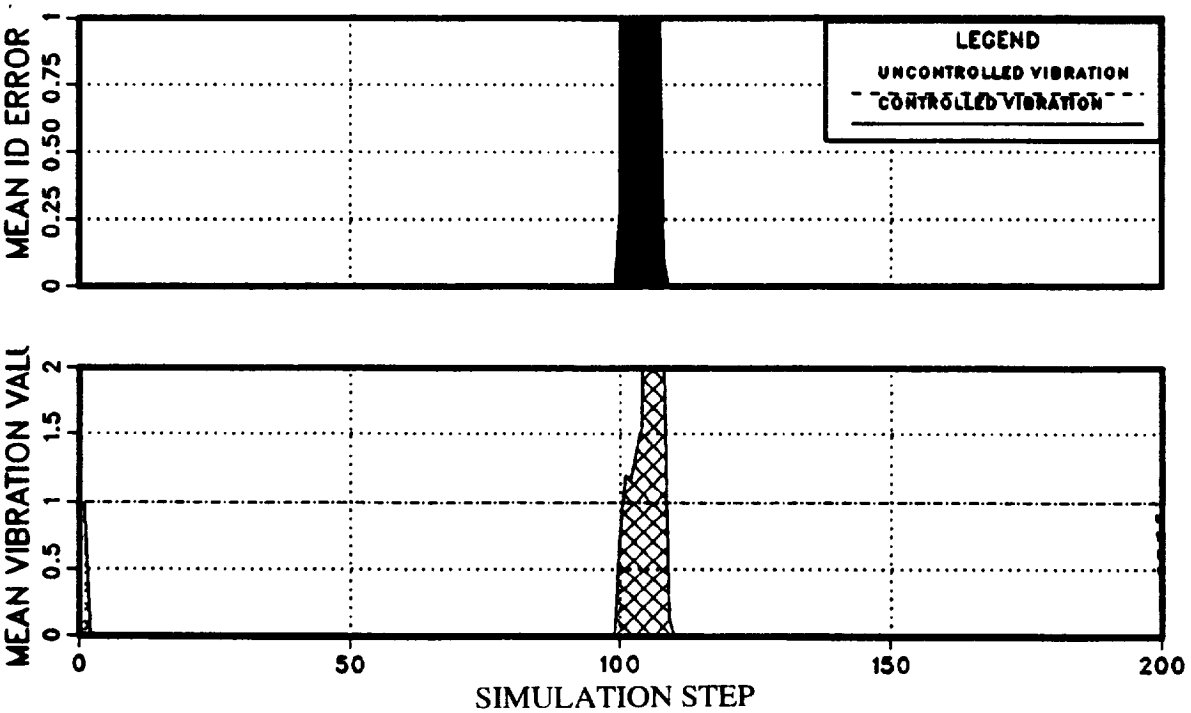

Figure 32. Closed-loop weighted-least-squares identification error and vibration for no measurement noise using batch size n = 8 and "zero-vibration" defined as 0.05 (Local Model).

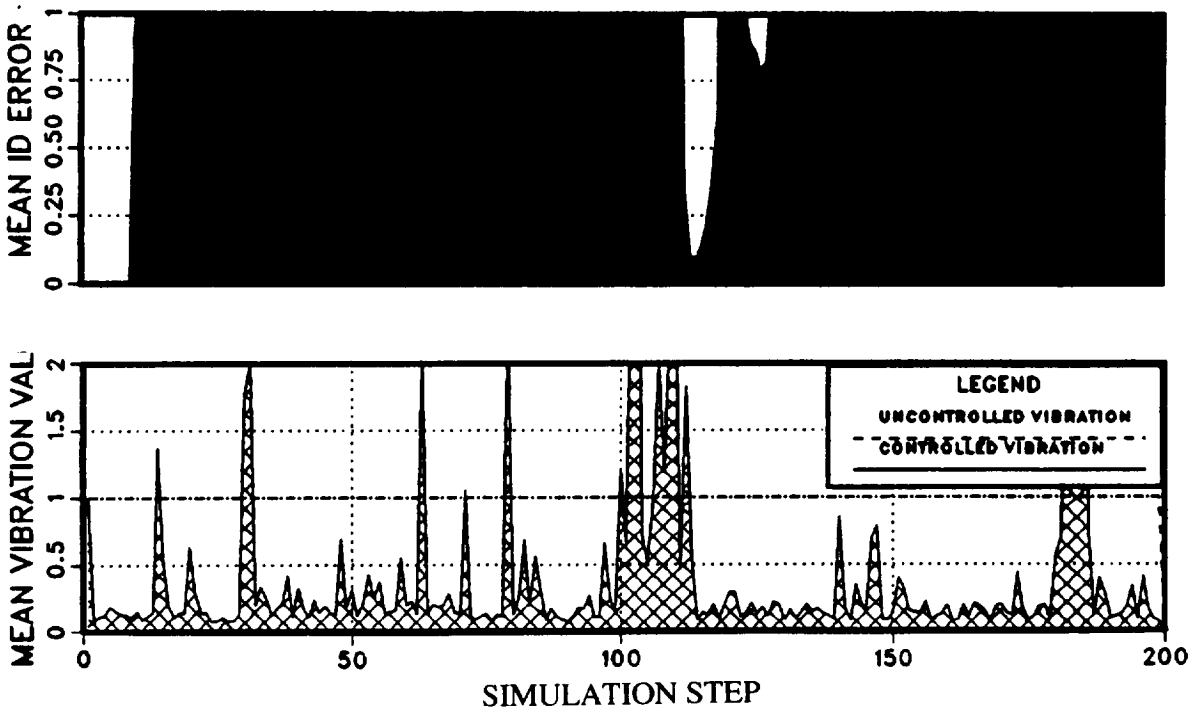

Figure 33. Closed-loop weighted-least-squares identification error and vibration for 10% measurement noise using batch size n = 8 and "zero-vibration" defined as 0.05 (Local Model).

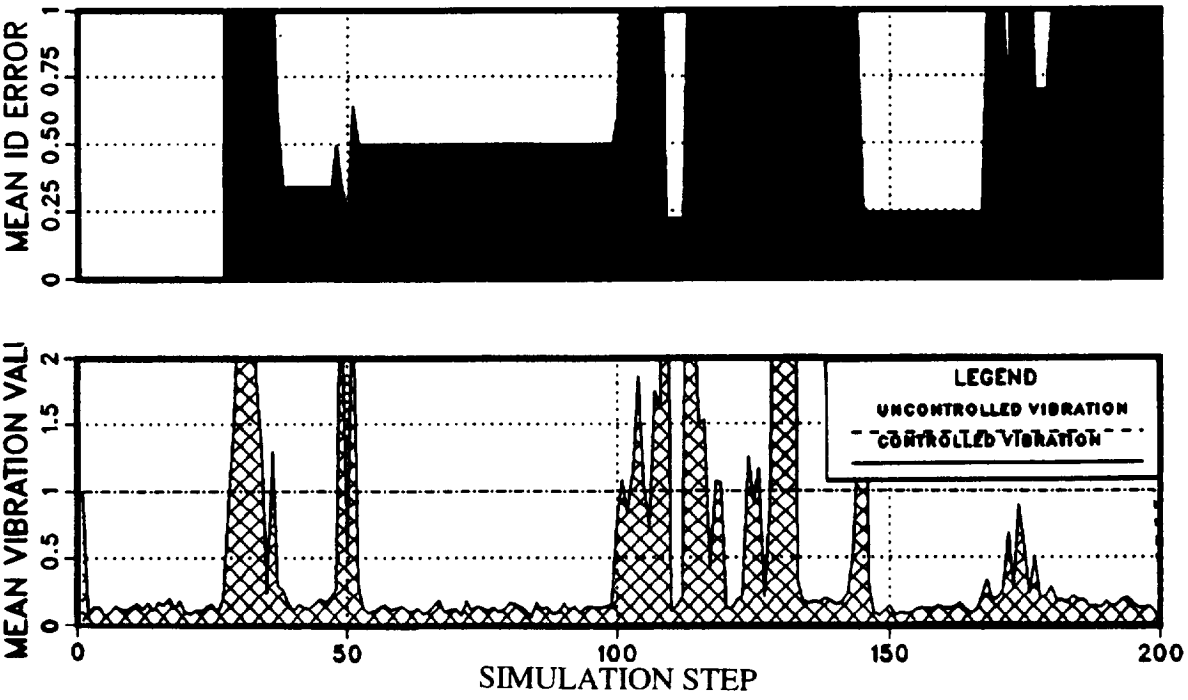

Figure 34. Closed-loop weighted-least-squares identification error and vibration for 10% measurement noise using batch size n = 8 and "zero-vibration" defined as 0.20 (Local Model).

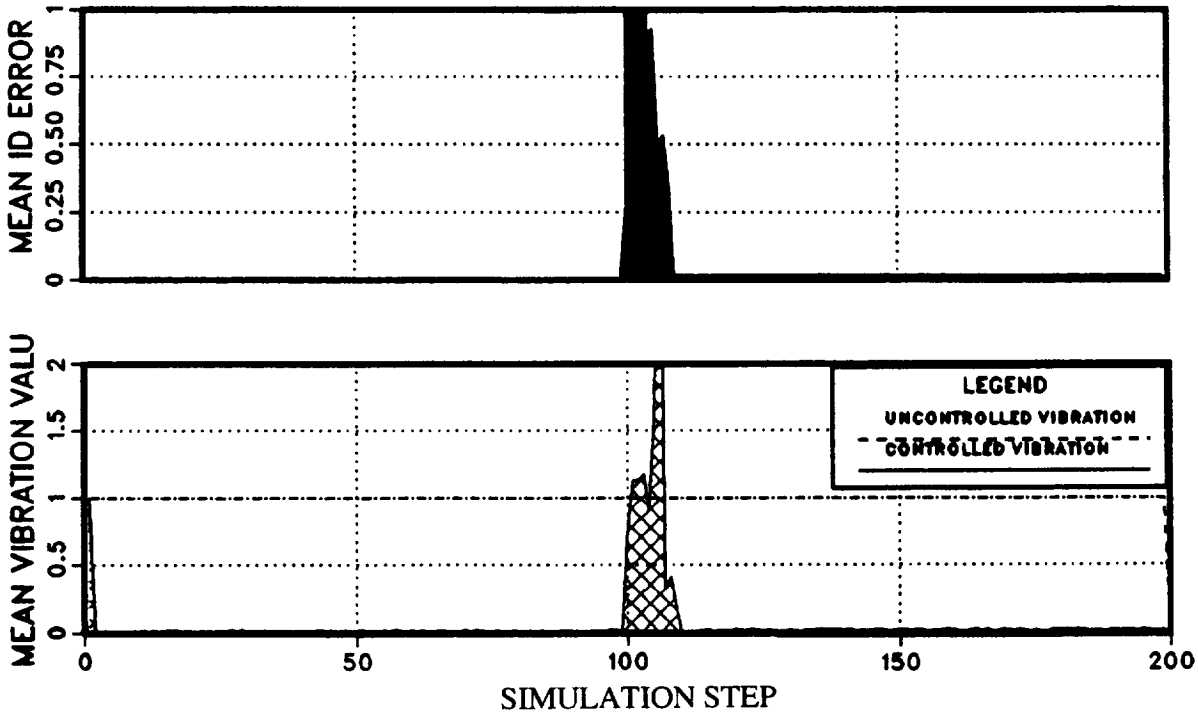

(a)

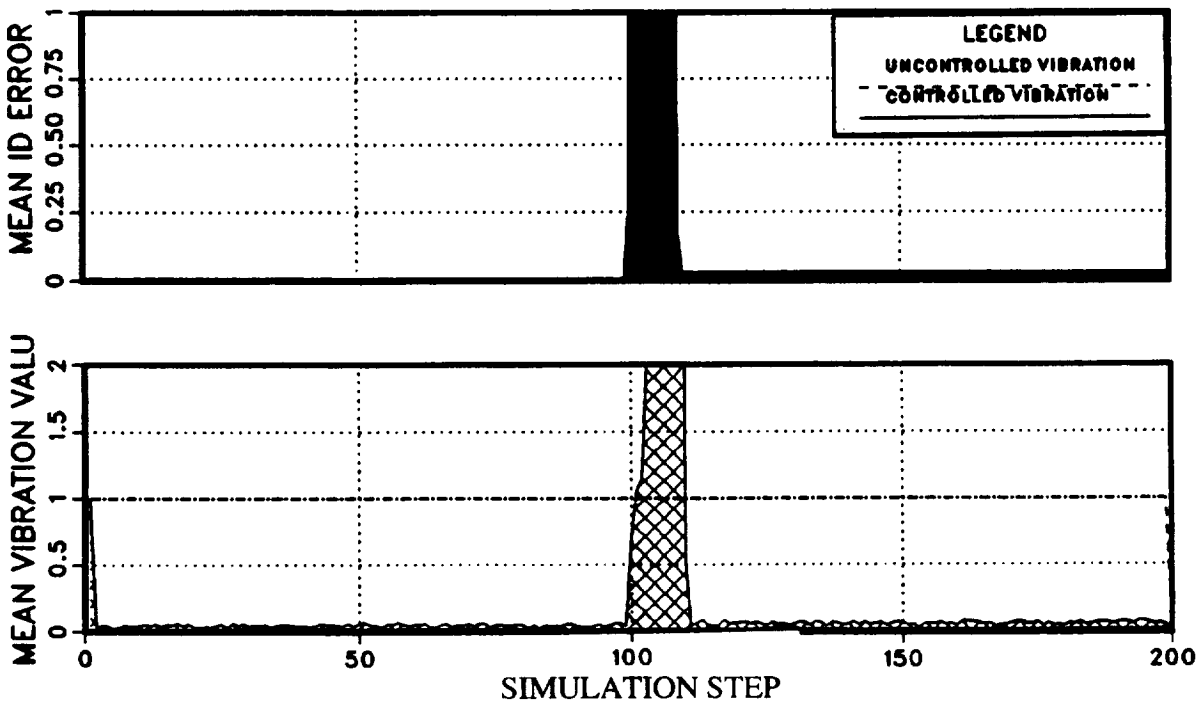

(b)

Figure 35 (part 1). Closed-loop weighted-least-squares identification error and vibration using batch size n = 8 and "zero-vibration" defined as 0.15: (a) 1% measurement noise; (b) 3% measurement noise (Local Model).

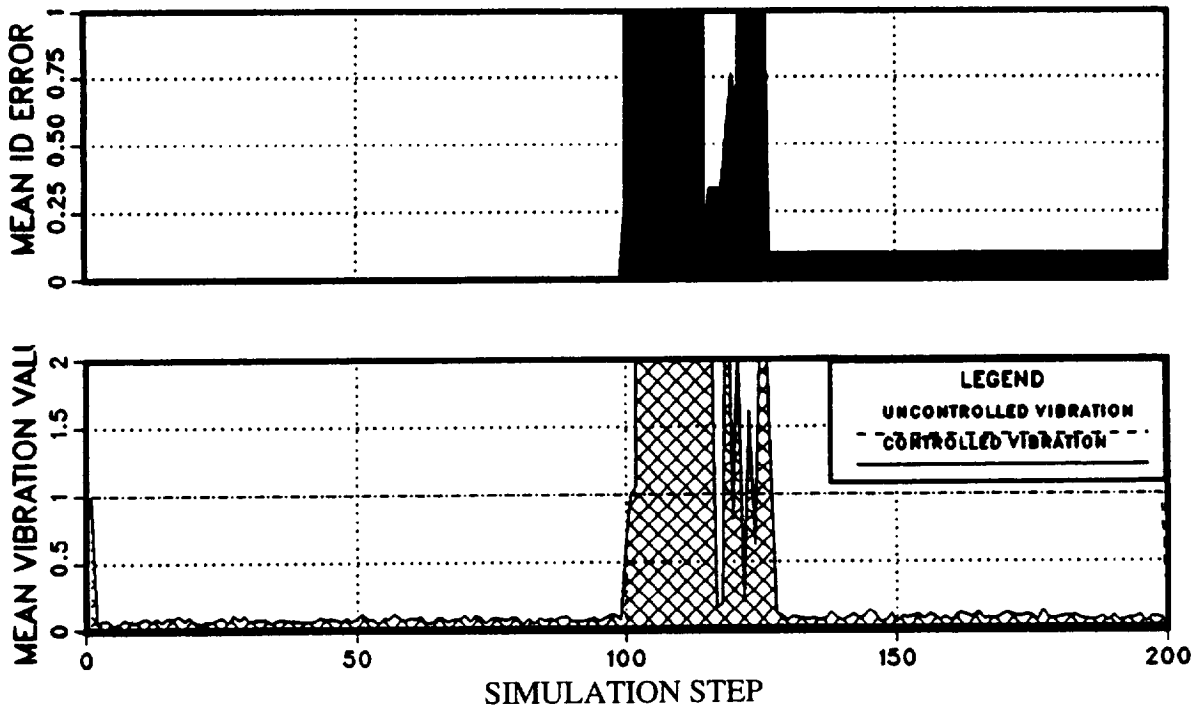

(c)

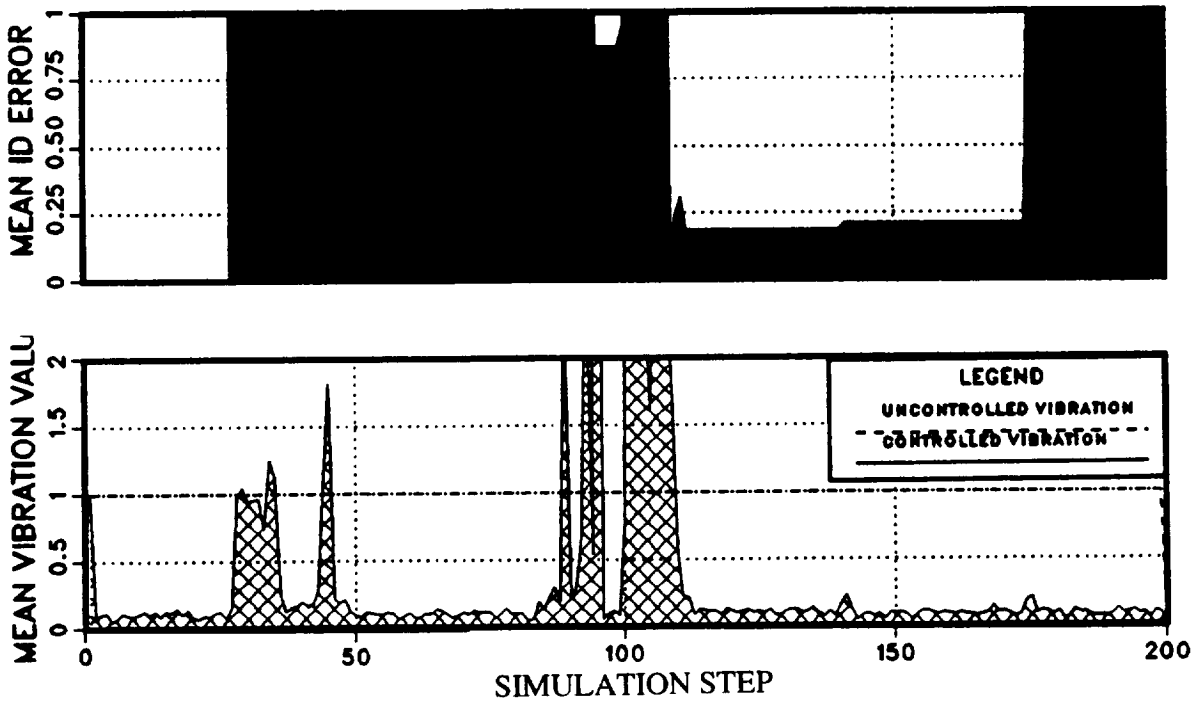

(d)

Figure 35 (part 2). Closed-loop weighted-least-squares identification error and vibration using batch size n = 8 and "zero-vibration" defined as 0.15: (c) 5% measurement noise; (d) 7.5% measurement noise (Local Model).

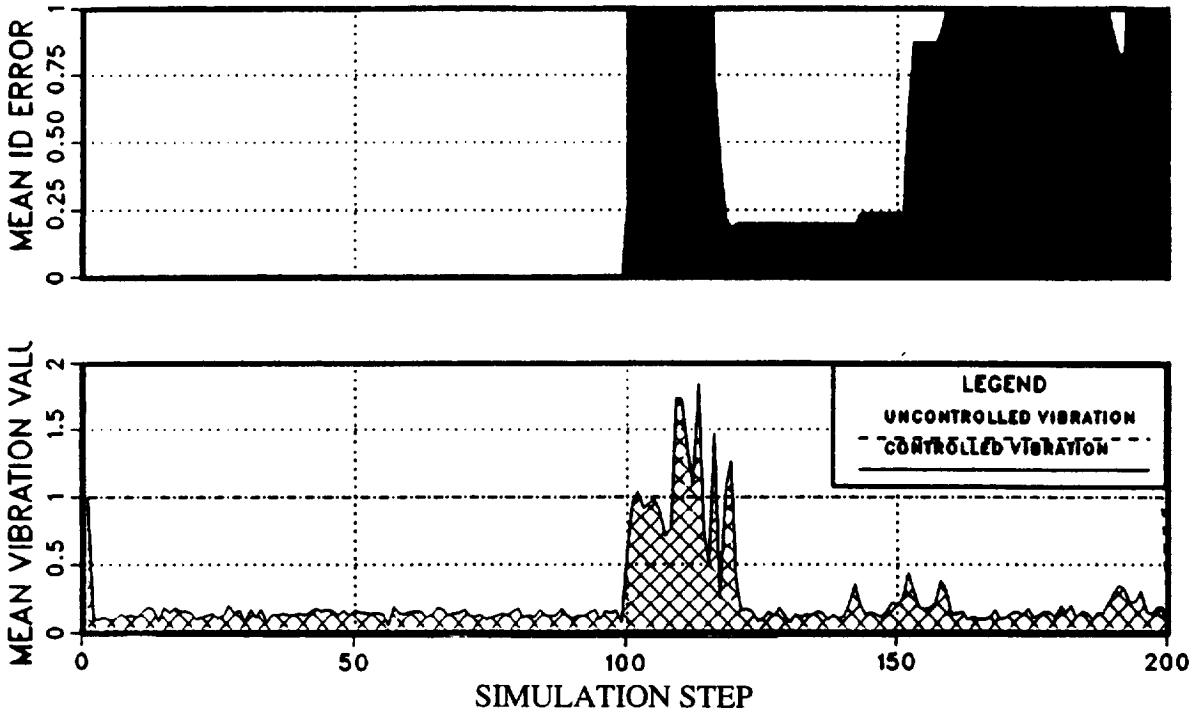

(a)

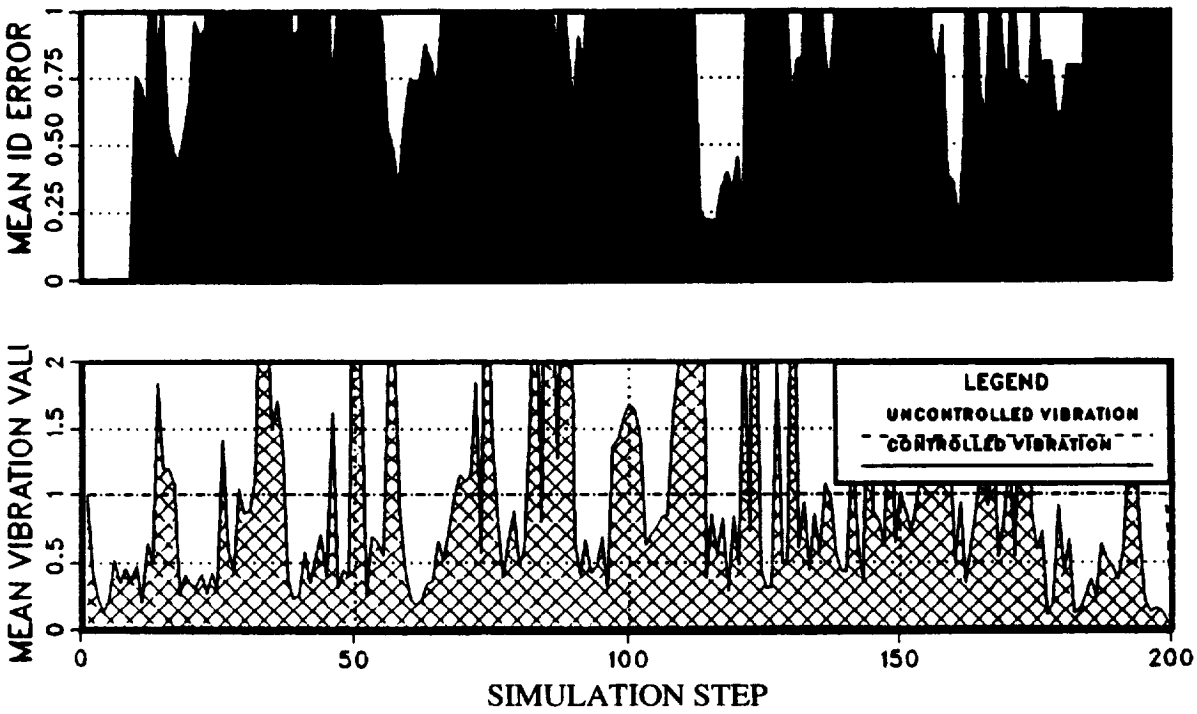

(b)

Figure 36. Closed-loop weighted-least-squares identification error and vibration for 10% measurement noise using batch size n = 8 and "zero-vibration" defined as 0.20, showing effect of random perturbation: (a) 10% probing; (b) 50% probing (Local Model).

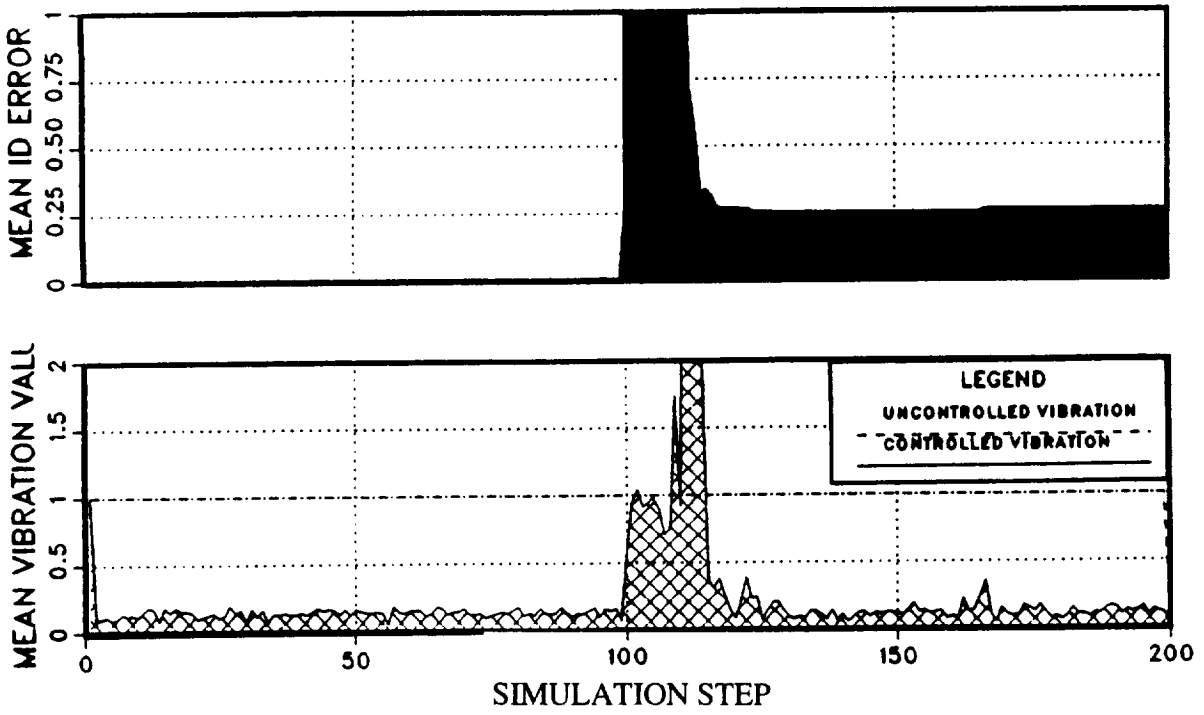

(a)

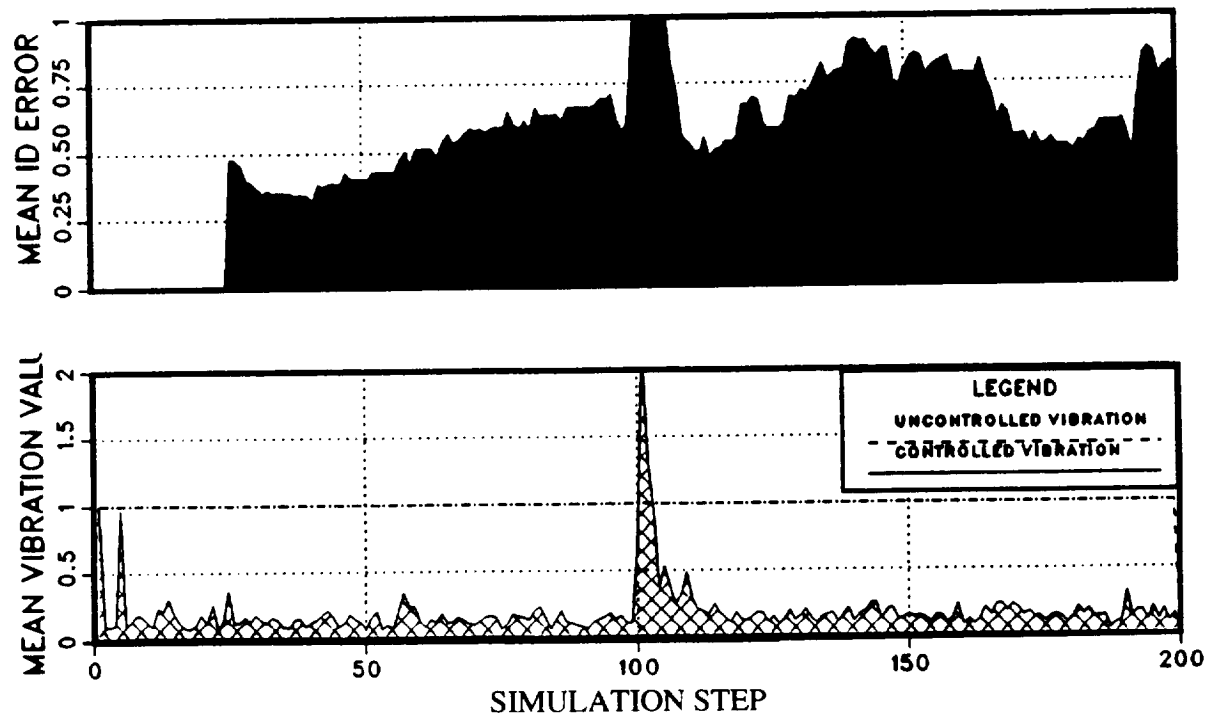

(b)

Figure 37 (part 1). Closed-loop weighted-least-squares identification error and vibration for 10% measurement noise using batch size n = 24: (a) "zero-vibration" of 0.20, 10% probing; (b) "zero-vibration" of 0.10, 10% probing (Local Model).

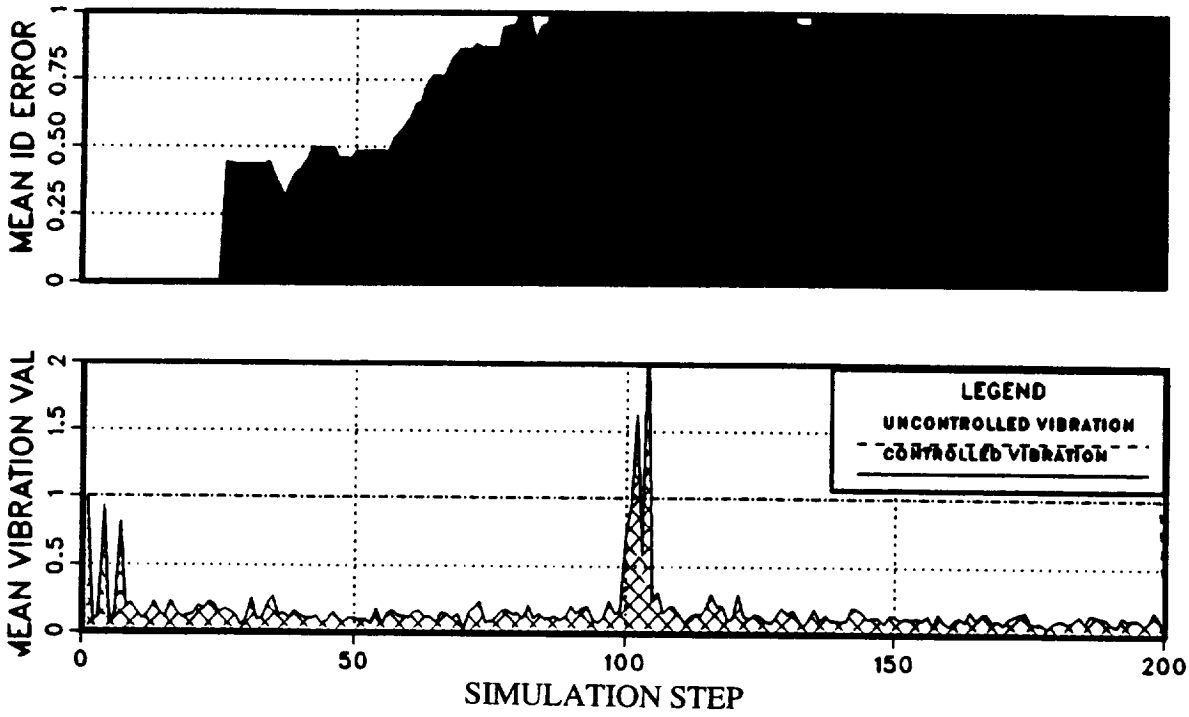

Figure 37 (part 2). Closed-loop weighted-least-squares identification error and vibration for 10% measurement noise using batch size n = 24: (c) "zero-vibration" of 0.10, 5% probing (Local Model).

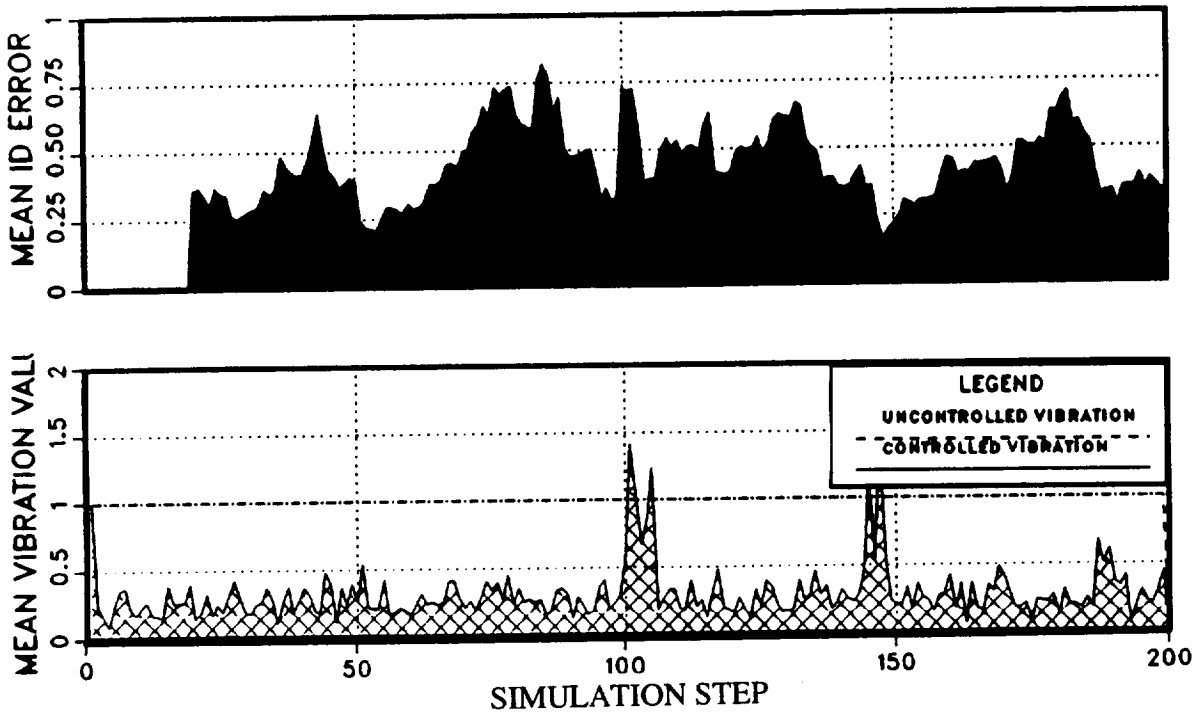

(a)

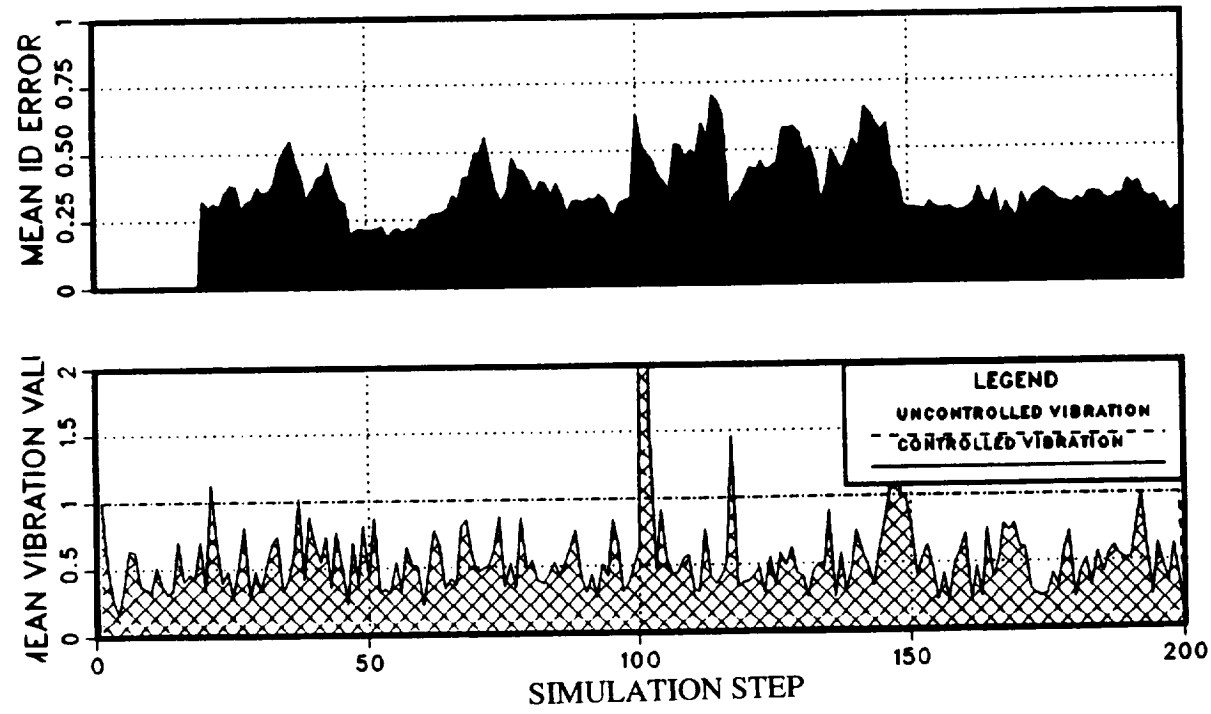

(b)

Figure 38 (part 1). Closed-loop weighted-least-squares identification error and vibration for 10% measurement noise using batch size n =18 and "zero-vibration" of 0.0: (a) 30% probing; (b) 60% probing (Local Model).

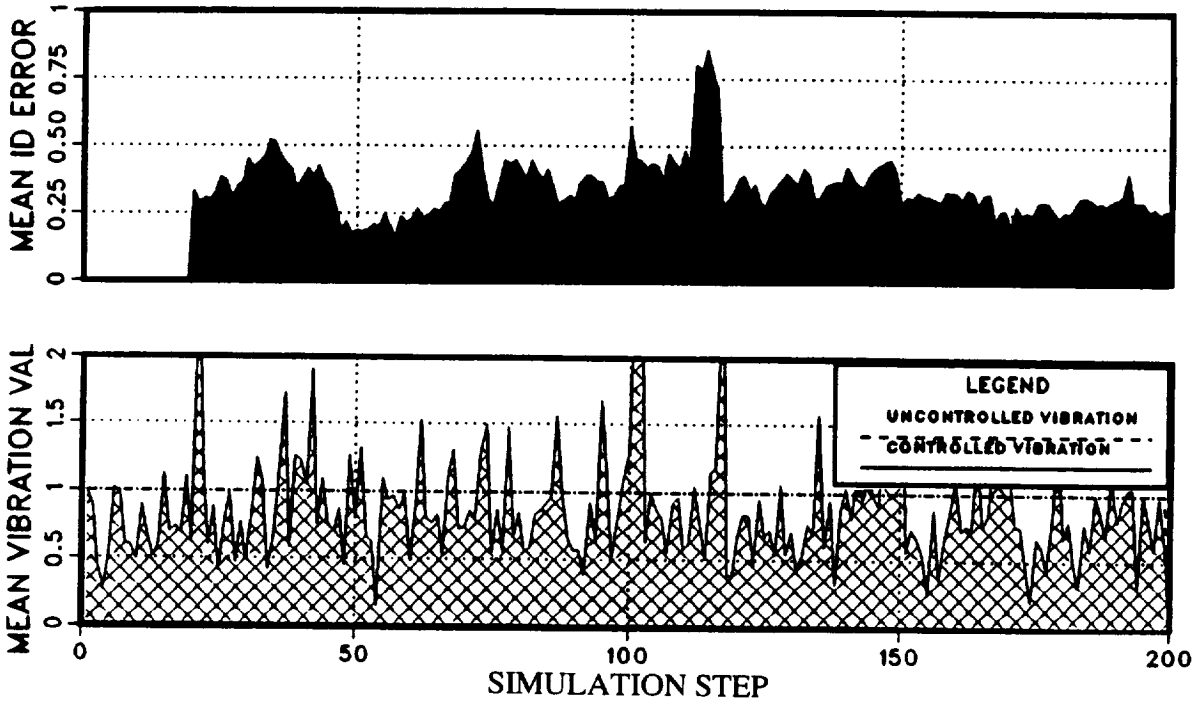

(c)

Figure 38 (part 2). Closed-loop weighted-least-squares identification error and vibration for 10% measurement noise using batch size n =18 and "zero-vibration" of 0.0: (c) 100% probing (Local Model).

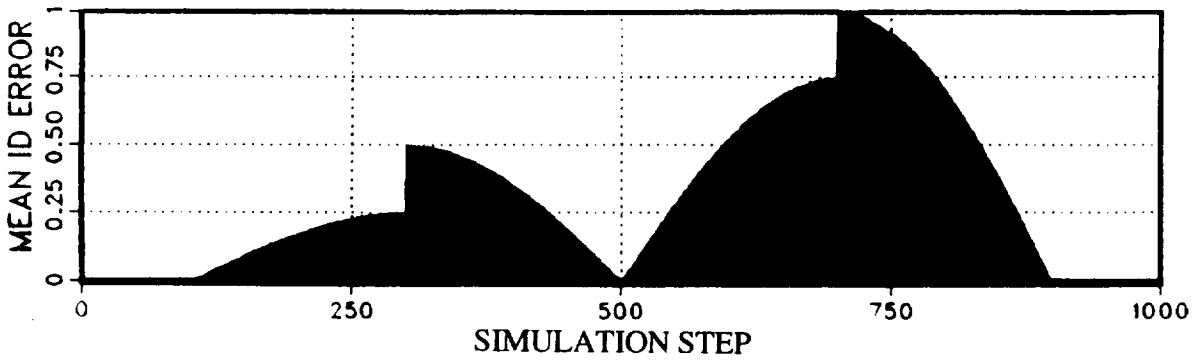

Figure 39. Identification error produced by variation of the system transfer matrix for the case of no on-line identification (Local Model).

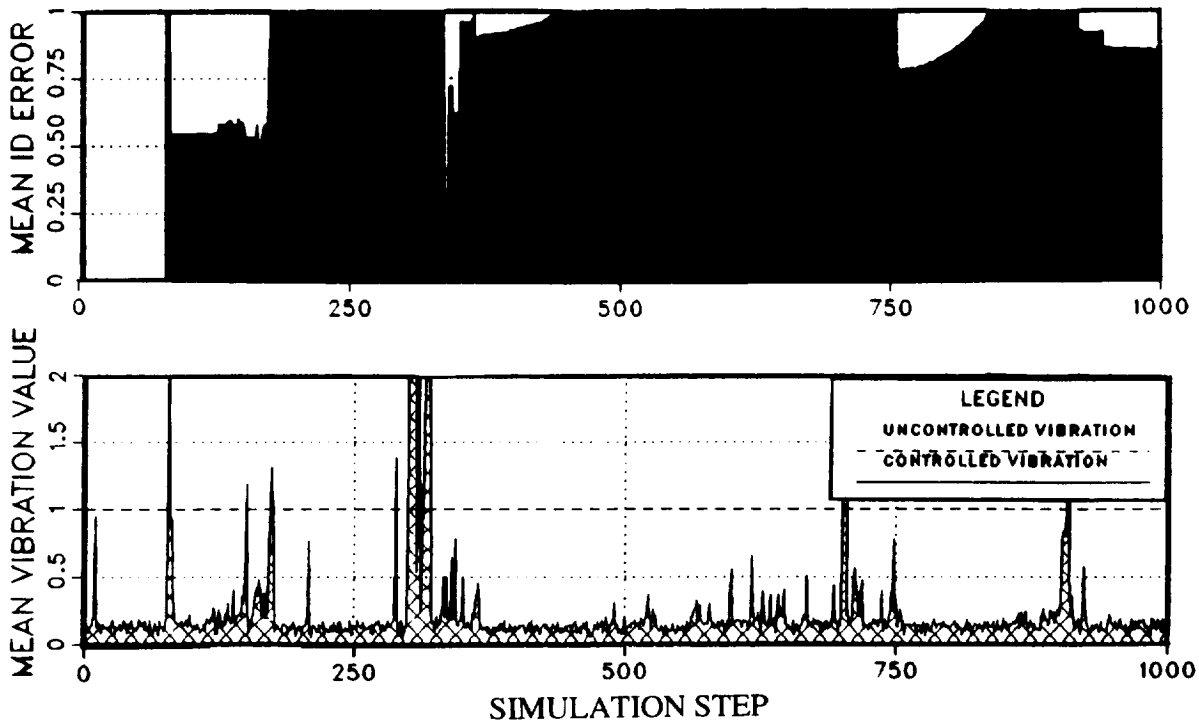

Figure 40. Closed-loop weighted-least-squares identification error and vibration for 10% measurement noise using batch size n = 24: "zero-vibration" of 0.20 for the case of continuous transfer-matrix variation (Local Model).

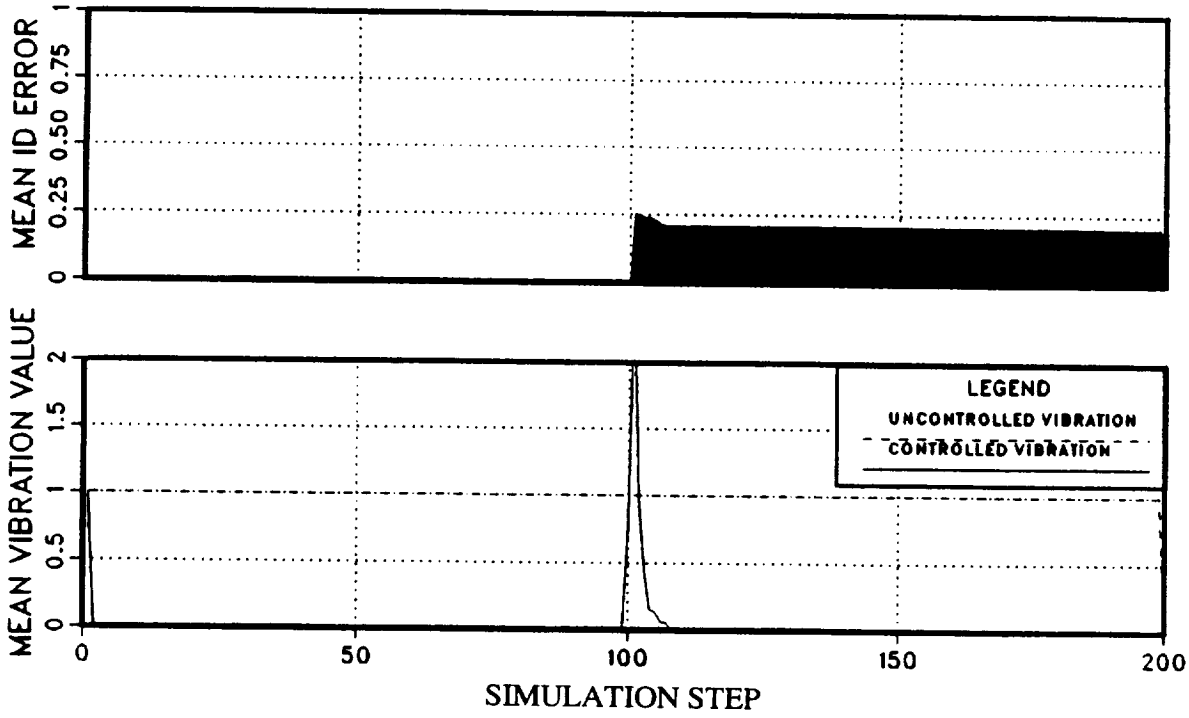

(a)

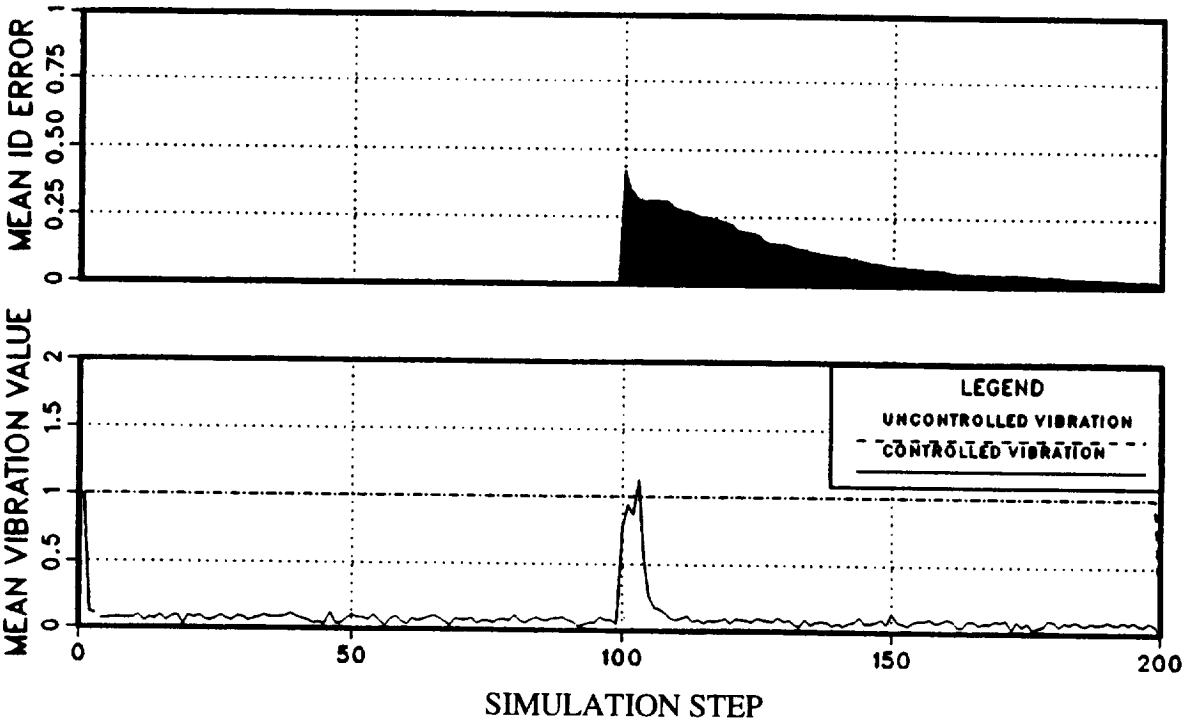

(b)

Figure 41. Closed-loop Kalman filter identification error and vibration for no measurement noise, r = 1, $\mathbf{M} = 10 * \mathbf{I}_6$, $\mathbf{Q} = 10 * \mathbf{I}_6$: (a) no probing; (b) 10% probing (Local Model).

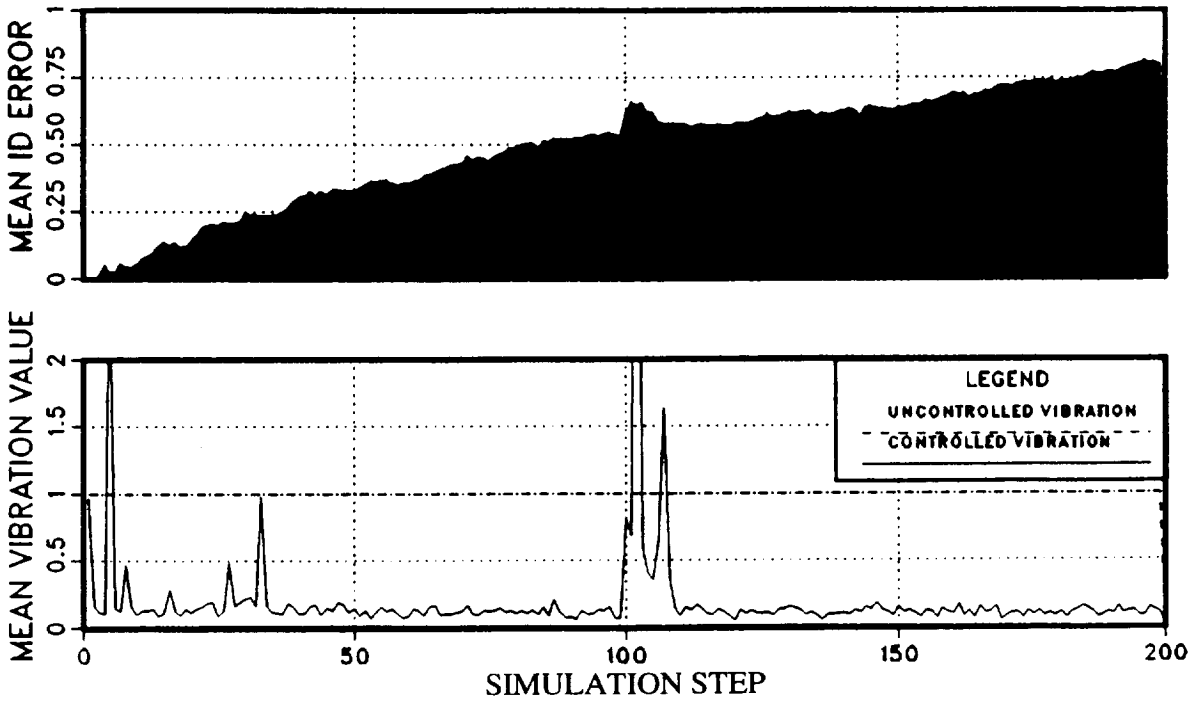

Figure 42. Closed-loop Kalman filter identification error and vibration for 10% measurement noise, r = 1, $\mathbf{M} = 10 * \mathbf{I}_6$, and $\mathbf{Q} = 10 * \mathbf{I}_6$, showing identification instability without probing (Local Model).

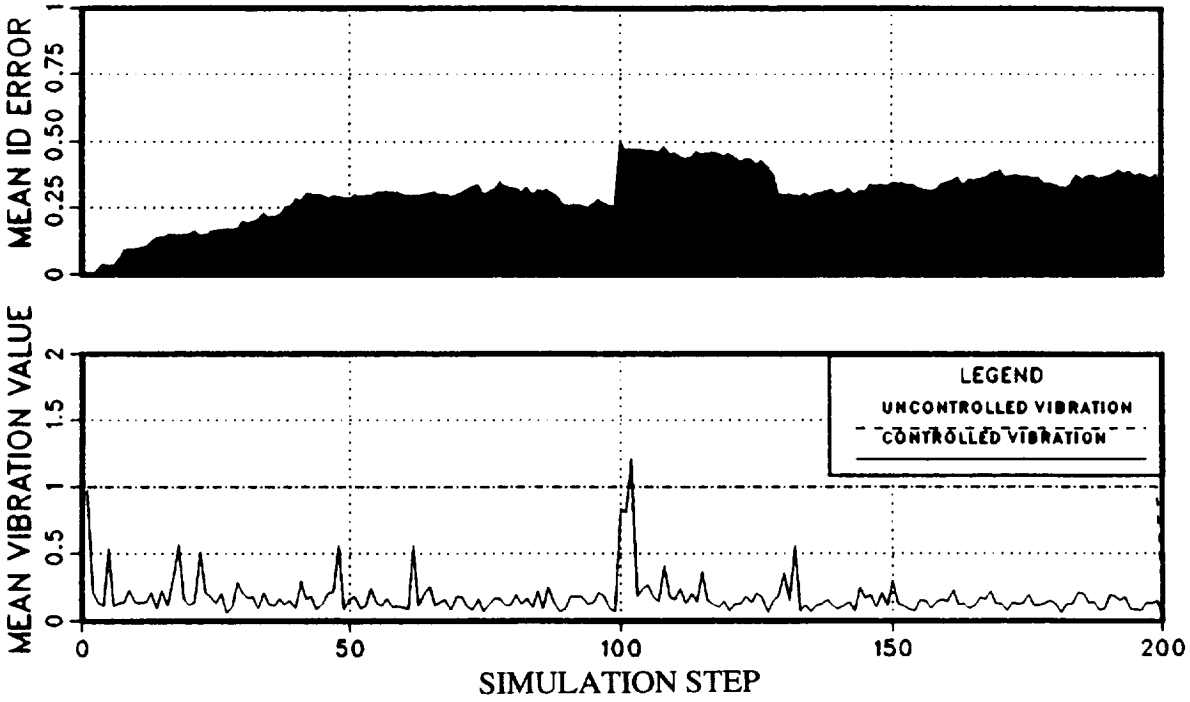

Figure 43. Closed-loop Kalman filter identification error and vibration for 10% measurement noise, r = 1, $\mathbf{M} = 10 * \mathbf{I}_6$, $\mathbf{Q} = 10 * \mathbf{I}_6$, and 10% probing (Local Model).

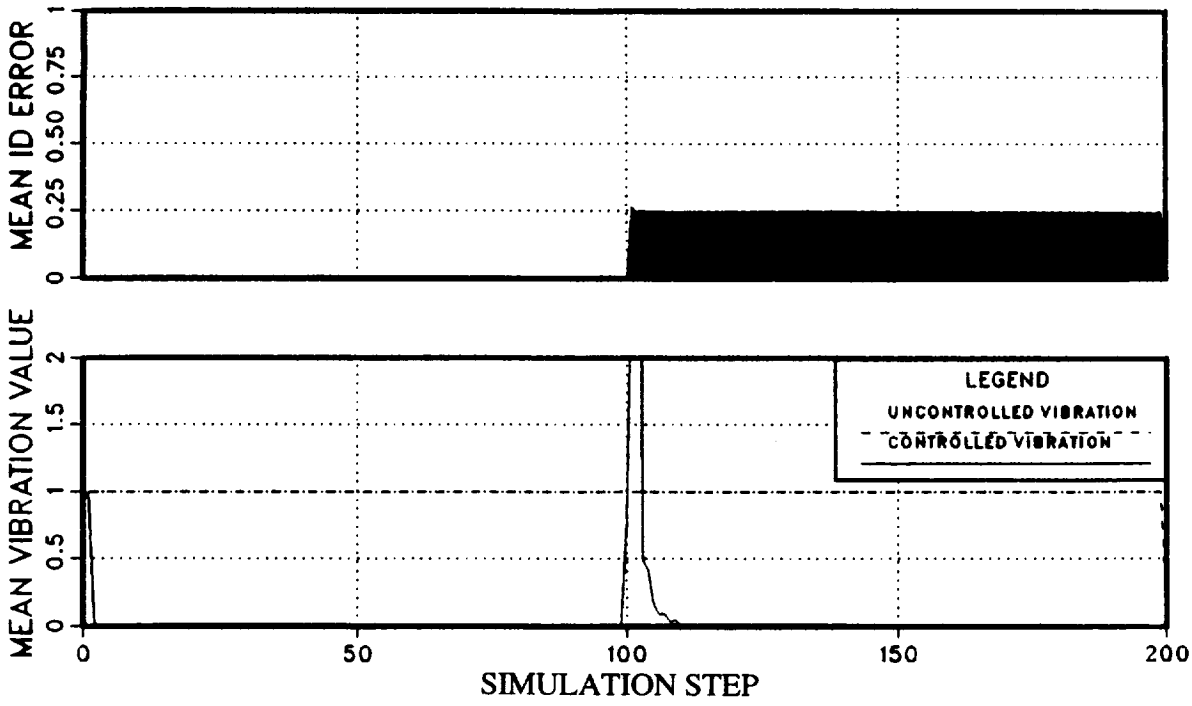

Figure 44. Closed-loop Kalman filter identification error and vibration for no measurement noise, r = 100, $\mathbf{M} = \mathbf{I}_6$, and $\mathbf{Q} = 10 * \mathbf{I}_6$ (Local Model).

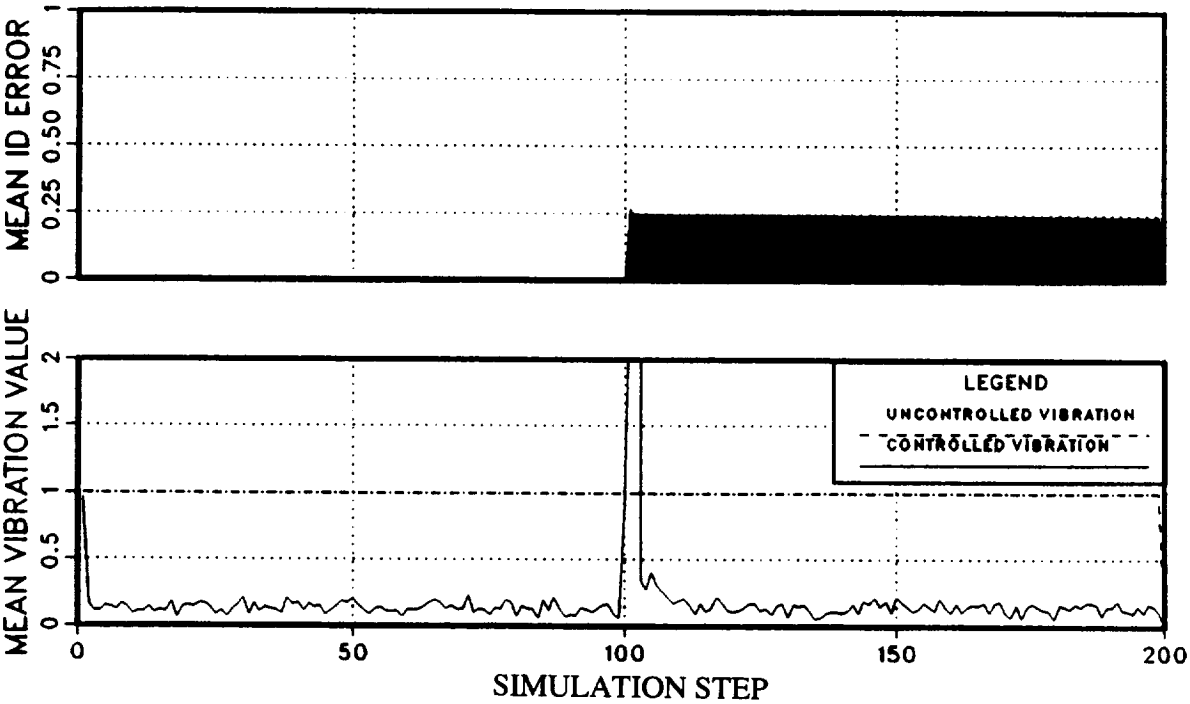

Figure 45. Closed-loop Kalman filter identification error and vibration for 10% measurement noise, r = 100, $\mathbf{M} = \mathbf{I}_6$, and $\mathbf{Q} = 10 * \mathbf{I}_6$ (Local Model).

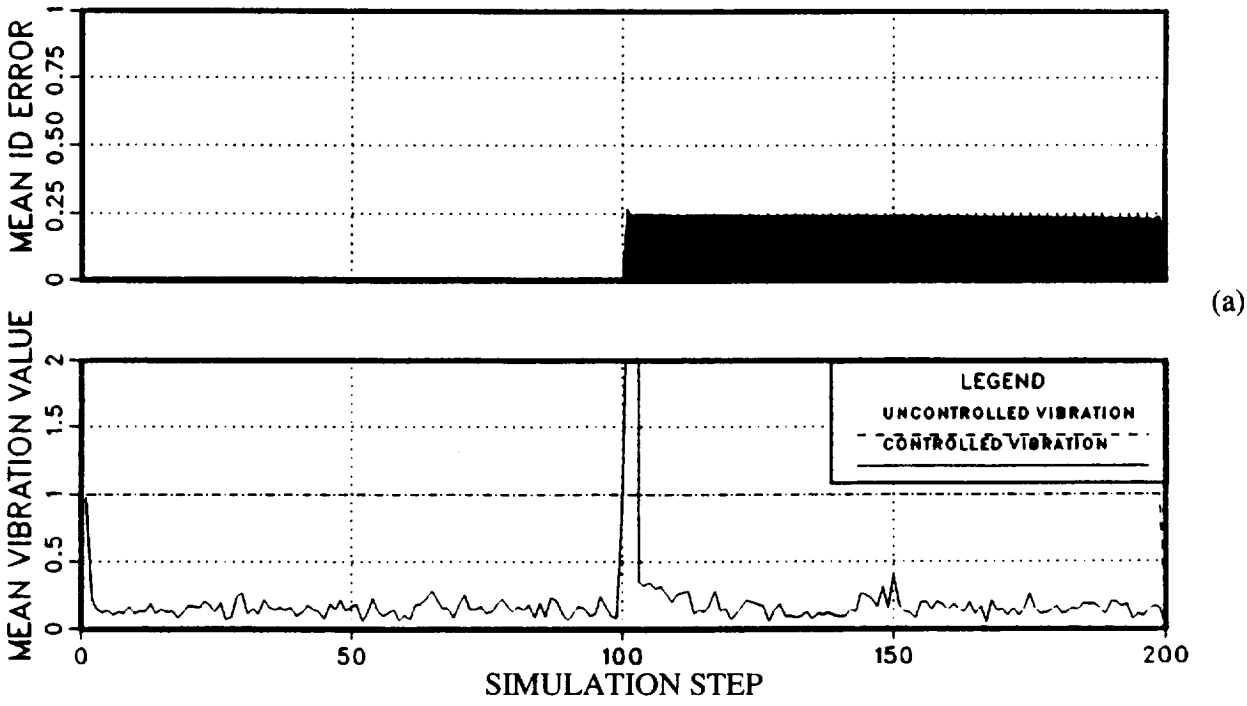

(a)

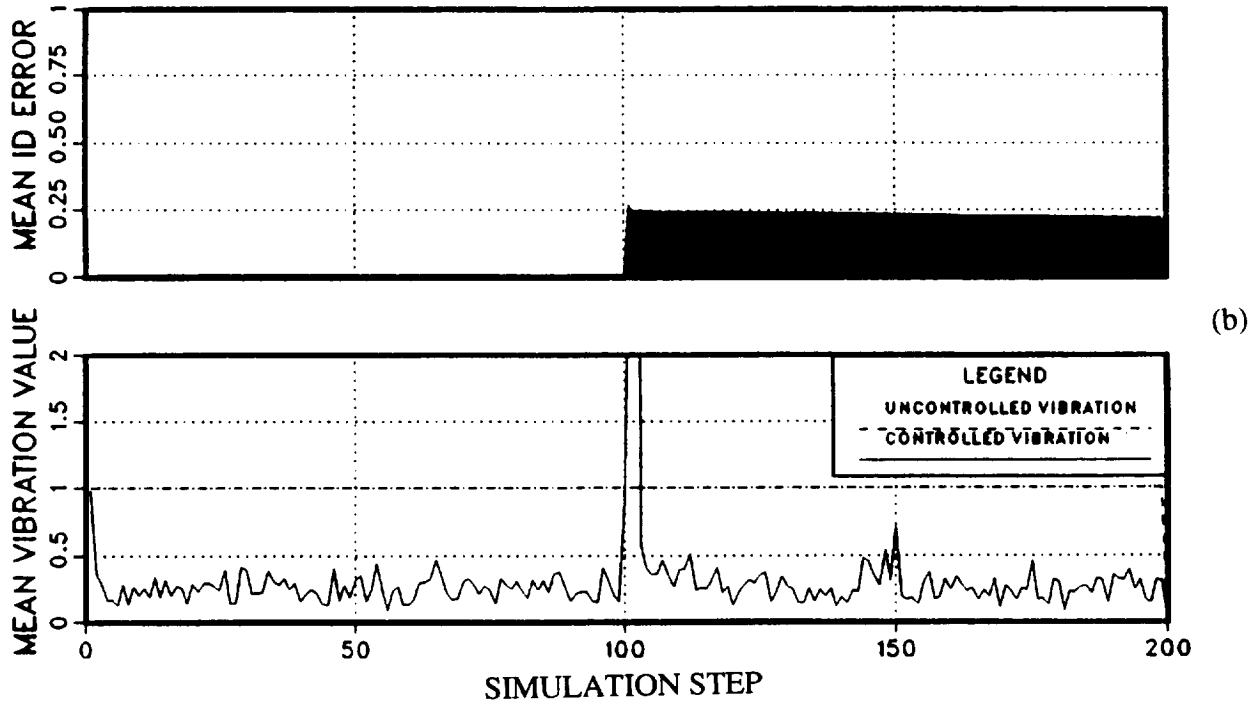

(b)

Figure 46 (part 1). Closed-loop Kalman filter identification error and vibration for 10% measurement noise, r = 100, $\mathbf{M} = \mathbf{I}_6$, $\mathbf{Q} = 10 * \mathbf{I}_6$: (a) 10% probing; (b) 30% probing (Local Model).

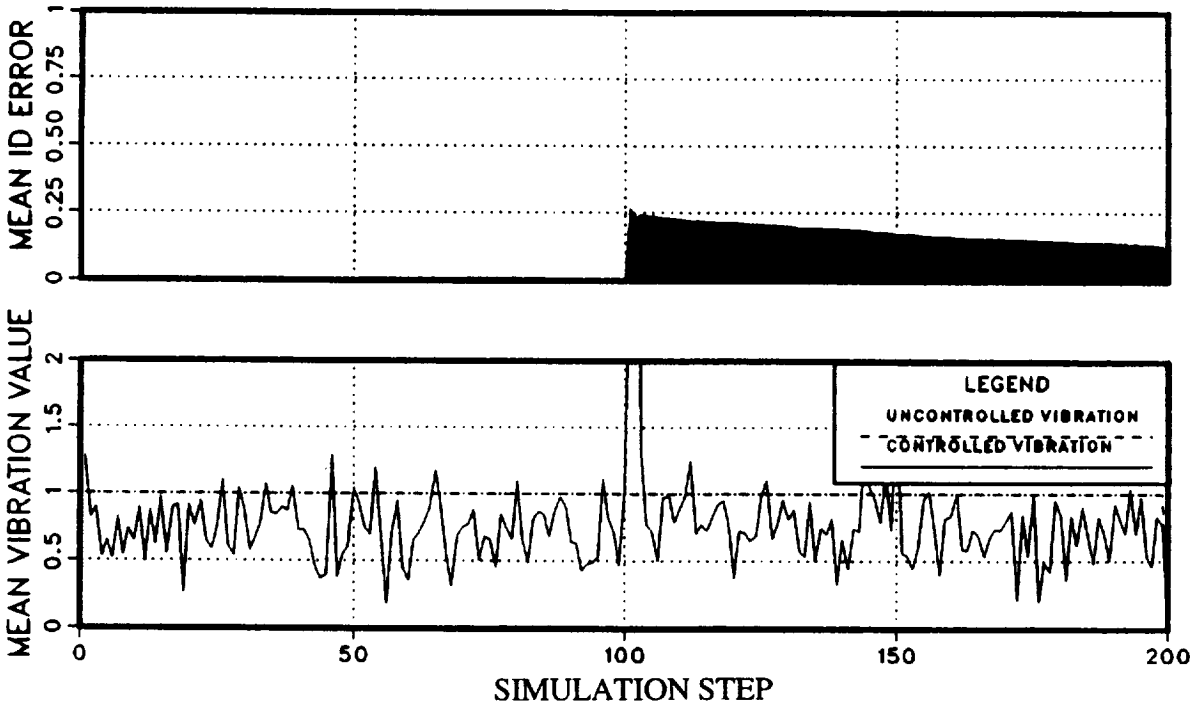

(c)

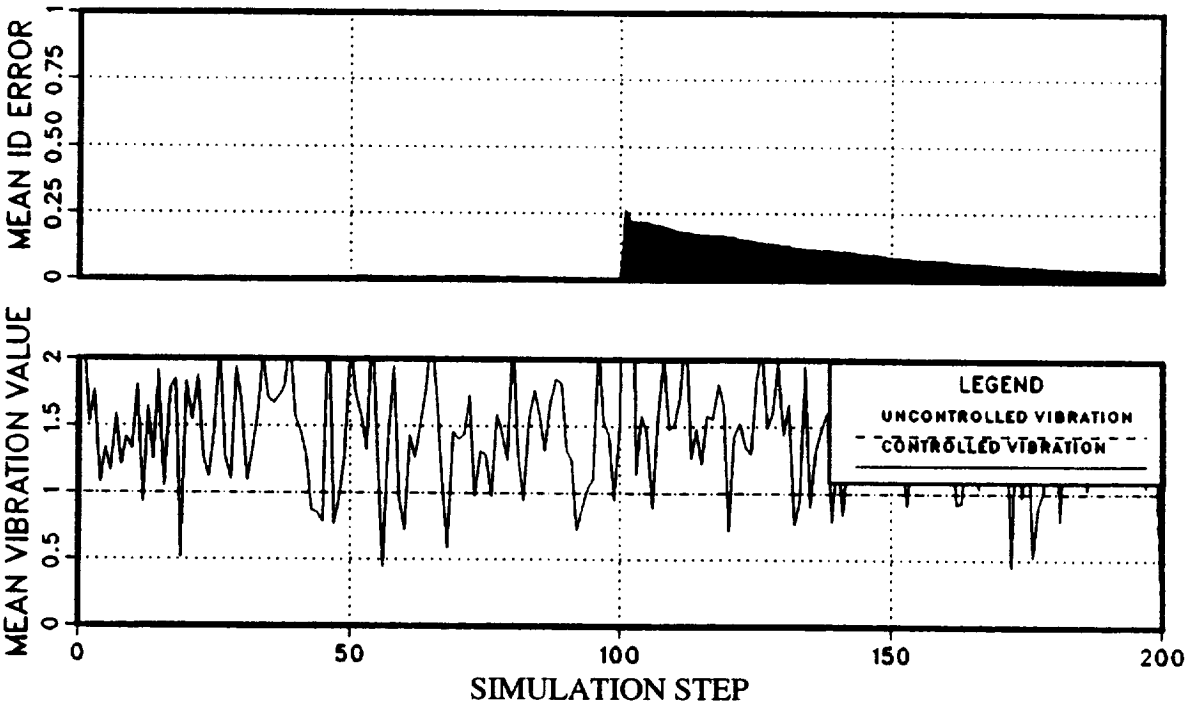

(d)

Figure 46 (part 2). Closed-loop Kalman filter identification error and vibration for 10% measurement noise, r = 100, $\mathbf{M} = \mathbf{I}_6$, $\mathbf{Q} = 10 * \mathbf{I}_6$: (c) 100% probing; (d) 200% probing (Local Model).

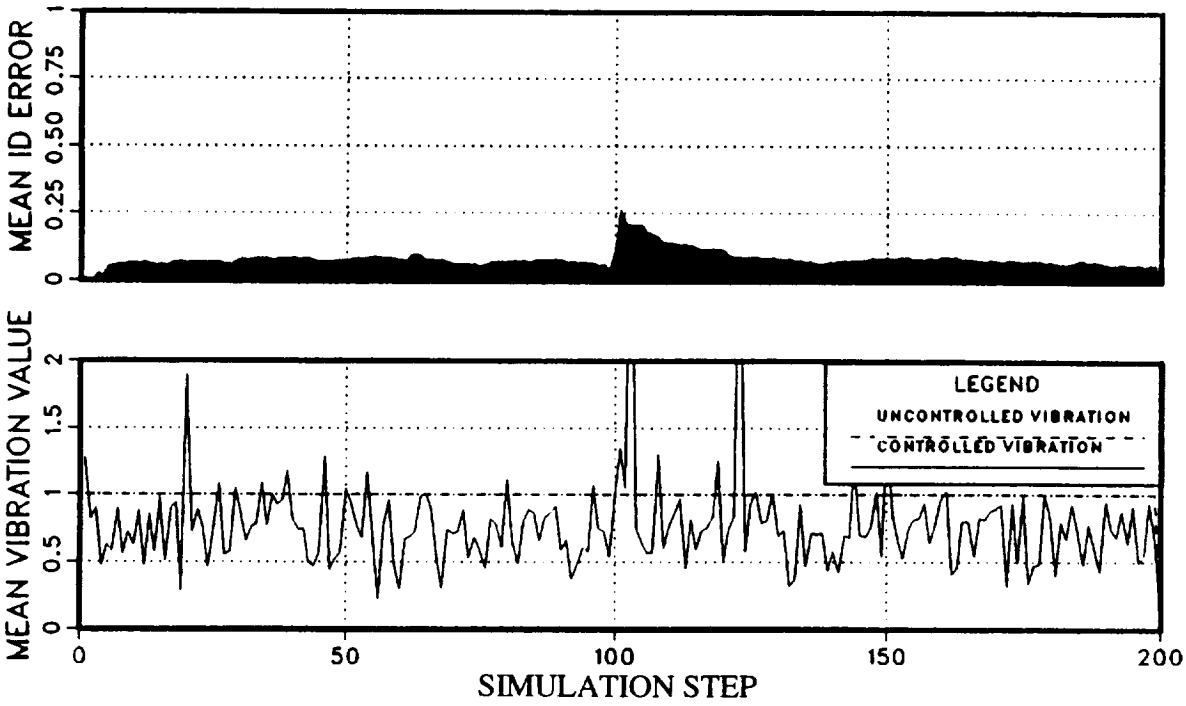

Figure 47. Closed-loop Kalman filter identification error and vibration for 10% measurement noise, r = 1, $\mathbf{M} = 10 * \mathbf{I}_6$, $\mathbf{Q} = 10 * \mathbf{I}_6$, and 100% probing (Local Model).

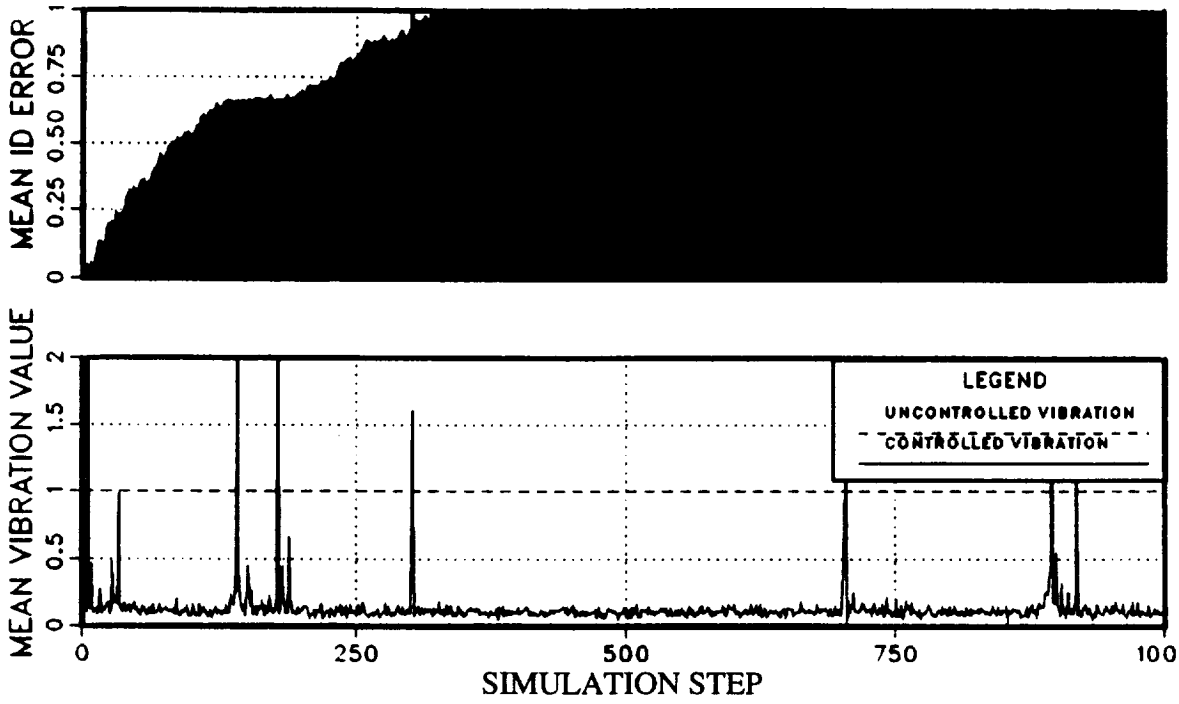

(a)

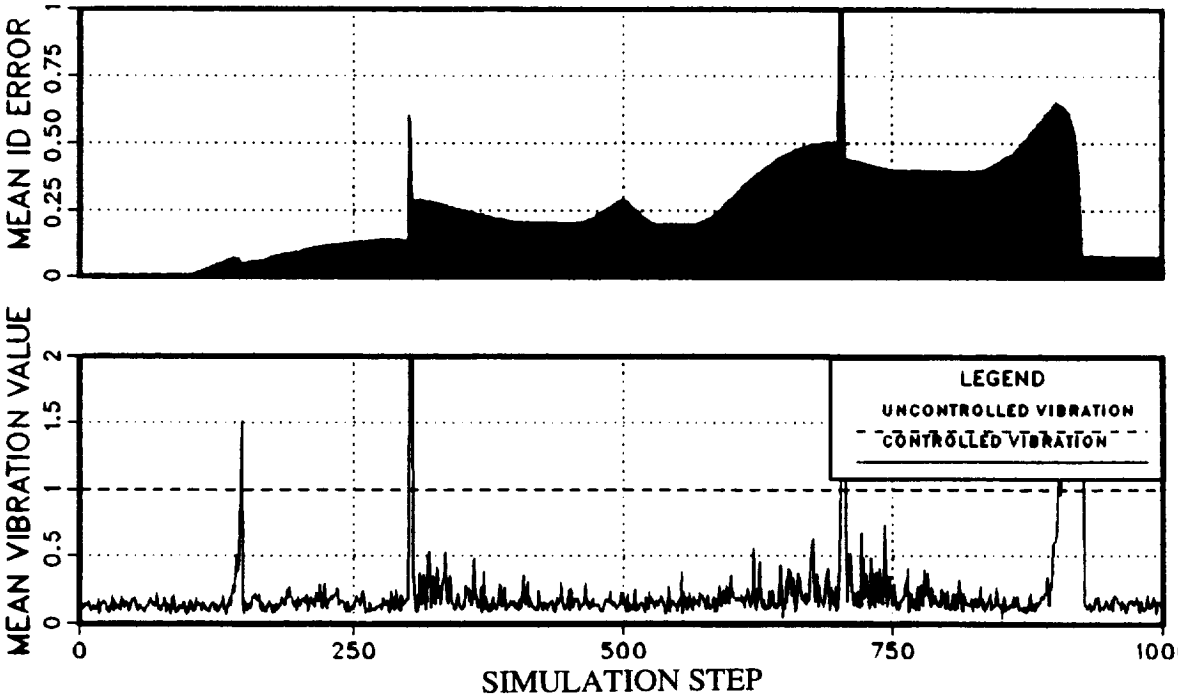

(b)

Figure 48. Closed-loop Kalman filter identification error and vibration for 10% measurement noise and continuous transfer-matrix variation, and $\mathbf{Q} = 10 * \mathbf{I}_6$: (a) r = 1, $\mathbf{M} = 10 * \mathbf{I}_6$; (b) r = 100, $\mathbf{M} = \mathbf{I}_6$ (Local Model).

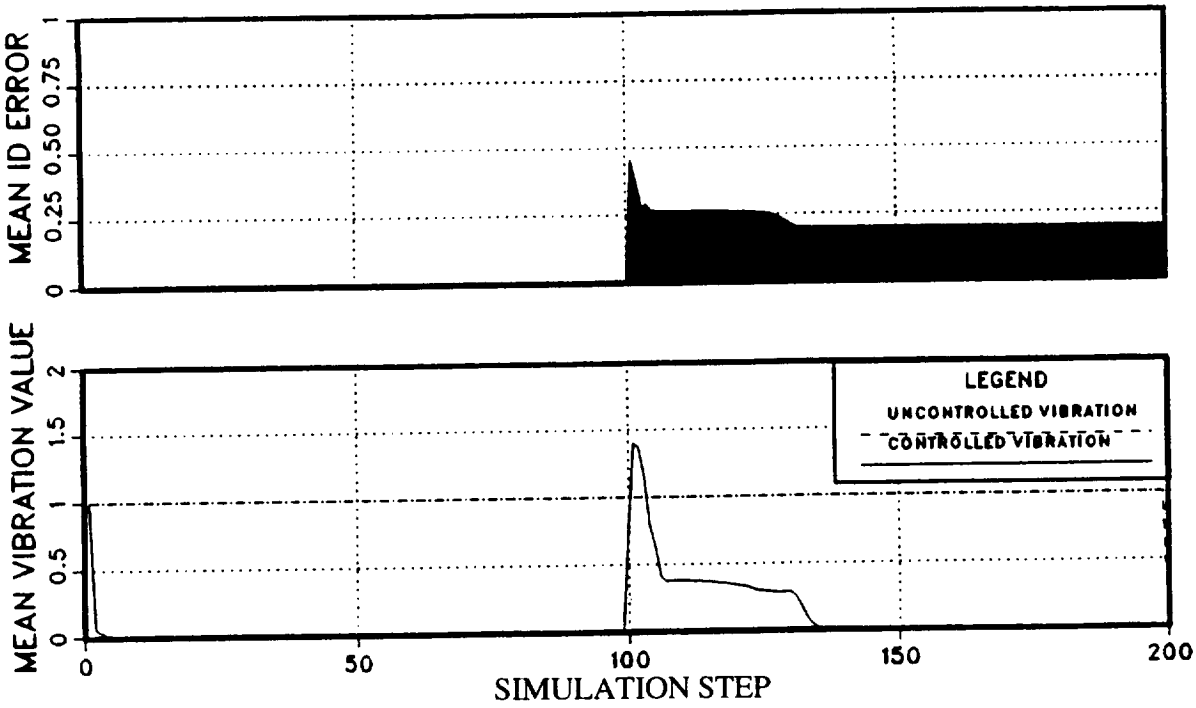

Figure 49. Closed-loop LMS filter identification error and vibration for no measurement noise and no probing, $\mathbf{K}_S = 0.3$ (Local Model).

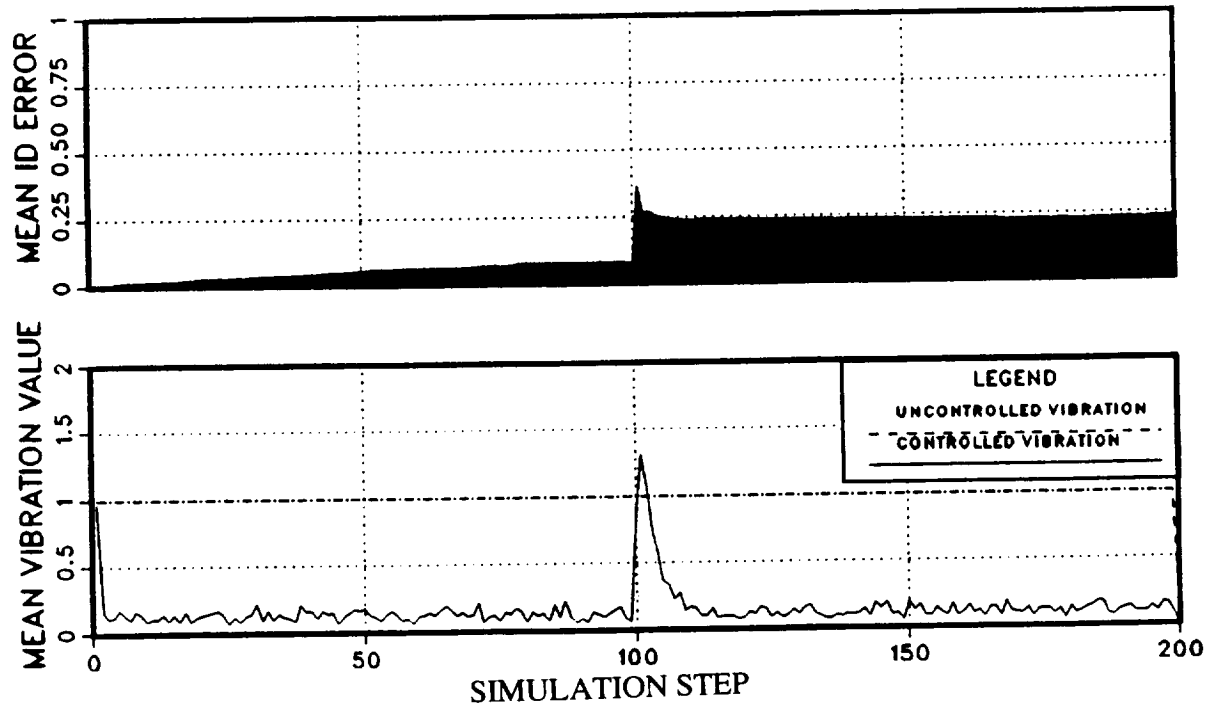

Figure 50. Closed-loop LMS filter identification error and vibration for 10% measurement noise and no probing, $\mathbf{K}_S = 0.3$ (Local Model).

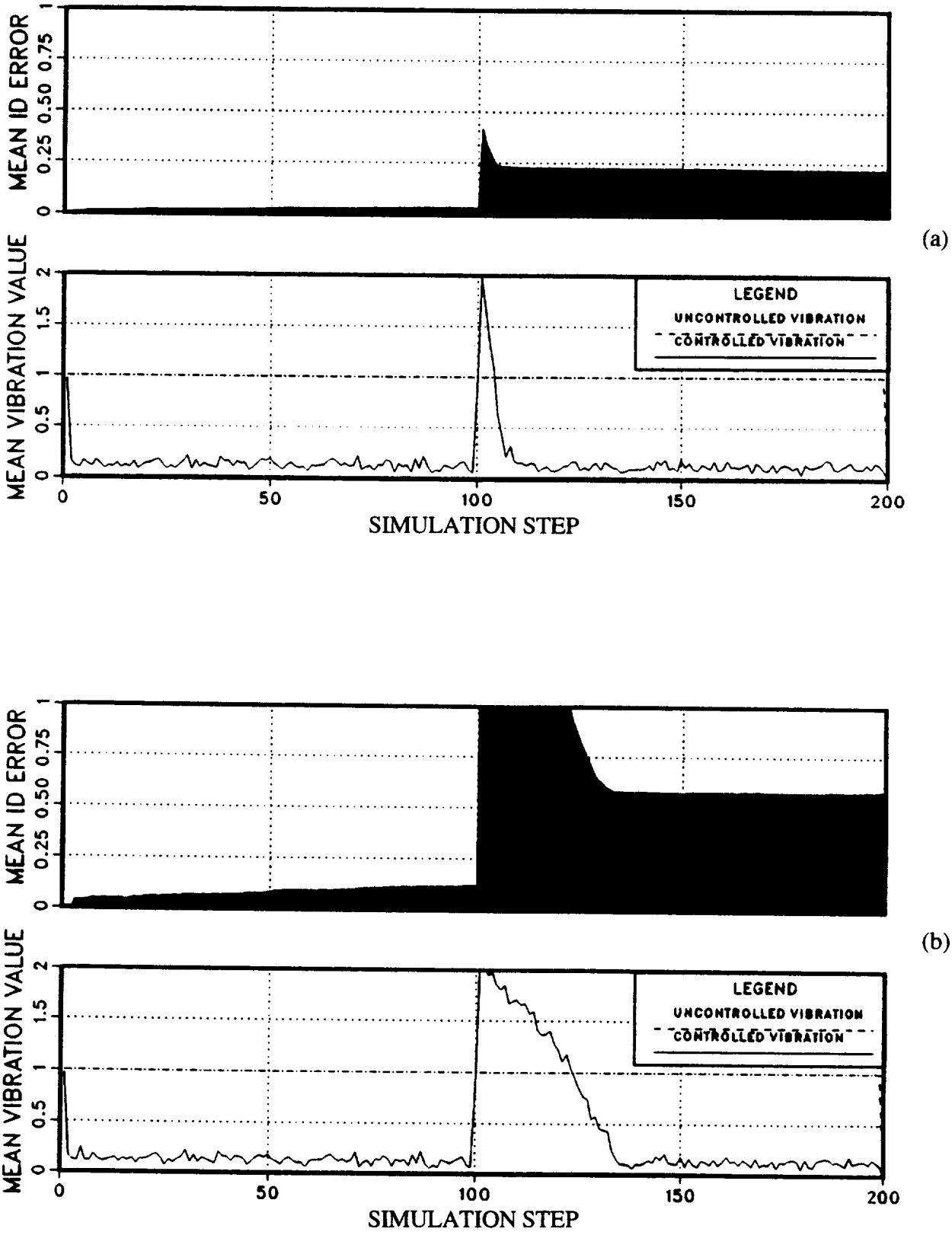

Figure 51. Closed-loop LMS filter identification error and vibration for 10% measurement noise and no probing: (a) $\mathbf{K}_S = 0.1$; (b) $\mathbf{K}_S = 0.5$ (Local Model).

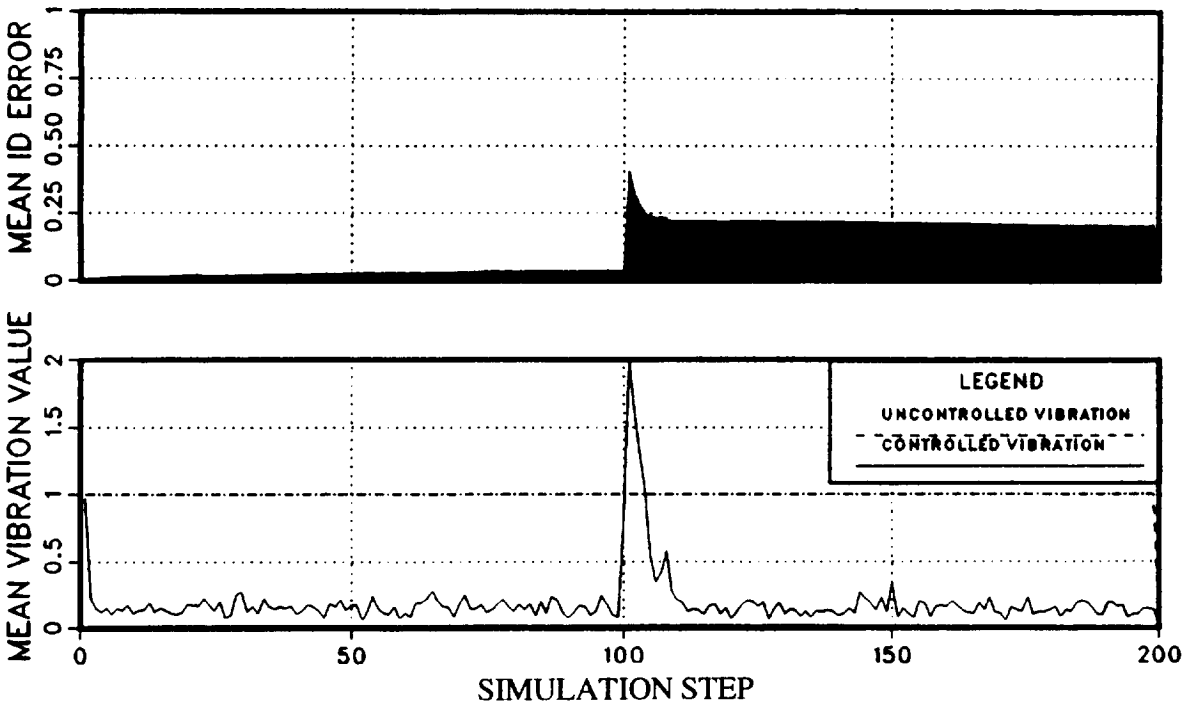

Figure 52. Closed-loop LMS filter identification error and vibration for 10% measurement noise, $\mathbf{K}_S = 0.1$, and 10% probing (Local Model).

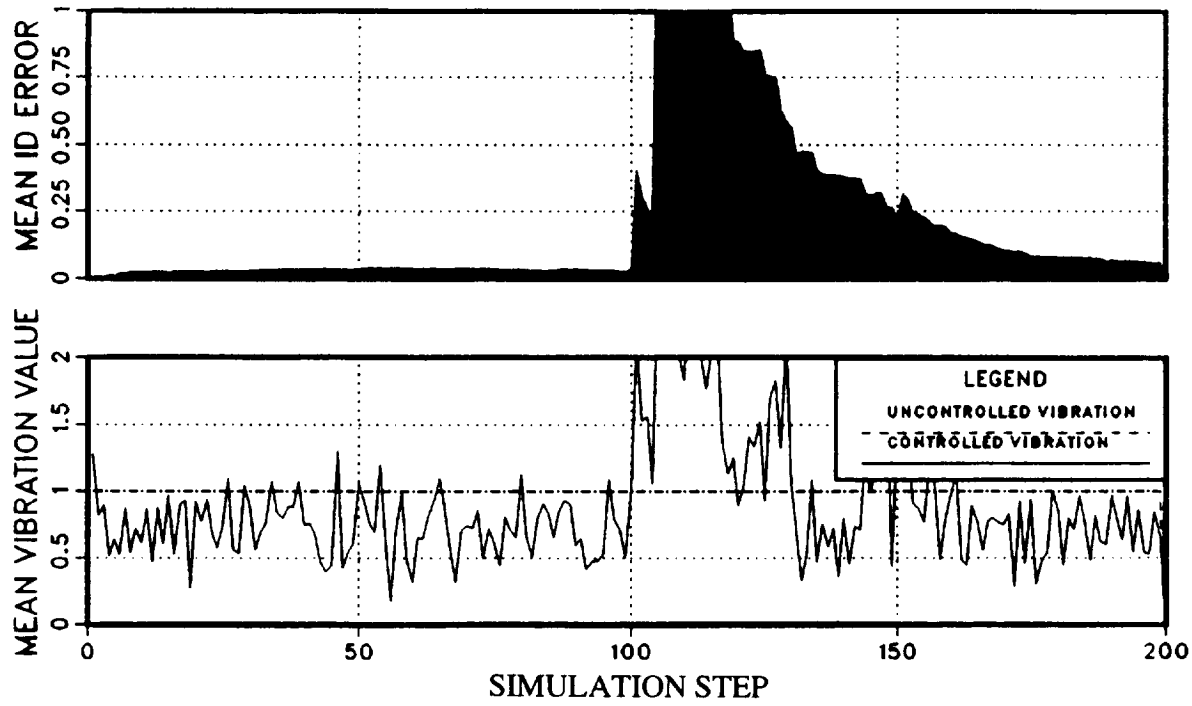

Figure 53. Closed-loop LMS filter identification error and vibration for 10% measurement noise, $\mathbf{K}_S = 0.1$, and 100% probing (Local Model).

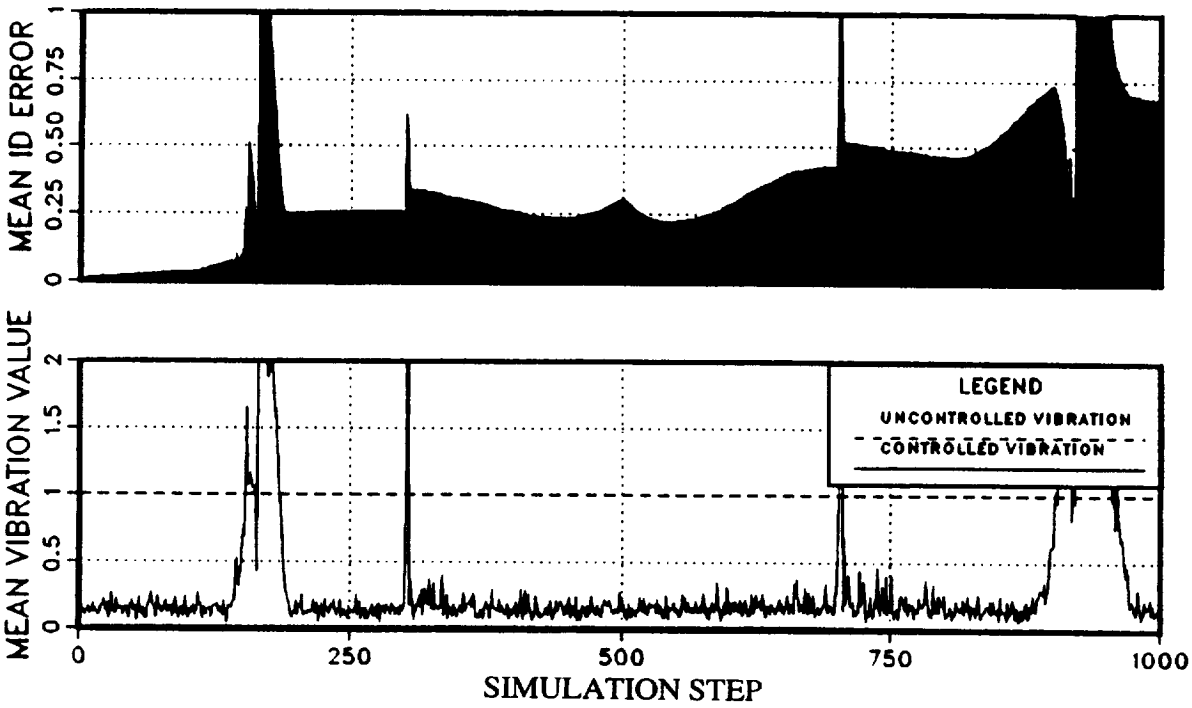

Figure 54. Closed-loop LMS filter identification error and vibration for 10% measurement noise, $\mathbf{K}_S = 0.1$, and 100% probing for continuous transfer-matrix variation (Local Model).

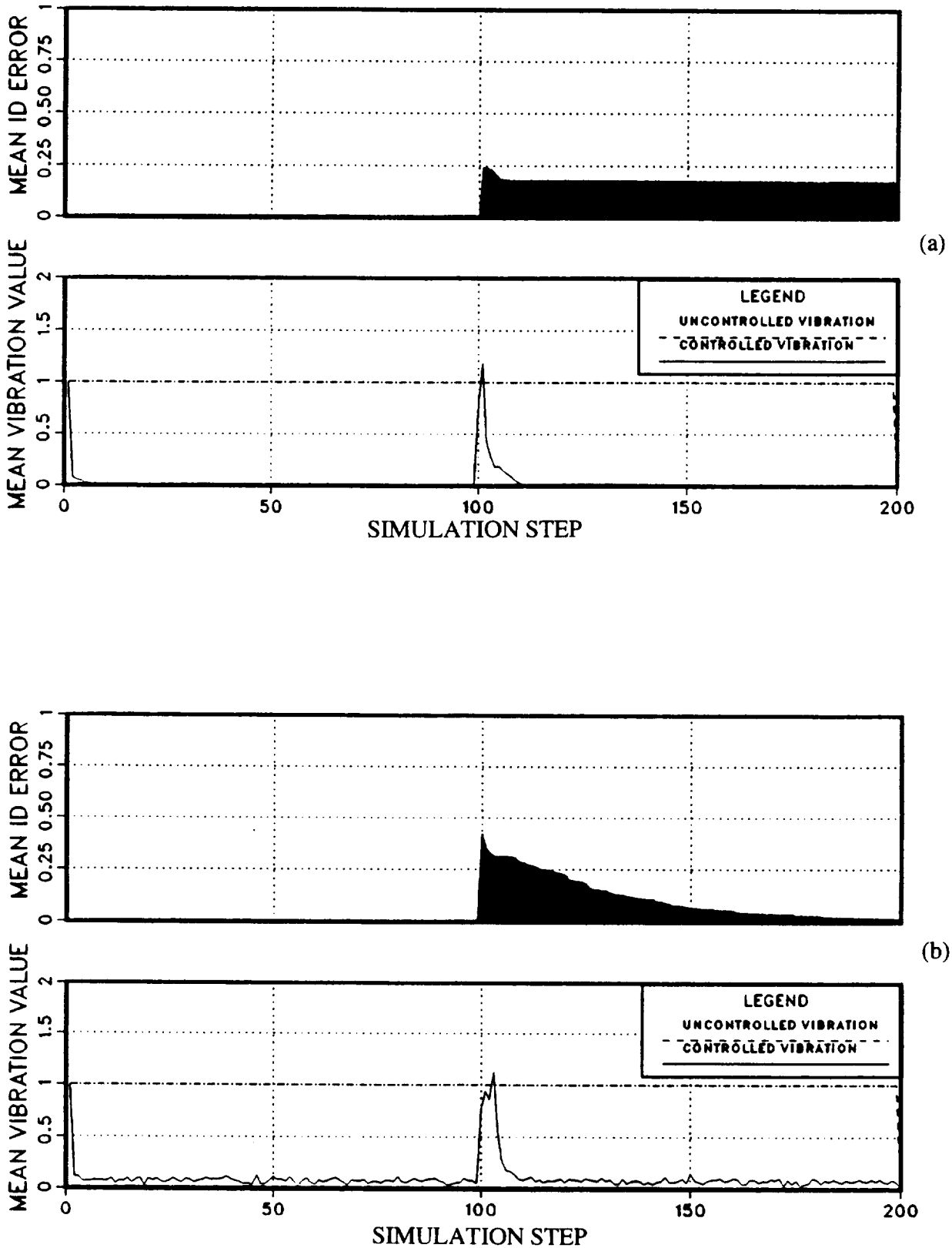

Figure 55. Closed-loop generalized Kalman filter identification error and vibration for no measurement noise, $\mathbf{R} = 1$, $\mathbf{M} = 10 * \mathbf{I}_6$, and multi-step batch size n = 1: (a) no probing; (b) 10% probing (Local Model).

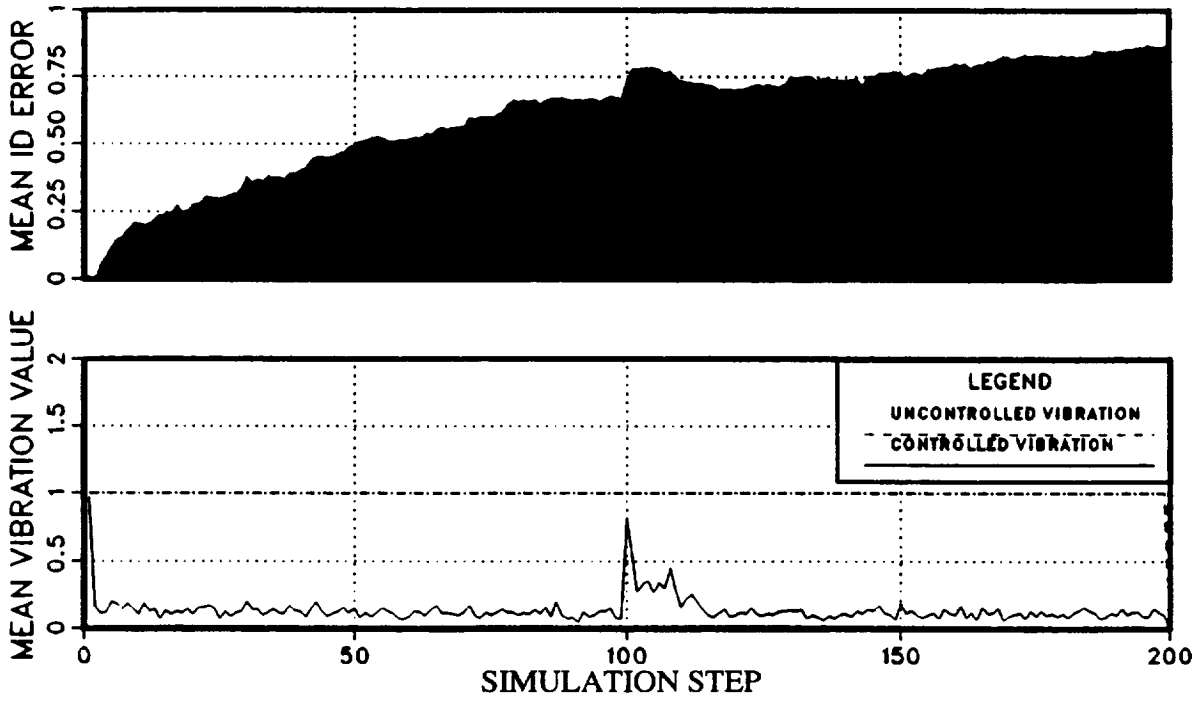

Figure 56. Closed-loop generalized Kalman filter identification error and vibration for 10% measurement noise, $\mathbf{R} = 1$, $\mathbf{M} = 10 * \mathbf{I}_6$, multi-step batch size n = 1, and no probing (Local Model).

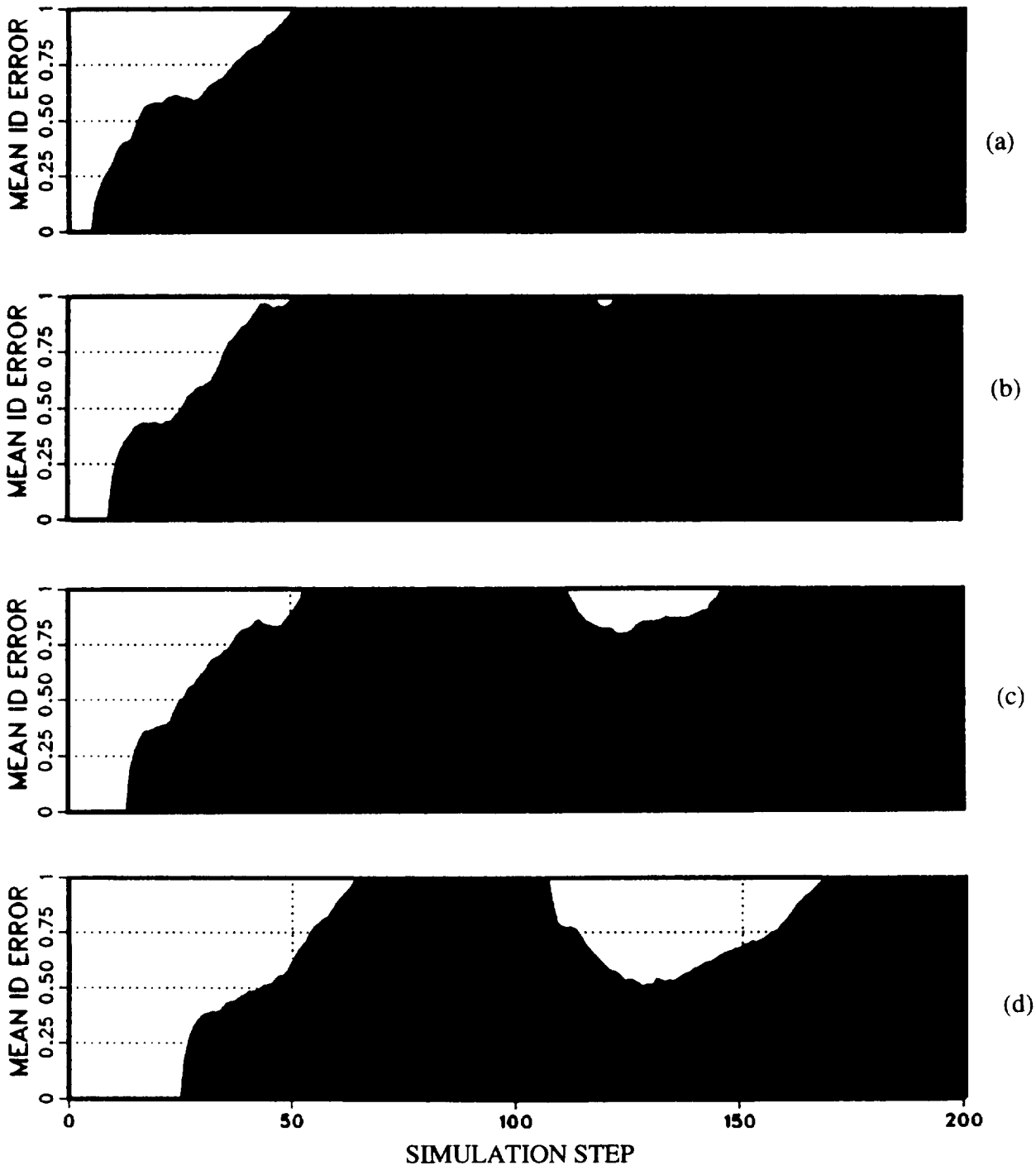

Figure 57. Closed-loop generalized Kalman filter identification error for 10% measurement noise, no probing, r = 1, and $\mathbf{M} = 10 * \mathbf{I}_6$, showing effect of multi-step batch size n: (a) n = 4; (b) n = 8; (c) n = 12; (d) n = 24 (Local Model).

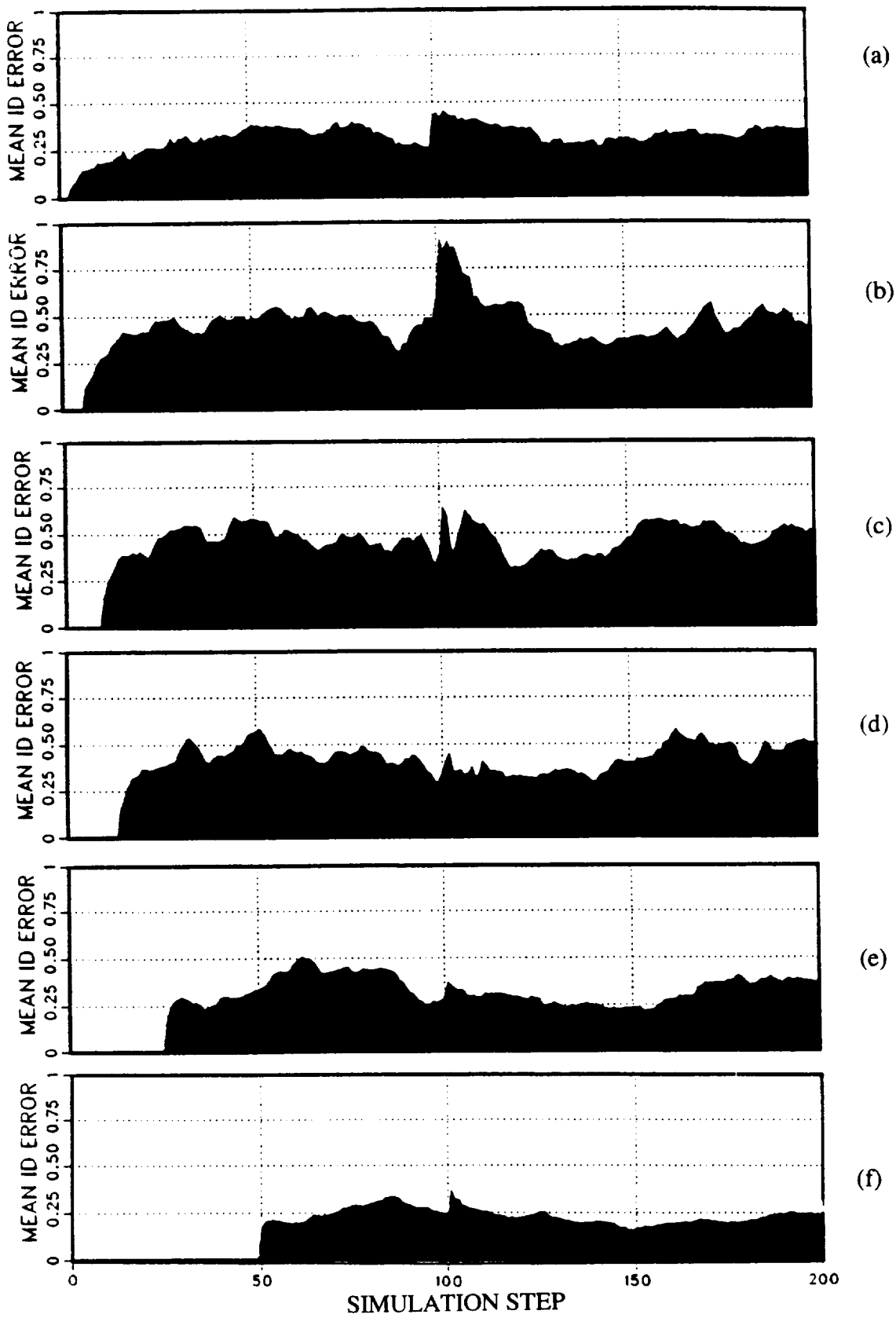

Figure 58. Closed-loop generalized Kalman filter identification error for 10% measurement noise, 10% probing, $\mathbf{R} = 1$, and $\mathbf{M} = 10 * \mathbf{I}_6$, showing effect of multi-step batch size n: (a) n = 1; (b) n = 4; (c) n = 8; (d) n = 12; (e) n = 24; (f) n = 48 (Local Model).

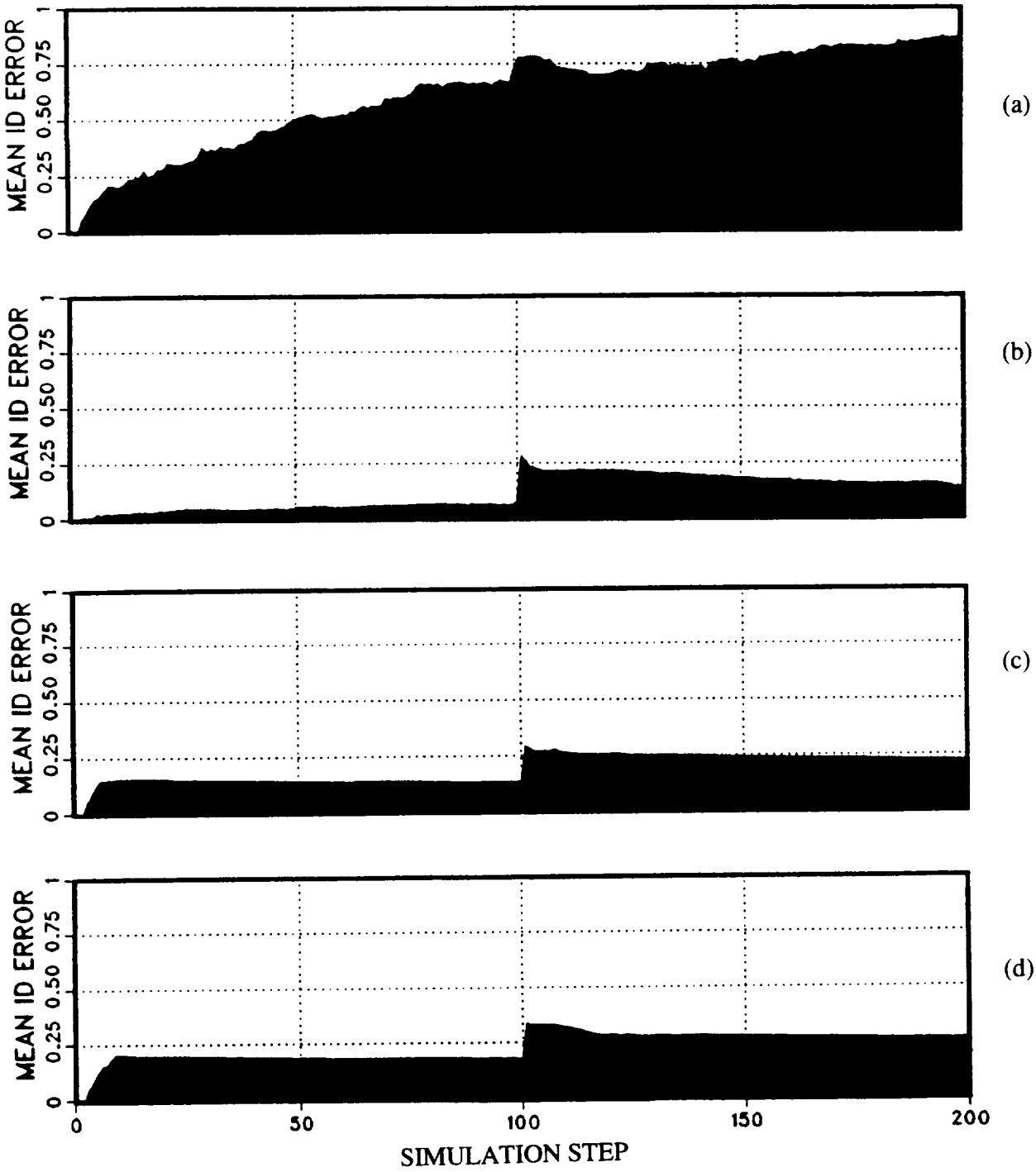

Figure 59. Closed-loop generalized Kalman filter identification error for 10% measurement noise, 10% probing, multi-step batch size n = 1, **R** = 1, and **M** = 10 * $\mathbf{I}_6$, showing effect of the cycles-averaged CA: (a) CA = 1; (b) CA = 4; (c) CA = 8; (d) CA = 12 (Local Model).

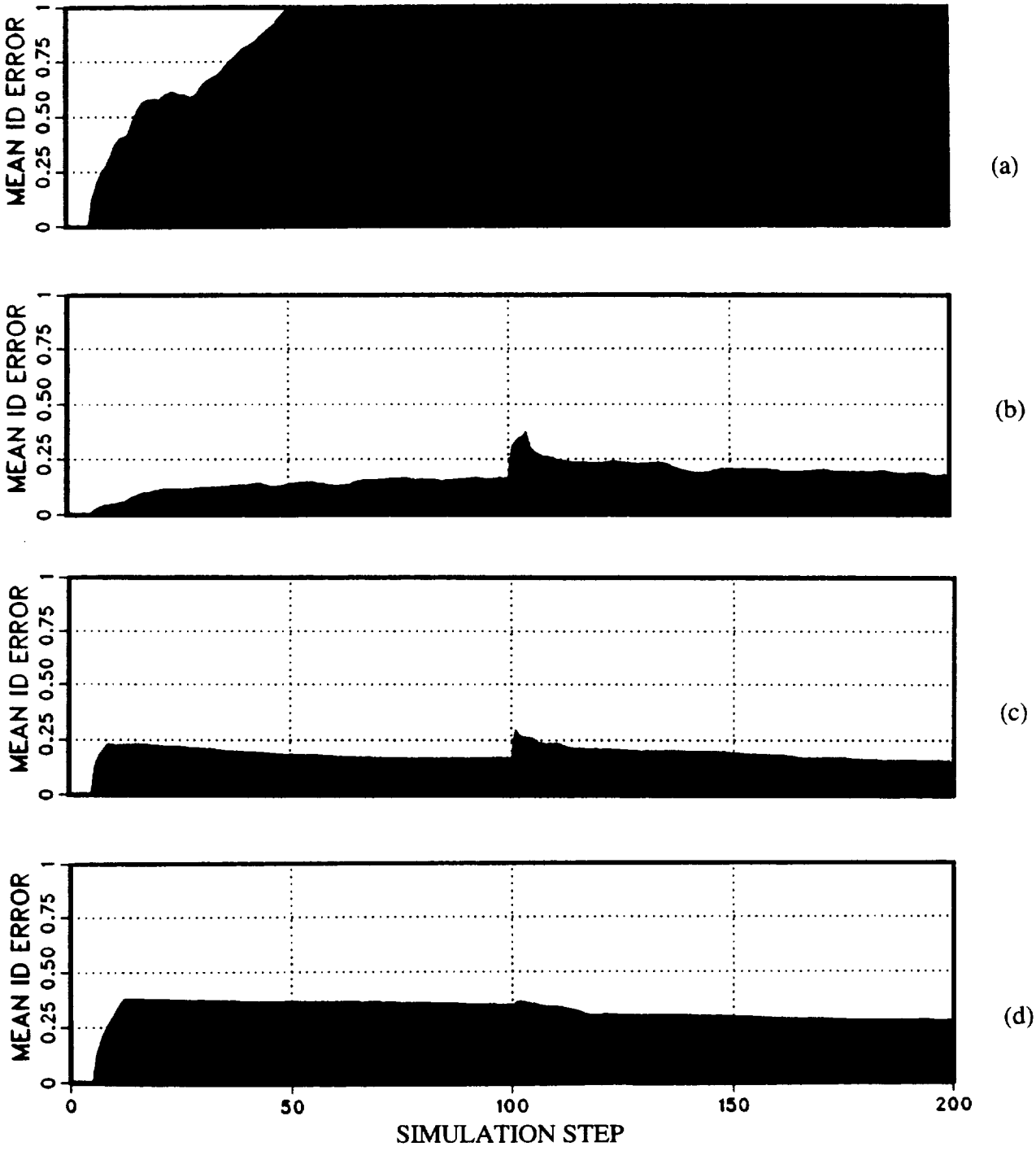

Figure 60. Closed-loop generalized Kalman filter identification error for 10% measurement noise, 10% probing, multi-step batch size n = 4, $\mathbf{R}$ = 1, and $\mathbf{M} = 10 * \mathbf{I}_6$, showing effect of cycles-averaged CA: (a) CA = 1; (b) CA = 4; (c) CA = 8; (d) CA = 12 (Local Model).

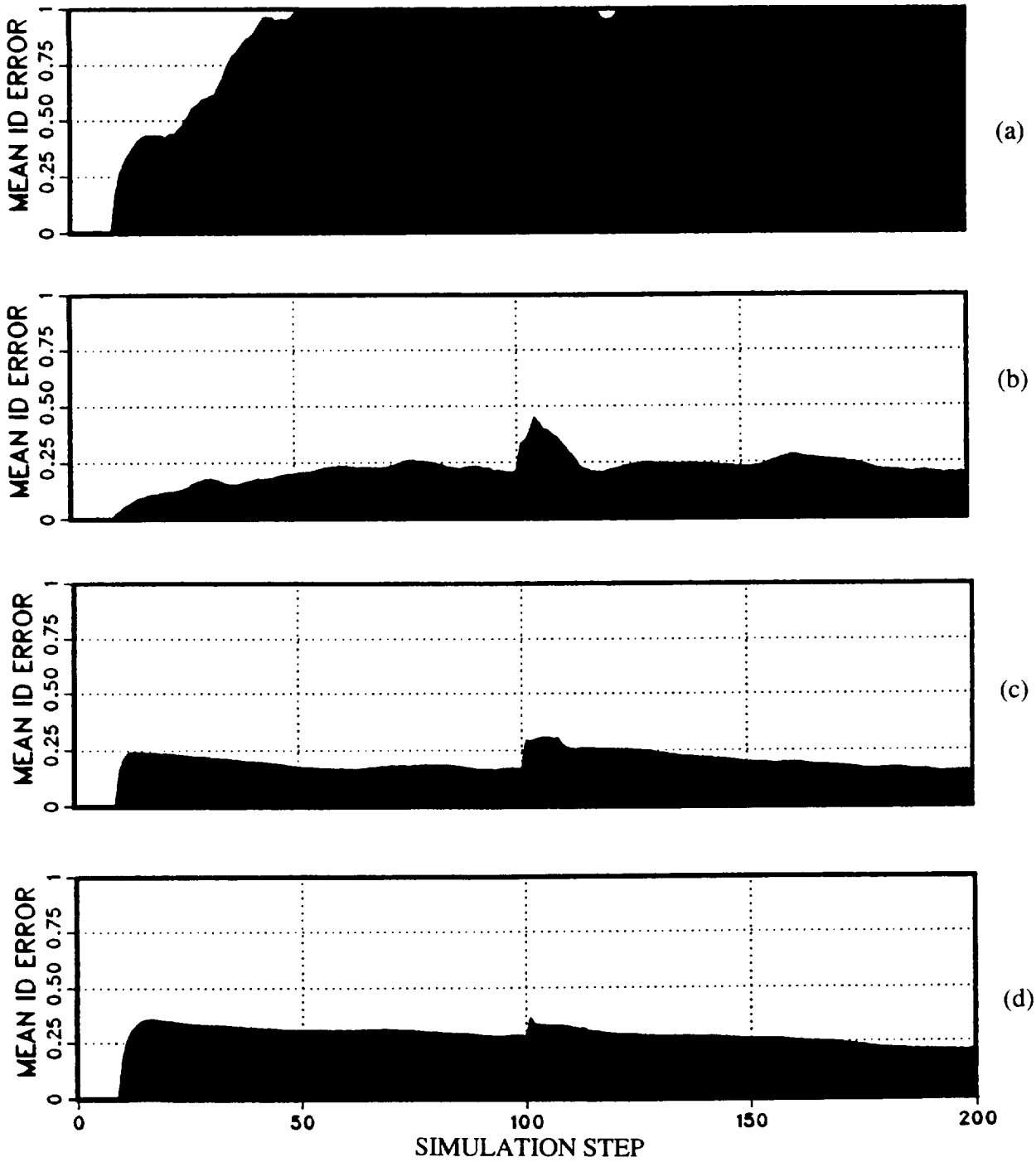

Figure 61. Closed-loop generalized Kalman filter identification error for 10% measurement noise, 10% probing, multi-step batch size n = 8, $\mathbf{R} = 1$, and $\mathbf{M} = 10 * \mathbf{I}_6$, showing effect of cycles-averaged CA: (a) CA = 1; (b) CA = 4; (c) CA = 8; (d) CA = 12 (Local Model).

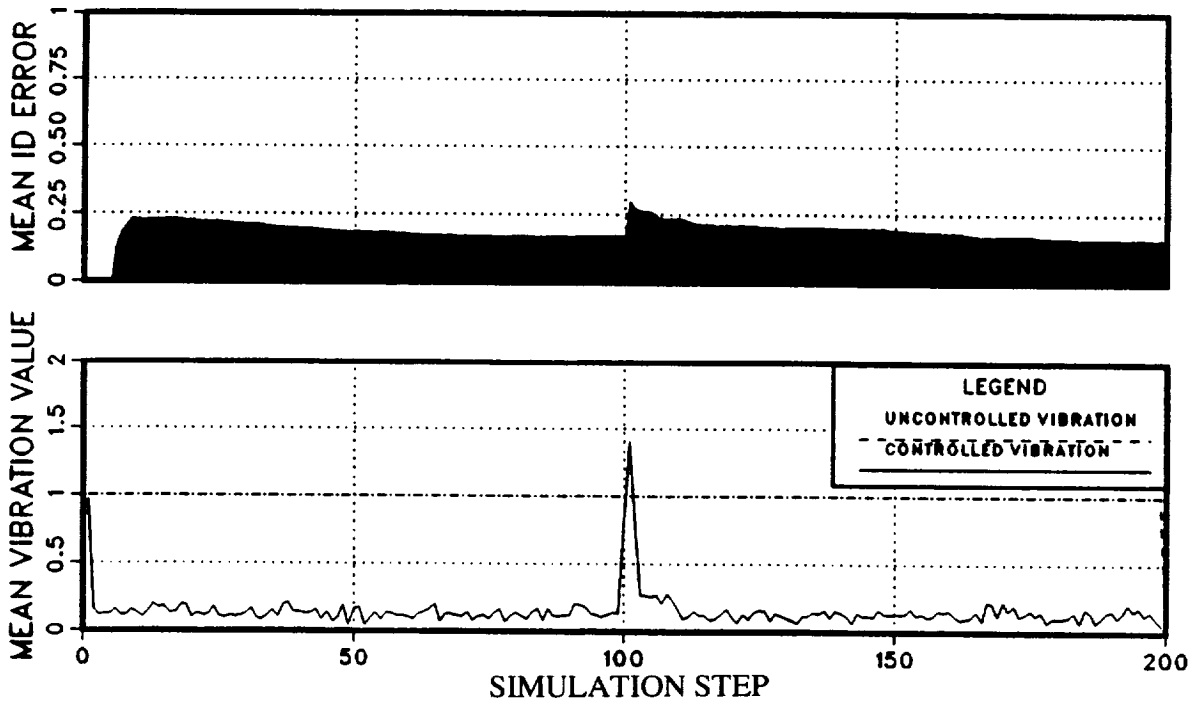

(a)

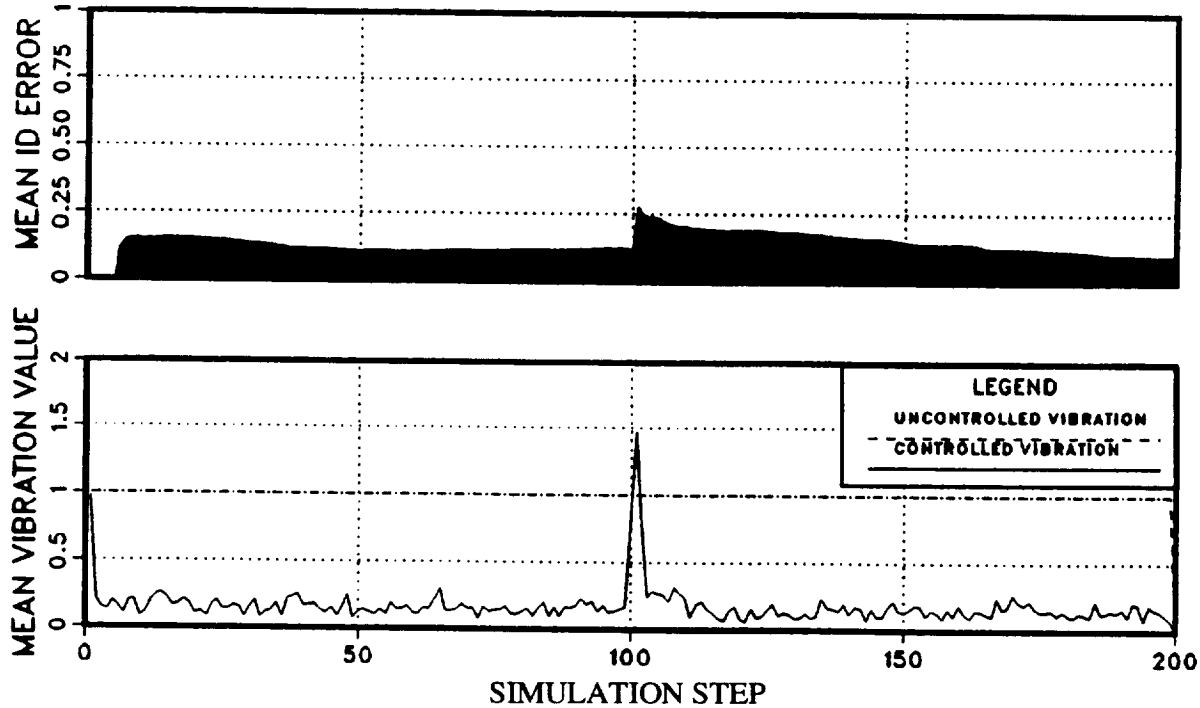

(b)

Figure 62. Closed-loop generalized Kalman filter identification error and vibration for 10% measurement noise, multi-step batch size n = 4, 8-cycle average, $\mathbf{R} = 1$, and $\mathbf{M} = 10 * \mathbf{I}_6$, showing effect of (a) no probing; (b) 10% probing (Local Model).

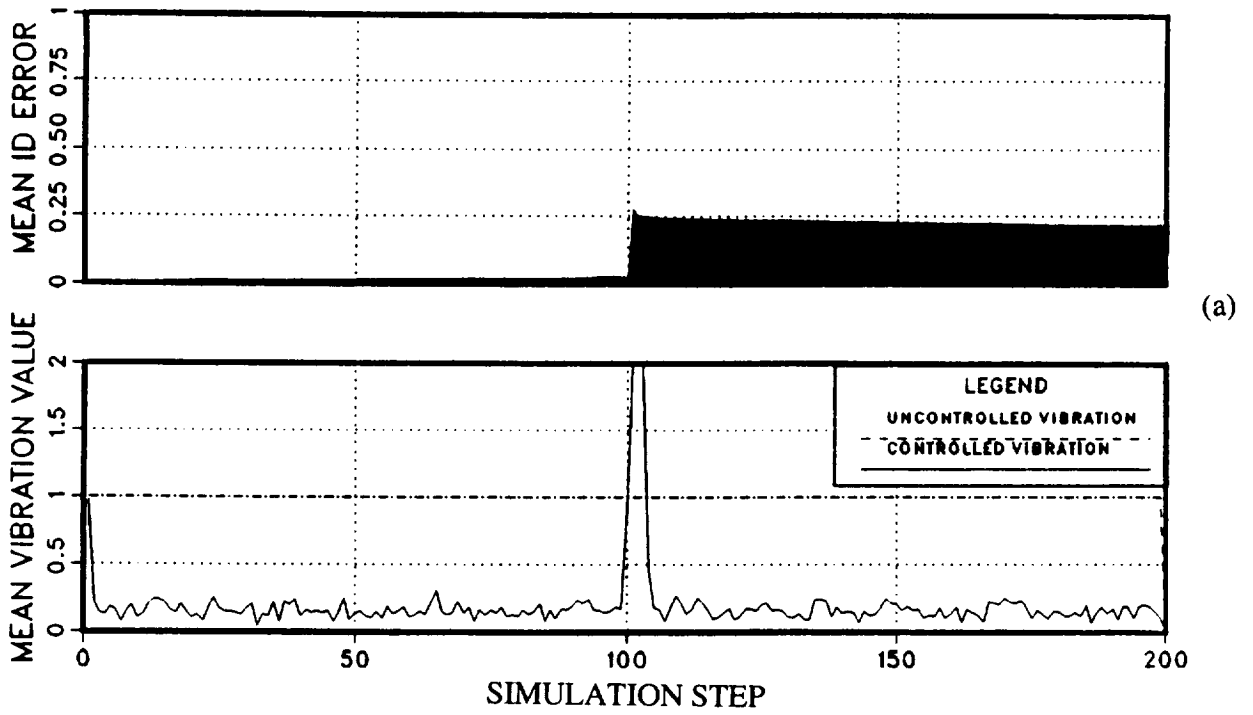

(a)

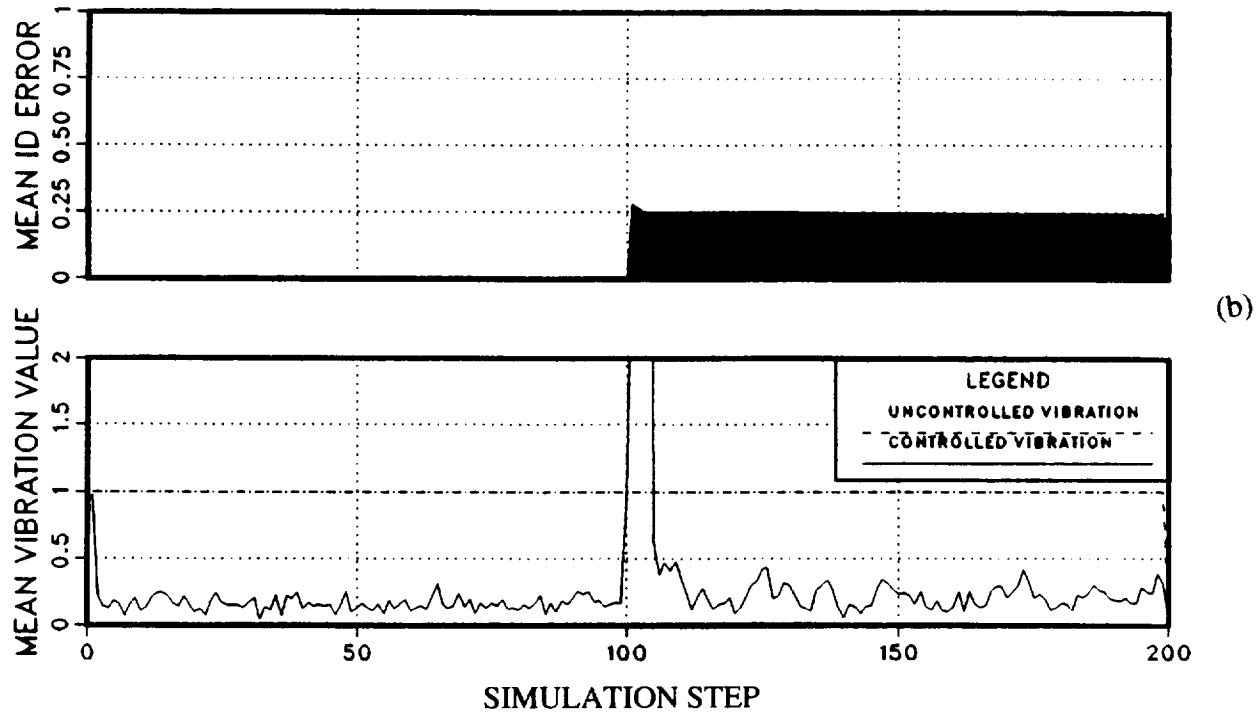

(b)

Figure 63. Closed-loop generalized Kalman filter identification error and vibration for 10% measurement noise, multi-step batch size n = 4, $\mathbf{R} = 100$, $\mathbf{M} = \mathbf{I}_6$, and 10% probing, showing effect of (a) no cycle averaging; (b) 8-cycle averaging (Local Model).

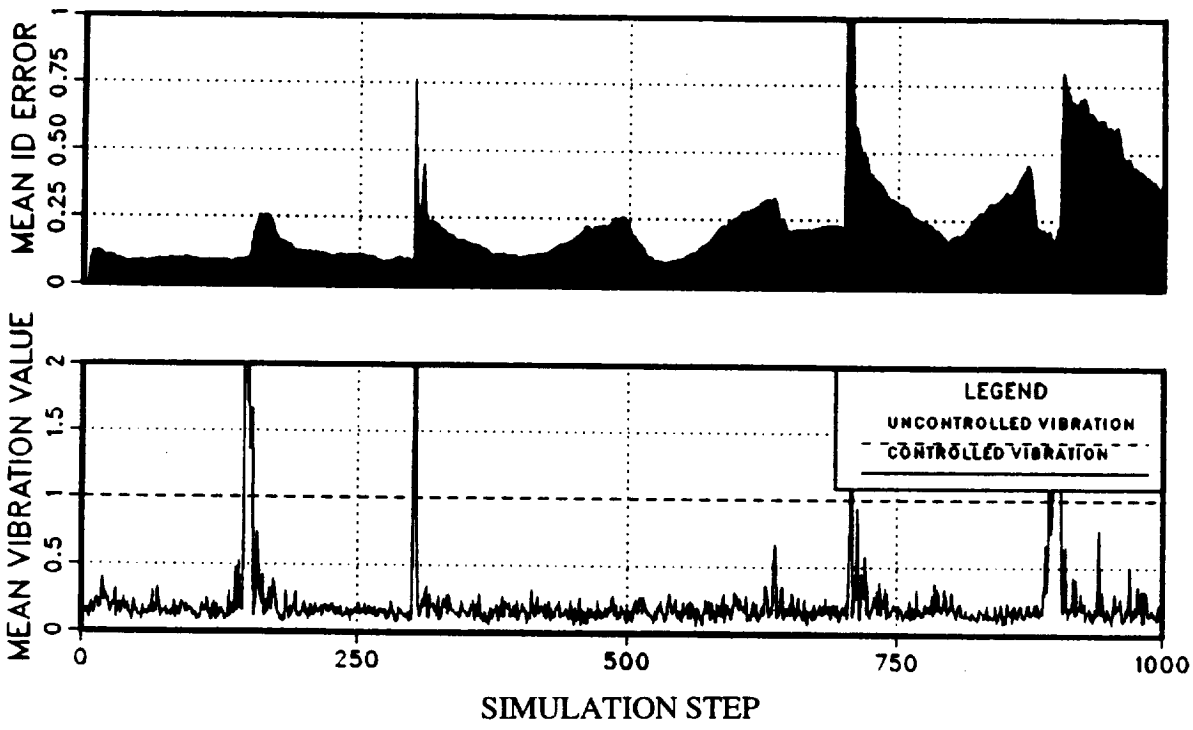

(a)

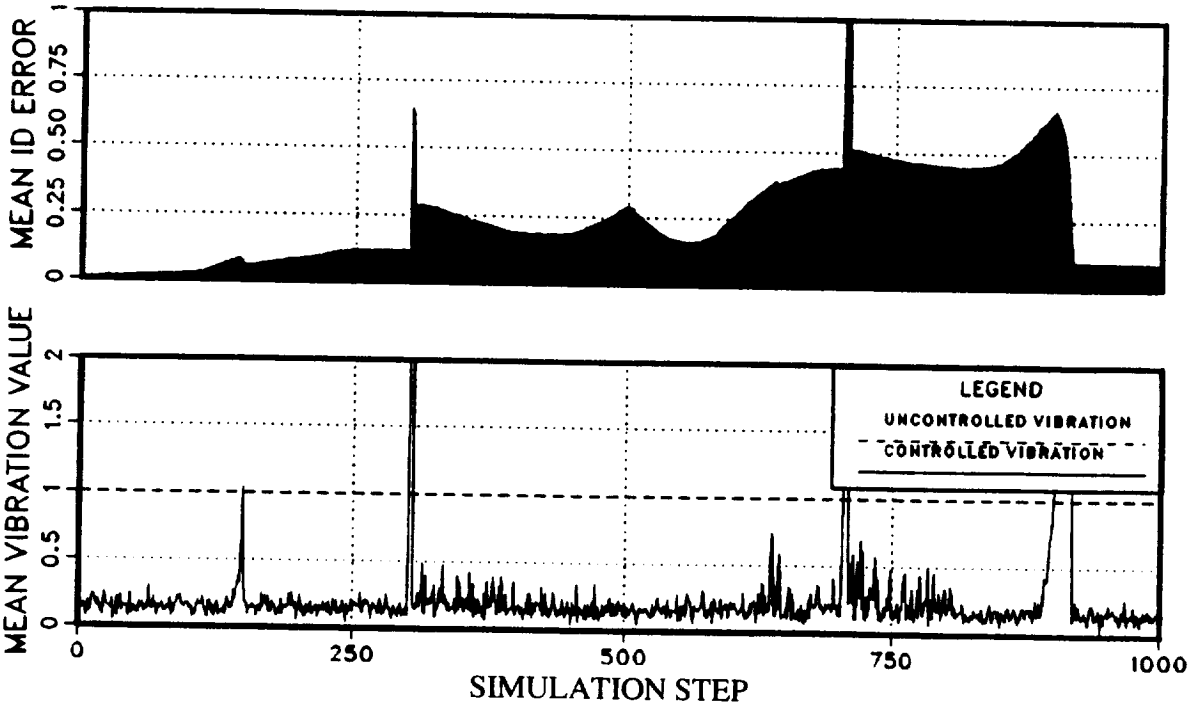

(b)

Figure 64. Closed-loop generalized Kalman filter identification error and vibration for 10% measurement noise, batch size n = 4, and 10% probing for the case of continuous transfer-matrix variation, showing (a) $\mathbf{R} = 1$, $\mathbf{M} = 10 * \mathbf{I}_6$, CA = 8; (b) $\mathbf{R} = 100$, $\mathbf{M} = \mathbf{I}_6$, CA = 1 (Local Model).

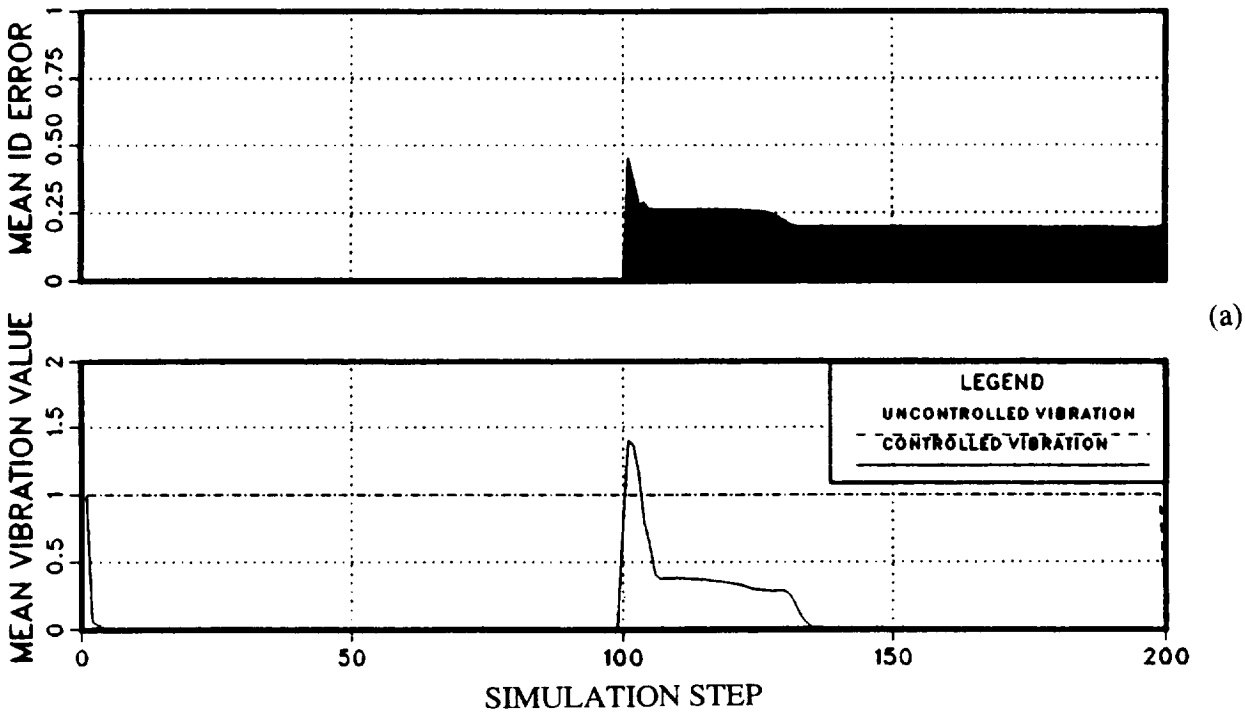

(a)

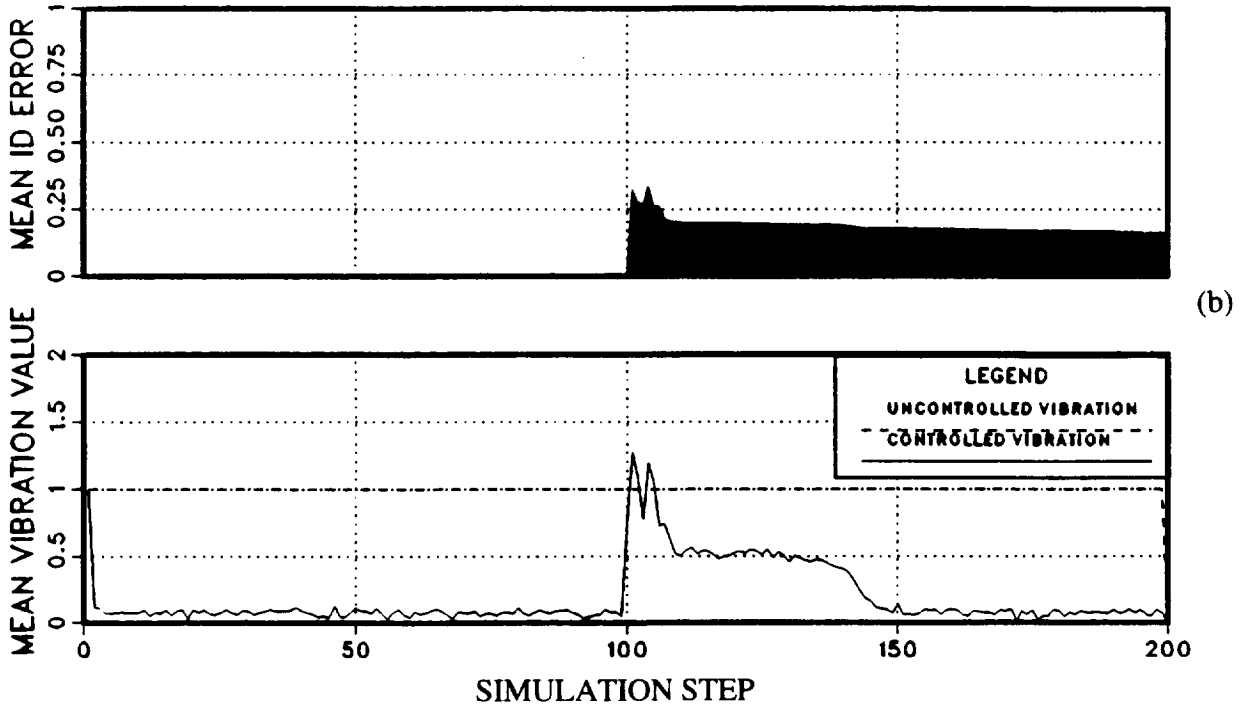

(b)

Figure 65. Closed-loop generalized LMS filter identification error and vibration for no measurement noise, $\mathbf{K}_S = 0.3 * \mathbf{I}_6$, multi-step batch size n = 1: (a) no probing; (b) 10% probing (Local Model).

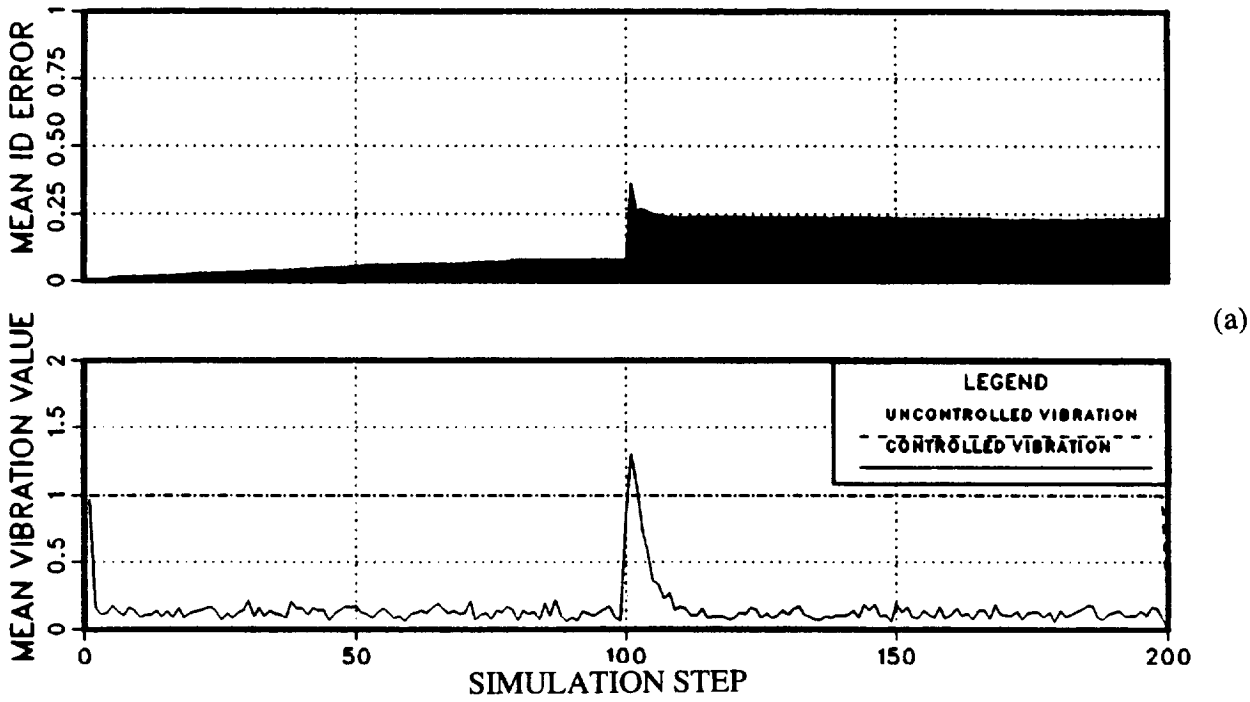

(a)

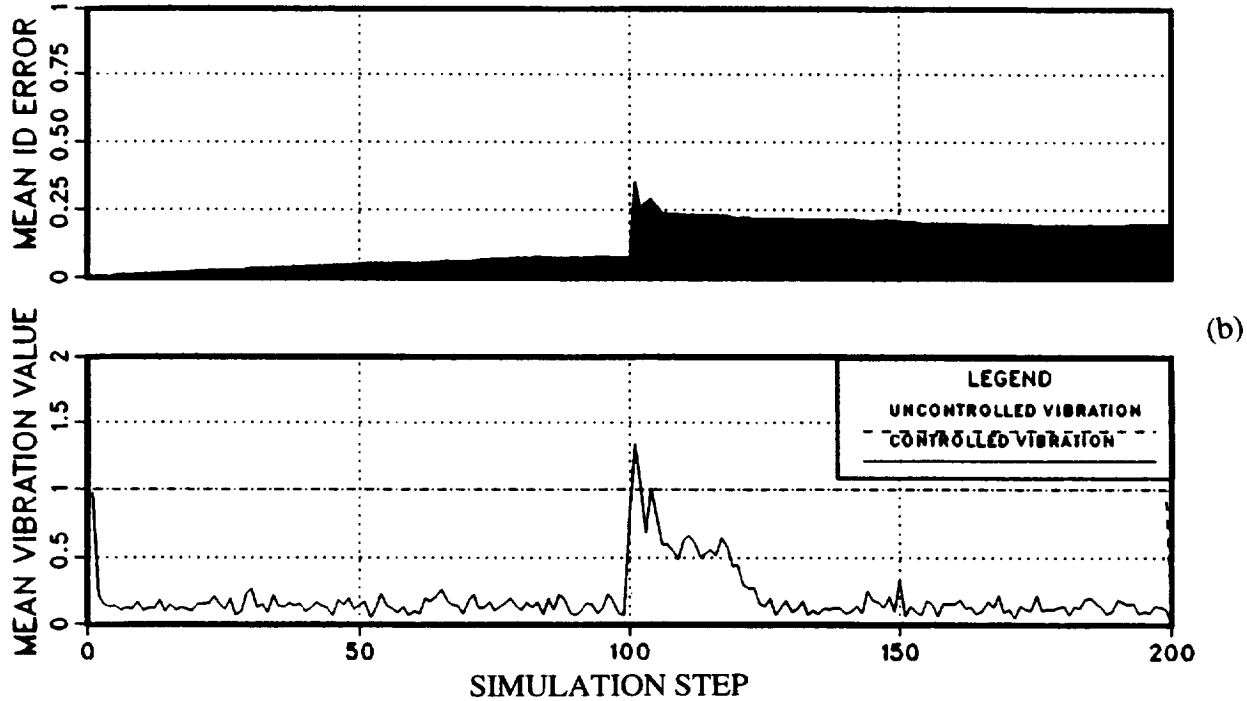

(b)

Figure 66. Closed-loop generalized LMS filter identification error and vibration for 10% measurement noise, $\mathbf{K}_S = 0.3 * \mathbf{I}_6$, multi-step batch size n =1: (a) no probing; (b) 10% probing (Local Model).

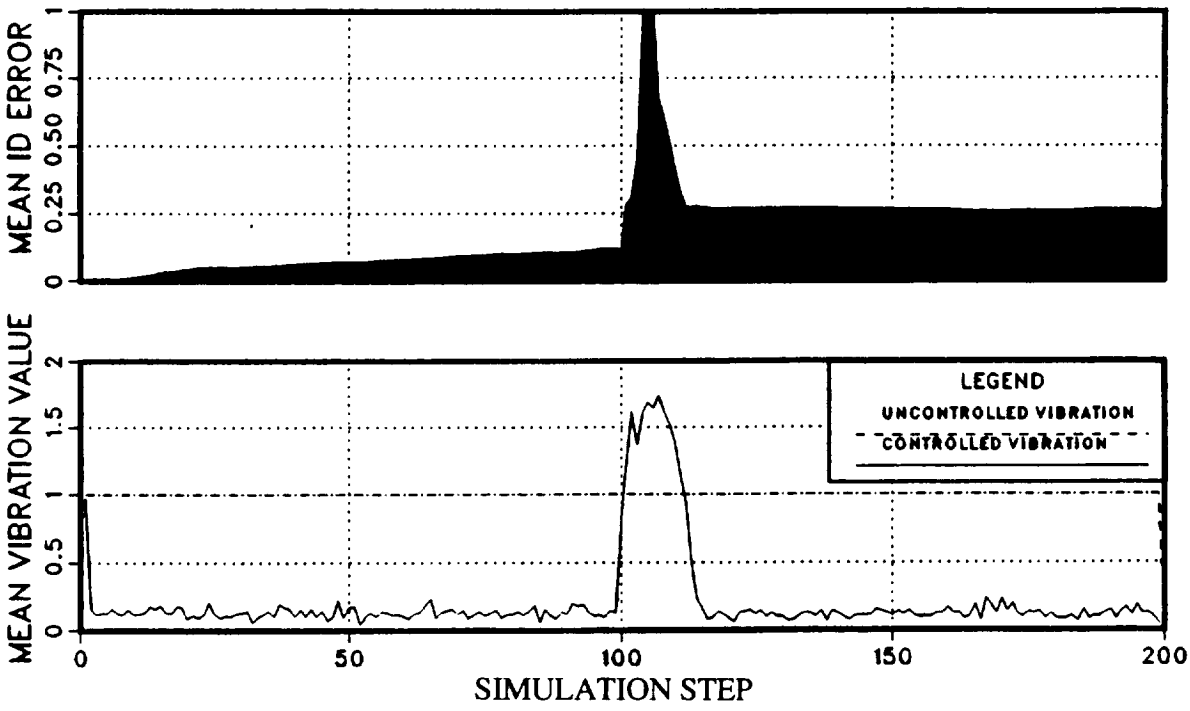

(a)

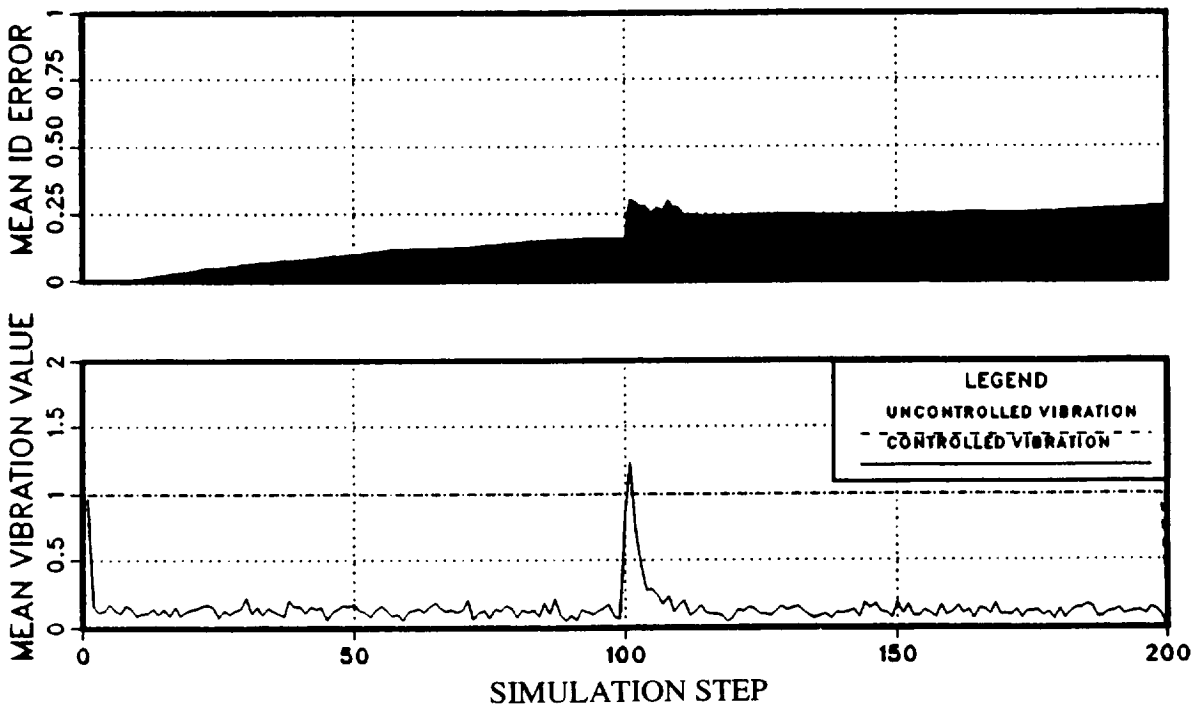

(b)

Figure 67 (part 1). Closed-loop generalized LMS filter identification error and vibration for 10% measurement noise, no probing, and $\mathbf{K}_S = 0.1 * \mathbf{I}_6$, showing effect of multi-step batch size n: (a) n = 4; (b) n = 8 (Local Model).

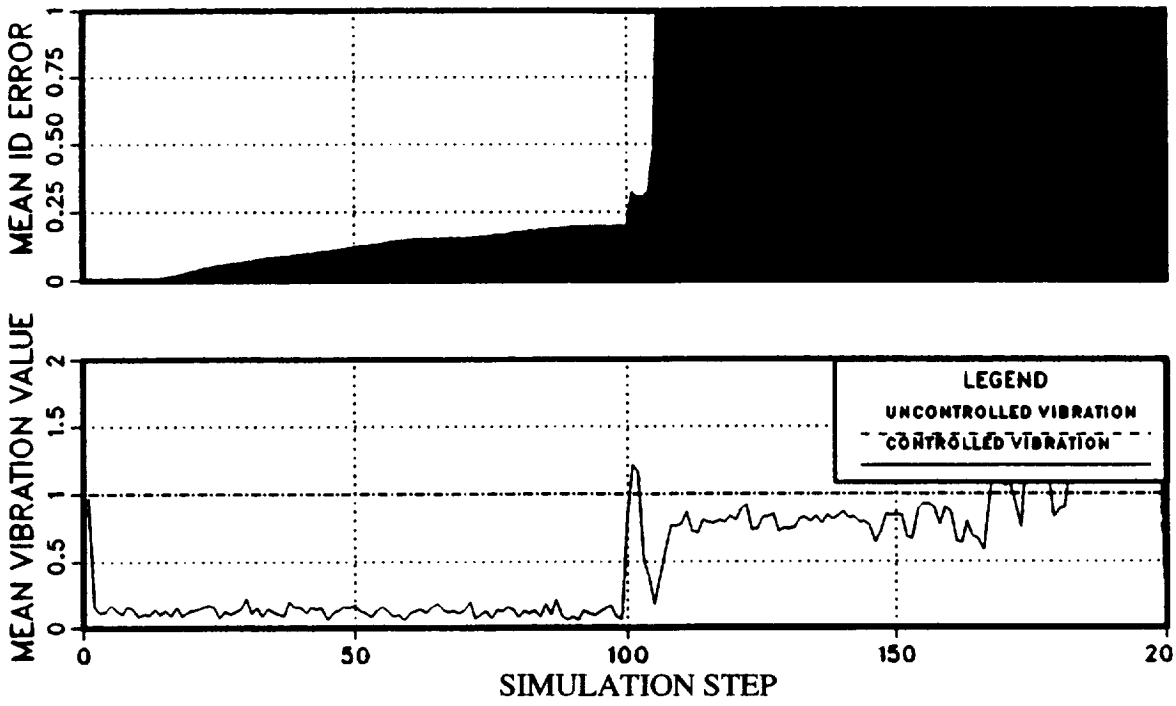

(c)

Figure 67 (part 2). Closed-loop generalized LMS filter identification error and vibration for 10% measurement noise, no probing, and $\mathbf{K}_S = 0.1 * \mathbf{I}_6$, showing effect of multi-step batch size n: (c) n = 12 (Local Model).

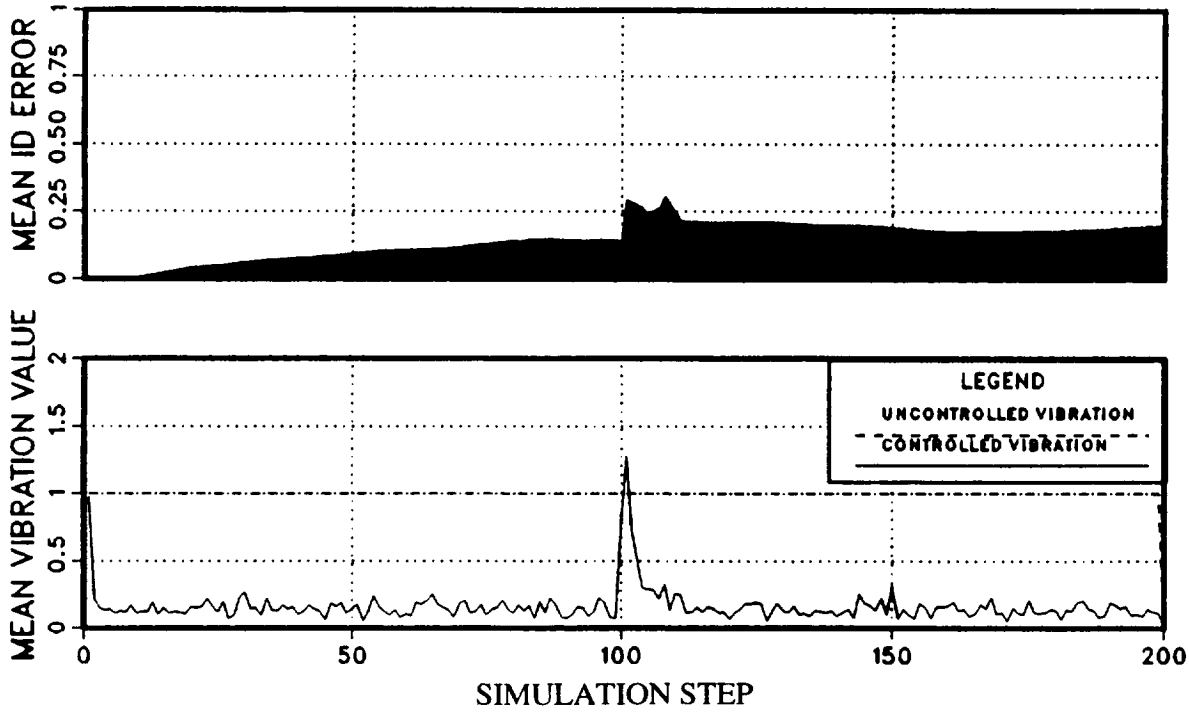

Figure 68. Closed-loop generalized LMS filter identification error and vibration for 10% measurement noise, 10% probing, $\mathbf{K}_S = 0.1 * \mathbf{I}_6$, multi-step batch size n = 8 (Local Model).

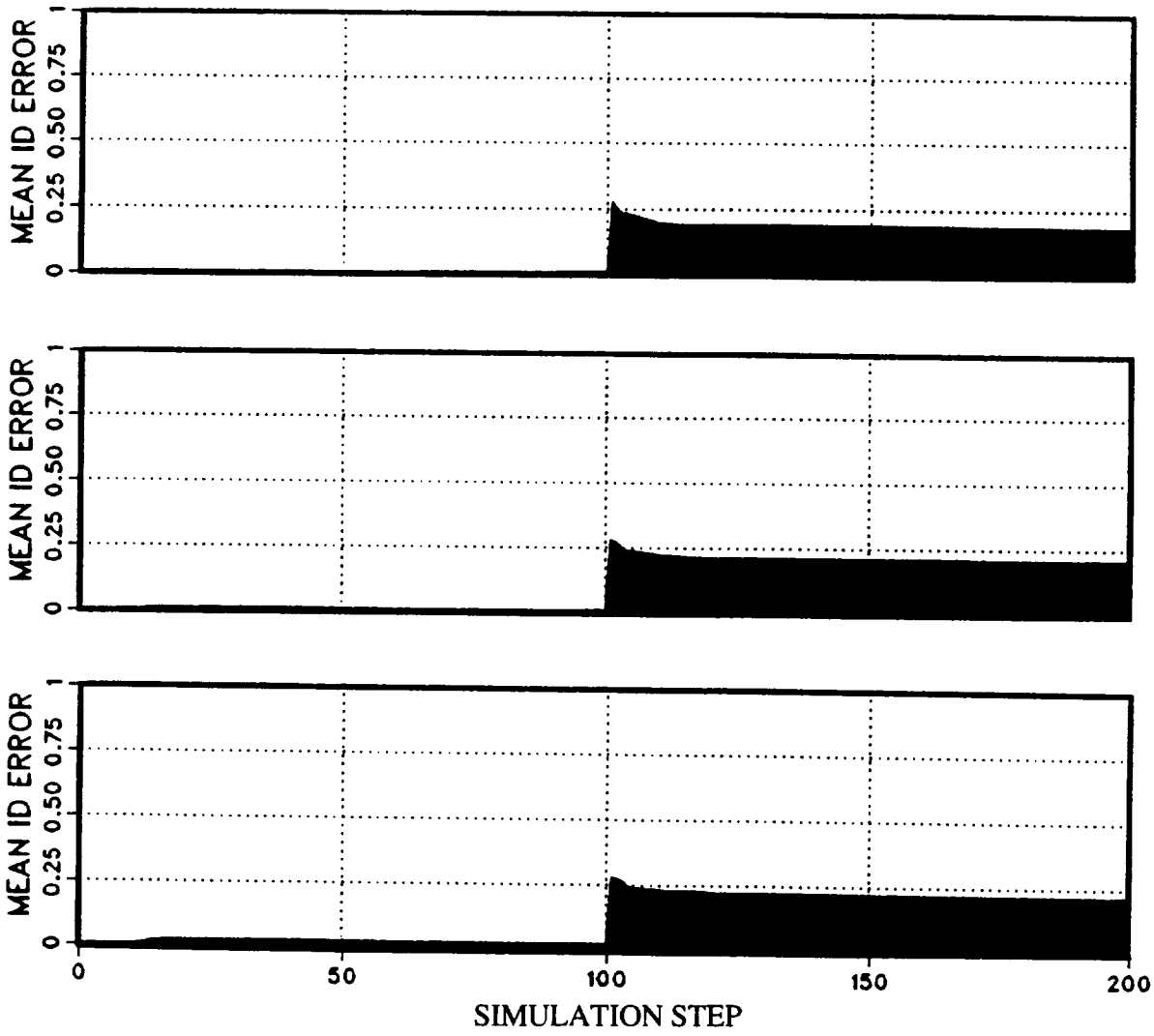

Figure 69. Closed-loop generalized LMS filter identification error for 10% measurement noise, 10% probing, multi-step batch size n = 8, and $\mathbf{K}_S = 0.1 * \mathbf{I}_6$, showing effect of cycles-averaged CA: (a) CA = 4; (b) CA = 8; (c) CA = 12 (Local Model).

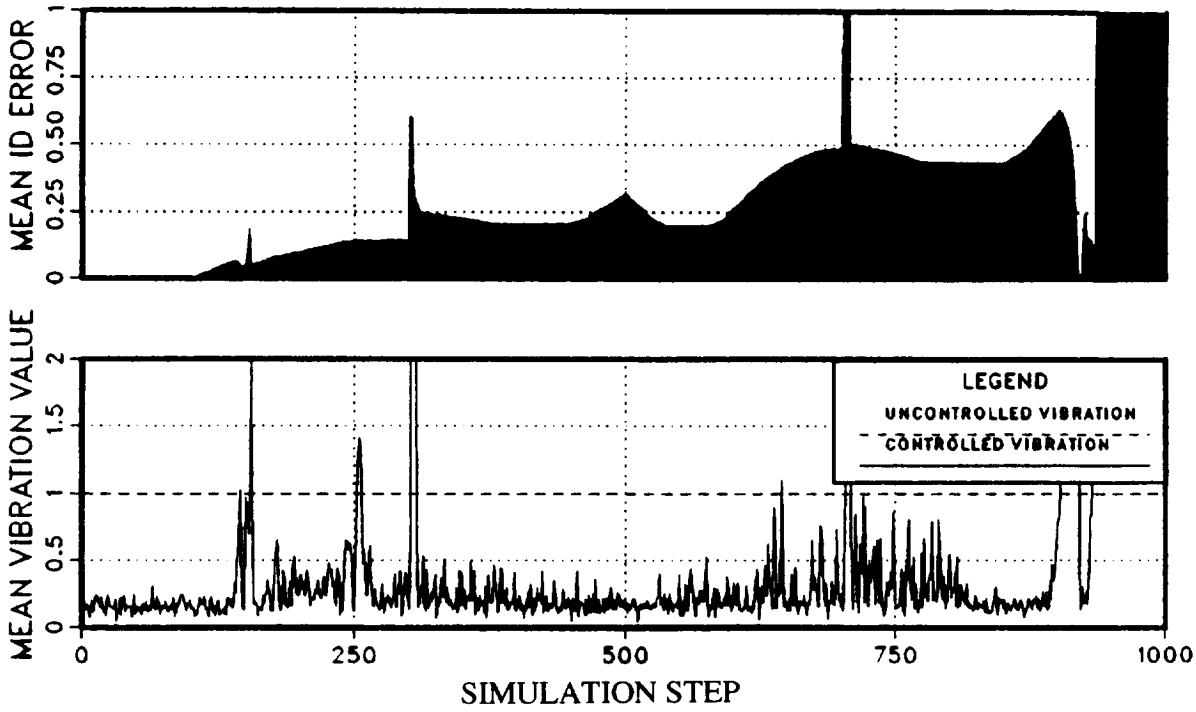

Figure 70. Closed-loop generalized LMS filter identification error for 10% measurement noise, 10% probing, multi-step batch size n = 4, 4-cycle averaging, and $\mathbf{K}_S = 0.01 * \mathbf{I}_6$ for the case of continuous transfer-matrix variation (Local Model).

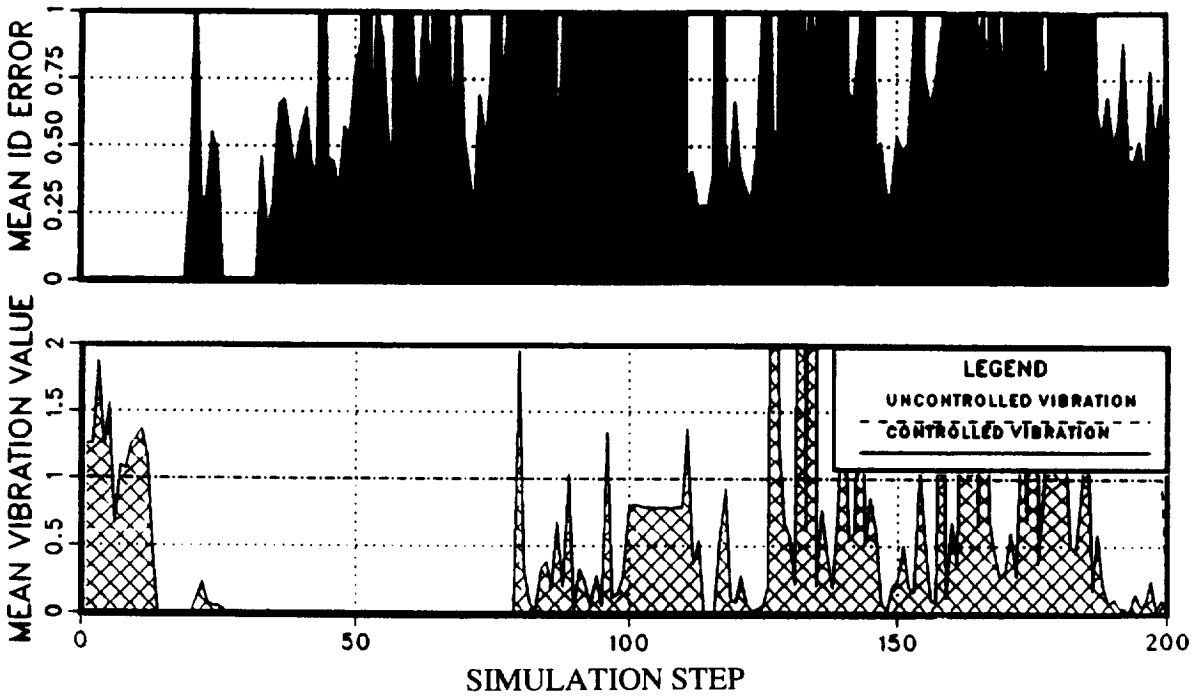

Figure 71. Closed-loop weighted-least-squares identification error and vibration for no measurement noise, no probing, and batch size n = 12 (Global Model).

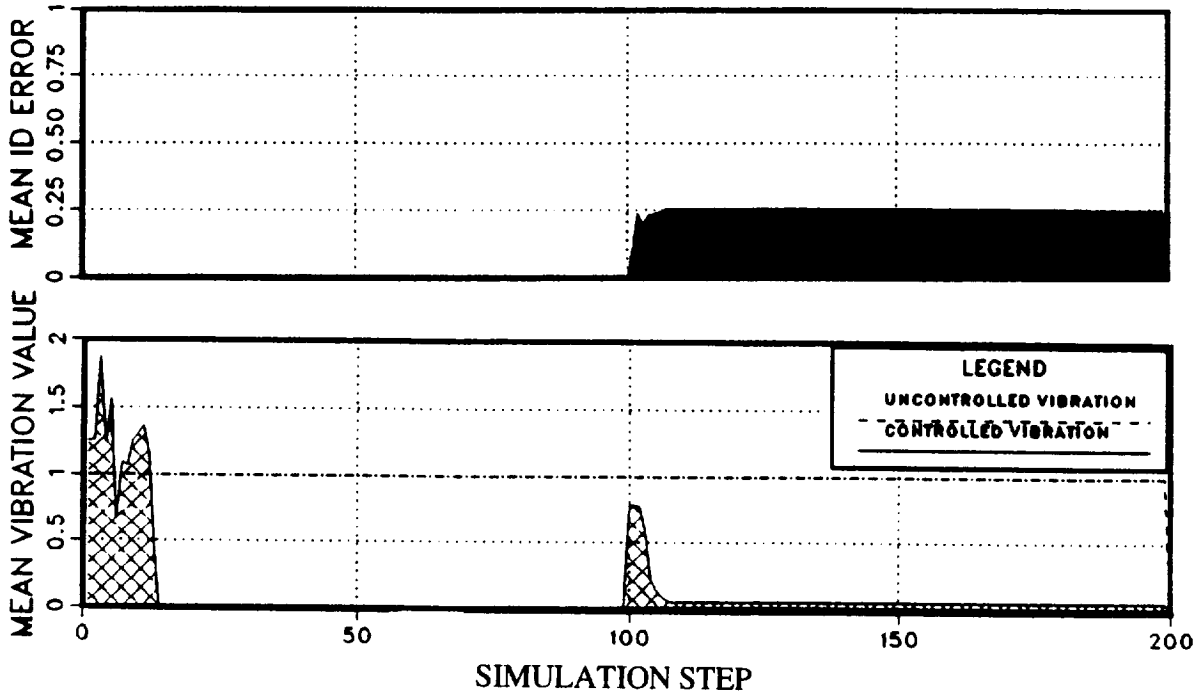

Figure 72. Closed-loop weighted-least-squares identification error and vibration for no measurement noise, no probing, batch size n = 12, and "zero-vibration" defined as 0.05 of baseline (Global Model).

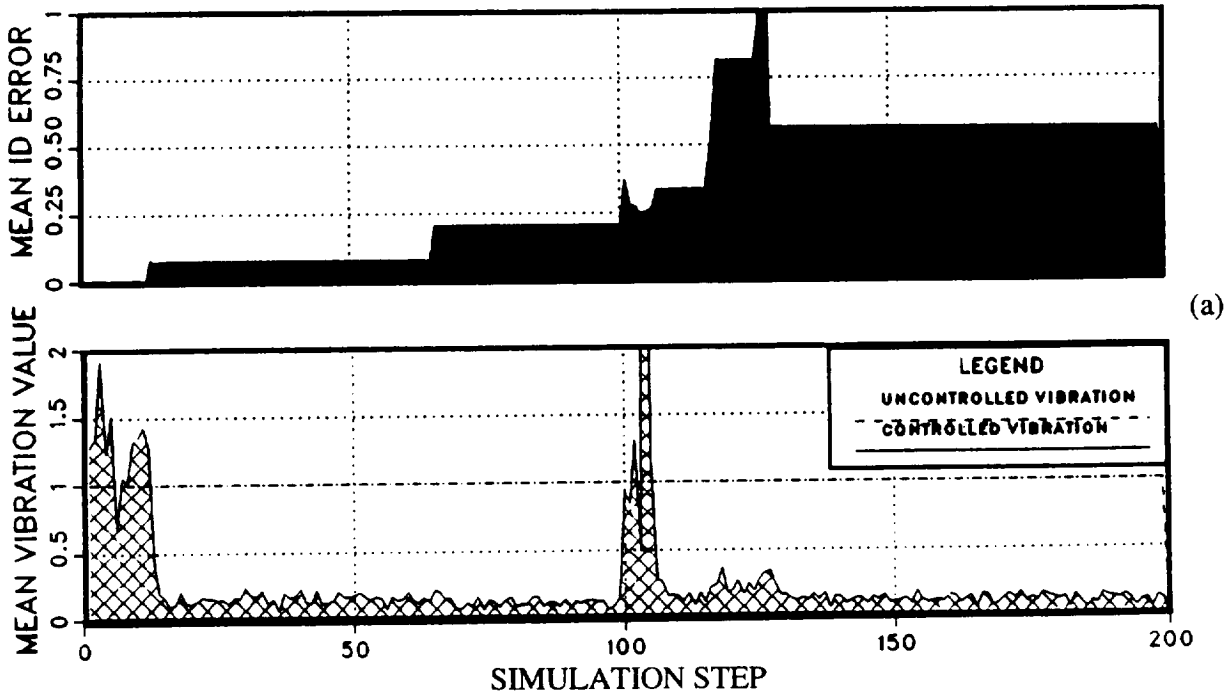

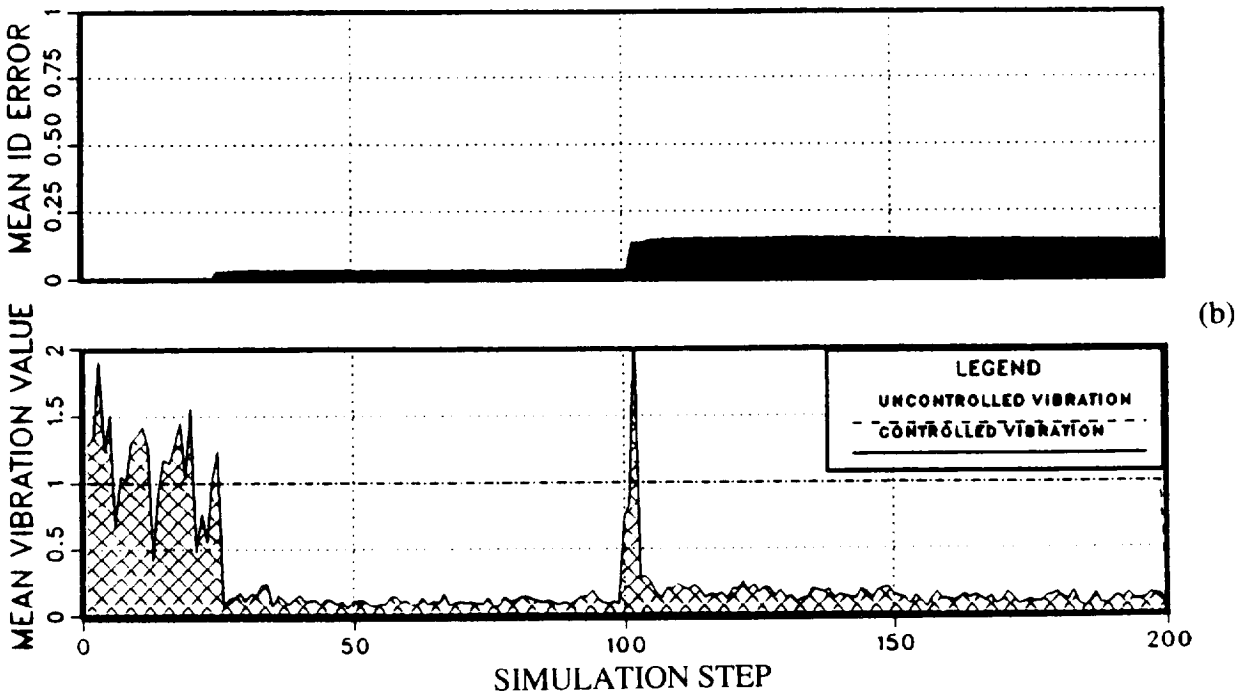

Figure 73. Closed-loop weighted-least-squares identification error and vibration for 10% measurement noise, no probing, and "zero-vibration" defined as 0.20 of baseline showing effect of batch size n: (a) n = 12; (b) n = 24 (Global Model).

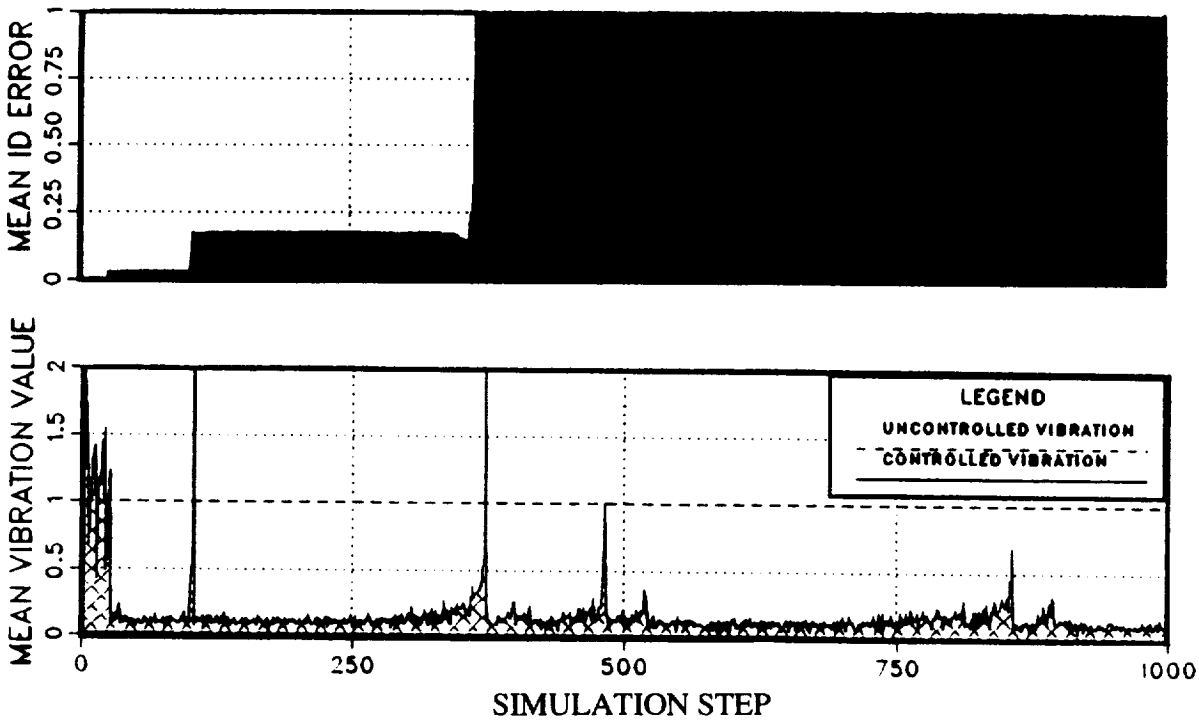

Figure 74. Closed-loop weighted-least-squares identification error and vibration for 10% measurement noise using batch size n = 24 with "zero-vibration" of 0.20 for the case of continuous transfer-matrix variation (Global Model).

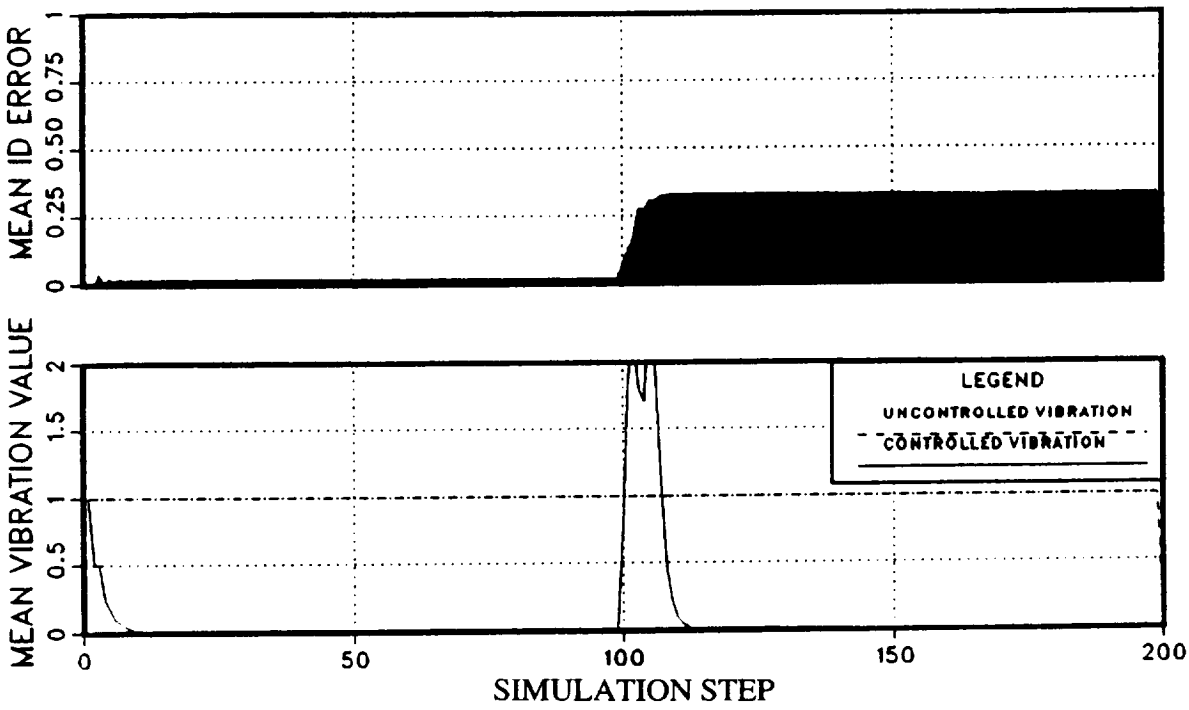

(a)

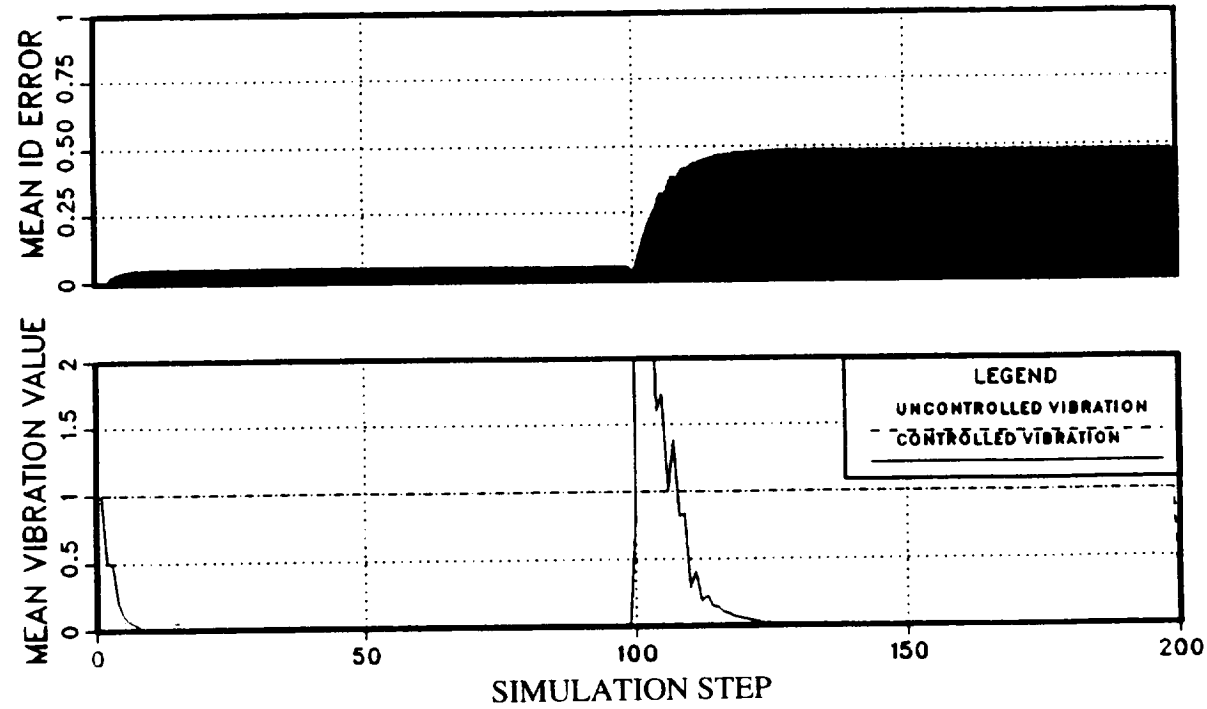

(b)

Figure 75 (part 1). Closed-loop Kalman filter identification error and vibration for no measurement noise, no probing, and $\mathbf{Q} = 10 * \mathbf{I}_6$, showing effect of tuning: (a) r = 1, $\mathbf{M} = \mathbf{I}_6$; (b) r = 10, $\mathbf{M} = \mathbf{I}_6$ (Global Model).

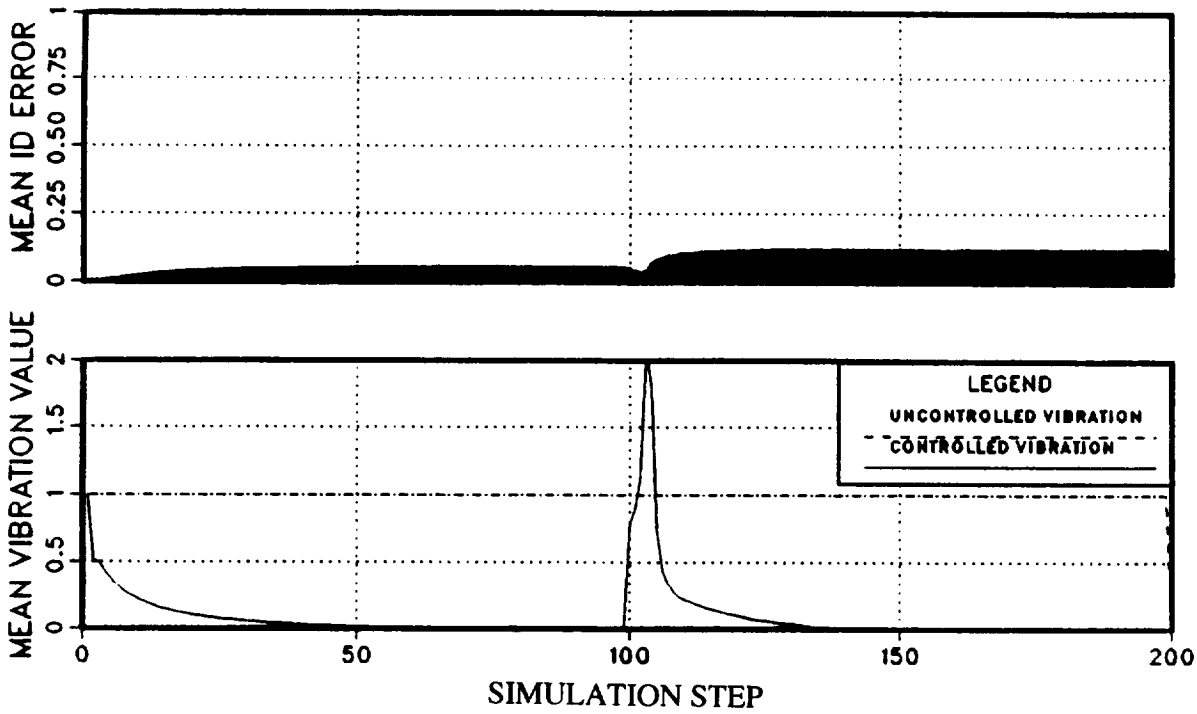

(c)

Figure 75 (part 2). Closed-loop Kalman filter identification error and vibration for no measurement noise, no probing, and $\mathbf{Q} = 10 * \mathbf{I}_6$, showing effect of tuning: (c) r = 100, $\mathbf{M} = \mathbf{I}_6$ (Global Model).

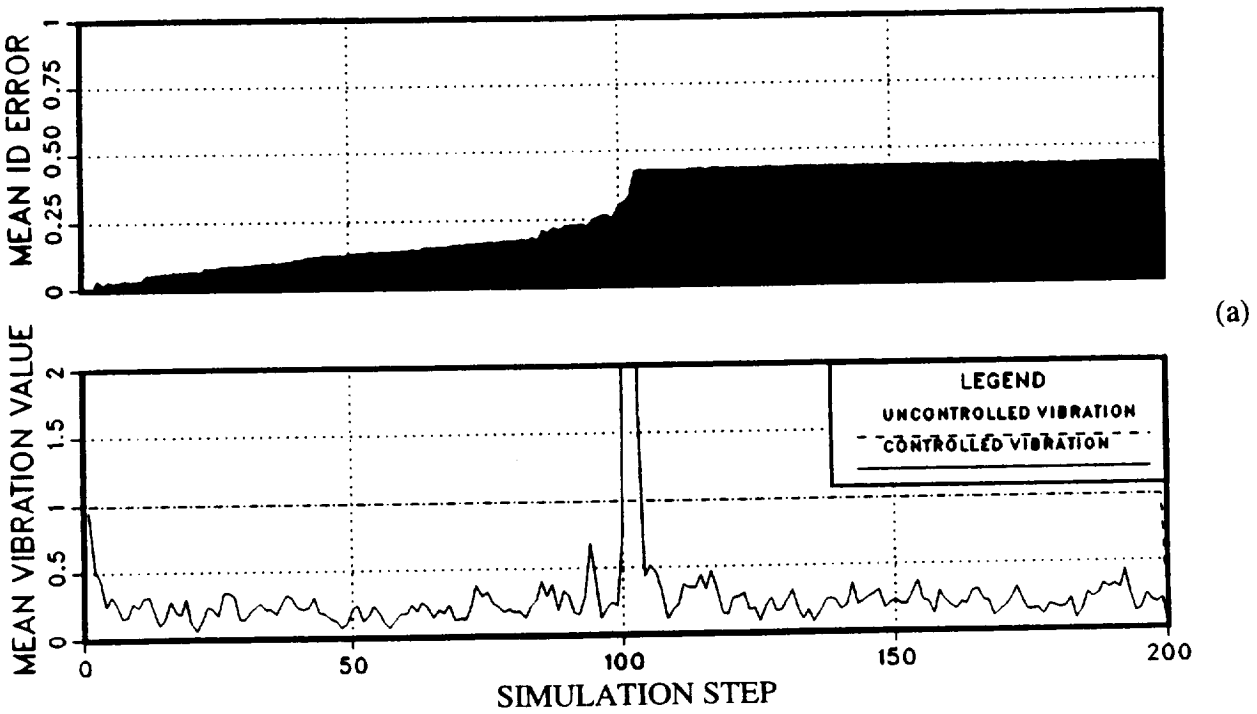

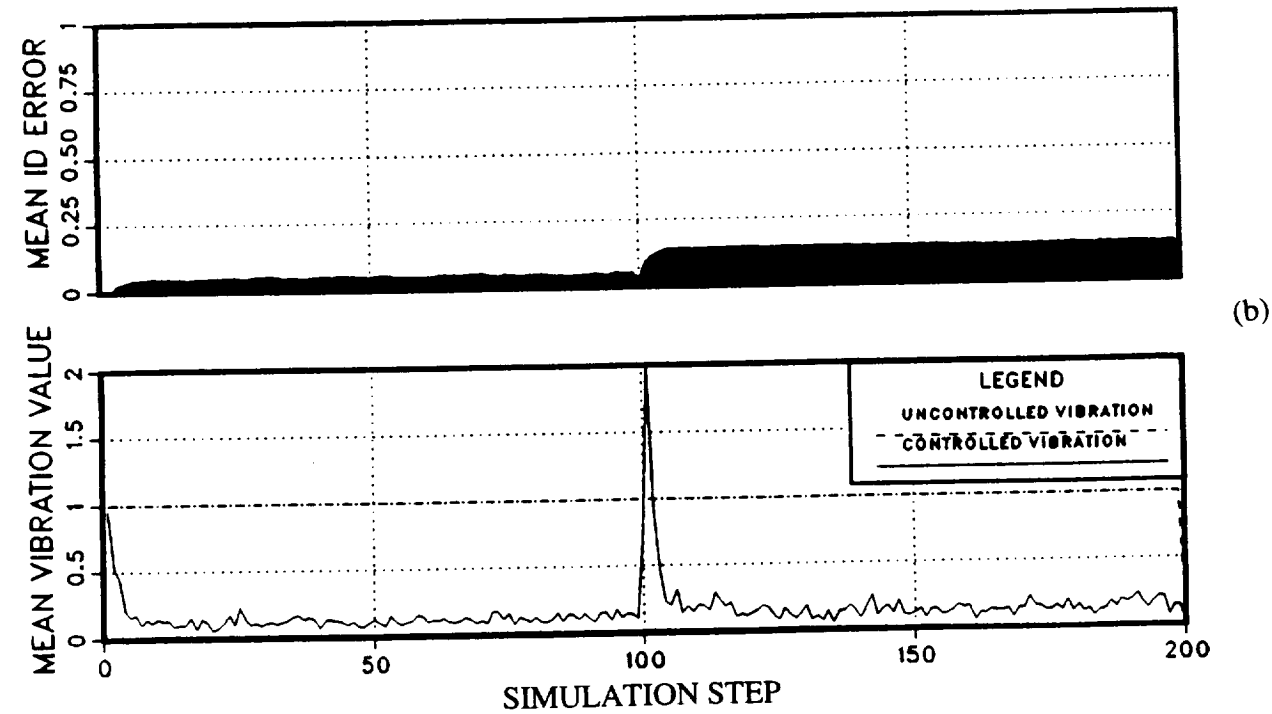

Figure 76 (part 1). Closed-loop Kalman filter identification error and vibration for 10% measurement noise, no probing, and $\mathbf{Q} = 10 * \mathbf{I}_6$, showing effect of tuning: (a) r = 1, $\mathbf{M} = \mathbf{I}_6$; (b) r = 10, $\mathbf{M} = \mathbf{I}_6$ (Global Model).

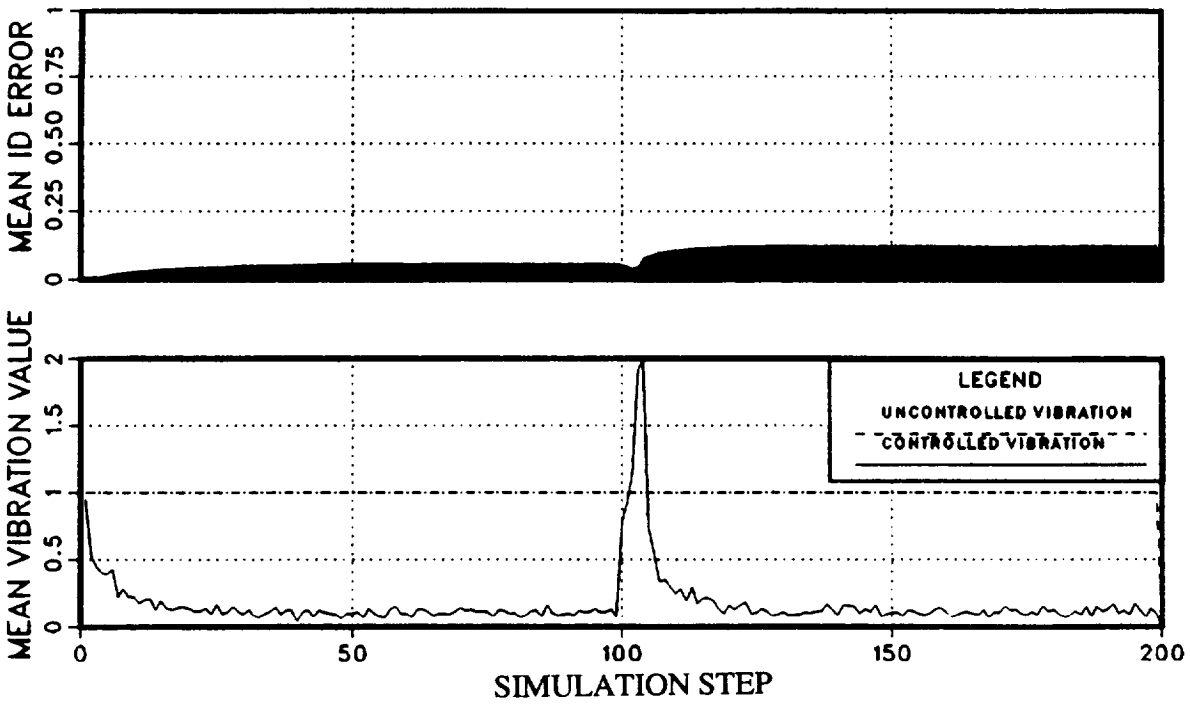

(c)

Figure 76 (part 2). Closed-loop Kalman filter identification error and vibration for 10% measurement noise, no probing, and $\mathbf{Q} = 10 * \mathbf{I}_6$, showing effect of tuning: (c) r = 100, $\mathbf{M} = \mathbf{I}_6$ (Global Model).

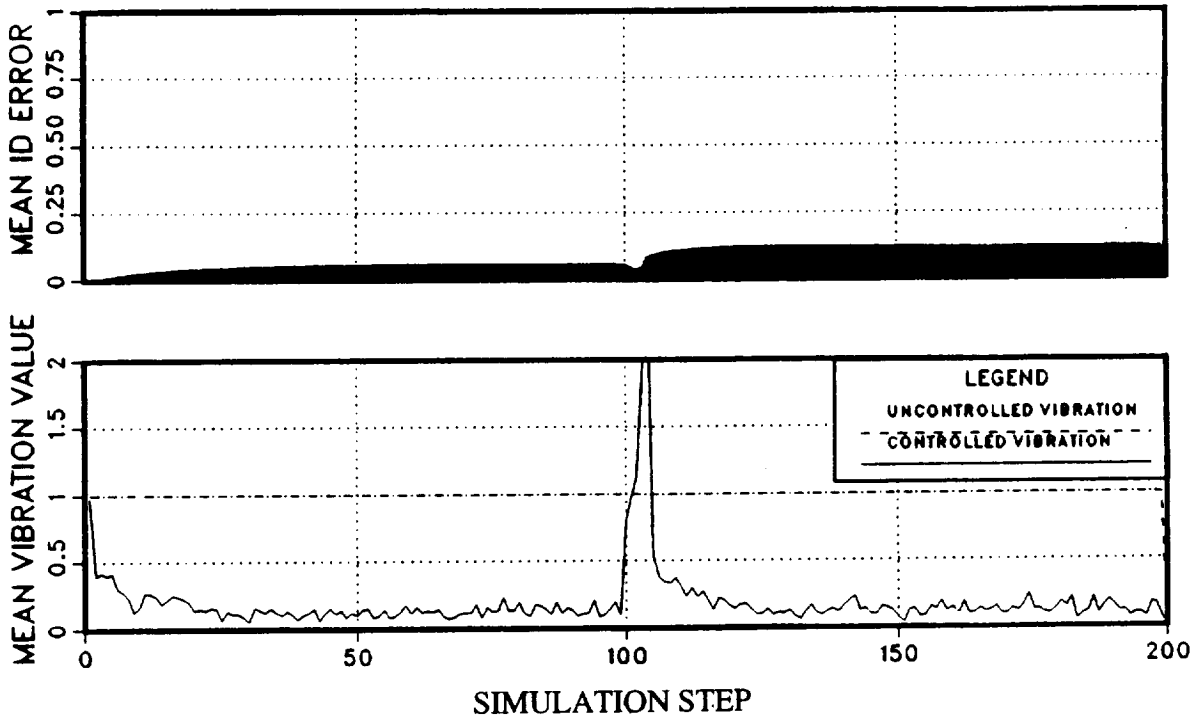

Figure 77. Closed-loop Kalman filter identification error and vibration for 10% measurement noise, $\mathbf{Q} = 10 * \mathbf{I}_6$, r = 100, and $\mathbf{M} = \mathbf{I}_6$ with 10% probing (Global Model).

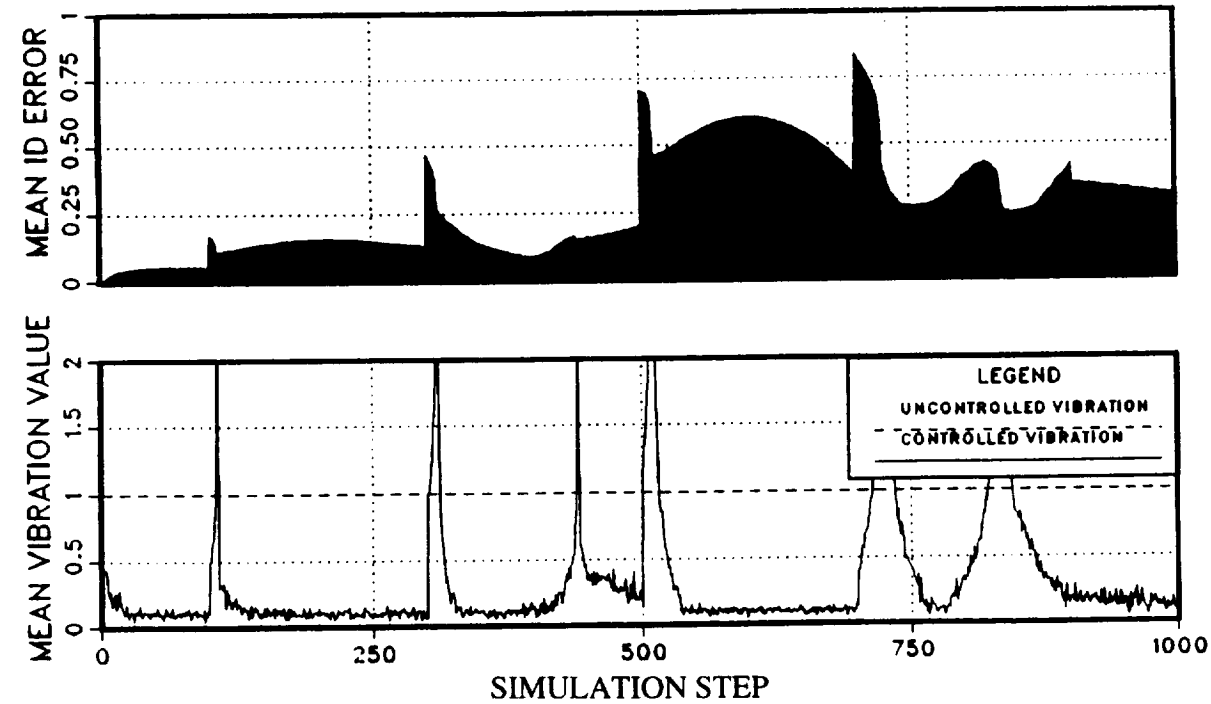

Figure 78. Closed-loop Kalman filter identification error and vibration for 10% measurement noise, 10% probing, r = 100, $\mathbf{M} = \mathbf{I}_6$, and $\mathbf{Q} = 10 * \mathbf{I}_6$, showing effect of continuous transfer-matrix variation (Global Model).

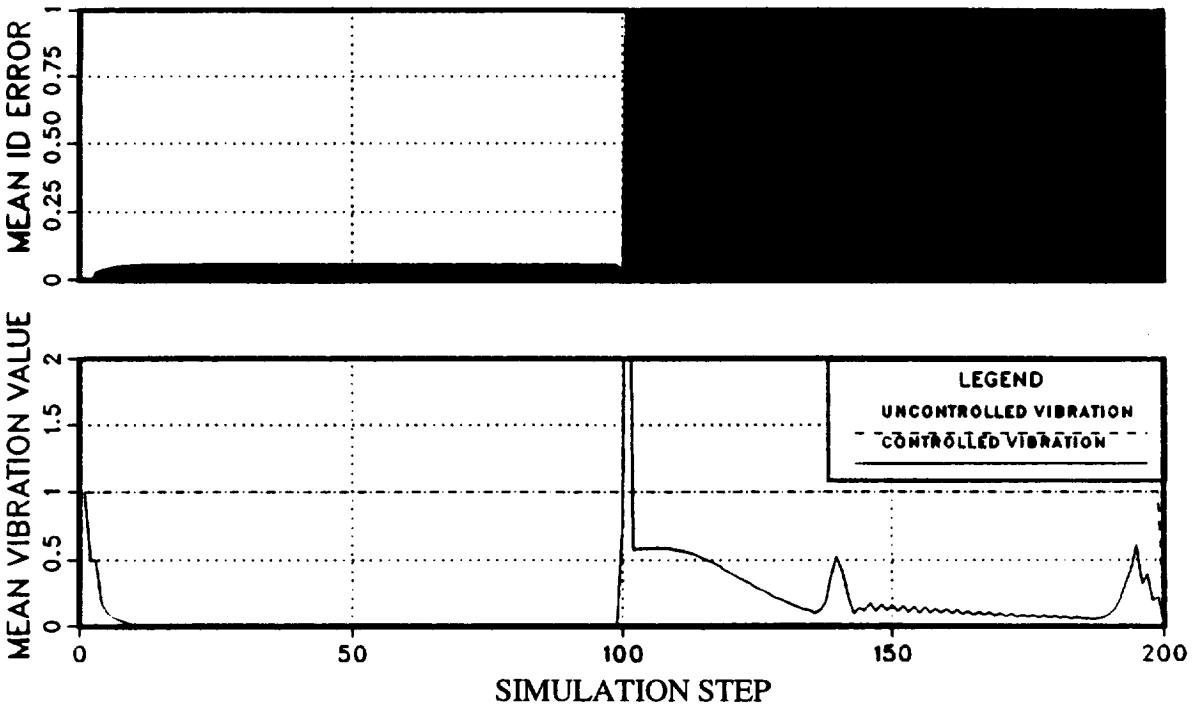

(a)

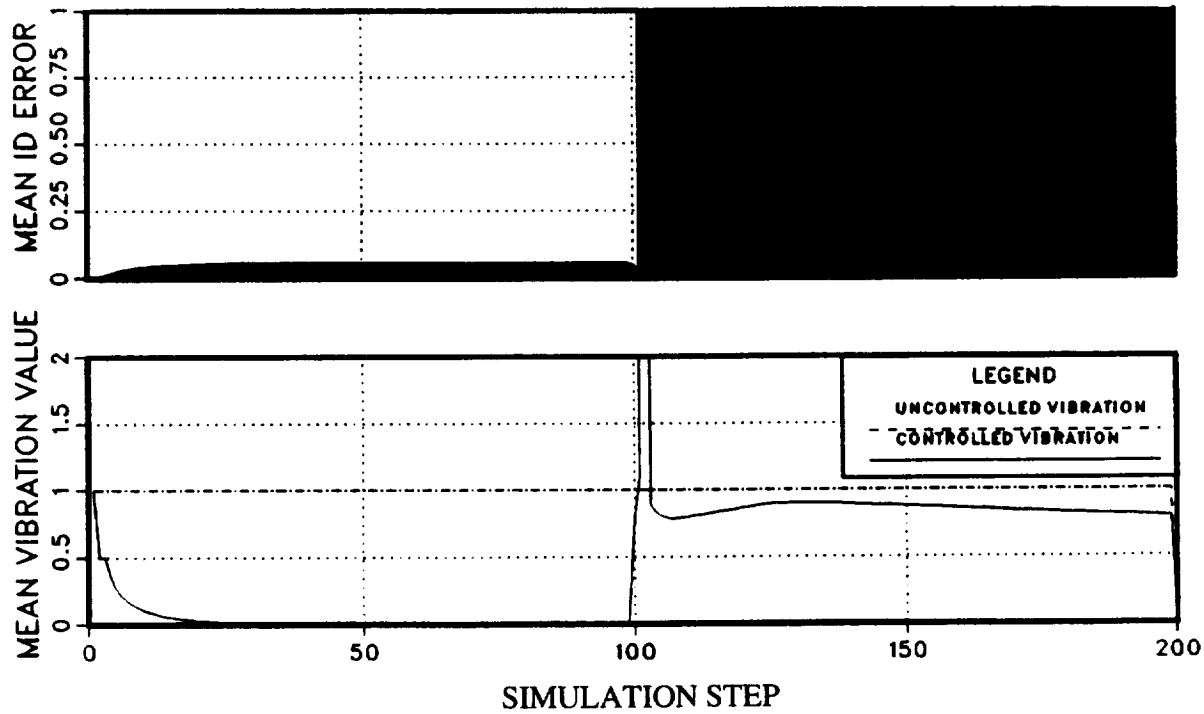

(b)

Figure 79 (part 1). Closed-loop LMS filter identification error and vibration for no measurement noise and no probing, showing effect of (a) $\mathbf{K}_S = 0.05$; (b) $\mathbf{K}_S = 0.02$ (Global Model).

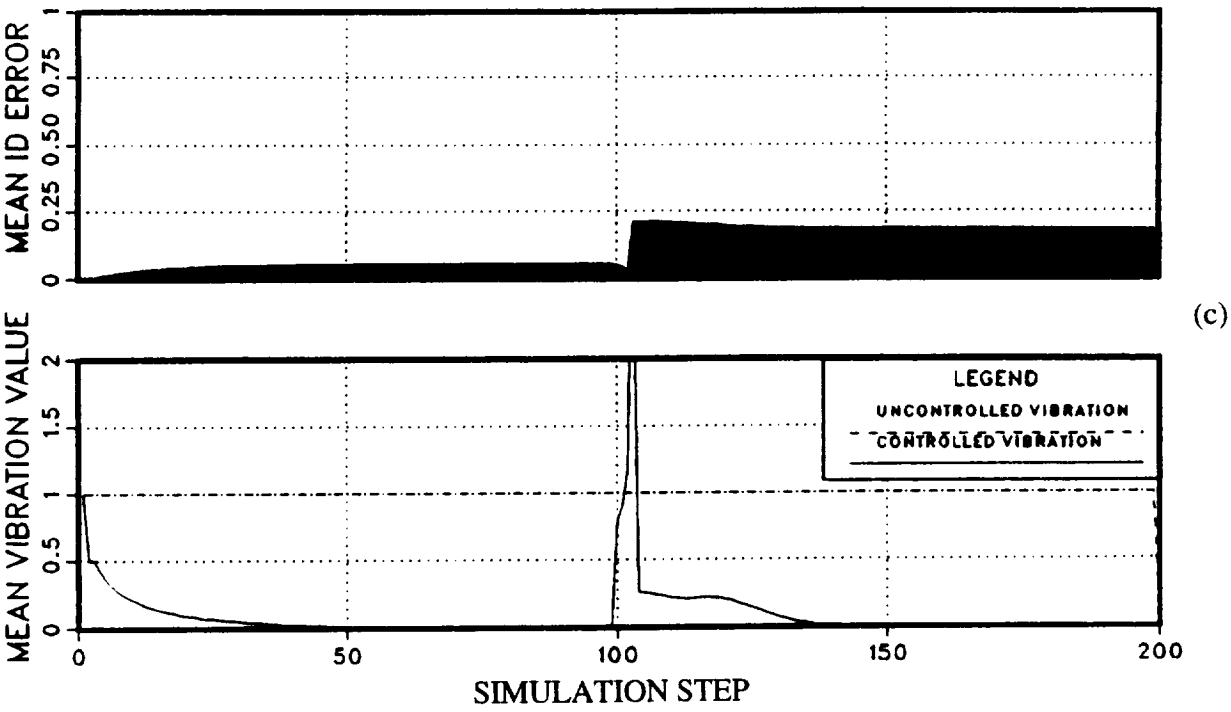

(c)

Figure 79 (part 2). Closed-loop LMS filter identification error and vibration for no measurement noise and no probing, showing effect of (c) $\mathbf{K}_S = 0.01$ (Global Model).

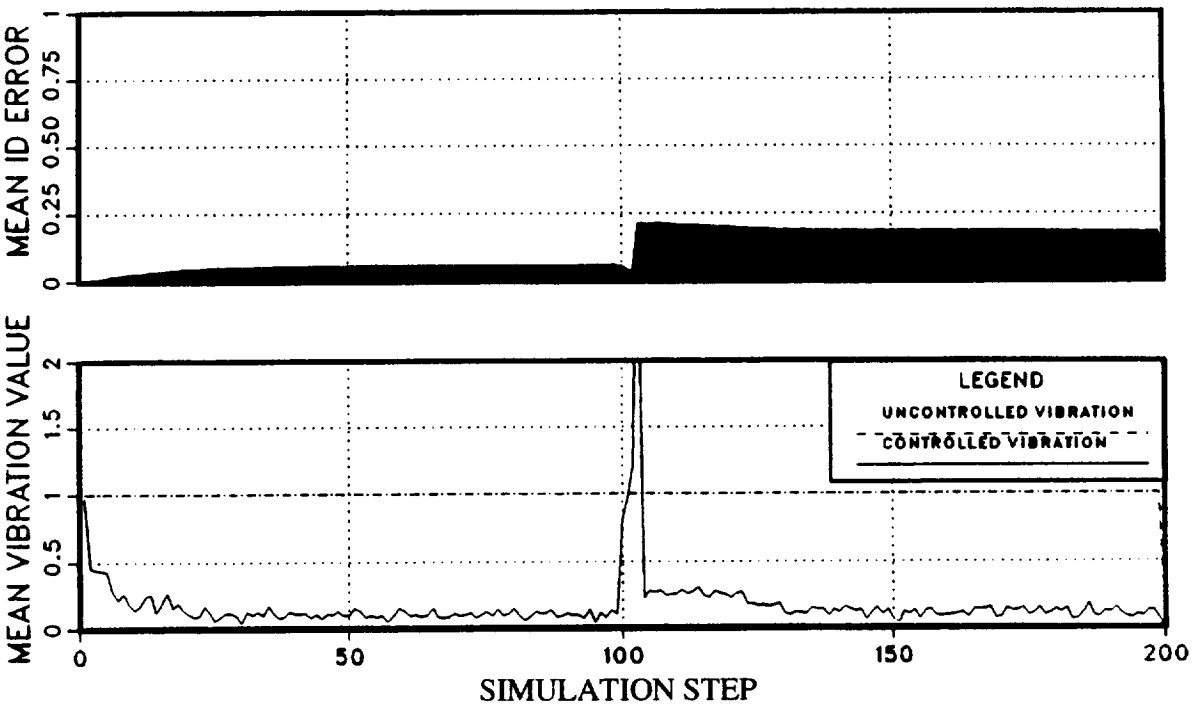

Figure 80. Closed-loop LMS filter identification error and vibration for no probing with $\mathbf{K}_S = 0.01$, showing effect of 10% measurement noise (Global Model).

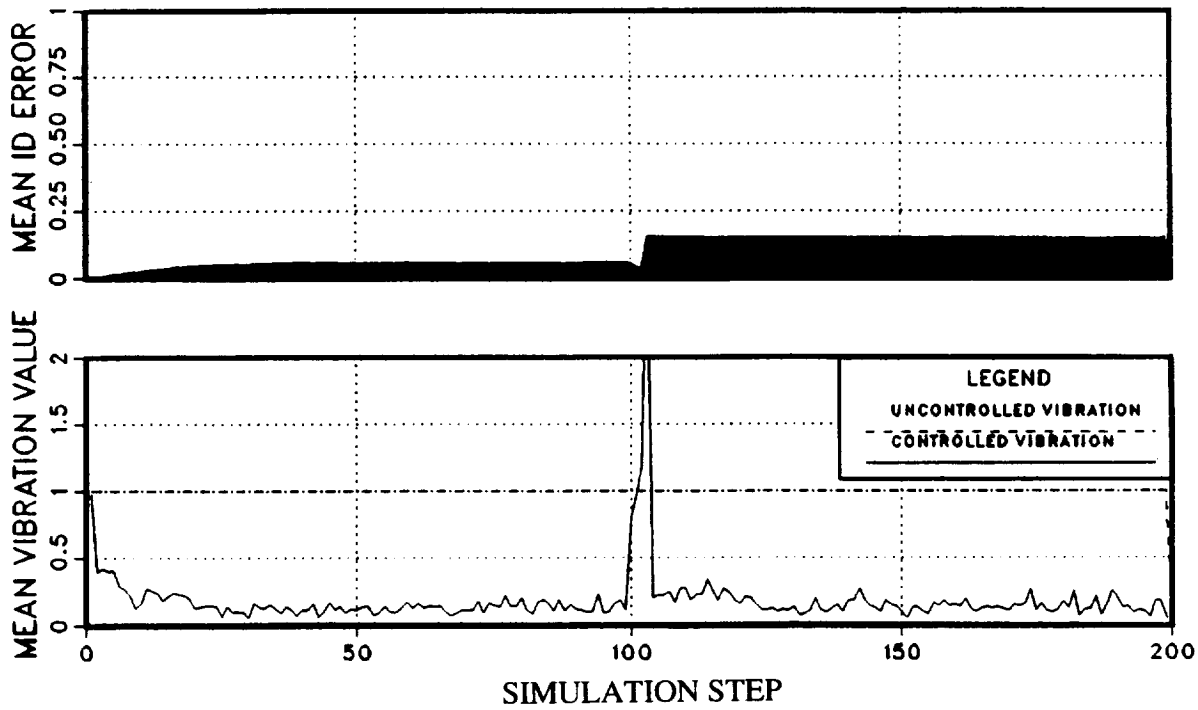

Figure 81. Closed-loop LMS filter identification error and vibration for 10% measurement noise and $\mathbf{K}_S = 0.01$ showing effect of 10% probing (Global Model).

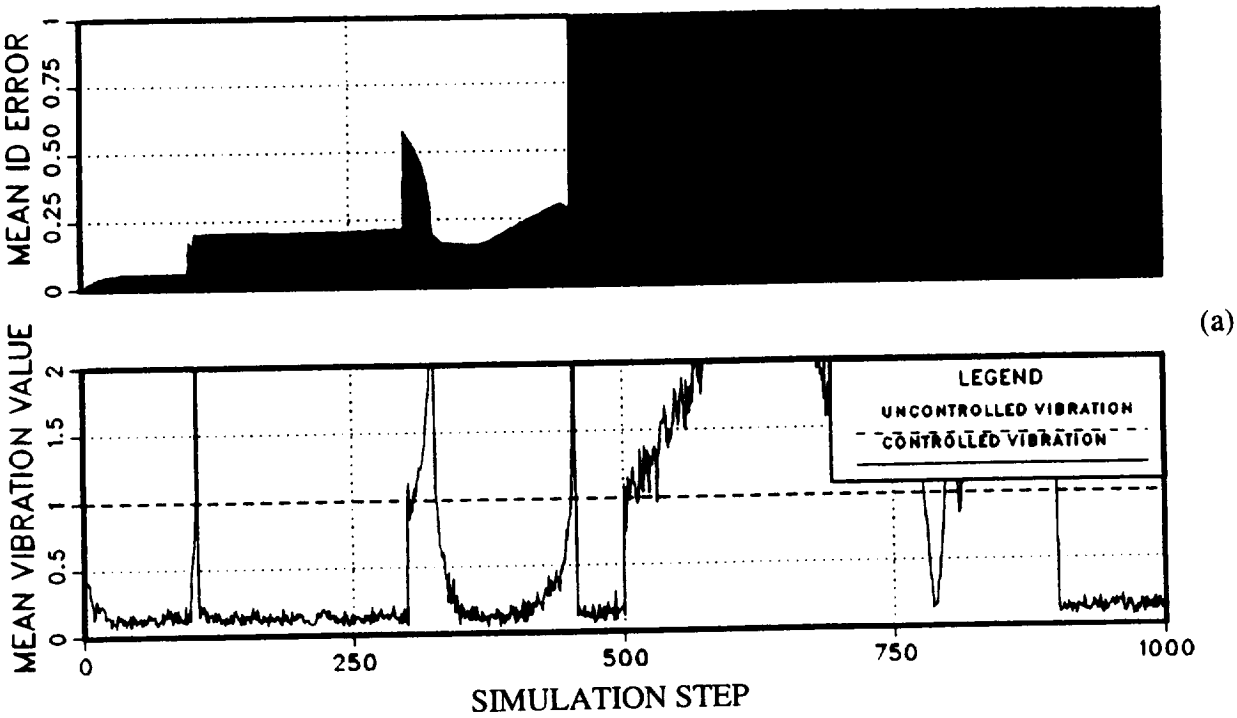

(a)

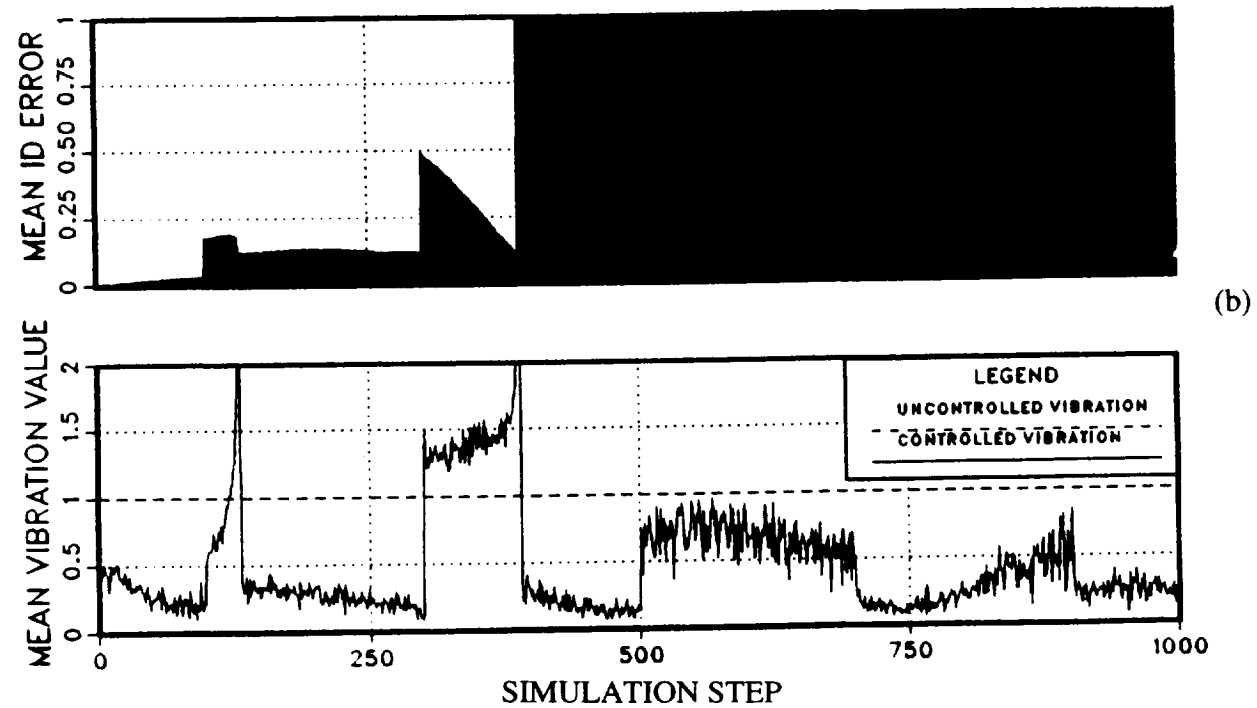

(b)

Figure 82. Closed-loop LMS filter identification error and vibration for 10% measurement noise and 10% probing, showing effect of continuous transfer-matrix variation: (a) $\mathbf{K}_S = 0.01$; (b) $\mathbf{K}_S = 0.001$ (Global Model).

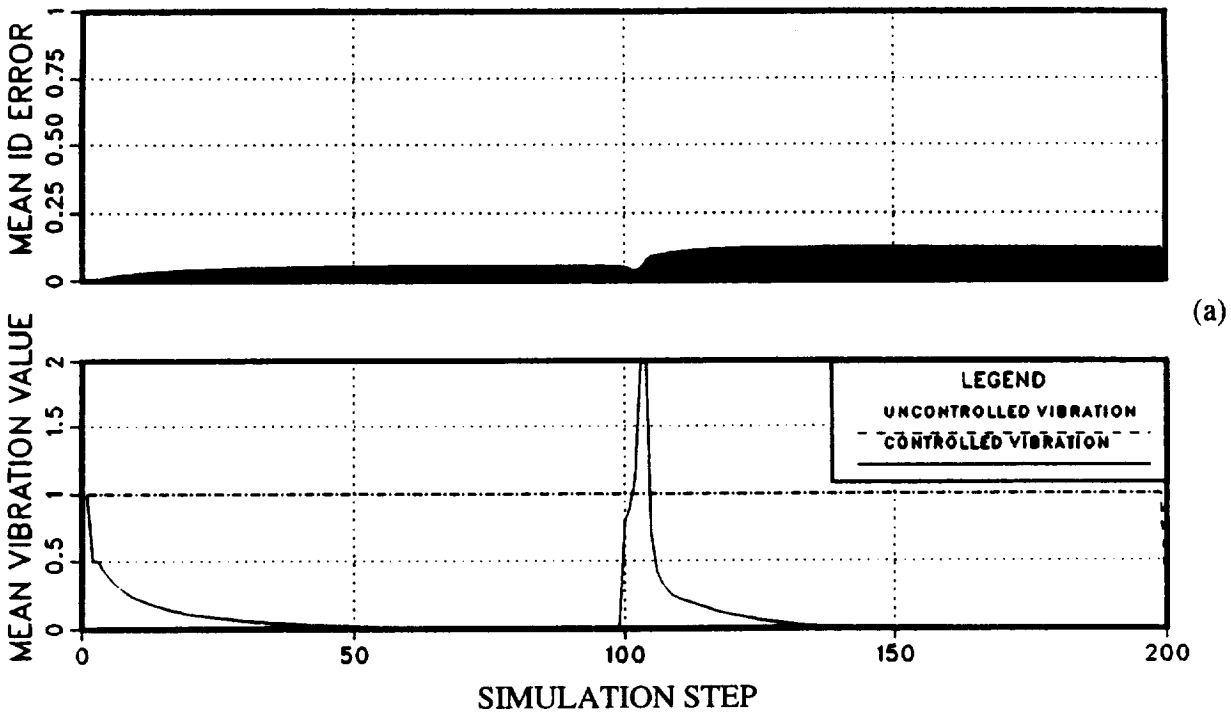

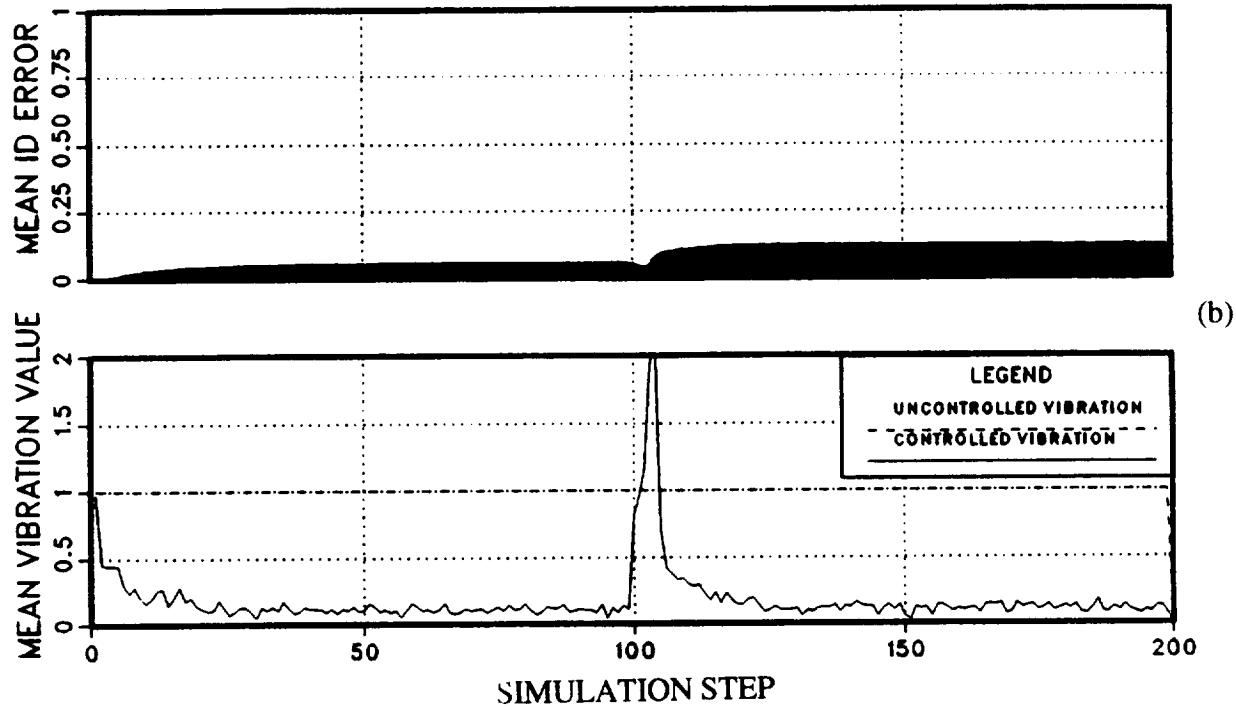

Figure 83. Closed-loop generalized Kalman filter identification error and vibration for no probing, $\mathbf{R} = 100$, $\mathbf{M} = \mathbf{I}_6$, and multi-step batch size n = 1: (a) no measurement noise; (b) 10% measurement noise (Global Model).

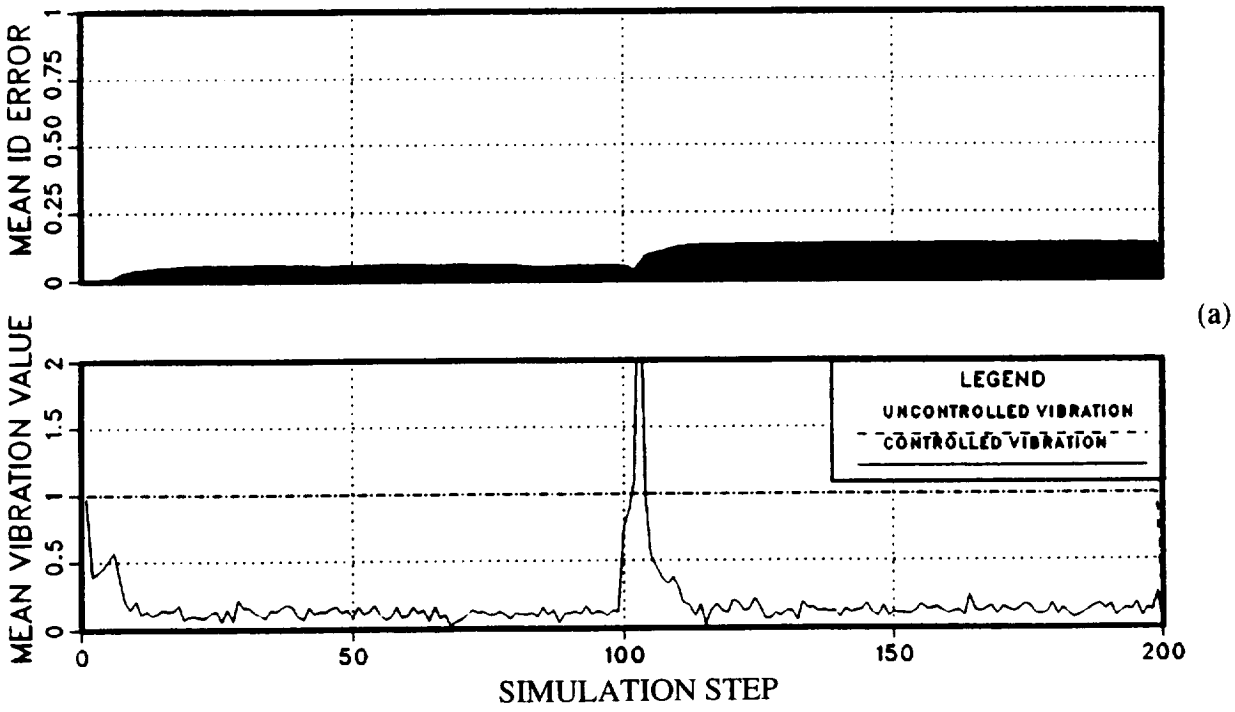

(a)

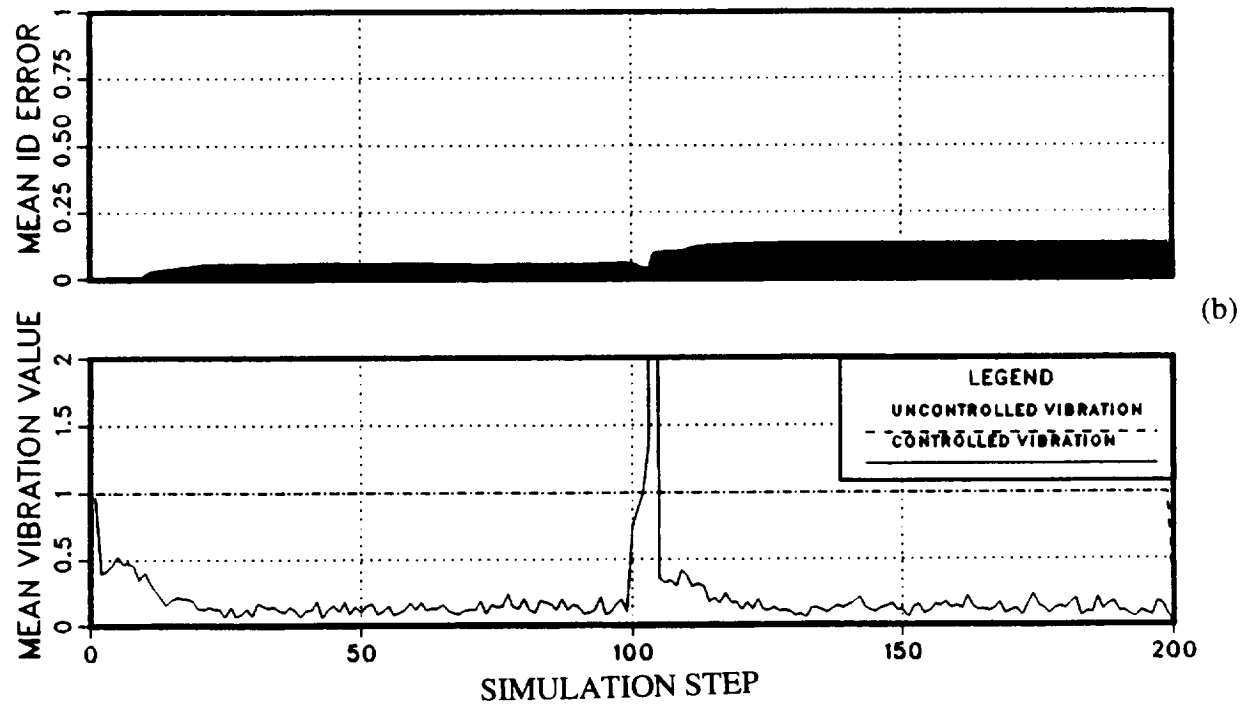

(b)

Figure 84. Closed-loop generalized Kalman filter identification error and vibration for 10% measurement noise, $\mathbf{R} = 100$, and $\mathbf{M} = \mathbf{I}_6$, showing effect of multi-step batch size n: (a) n = 4; (b) n = 6 (Global Model).

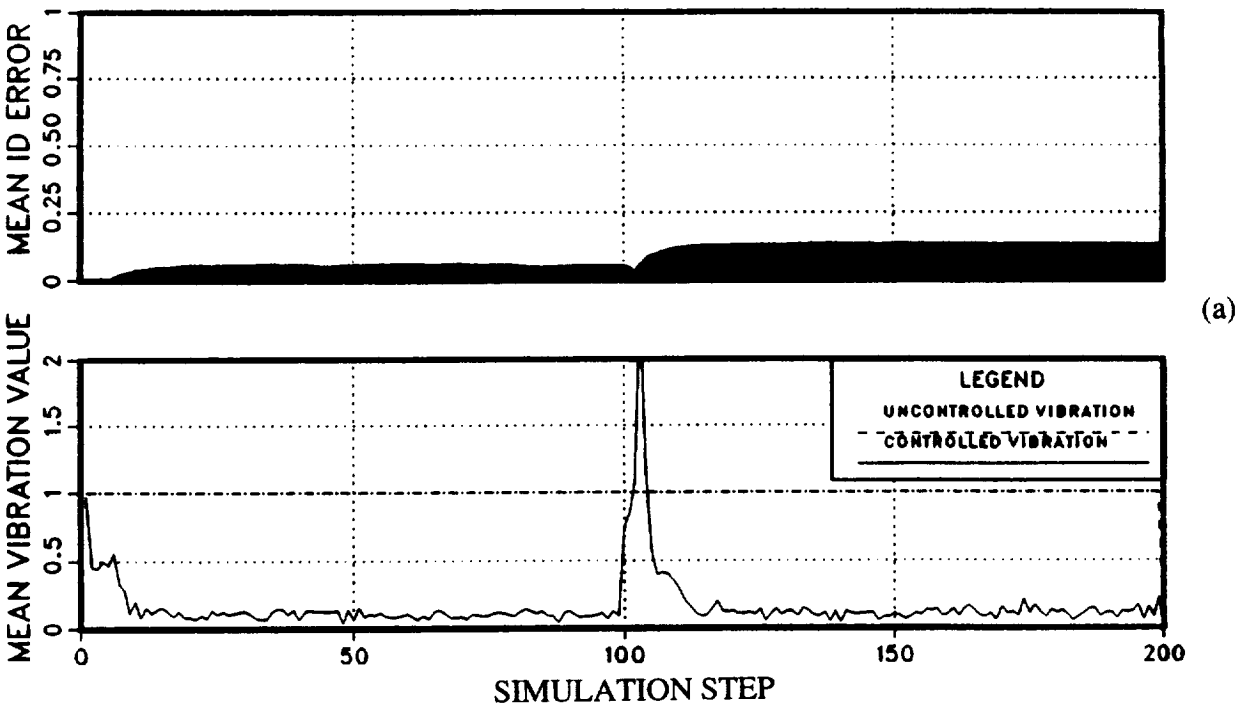

(a)

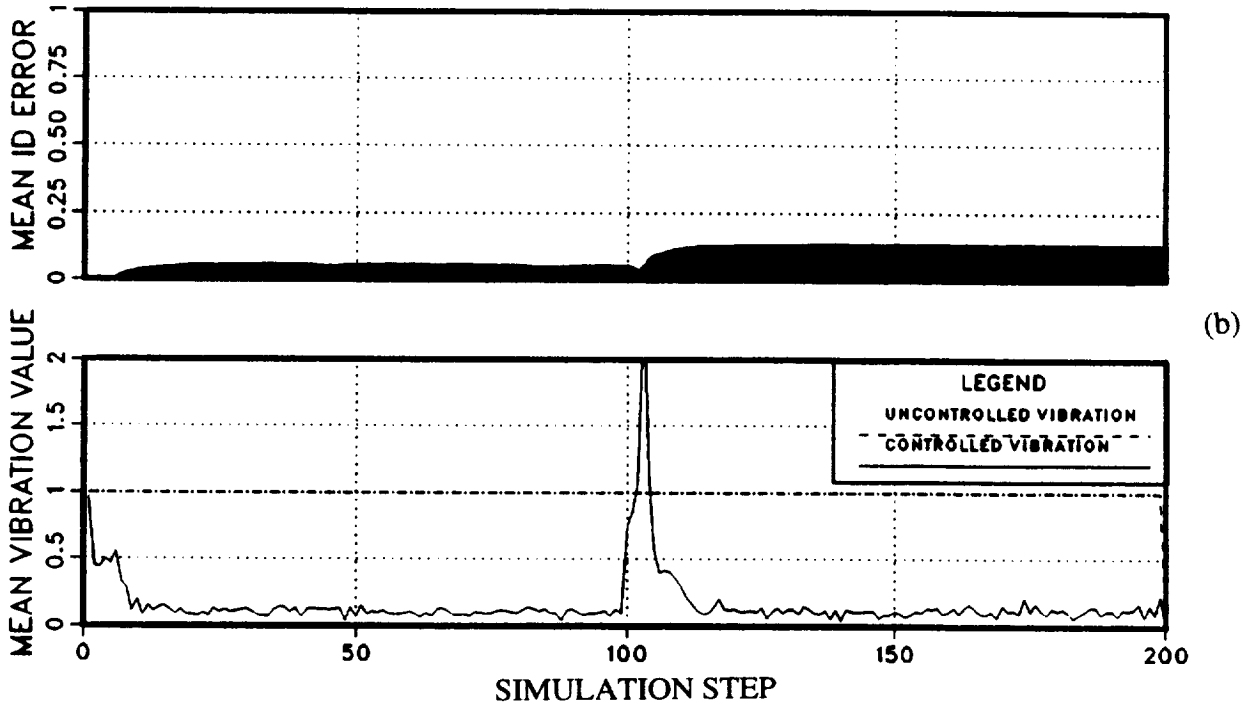

(b)

Figure 85. Closed-loop generalized Kalman filter identification error and vibration for 10% measurement noise, $\mathbf{R} = 100$, $\mathbf{M} = \mathbf{I}_6$, and multi-step batch size n = 4 showing effect of CA: (a) 4-cycle averaging; (b) 8-cycle averaging (Global Model).

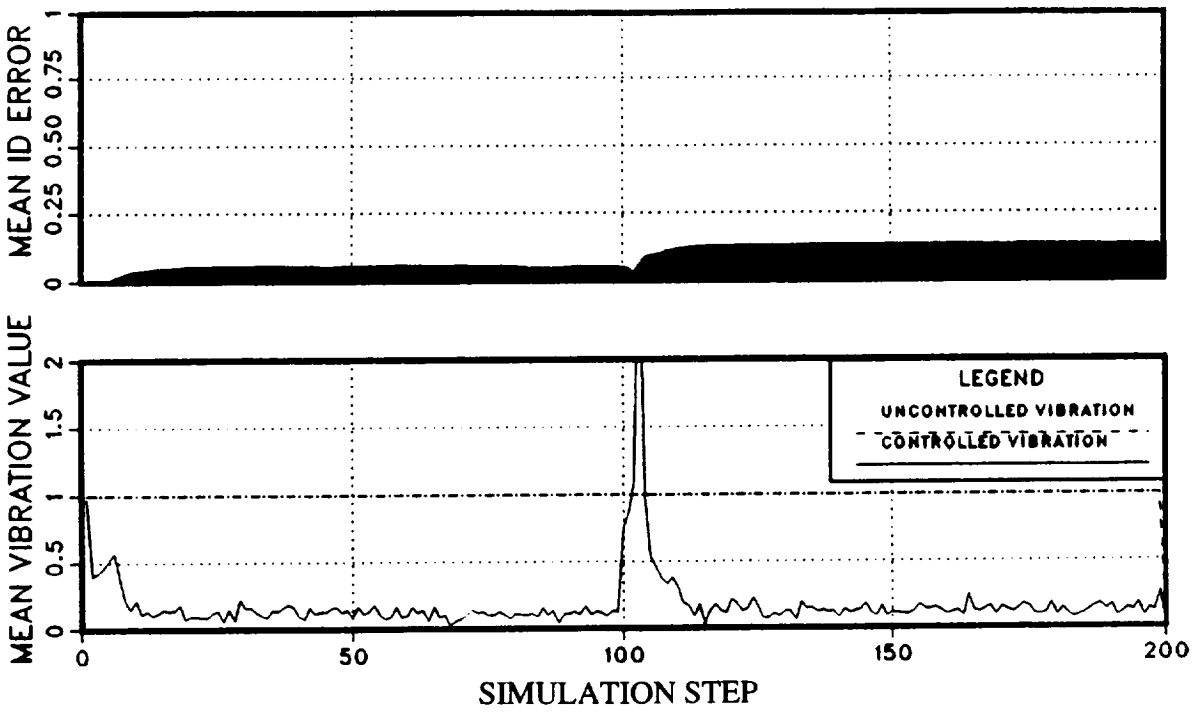

Figure 86. Closed-loop generalized Kalman filter identification error and vibration for 10% measurement noise, $\mathbf{R} = 100$, $\mathbf{M} = \mathbf{I}_6$, multi-step batch size n = 4, and 8-cycle averaging showing effect of 10% probing (Global Model).

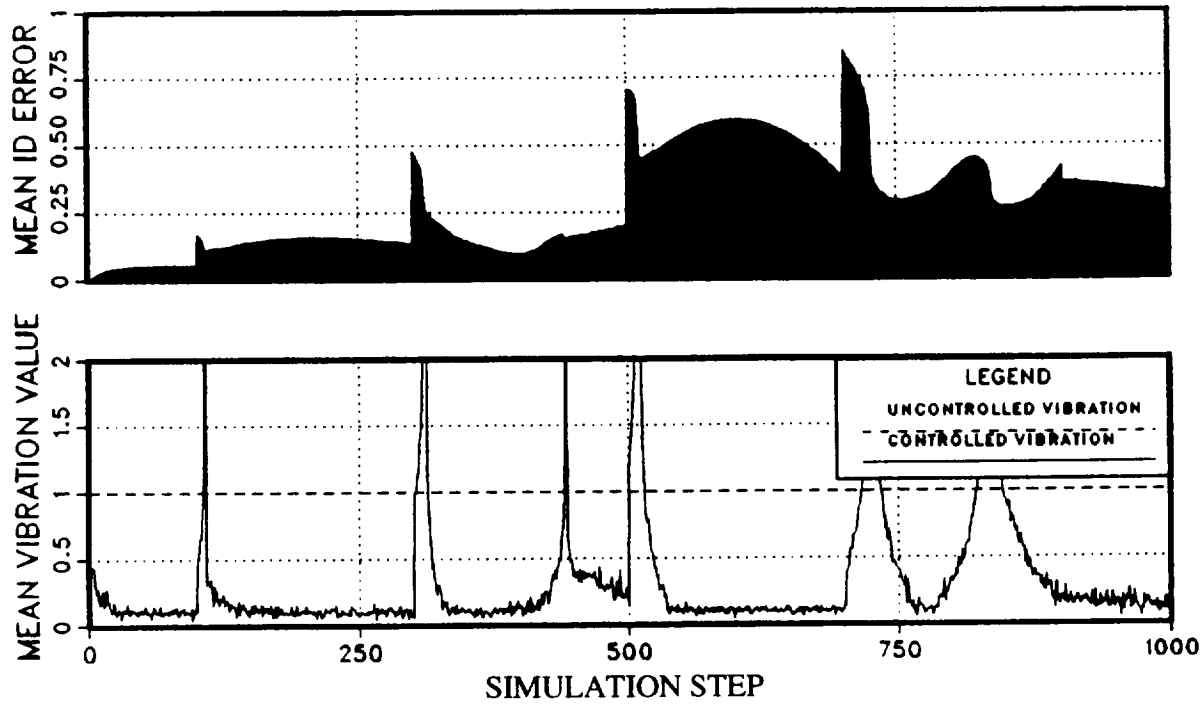

Figure 87. Closed-loop generalized Kalman filter identification error and vibration for 10% measurement noise, no probing, $\mathbf{R} = 100$, $\mathbf{M} = \mathbf{I}_6$, multi-step batch size n = 1, and no cycle averaging, showing effect of continuous transfer-matrix variation (Global Model).

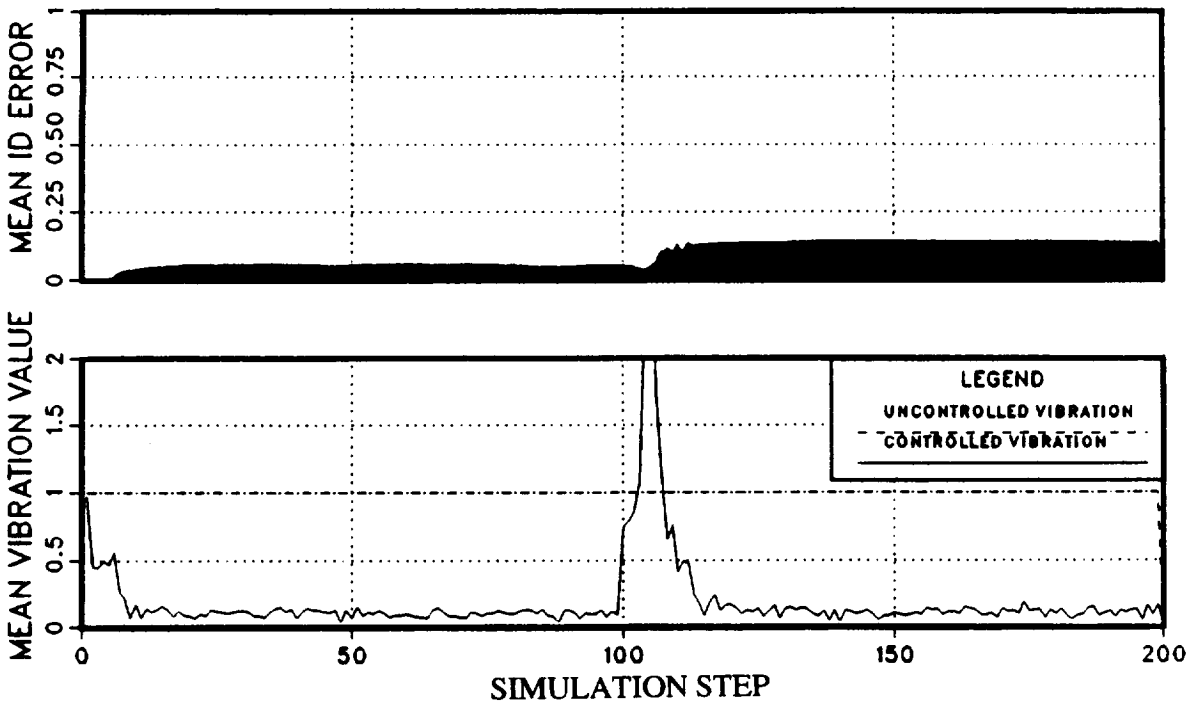

Figure 88. Closed-loop generalized LMS filter identification error and vibration for 10% measurement noise, no probing, $\mathbf{K}_S = 0.01 * \mathbf{I}_6$, multi-step batch size n = 4 and 4-cycle averaging (Global Model).

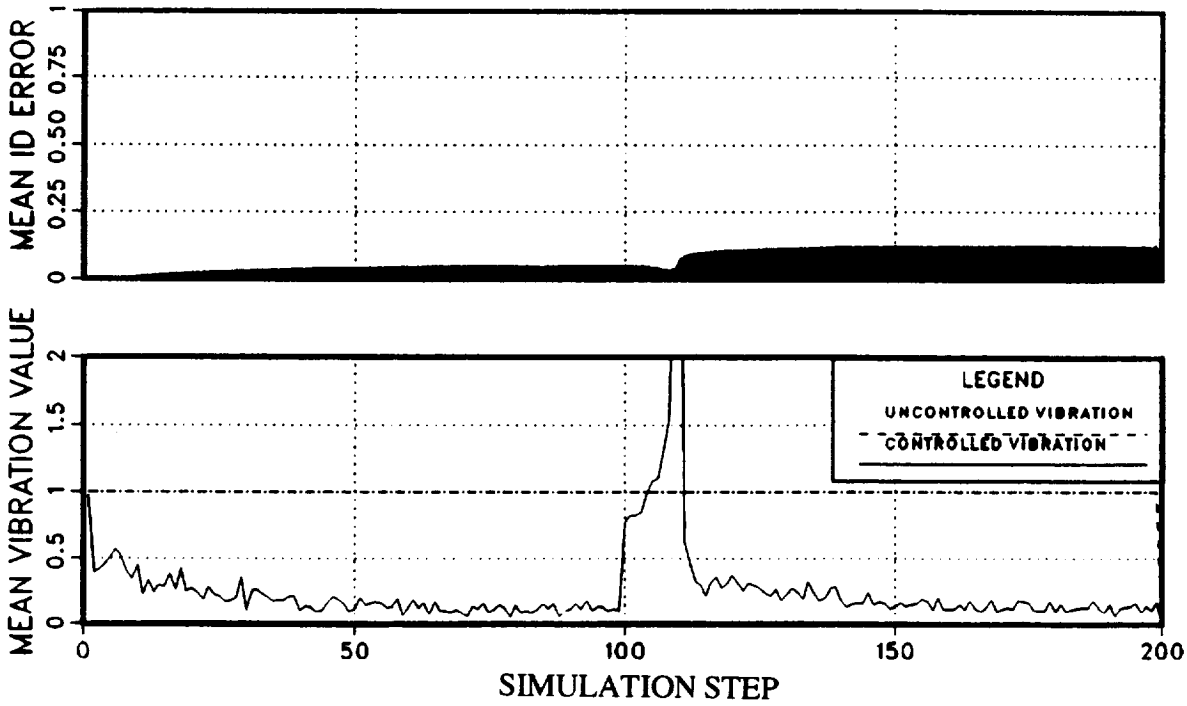

Figure 89. Closed-loop generalized LMS filter identification error and vibration for 10% measurement noise, 10% probing, $\mathbf{K}_S = 0.001 * \mathbf{I}_6$, multi-step batch size n = 4, and no cycle averaging (Global Model).

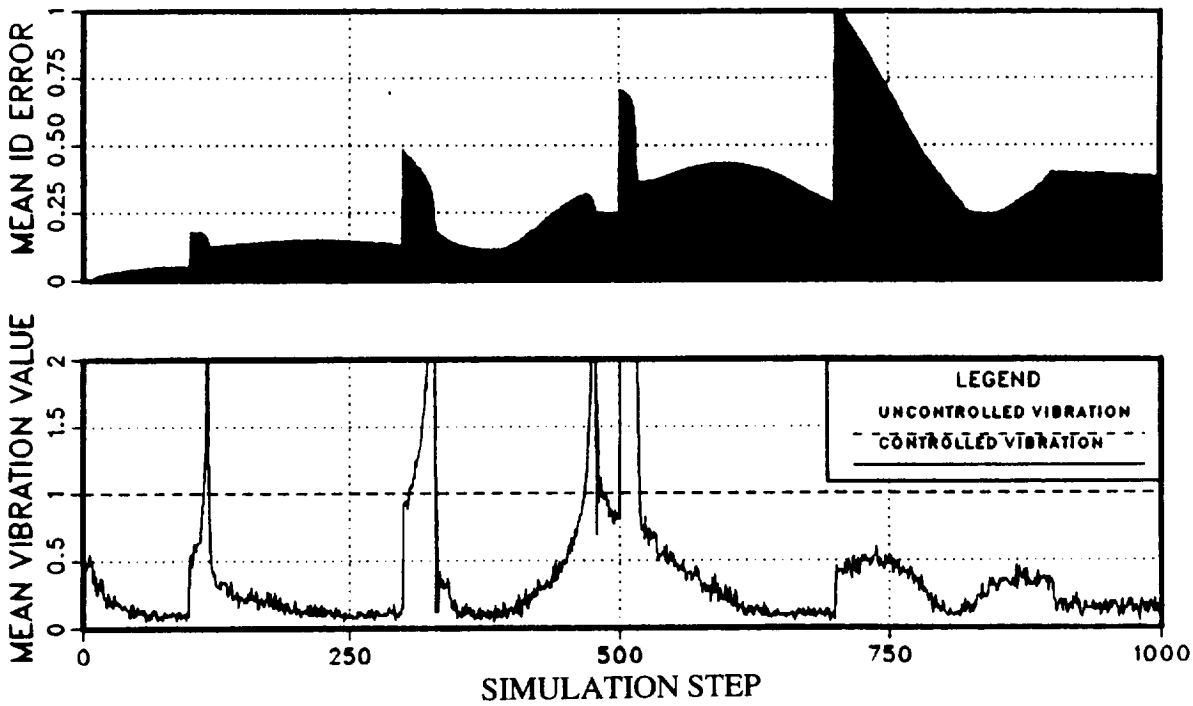

Figure 90. Closed-loop generalized LMS filter identification error and vibration for 10% measurement noise, no probing, $\mathbf{K}_S = 0.001 * \mathbf{I}_6$, multi-step batch size n = 4, and no cycle averaging, showing effect of continuous transfer-matrix variation (Global Model).

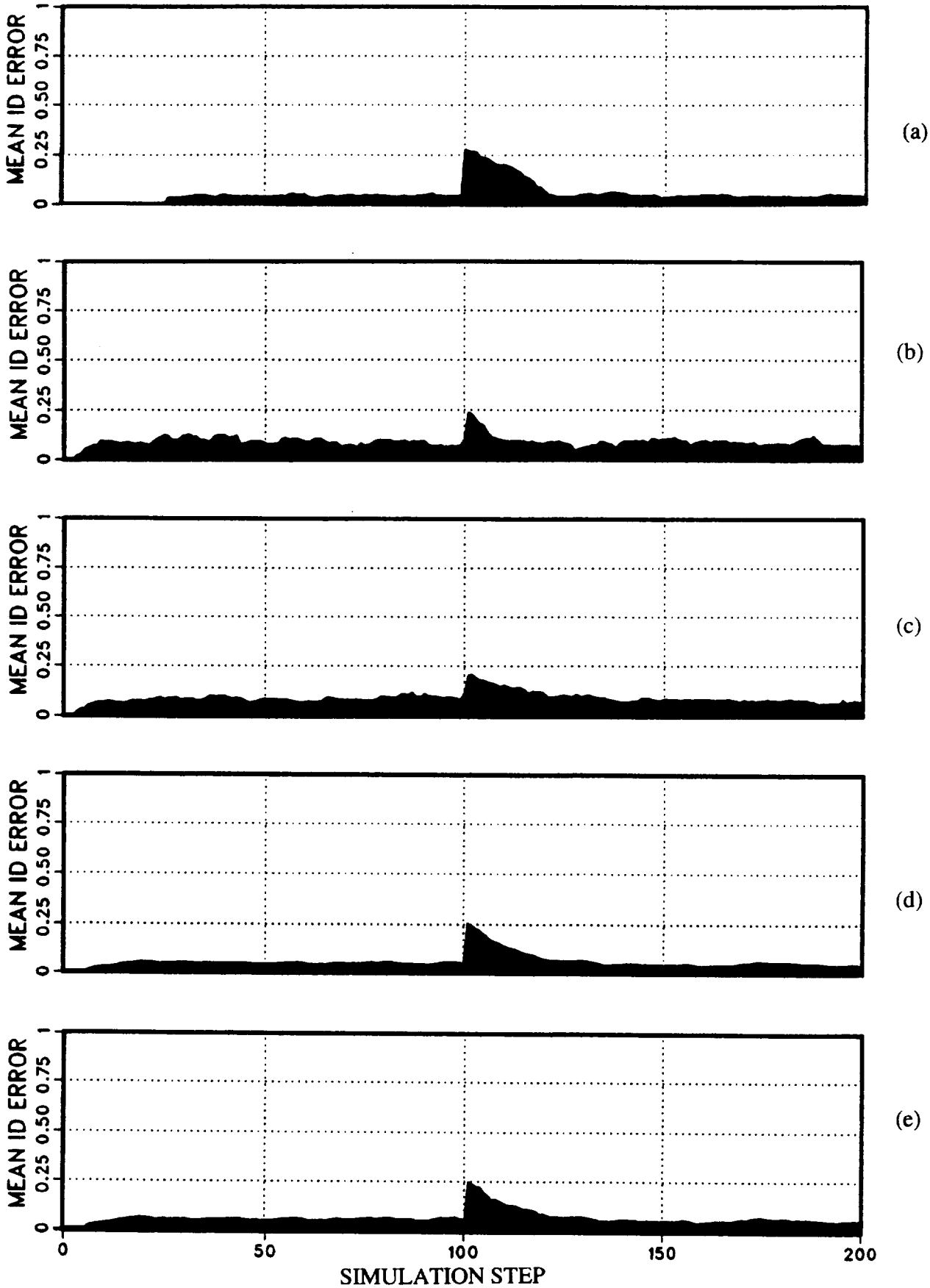

Figure 91. Comparison of local model, open-loop identification error for 10% measurement noise: (a) weighted least squares with batch size n = 24; (b) Kalman filter, $\mathbf{M} = 10 * \mathbf{I}_6$, r = 1, $\mathbf{Q} = 10$; (c) LMS filter, $\mathbf{K}_S = 0.3$; (d) generalized Kalman filter, multi-step batch size n = 4, $\mathbf{M} = \mathbf{I}_6$, $\mathbf{R} = 10$; (e) generalized LMS filter, multi-step batch size n = 4, $\mathbf{K}_S = 0.1 * \mathbf{I}_6$.

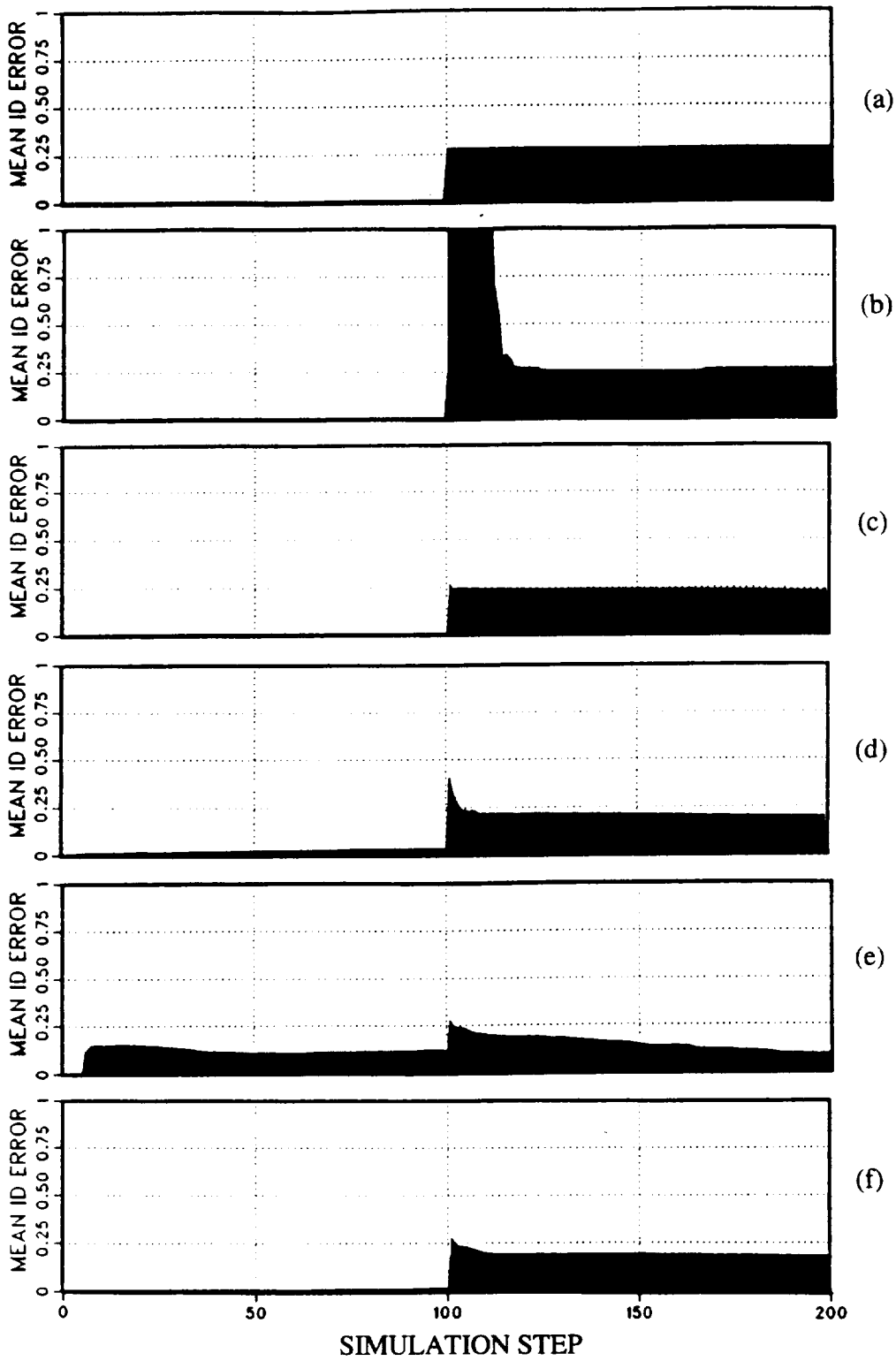

Figure 92. Comparison of Local Model, closed-loop identification error for the case of 10% measurement noise and a single change in the transfer matrix at simulation step 100: (a) error without identification; (b) weighted least squares with n = 24, 10% probing, and "zero-vibration" = 0.20; (c) Kalman filter with r = 100, $\mathbf{M} = \mathbf{I}_6$, $\mathbf{Q} = 10 * \mathbf{I}_6$, and 10% probing; (d) LMS filter with $\mathbf{K}_S = 0.1$ and 10% probing; (e) generalized Kalman filter with $\mathbf{R} = 1$, $\mathbf{M} = 10 * \mathbf{I}_6$, batch size n = 4, 4-cycle averaging, and 10% probing; (f) generalized LMS filter with $\mathbf{K}_S = 0.1 * \mathbf{I}_6$, batch size n = 8, and 4-cycle averaging.

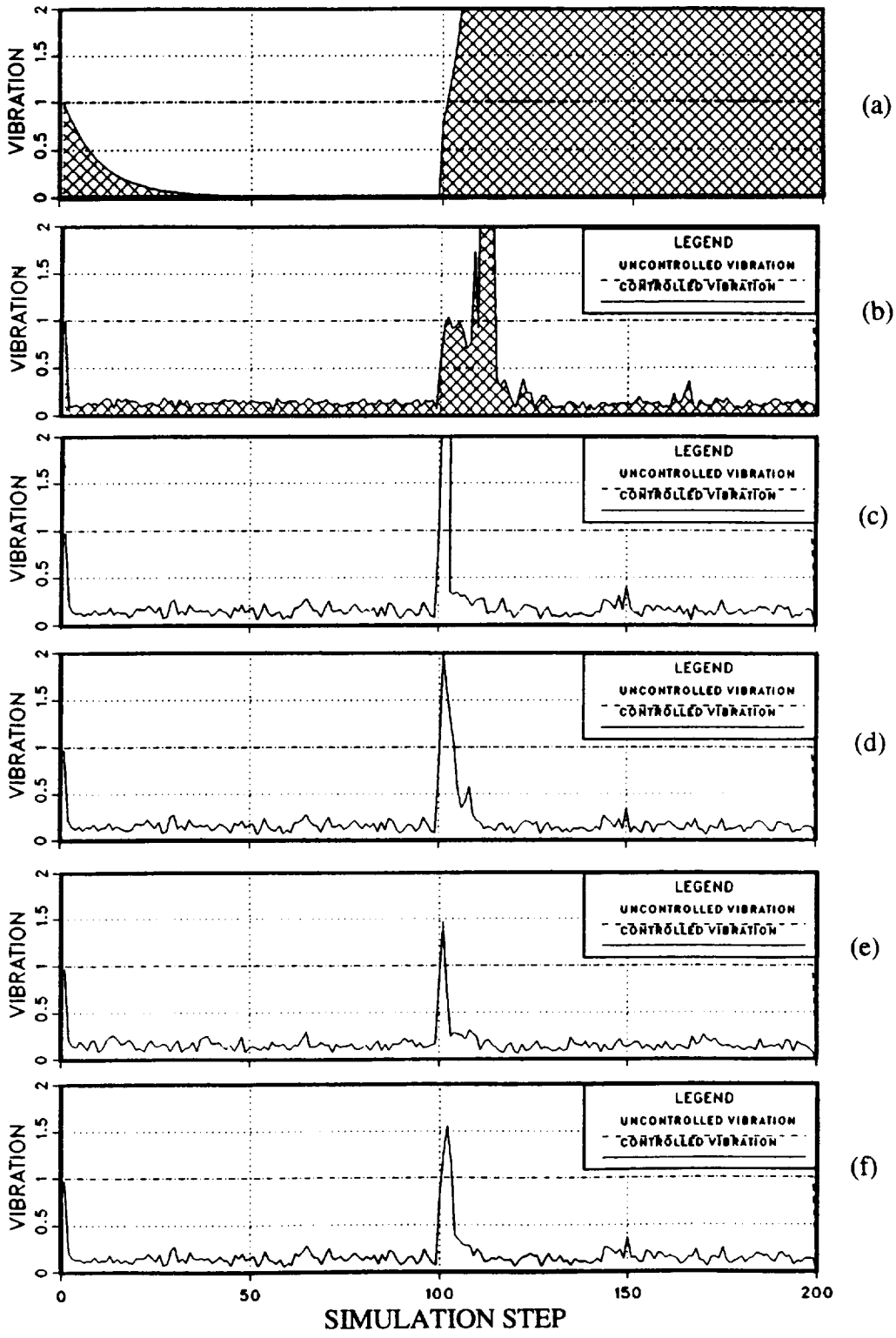

Figure 93. Comparison of Local Model, closed-loop vibration index for the case of 10% measurement noise and a single change in the transfer matrix at simulation step 100: (a) without identification; (b) weighted least squares with n = 24, 10% probing, and "zero-vibration" = 0.20; (c) Kalman filter with r = 100, $\mathbf{M} = \mathbf{I}_6$, $\mathbf{Q} = 10 * \mathbf{I}_6$, and 10% probing; (d) LMS filter with $\mathbf{K}_S = 0.1$ and 10% probing; (e) generalized Kalman filter with $\mathbf{R} = 1$, $\mathbf{M} = 10 * \mathbf{I}_6$, batch size n = 4, 4-cycle averaging, and 10% probing; (f) generalized LMS filter with $\mathbf{K}_S = 0.1 * \mathbf{I}_6$, batch size n = 8, and 4-cycle averaging.

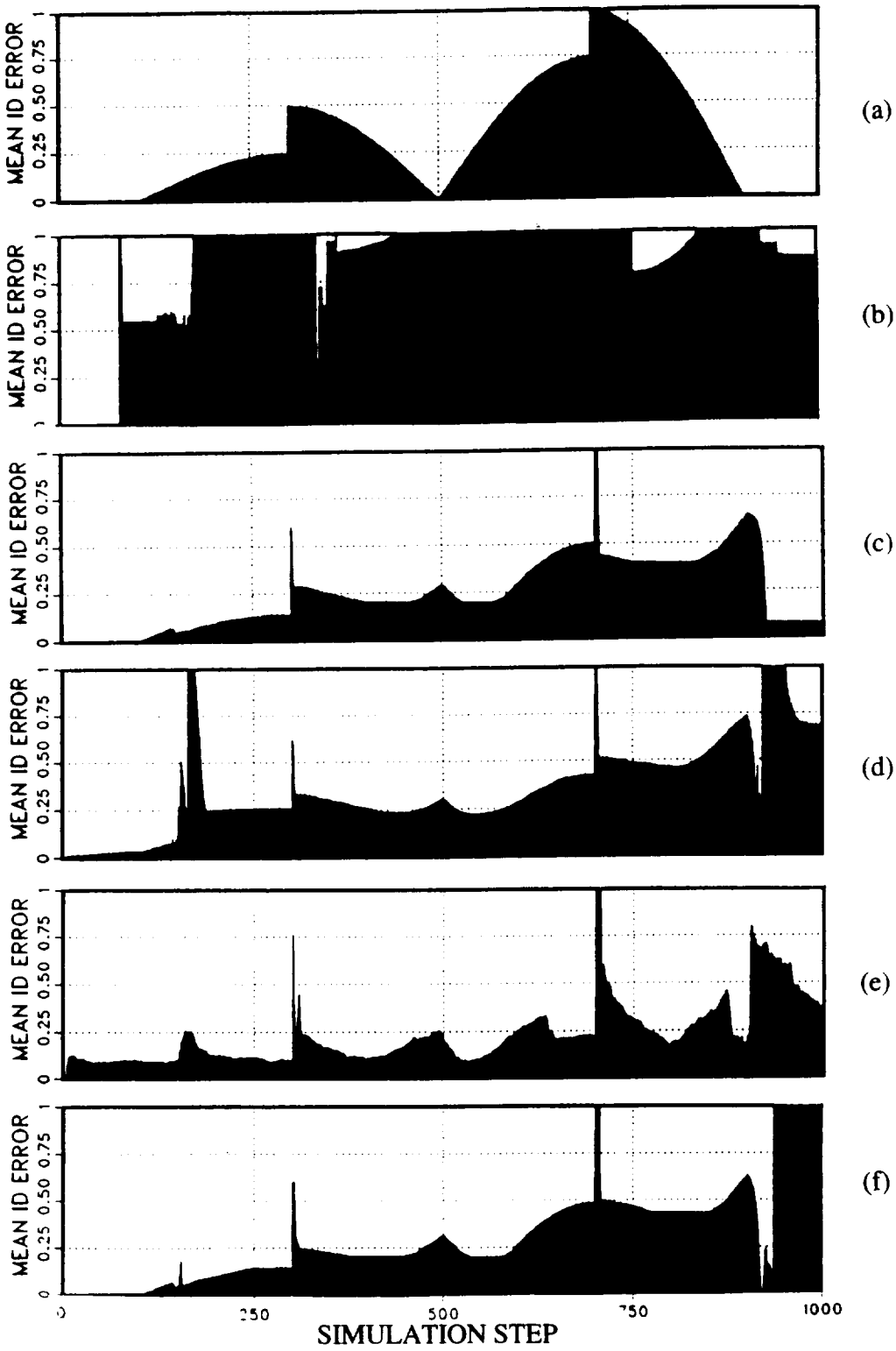

Figure 94. Comparison of Local Model, closed-loop identification error for the case of 10% measurement noise and continuous variation of the transfer matrix: (a) error without identification; (b) weighted least squares with n = 24 and "zero-vibration" = 0.20; (c) Kalman filter with r = 100, $\mathbf{M} = \mathbf{I}_6$, $\mathbf{Q} = 10 * \mathbf{I}_6$; (d) LMS filter with $\mathbf{K}_S = 0.1$ and 10% probing; (e) generalized Kalman filter with $\mathbf{R} = 1$, $\mathbf{M} = 10 * \mathbf{I}_6$, batch size n = 4, 8-cycle averaging, and 10% probing; (f) generalized LMS filter with $\mathbf{K}_S = 0.01 * \mathbf{I}_6$, batch size n = 4, no cycle averaging, and 10% probing.

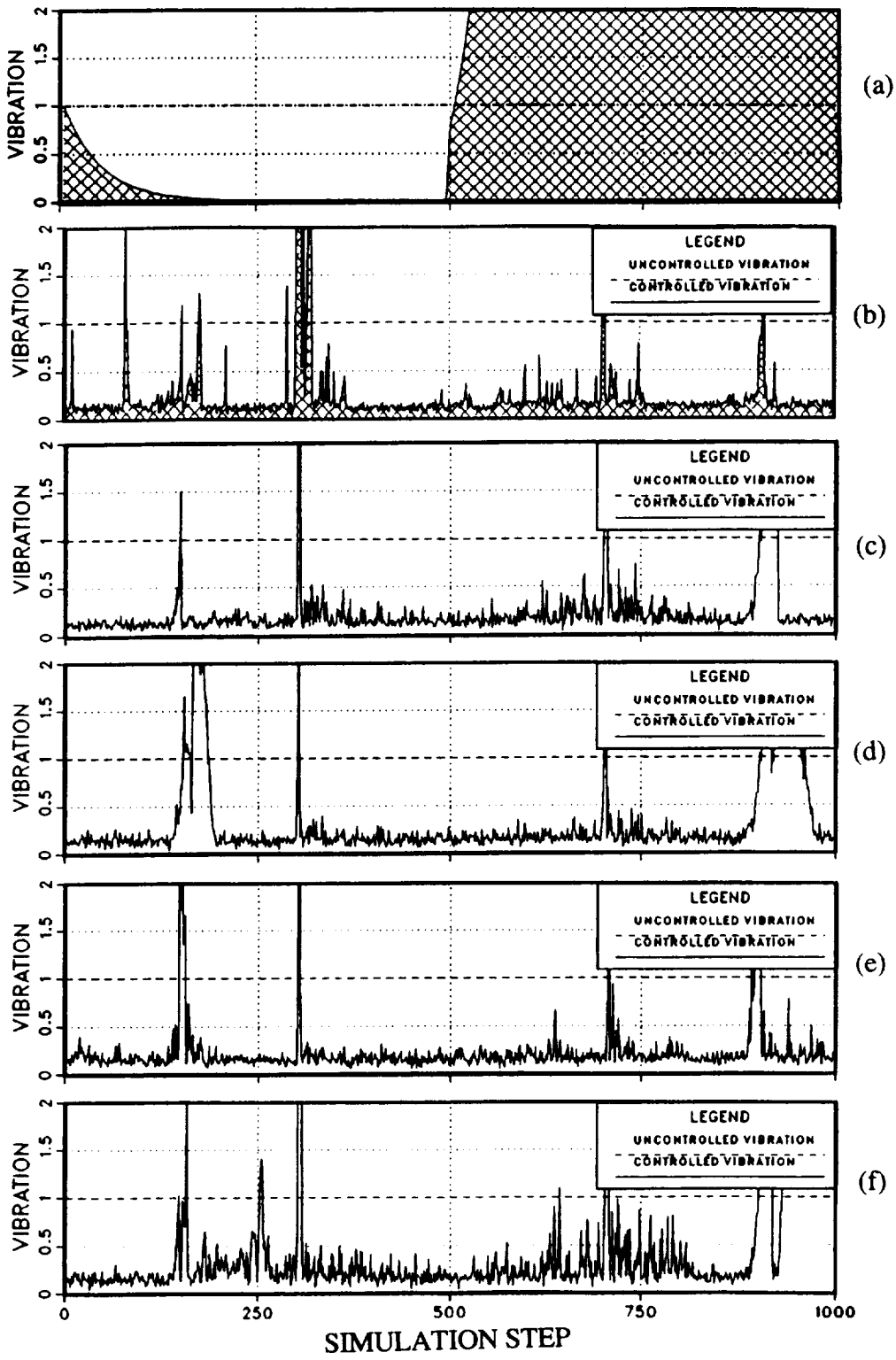

Figure 95. Comparison of Local Model, closed-loop vibration index for the case of 10% measurement noise and continuous variation of the transfer matrix: (a) without identification; (b) weighted least squares with n = 24 and "zero-vibration" = 0.20; (c) Kalman filter with r = 100, $\mathbf{M} = \mathbf{I}_6$, $\mathbf{Q} = 10$; (d) LMS filter with $\mathbf{K}_S = 0.1$ and 10% probing; (e) generalized Kalman filter with $\mathbf{R} = 1$, $\mathbf{M} = 10 * \mathbf{I}_6$, batch size n = 4, 8-cycle averaging, and 10% probing; (f) generalized LMS filter with $\mathbf{K}_S = 0.01 * \mathbf{I}_6$, batch size n = 4, no cycle averaging, and 10% probing.

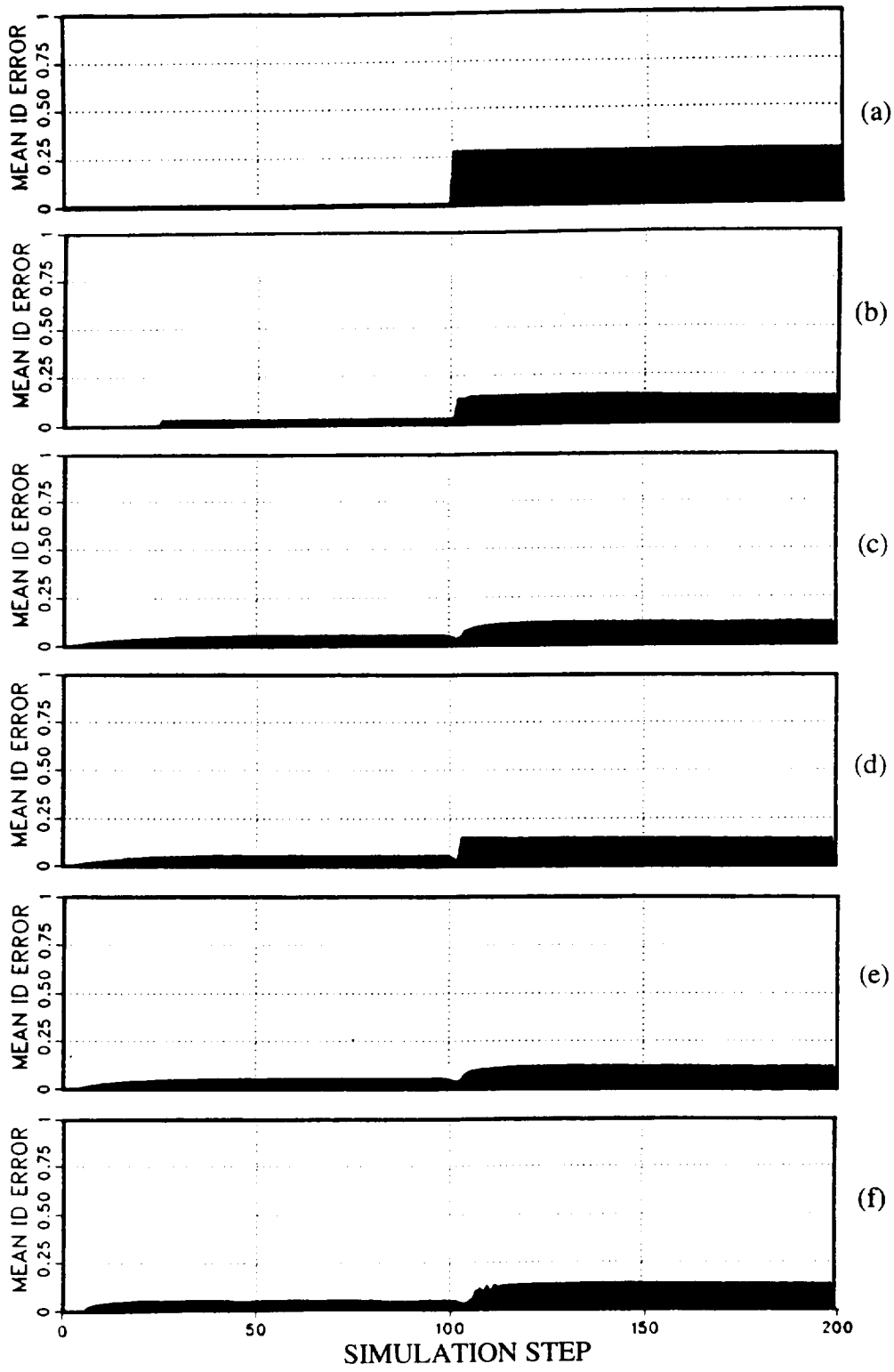

Figure 96. Comparison of global model, closed-loop identification error for the case of 10% measurement noise and a single change in the transfer matrix at simulation step 100: (a) error without identification; (b) weighted least squares with n = 24 and "zero-vibration" = 0.20; (c) Kalman filter with r = 100, $\mathbf{M} = \mathbf{I}_6$, $\mathbf{Q} = 10 * \mathbf{I}_6$, and 10% probing; (d) LMS filter with $\mathbf{K}_S = 0.01$ and 10% probing; (e) generalized Kalman filter with $\mathbf{R} = 100$, $\mathbf{M} = \mathbf{I}_6$, batch size n = 1, and no cycle-averaging; (f) generalized LMS filter with $\mathbf{K}_S = 0.01 * \mathbf{I}_6$, batch size n = 4, and 4-cycle averaging.

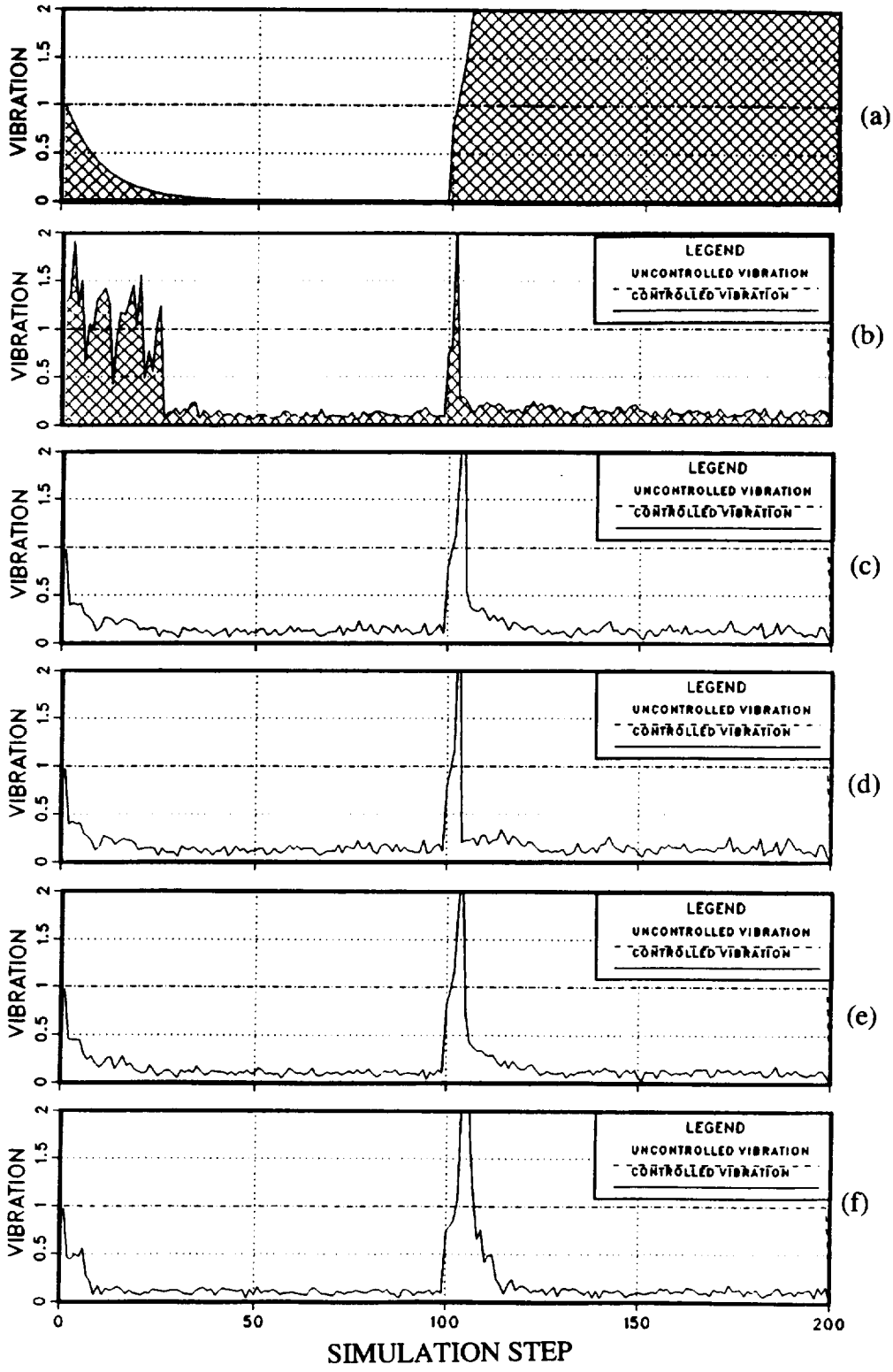

Figure 97. Comparison of global model, closed-loop vibration index for the case of 10% measurement noise and a single change in the transfer matrix at simulation step 100: (a) without identification; (b) weighted least squares with n = 24 and "zero-vibration" = 0.20; (c) Kalman filter with r = 100, $\mathbf{M} = \mathbf{I}_6$, $\mathbf{Q} = 10 * \mathbf{I}_6$, and 10% probing; (d) LMS filter with $\mathbf{K}_S = 0.01$ and 10% probing; (e) generalized Kalman filter with $\mathbf{R} = 100$, $\mathbf{M} = \mathbf{I}_6$, batch size n = 1, and no cycle-averaging; (f) generalized LMS filter with $\mathbf{K}_S = 0.01 * \mathbf{I}_6$, batch size n = 4, and 4-cycle averaging.

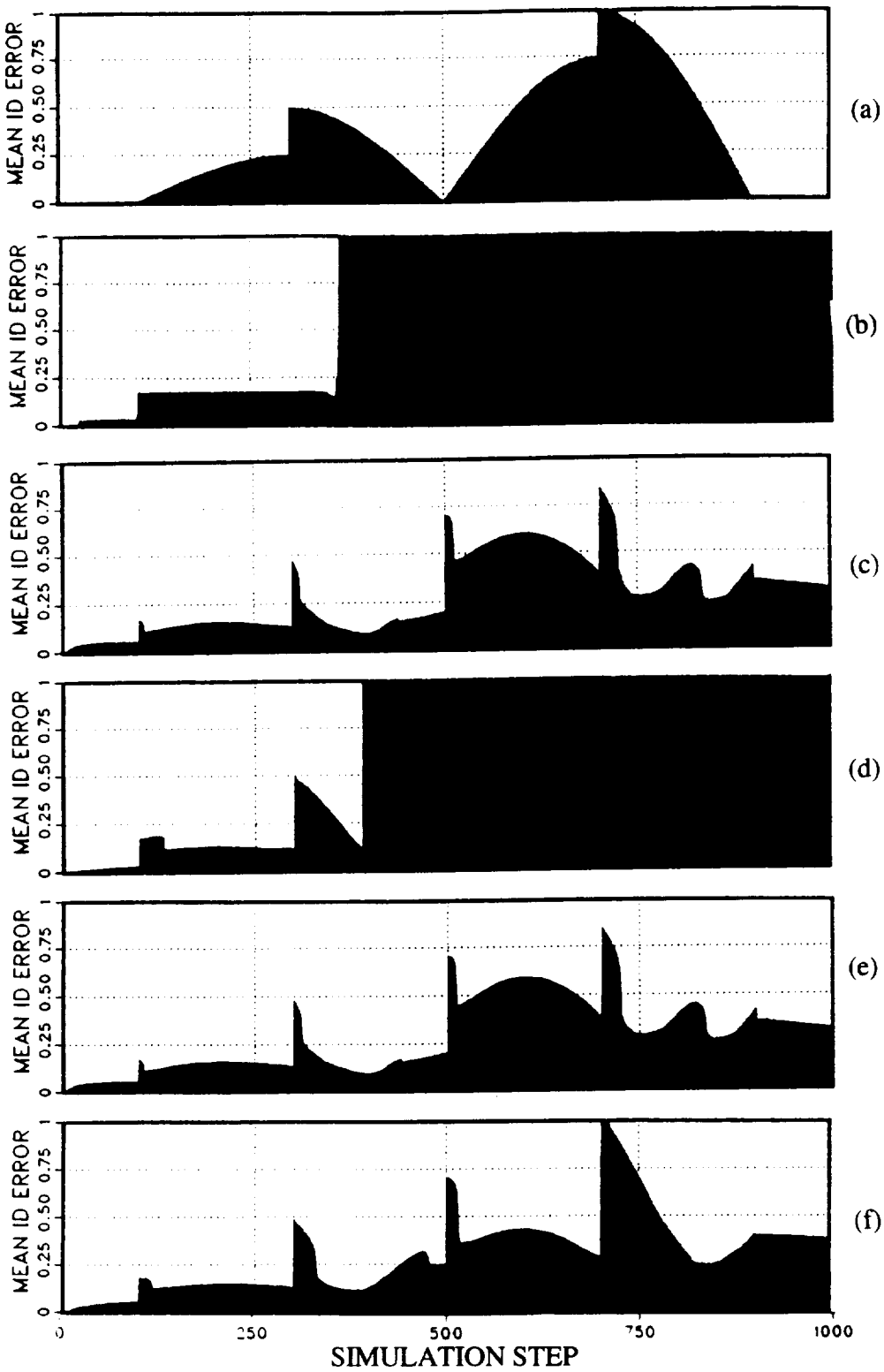

Figure 98. Comparison of global model, closed-loop identification error for the case of 10% measurement noise and continuous variation of the transfer matrix: (a) error without identification; (b) weighted least squares with n = 24 and "zero-vibration" = 0.20; (c) Kalman filter with r = 100, $\mathbf{M} = \mathbf{I}_6$, and $\mathbf{Q} = 10 * \mathbf{I}_6$; (d) LMS filter with $\mathbf{K}_S = 0.001$ and 10% probing; (e) generalized Kalman filter with $\mathbf{R} = 100$, $\mathbf{M} = \mathbf{I}_6$, batch size n = 1, and no cycle-averaging; (f) generalized LMS filter with $\mathbf{K}_S = 0.001 * \mathbf{I}_6$, batch size n = 4, and 4-cycle averaging.

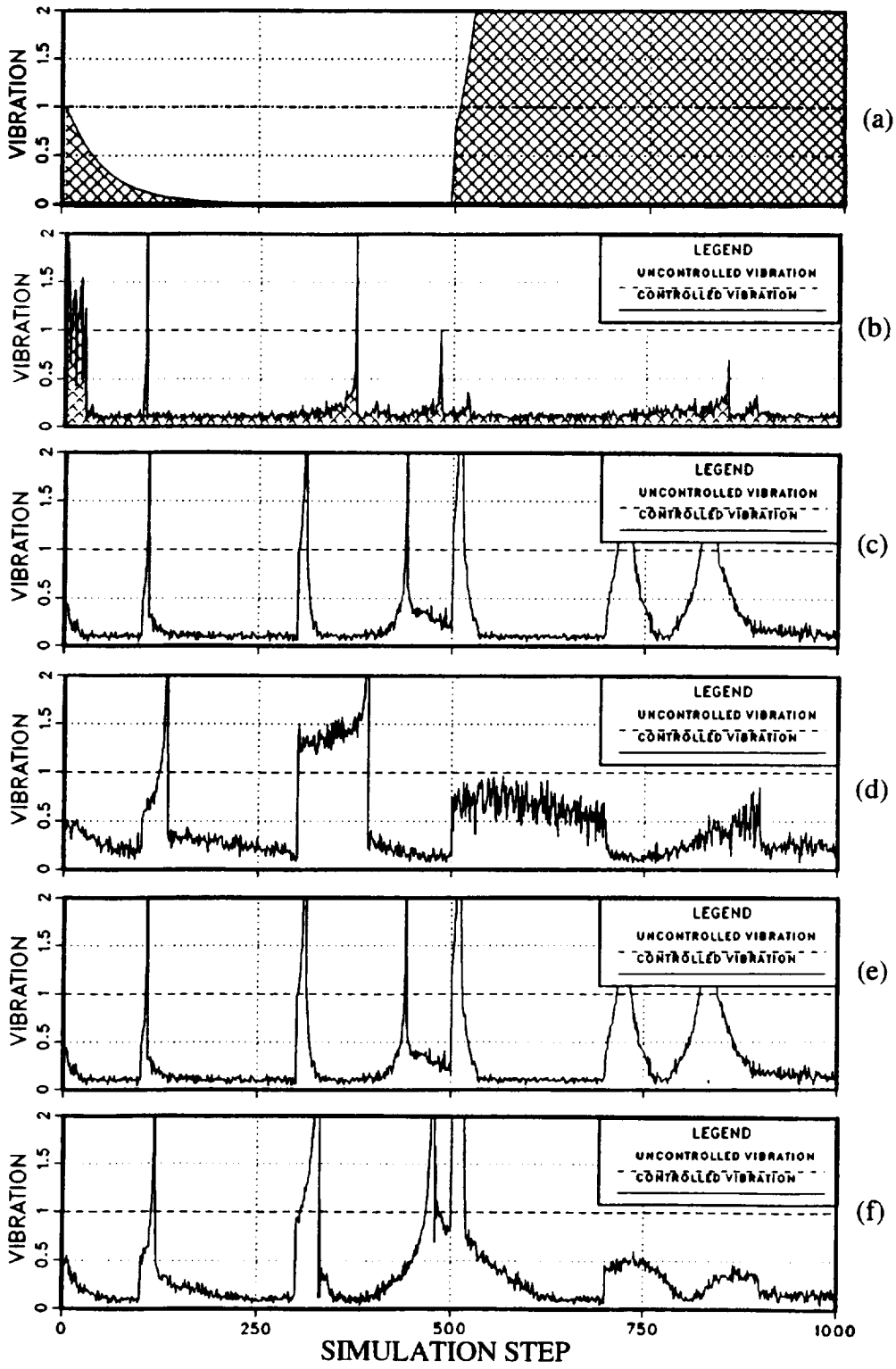

Figure 99. Comparison of global model, closed-loop vibration index for the case of 10% measurement noise and continuous variation of the transfer matrix: (a) without identification; (b) weighted least squares with n = 24 and "zero-vibration" = 0.20; (c) Kalman filter with r = 100, $\mathbf{M} = \mathbf{I}_6$, and $\mathbf{Q} = 10$; (d) LMS filter with $\mathbf{K}_S = 0.001$ and 10% probing; (e) generalized Kalman filter with R = 100, $\mathbf{M} = \mathbf{I}_6$, batch size n = 1, and no cycle-averaging; (f) generalized LMS filter with $\mathbf{K}_S = 0.001 * \mathbf{I}_6$, batch size n = 4, and 4-cycle averaging.

REPORT DOCUMENTATION PAGE

Form Approved
OMB No. 0704-0188

1. AGENCY USE ONLY *(Leave blank)*	2. REPORT DATE	3. REPORT TYPE AND DATES COVERED
	May 1998	Technical Paper

4. TITLE AND SUBTITLE

Comparison of Five System Identification Algorithms for Rotorcraft Higher Harmonic Control

5. FUNDING NUMBERS

6. AUTHOR(S)

Stephen Jacklin

7. PERFORMING ORGANIZATION NAME(S) AND ADDRESS(ES)

Ames Research Center
Moffett Field, CA 94035-1000

8. PERFORMING ORGANIZATION REPORT NUMBER

A-977183

9. SPONSORING/MONITORING AGENCY NAME(S) AND ADDRESS(ES)

National Aeronautics and Space Administration
Washington, DC 20546-0001

10. SPONSORING/MONITORING AGENCY REPORT NUMBER

NASA/TP–1998-207687

11. SUPPLEMENTARY NOTES

Point of Contact: Stephen Jacklin, Ames Research Center, MS T12-B, Moffett Field, CA 94035-1000
(650) 604-4567

12a. DISTRIBUTION/AVAILABILITY STATEMENT

Unclassified-Unlimited
Subject Category – 01, 63

Availability: NASA CASI (301) 621-0390

12b. DISTRIBUTION CODE

Distribution: Standard

13. ABSTRACT ***(Maximum 200 words)***

This report presents an analysis and performance comparison of five system identification algorithms. The methods are presented in the context of identifying a frequency-domain transfer matrix for the higher harmonic control (HHC) of helicopter vibration. The five system identification algorithms include three previously proposed methods: (1) the weighted-least-squares-error approach (in moving-block format), (2) the Kalman filter method, and (3) the least-mean-squares (LMS) filter method. In addition there are two new ones: (4) a generalized Kalman filter method and (5) a generalized LMS filter method. The generalized Kalman filter method and the generalized LMS filter method were derived as extensions of the classic methods to permit identification by using more than one measurement per identification cycle. Simulation results are presented for conditions ranging from the ideal case of a stationary transfer matrix and no measurement noise to the more complex cases involving both measurement noise and transfer-matrix variation. Both open-loop identification and closed-loop identification were simulated. Closed-loop mode identification was more challenging than open-loop identification because of the decreasing signal-to-noise ratio as the vibration became reduced. The closed-loop simulation considered both local-model identification, with measured vibration feedback and global-model identification with feedback of the identified uncontrolled vibration. The algorithms were evaluated in terms of their accuracy, stability, convergence properties, computation speeds, and relative ease of implementation.

14. SUBJECT TERMS

System identification, Higher harmonic control, Helicopter vibration control, Active vibration control, Kalman filter

15. NUMBER OF PAGES

154

16. PRICE CODE

A08

17. SECURITY CLASSIFICATION OF REPORT	18. SECURITY CLASSIFICATION OF THIS PAGE	19. SECURITY CLASSIFICATION OF ABSTRACT	20. LIMITATION OF ABSTRACT
Unclassified	Unclassified		